VOLUME 12 (1959) No. 6

NUCLEAR PHYSICS

JOURNAL DEVOTED TO THE EXPERIMENTAL AND THEORETICAL STUDY OF THE FUNDAMENTAL CONSTITUENTS OF MATTER AND THEIR INTERACTIONS

EDITOR: L. ROSENFELD - COPENHAGEN

P. BOSKMA and H. DE WAARD, Excited states of ^{166}Er 533

F. W. K. FIRK and M. C. MOXON, The determination of neutron resonance parameters of tungsten by the transmission method 552

J. R. WATERS, J. E. EVANS, B. B. KINSEY and G. H. WILLIAMS, Spins and radiation widths of the low energy neutron resonances in tungsten 563

J. M. FERGUSON, Fe^{59} decay scheme. 579

MINORU YONEZAWA, Remarks on the decay interactions in the K_{e2} process . 589

PETER HILLMAN, ARNE JOHANSSON, GUNNAR TIBELL and HELGE TYRÉN, Inelastic scattering of high energy protons by helium: an excited level? 596

K. V. LAURIKAINEN and O. VARHO, Phenomenological two-nucleon potentials and the deuteron, II 606

K. MAACK BISGÅRD, P. DAHL and K. OLESEN, Multipolarities of U^{233} transitions 612

R. H. LEMMER, TH. A. J. MARIS and Y. C. TANG, On the imaginary optical potential 619

L. E. H. TRAINOR and P. C. SOOD, Nature of nuclear matter in the free-meson lattice model 625

RICHARD BLANKENBECLER, MARVIN L. GOLDBERGER and FRANCIS R. HALPERN Elastic neutron-deuteron scattering 629

K. HELMERS, On symplectic invariance of the energy matrix a nuclear j^N configuration 647

L. J. B. GOLDFARB, On the detection of deuteron polarization 657

CORNELIUS P. BROWNE, Energy levels of Na^{22} from the $Mg^{24}(d, \alpha)Na^{22}$ and $Mg^{25}(p, \alpha)Na^{22}$ reactions 662

R. K. GIRGIS and R. VAN LIESHOUT, The level scheme of ^{134}Ba. Some features of the NaI summing spectrometer. 672

Author Index 689

Subject Index 694

NORTH-HOLLAND PUBLISHING COMPANY-AMSTERDAM

September (1) 1959

LAST NUMBER OF THIS VOLUME

EDITORIAL BOARD

AUSTRALIA & NEW ZEALAND:	H. Messel (Sydney), M. L. Oliphant (Canberra)
AUSTRIA:	B. Karlik, (Vienna), H. Thirring (Vienna)
BELGIUM:	M. de Hemptinne (Louvain), J. Verhaeghe (Ghent)
CANADA:	G. Volkoff (Vancouver)
DENMARK:	C. Møller (Copenhagen), S. Rozental (Copenhagen)
FINLAND:	L. Simons (Helsinki)
FRANCE:	A. Berthelot (Saclay), S. Gorodetzky (Strasbourg)
GERMANY (DEM. REP.):	G. Hertz (Leipzig)
GERMANY (FED. REP.):	W. Gentner (Freiburg i. B.), J. H. D. Jensen (Heidelberg)
GREAT BRITAIN:	S. Devons (Manchester), T. H. R. Skyrme (Harwell)
HUNGARY:	L. Janossy (Budapest)
INDIA:	H. Bhabha (Bombay), R. Ramanna (Trombay)
IRISH REPUBLIC:	J. McConnell (Maynooth)
ISRAEL:	G. Racah (Jerusalem)
ITALY:	E. Amaldi (Rome)
JAPAN:	S. Kikuchi (Tokyo), S. Tomonaga (Tokyo)
MEXICO:	M. Moshinsky (Mexico)
NETHERLANDS:	H. Brinkman (Groningen), S. R. de Groot (Leiden)
NORWAY:	E. Hylleraas (Oslo), A. Lundby (Oslo), H. Wergeland (Trondheim)
POLAND:	L. Infeld (Warsaw)
PORTUGAL:	J. M. Araújo (Porto), J. R. de Almeida Santos (Coimbra)
SOUTH AMERICA:	G. Beck (Saõ Paulo), J. Leite Lopes (Rio de Janeiro)
SPAIN:	J. M. Otero (Madrid), C. Sanchez del Rio (Madrid)
SWEDEN:	O. Klein (Stockholm), K. Siegbahn (Uppsala), I. Waller (Uppsala)
SWITZERLAND:	P. Huber (Basel), P. Scherrer (Zürich)
U.A.R. & ARAB COUNTRIES:	F. El Bedewi (Alexandria), M. G. Nooh (Cairo)
U.S.A.	H. H. Barschall (Madison, Wisconsin), V. Weisskopf (Cambridge, Mass.)
U.S.S.R.:	M. A. Markov (Moscow), I. S. Shapiro (Moscow), D. V. Skobeltzyn (Moscow)
YUGOSLAVIA:	I. Supek (Zagreb)

CONTRIBUTIONS may be sent to the Editor, Professor L. Rosenfeld, NORDITA, Blegdamsvej 17, Copenhagen Ø, either directly, or preferably through the intermediary of one of the members of the Editorial Board of the country or region in which the author is working. They may be written in English, French or German.

NUCLEAR PHYSICS is published in Fortnightly issues. The subscription price per volume of 700 pages is fl 57.00; 114s; a 15.00. Post-free.

SUBSCRIPTIONS should be sent to the publishers, NORTH-HOLLAND PUBLISHING COMPANY, P.O.Box 103, Amsterdam or to any subscription-agent.

BOOKS FOR REVIEW should be sent to Professor Rosenfeld.

No part of this issue may be reproduced in any form, by print, photoprint, microfilm or any other means without written permission from the publisher. Reprints, photoprints or microfilms are obtainable at cost from the publisher.

Printed in the Netherlands

NUCLEAR PHYSICS

ASSISTANT EDITOR

The Editor of NUCLEAR PHYSICS requires the assistance of a theoretical physicist for the reading and preparation of manuscripts for the press. The main requirements are:

(1) interest in and acquaintance with the methods of field theory and nuclear physics,

(2) interest in obtaining experience in the techniques of typography and editing,

(3) good knowledge of English.

The candidate is expected to reside in Copenhagen and may

(a) either be engaged on a full-time basis

(b) or be given the opportunity of pursuing research on a part-time basis.

The conditions of employment (salary, pension scheme, etc.) will be on the academic level, depending on the status and experience of the candidate.

Applications with details of scientific education and references should be sent to:

Professor L. Rosenfeld, NORDITA, Blegdamsvej 17,
COPENHAGEN, Denmark

NUCLEAR PHYSICS

EDTIORIAL BOARD

AUSTRALIA & NEW ZEALAND:	H. Messel (Sydney), M. L. Oliphant (Canberra)
AUSTRIA:	B. Karlik, (Vienna), H. Thirring (Vienna)
BELGIUM:	M. de Hemptinne (Louvain), J. Verhaeghe (Ghent)
CANADA:	G. Volkoff (Vancouver)
DENMARK:	C. Møller (Copenhagen), S. Rozental (Copenhagen)
FINLAND:	L. Simons (Helsinki)
FRANCE:	A. Berthelot (Saclay), S. Gorodetzky (Strasbourg)
GERMANY (DEM. REP.):	G. Hertz (Leipzig)
GERMANY (FED. REP.):	W. Gentner (Freiburg i. B.), J. H. D. Jensen (Heidelberg)
GREAT BRITAIN:	S. Devons (Manchester), T. H. R. Skyrme (Harwell)
HUNGARY:	L. Janossy (Budapest)
INDIA:	H. Bhabha (Bombay), R. Ramanna (Trombay)
IRISH REPUBLIC:	J. McConnell (Maynooth)
ISRAEL:	G. Racah (Jerusalem)
ITALY:	E. Amaldi (Rome)
JAPAN:	S. Kikuchi (Tokyo), S. Tomonaga (Tokyo)
MEXICO:	M. Moshinsky (Mexico)
NETHERLANDS:	H. Brinkman (Groningen), S. R. de Groot (Leiden)
NORWAY:	E. Hylleraas (Oslo), A. Lundby (Oslo), H. Wergeland (Trondheim)
POLAND:	L. Infeld (Warsaw)
PORTUGAL:	J. M. Araújo (Porto), J. R. de Almeida Santos (Coimbra)
SOUTH AMERICA:	G. Beck (Saõ Paulo), J. Leite Lopes (Rio de Janeiro)
SPAIN:	J. M. Otero (Madrid), C. Sanchez del Rio (Madrid)
SWEDEN:	O. Klein (Stockholm), K. Siegbahn (Uppsala), I. Waller (Uppsala)
SWITZERLAND:	P. Huber (Basel), P. Scherrer (Zürich)
U.A.R. & ARAB COUNTRIES:	F. El Bedewi (Alexandria), M. G. Nooh (Cairo)
U.S.A.	H. H. Barschall (Madison, Wisconsin), V. Weisskopf (Cambridge, Mass.)
U.S.S.R.:	M. A. Markov (Moscow), I. S. Shapiro (Moscow), D. V. Skobeltzyn (Moscow)
YUGOSLAVIA:	I. Supek (Zagreb)

NUCLEAR PHYSICS

JOURNAL DEVOTED TO THE EXPERIMENTAL AND THEORETICAL STUDY OF THE FUNDAMENTAL CONSTITUENTS OF MATTER AND THEIR INTERACTIONS

EDITOR: L. ROSENFELD · COPENHAGEN

VOLUME XII

JUNE 1959—SEPTEMBER 1959

NORTH-HOLLAND PUBLISHING COMPANY - AMSTERDAM

PRINTED IN THE NETHERLANDS

1.E.1:
4.E

Nuclear Physics **12** (1959) 533—551; © *North-Holland Publishing Co., Amsterdam*
Not to be reproduced by photoprint or microfilm without written permission from the publisher

EXCITED STATES OF ^{166}Er

P. BOSKMA and H. DE WAARD

Natuurkundig Laboratorium der Rijksuniversiteit Groningen

Received 4 May 1959

Abstract: The level scheme of ^{166}Er has been studied from the decays of ^{166}Ho*(> 30y) and ^{166}Tm(7.7h) by means of scintillation and β-spectroscopic coincidence techniques. A discussion is given about the character of the excited states of ^{166}Er.

1. Introduction

The rotation-vibration structure of nuclear spectra, predicted by the Bohr-Mottelson model for strongly deformed nuclei, has been found experimentally for several rare earth elements, in which the number of protons and neutrons is sufficiently far from the magic numbers 50 and 82. This paper deals with such an example: the nuclear level spectrum of ^{166}Er. Its trends are consistent with the theoretical predictions.

Earlier investigators studied the ^{166}Ho* decay by means of scintillation methods and gamma-gamma coincidence experiments, but no measurements of the conversion electron and beta spectrum, as reported here, have as yet been published. In the ^{166}Tm decay only the scintillation gamma spectrum and the low energy conversion lines have previously been studied. This paper also describes conversion electron-gamma and gamma-gamma coincidence experiments and proposes a level scheme for the more intense transitions.

2. Survey of Previous Results

The excited states of ^{166}Er had been studied from the radioactive decays of ^{166}Ho(27 h), ^{166}Ho*(> 30y) and ^{166}Tm(7.7 h). As these parent nuclei have widely different spins, the data obtained from their decay about the levels in ^{166}Er supplement each other.

The decay of ^{166}Ho(27h) has been studied rather thoroughly [1–5]). Five gamma rays were detected, the lowest of which has an energy of 80 keV, indicating a first rotational level. Three other gamma rays of much lower intensity start from two levels at 1458 and 1620 keV with spin 0 and 1 respectively, the first level having positive parity. This was concluded from angular correlation measurements by Fraser and Milton [4]). The fifth

gamma ray, observed only by Cork *et al.*[5]), de-excites a level at 970 keV. There are two rather intense beta spectra, one to the ground state and one to the 80 keV state. Three components of lower intensity populate the 970, 1458 and 1620 keV excited states. An assignment 0- was proposed for the 27 h ^{166}Ho-state.

The long lived ^{166}Ho activity was first identified and studied by Butement [6]) by means of Geiger counters and absorption techniques. A second study by Milton, Fraser and Milton [7,8]) with gamma scintillation coincidence techniques revealed 5 gamma rays in cascade of energies 80, 188, 283, 725 and 845 keV. A recent investigation by Grace, Taylor and Trecay [9]) with scintillation counters reported two gamma rays of 438 and 537 keV. On the basis of gamma-gamma coincidence results they propose a different level scheme, partly contradictory to that of Milton *et al.* Apart from a determination of the energies of the conversion electrons of the three lowest gamma rays by Graham and Clark [3]), no beta spectrometer measurements have been reported before the work to be described here was started. This may be due to the very low specific activity available.

^{166}Tm(7.7 h) decays by electron capture and a small amount of β^+-emission to ^{166}Er. The isotope was first produced and identified by Wilkinson and Hicks [10]). Nervik and Seaborg [11]) measured gamma energies of 80, 112, 140, 180, 670, 800 and 1320 keV in an equilibrium mixture of ^{166}Yb and ^{166}Tm. Gorodinskii *et al.*[12]) also investigated the spallation products of tantalum and found gamma lines of 80, 180, 690 and 780 keV in the ^{166}Tm decay. Mihelich *et al.*[13]) found transitions in the low energy region of 80.7, 154.6, 184.7, 194.8 and 215.4 keV, using a photographic permanent magnet beta-spectrometer. No decay schemes were published.

3. Decay of ^{166}Ho*(>30y)

3.1. SINGLE COUNT SPECTRA

Spectroscopically pure Ho_2O_3 was irradiated at the Materials Testing Reactor in Idaho (USA) for one month at a neutron flux of about 10^{14} neutrons/cm^2 sec. After the short lived activity had died down completely, an ion exchange column separation was performed to get rid of possible contaminations by other rare earths. No such impurities appeared to be present because no noticeable difference was found between the gamma spectra of the purified sample and the original material. Sources for beta-spectroscopical measurements were prepared by spreading some Ho_2O_3 powder suspended in a 5% zapon lacquer solution evenly on a teflon backing of 0.4 mg/cm^2. Due to the very low specific activity of the material, rather thick sources had to be used (about 0.5 mg/cm^2).

A *single count scintillation spectrum*, using a $1\frac{3}{4}'' \times 2''$ NaI(Tl) crystal, was

recorded with a multichannel kick-sorter. This spectrum, which shows photopeaks corresponding to gamma energies of 60, 80, 105, 180, 280, 420, 530, 710 and 820 keV was analyzed to determine the relative intensities of the various transitions. Table 1 lists these intensities, obtained from the area's under the analyzed photopeaks, after correction for the efficiency and the photofraction of the crystal, together with measurements of previous authors. A correction for internal conversion is made for the 80 and 180 keV gamma rays, assuming these transitions to be of E2 character.

TABLE 1

Gamma energies in keV and relative intensities from an analysis of the single count spectrum of ^{166}Ho*

This paper		Butement [6])		Milton *et al.* [7, 8])		Grace *et al.*[9])	
Energies	Intensities	Energies	Intensities	Energies	Intensities	Energies	Intensities
80	100	95	—	80.2±0.5	100	80	110
105	5	—	—	—	—	—	—
180	100	212	—	188	100	183	100
280	35	280	—	283	100	277	30
420	18	—	—	—	—	410	10
530	8	—	—	—	—	528	10
710	80	725	—	725	100	718	100
820	80	830	—	845	100	817	100

The *single count β-spectrum* was measured in a solenoidal beta-spectrometer. The conversion lines show long tails on their low energy sides, due to the source thickness. This thickness could be estimated from the line shift of the L 80.25 keV conversion line to be about 0.5 mg/cm^2. Table 2 lists and identifies the conversion lines after a correction for source thickness.

TABLE 2

Conversion lines in the ^{166}Ho*-decay and their identification

Energy of conv. line		Identification of conv. line	Gamma energy	Energy of conv. line		Identification of conv. line	Gamma energy
single	coinc.			single	coinc.		
70.8	69.4	L 80.25	80.25	351	351	K 409	409± 4
78.4	78.2	M 80.25	—	403	—	L 409	—
96	—	L 105	105±5	476	472	K 532	532± 7
125	123	K 182	182±1	—	522	L 532	—
173	171	L 182	—	652	638	K 700	700±14
—	217	K 275	275±2	759	759	K 817	817± 7
—	222	K 280	280±2	831	814	L 817	—

Energies in keV.

A Kurie-plot of the beta spectrum shows two components with maximum energies 1450±50 and 1000±50 keV, and relative intensities of about 10 and 85 %; the corresponding *lower limits* of the log *ft* values are 11.6 and 10.9.

3.2. COINCIDENCE SPECTRA

β—e⁻ coincidences. In order to reduce the contribution of the beta spectrum under the conversion lines, a spectrum of coincidences was recorded between electrons detected in a stilbene crystal placed directly behind the source and electrons analyzed in the beta spectrometer. The statistics of the higher energy conversion lines are rather poor because of the low intensity of the source. Except for the 80 and 182 keV transitions, for which the conver-

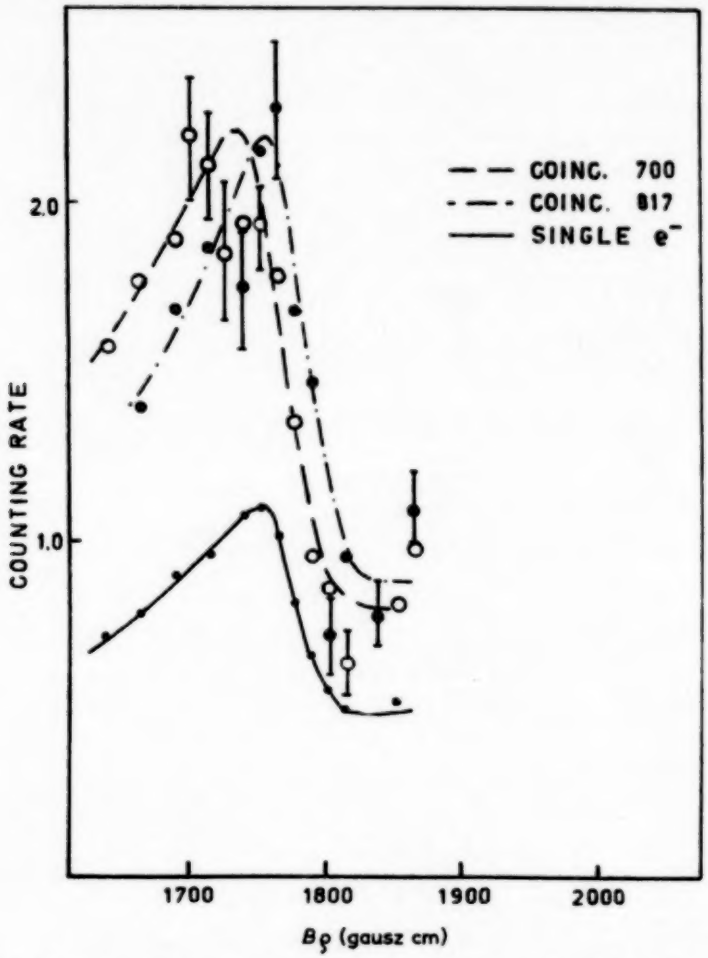

Fig. 1. γ—e⁻ coincidences on the two K conversion lines of the 275 and 280 keV transitions in ^{166}Ho*.

sion ratios are $L/(M+N) = 3.4 \pm 0.6$ and $K/(L+M) = 1.7 \pm 0.5$ respectively, no sufficiently accurate conversion ratios can be given.

γ—γ coincidences. Using two NaI(Tl) crystals of size $1\frac{3}{4}'' \times 2''$, gamma-gamma coincidence spectra were recorded on the multichannel pulse height analyzer, gating the spectrum from one counter on several parts of the spectrum from the other counter. The results are in good agreement with the experiments of Grace *et al.* [9]; for instance, we also find that the intensity of the 280 keV gamma is about half as large in the spectra coincident with the

817 and 700 keV gamma rays as in the single count spectrum. This result can be interpreted by assuming that there are really two different gamma lines both with an energy of about 280 keV.

γ—e$^-$ *coincidences.* In order to investigate if there are two different lines at about 280 keV, the electron spectrum corresponding to the K-conversion of lines with energies near 280 keV was measured, first in coincidence with the 817 keV gamma line and next with the 700 keV gamma line. Two con-

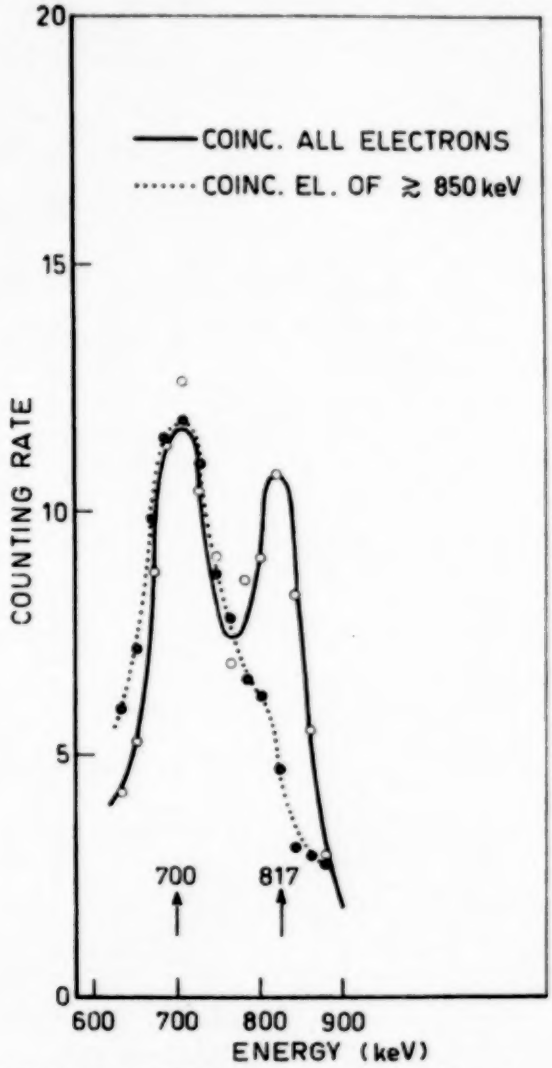

Fig. 2. Coincidences of the 700 and 817 gamma lines with different parts of the β-spectrum of ^{166}Ho*.

version lines with energies of 217 and 223 keV were thus found, as is shown in fig. 1.

The single count conversion spectrum, also given in this figure, shows only one peak, from which it is impossible to separate the two conversion lines. The energies of the corresponding gamma rays are estimated at 275 ± 2 and 280 ± 2 keV (see table 2).

To fix the position of the weak 105 keV transition in the level scheme, a coincidence gamma spectrum was gated on the top of the L105 conversion line. Since no difference between this spectrum and the single count spectrum was found, the 105 keV line must be in coincidence with all other gamma rays.

β—γ coincidences. The gamma spectrum was recorded in coincidence with different parts of the beta spectrum, detected by a 10 mm thick anthracene

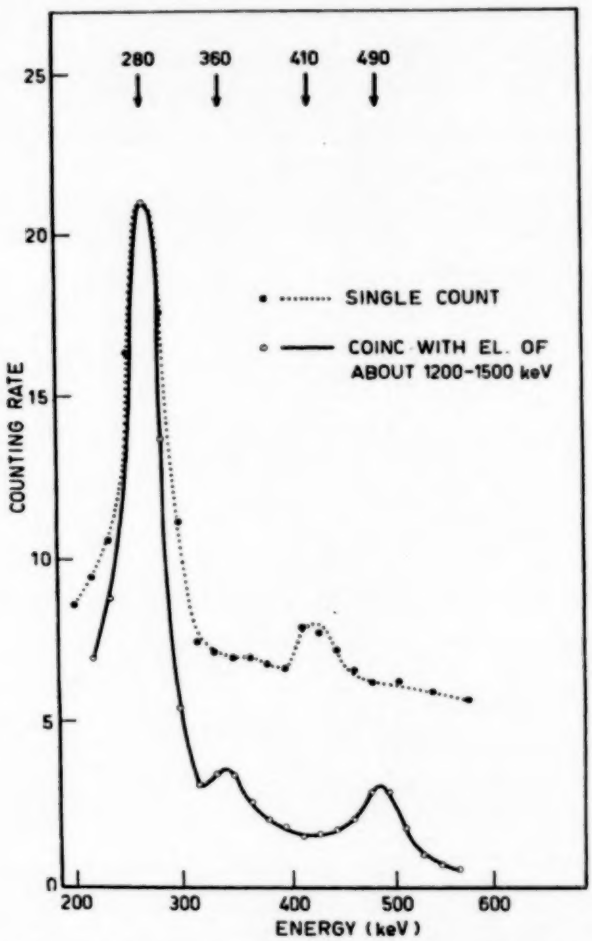

Fig. 3. Part of the gamma spectrum of $^{166}Ho^{*}$, coincident with electron energies of 1200—1500 keV.

crystal, in order to decide, which of the cascaded 700 and 817 keV gamma's is "on top". Gating the gamma spectrum on the higher energy part of the scintillation beta spectrum shows a large reduction of the intensity of the 817 keV line, as can be seen from fig. 2.

This line must therefore be on top. Gamma spectra in coincidence with beta-particles of 1200—1500 keV show two new lines (fig. 3) at 360 ± 20 and

490±30 keV. These lines could not be observed in the single count gamma spectrum because of their low intensity, but they can be seen very well in the coincidence spectrum, due to the reduction of the contribution of the higher energy gamma lines. Their intensities are estimated between 0.5 and 3 %.

3.3. DISCUSSION OF THE LEVEL SCHEME

A level scheme (fig. 4) can be given on the basis of these measurements, which is in good agreement with the decay scheme proposed by Grace *et al.* [9]).

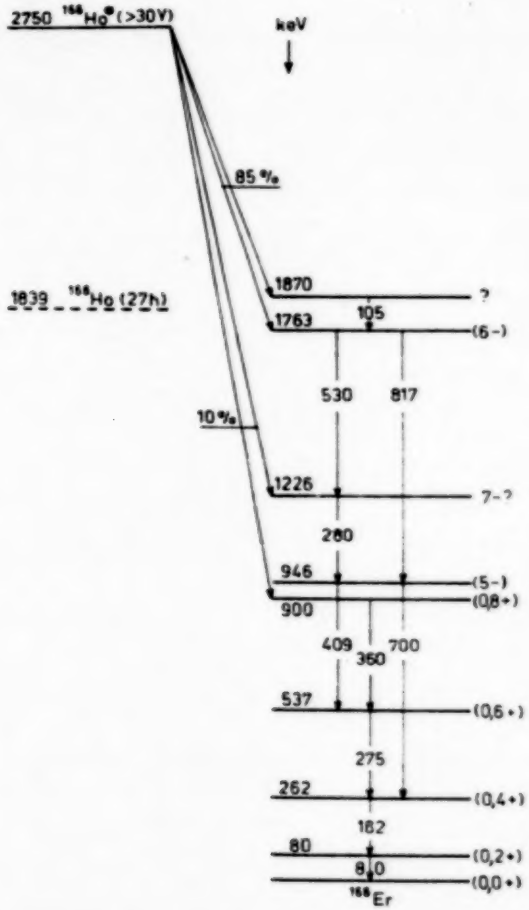

Fig. 4. Decay scheme of ^{166}Ho*(> 30y).

All authors agree that the 80.25 and 182 keV lines form a rotational band. The L/(M+N) ratio of the 80.25 and K/(L+M) ratio of the 182 keV transition are consistent with the theoretical values for E2 radiation. The ratio of the energies of the second and first rotational levels is 3.27±0.02, which may be compared with the theoretical value 3.33 for pure rotational levels. The difference gives a measure of the rotation-vibration interaction. A value 1.75±0.35 MeV is deduced from this difference for the vibration quanta

$\hbar\omega_\beta$ and $\hbar\omega_\gamma$, assuming $\hbar\omega_\beta = \hbar\omega_\gamma$ and using the notation of ref.[14]). A calculation of the energy of the third rotational level, taking into account the rotation-vibration interaction shows that the 275 keV line fits best between the second and third rotational level. Assuming the 275 keV transition to be of E2 character, its conversion coefficient can be determined using Rose's tables. A rough estimate of the K-conversion coefficient of the 280 keV line can now also be given, using the relative intensities deduced from the gamma-gamma coincidence spectra and from the conversion electron-gamma coincidence measurements on the 275 and 280 keV lines. A value $\alpha_K = (6.4 \pm 5.1) \times 10^{-2}$ is thus estimated, showing that the 280 keV transition may also have E2 character.

A calculation of the energy of the fourth rotational transition gives 362 ± 16 keV. The 360 ± 20 keV line found in the gamma spectrum coincident with high-energy beta-particles can be interpreted as this transition, populated by a separate β-component. The K-conversion coefficient of the 700 and 817 keV gamma rays can be determined using the relative intensity of 85 % for the 1000 keV β-component. Rough estimates of the α_K's of the 532 and 409 keV lines can be made if the relative intensities are taken equal, which can be argued from the gamma spectrum. Table 3 lists the experimental and theoretical conversion coefficients for those highest energy

TABLE 3

The K-conversion coefficients in the $^{166}Ho^*$-decay and the theoretical values calculated by Rose [15])

Gamma energy (keV)	Theoretical values acc. to Rose				Exp. value
	E1	E2	M1	M2	
817	1.8×10^{-3}	4.3×10^{-3}	8.8×10^{-3}	2.3×10^{-2}	$(3.0 \pm 0.8) \times 10^{-2}$
700	2.4×10^{-3}	6.1×10^{-3}	1.3×10^{-2}	3.7×10^{-2}	$(1.7 \pm 0.5) \times 10^{-2}$
532	4.2×10^{-3}	1.2×10^{-2}	2.7×10^{-2}	8.0×10^{-2}	$(6.3 \pm 2.0) \times 10^{-2}$
409	7.5×10^{-3}	2.2×10^{-2}	5.1×10^{-2}	1.7×10^{-1}	$(8.8 \pm 5.0) \times 10^{-2}$

gamma rays. A comparison shows that the K-conversion coefficient of the 817 keV line would be consistent with the calculated value for an M2 transition. The half life of the 1760 keV level can then be calculated for a single particle transition to be 3×10^{-9} sec. Delayed coincidence measurements between β- particles and Compton electrons of the 817 keV transition, both detected in stilbene crystals, however, give an upper limit to this half life of 2×10^{-10} sec. Anisotropy measurements of the 817 keV gamma radiation with oriented nuclei at very low termperatures ($\approx 0.02°$K), carried out by Postma *et al.* [16]) † in Leiden, are consistent with a quadrupole

† The authors gratefully acknowledge the communication of Postma's results prior to u[illegible] cation.

character of this radiation with about 2 % dipole admixture. Thus, its character must be E2(M1).

The conversion coefficient of the 700 keV gamma suggests M1 radiation. Measurements of the anisotropy and the linear polarization of the gamma-rays by Postma *et al.*[16]†, however, uniquely indicate that this character is E1

It must be concluded from these results, that the conversion coefficients for the 817 and 700 keV gamma are anomalously high by a factor of about 7. It has been pointed out by Church and Wesener [17]) and Nilsson and Rasmussen [18]) that this may happen for strongly deformed nuclei, when the gamma transition is hindered on the basis of the selection rules after Nilsson's model [19]), while the conversion process is unhindered.

Spins and parities can be assigned to various levels. The ground state of the even nucleus ^{166}Er is 0+. The quantum numbers (K, I, π) of the rotational levels at 80.25, 262, 537 and 900 keV are (0, 2+), (0, 4+), (0, 6+) and (0, 8+). The 946 keV level must be 5− to explain the E1 character of the 700 keV transition. Since the K quantum number of this level is not known, the intensity ratio for the decay of this level to two members of a rotational band cannot be calculated and verified.

The 1763 keV level decays by E2 emission to the 1226 and 946 keV excited states. Its parity must be negative, because the 946 keV state has negative parity.

The 1870 keV level cannot be assigned on the basis of the measurements. Also the position of the 490 keV gamma line is very difficult to settle.

The most probable value of the spin of the parent nucleus ^{166}Ho* is 8; a value 7, however, cannot be ruled out completely. According to Nilsson's calculations of single particle levels in deformed nuclei, a proposal can be made for the spins and parities of the odd proton and neutron in ^{166}Ho. The 67$^{\text{th}}$ proton is expected to be $\frac{7}{2}-$ or $\frac{1}{2}+$; the first value is in agreement with the ground state spin $\frac{7}{2}$ of ^{165}Ho. The 99$^{\text{th}}$ neutron should be $\frac{1}{2}-$ or $\frac{7}{2}+$; the second value is in agreement with the ground state spin $\frac{7}{2}$ of ^{167}Er. The ground state of ^{166}Ho(27h) has indeed a spin and parity 0−. These two particles cannot couple to a state 8−, which must be preferred on the basis of the high lower limit of the log ft value for the 1000 keV beta component. Such a high value can only be obtained if protons with angular momenta $\frac{11}{2}$ or $\frac{9}{2}$ play a part in forming this state. Since there is evidence from odd proton nuclei that the $h_{\frac{11}{2}}$ shell is being filled in this region, this assumption appears to be reasonable.

4. Decay of ^{166}Tm(7.7h)

4.1. SINGLE COUNT SPECTRA

Radioactive Tm isotopes were produced by 40 μAh irradiations of spectroscopically pure Er_2O_3 with 25 MeV deuterons at the Amsterdam cyclotron.

† The authors gratefully acknowledge the communication of Postma's results prior to publication.

Three Tm activities were identified in the sample on the basis of their half lives, viz. ^{165}Tm(29h), ^{166}Tm(7.7h) and ^{167}Tm(9.6d). By far the strongest activity was that of ^{166}Tm. Ion exchange column separations were carried out to obtain carrier free Tm activities. Sources for beta-spectroscopical measurements were made in the same way as the Ho-sources. In order to check the identification of the activities observed, spectroscopically pure Ho_2O_3 was irradiated at Amsterdam with a 4μAh dose of 50 MeV α-particles.

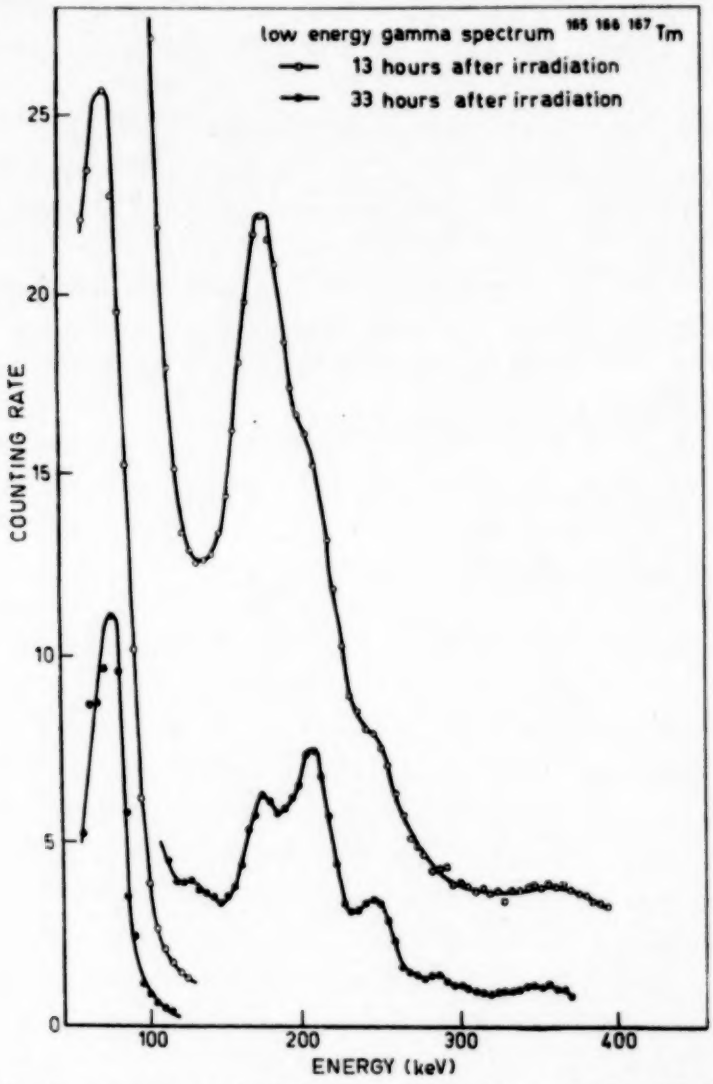

Fig. 5a. Low energy part of the gamma spectrum of some Tm-isotopes.

The same activities were found in the samples in a different intensity relation.

The *single count gamma spectrum* in a $1\frac{3}{4}'' \times 2''$ NaI(Tl) crystal is reproduced in figs. 5a and 5b.

The higher energy part (fig. 5b), which totally decays with a half life of 7.7h, shows photopeaks corresponding to gamma energies of 710, 790, 1180, 1270, 1550 and 2000 keV. Several of these lines had not been observed

before. The 1550 keV line is rather weak and its half width is much too large. Its existence is concluded unambiguously from an analysis of the spectrum and a comparison of two spectra measured with different distances between the source and the crystal. Relative intensities were also estimated from the analysis, correcting for photoefficiency and photofraction of the scintillation crystal.

The lower energy part of the spectrum (fig. 5a) shows a rather complicated conglomerate of lines, which decay with different half lives. It proved

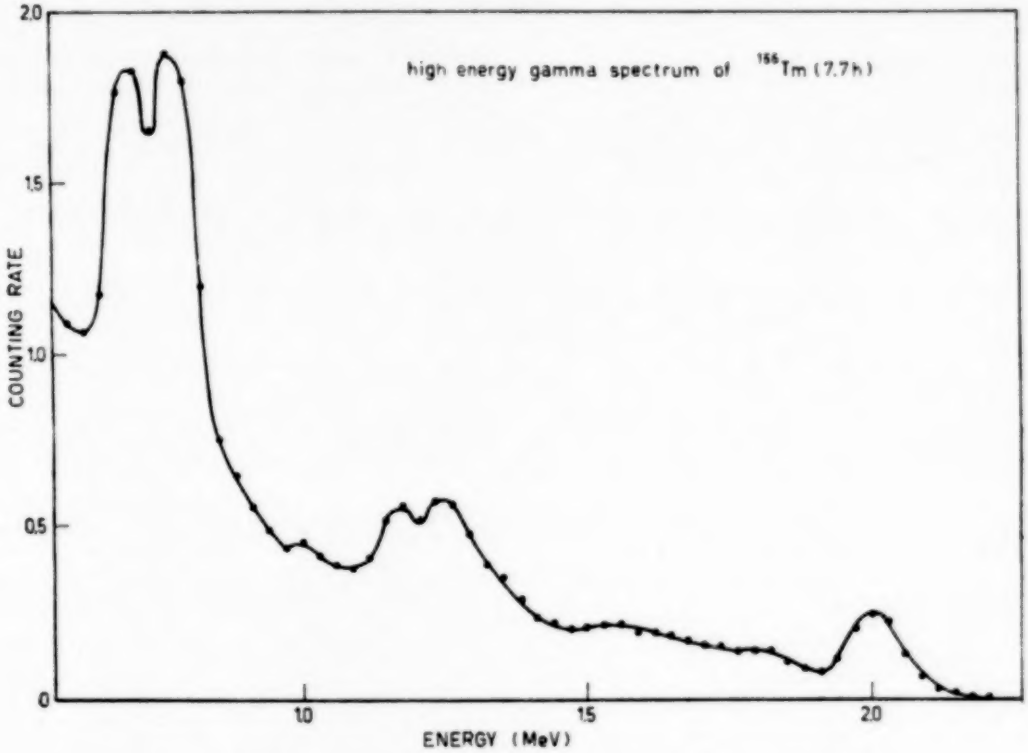

Fig. 5b. High energy part of the gamma spectrum of ^{166}Tm.

TABLE 4

γ-spectrum of Tm-isotopes

Gamma line (keV)	Intensity	Gamma line (keV)	Intensity
^{166}Tm (7.7h):			
80	100±30	1270	18
180	35±15	1550	7
464	10	2000	20
710	25	^{165}Tm (29h):	
790	30	243	—
1180	14	348	—
		^{167}Tm (9.6 d):	—
		207	—

difficult to analyze this part of the spectrum with reasonable accuracy into three components with the half lives mentioned above. A rough analysis was performed with the aid of the information obtained from the conversion electron spectrum. The results are listed in table 4.

No very precise values for the intensities of the 180 and 80 keV lines relative to the higher energy lines can be obtained from this gamma spectrum, because of its complex structure. The intensity ratio could be calculated very well from the conversion electron spectrum, however, assuming the 80 and 180 keV transitions to be of E2 character.

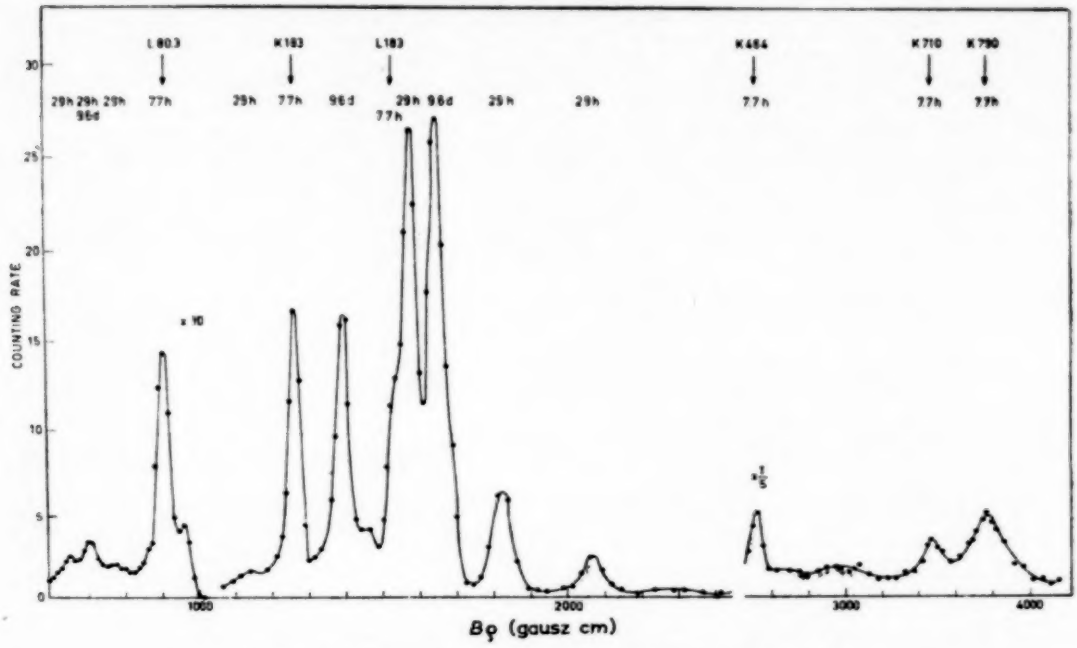

Fig. 6. Conversion electron spectrum of ^{166}Tm.

Fig. 6 shows *the conversion electron spectrum*, measured in our magnetic lens spectrometer. Table 5 lists the conversion lines, together with their half lives and identification.

A comparison is given of our measurements with those of Mihelich *et al.* [13]) for the three Tm isotopes 165, 166 and 167. We could not find the K conversion lines of the 154.6 and 215.4 keV gammas reported by Mihelich *et al.* [13]) in the 7.7h decay. This may be due to the smaller resolving power of our spectrometer, which caused an overlap of several conversion lines in this region. The lines at 238 and 292 keV are also interpreted as composite lines, each consisting of conversion lines of two different gamma rays. The K-conversion lines of the 297.8 and 296.5 keV transitions could impossibly be separated here. The small bumps in the spectrum at about 350 and 520 keV could not be interpreted satisfactorily. We could find no conversion lines of

TABLE 5

Conversion electron spectrum of Tm isotopes

Conversion Line		Gamma energy (keV)	Mihelich *et al.*[13])
Energy (keV)	Identification		
^{166}Tm(7.7h):			
70.9	L 80.2	80.2	80.7
77.2	M+N 80.2	80.2	80.7
—	—	—	154.6
124.8	K 183	183	184.7
135	K 192	192	194.8
175.6	L 183	183	184.7
—	—	—	215.4
^{165}Tm(29h):			
36.9	L 46.8	46.8	47.2
42.4	L 52.3	52.3	54.5
50.5	L 60.3	60.3	60.5
63.0	L 72.9	72.9	77.3
104.8	L 114.6	114.6	113.7
160	K 218	218	219.3
186	K 243	243	243.3
238	L+M 243	243	243.3
	K 296	296	296.5 297.8
292	L+M 296	296	296.5
	K 350	350	347.3
—	—	—	356.9
^{167}Tm (9.6d)			
42.4	L 52.3	52.3	57.1
198	L+M 207	207	208.3

the 112 and 140 keV transitions reported by Nervik and Seaborg [11]). Since these lines were neither observed by Mihelich *et al.* they are believed to be due to contaminations.

With a helical baffle mounted in the spectrometer *the positon spectrum* of ^{166}Tm was investigated. Two β^+-branches of low intensity were detected. From a Kurie plot their maximum energies were found to be 450 ± 80 and 1300 ± 100 keV. Their intensities were estimated at 1.8 % and 1.3 % by comparing them with the L+M+N conversion lines of the 80 keV transition and supposing that all decays proceed through this level. The corresponding 510 keV gamma annihilation radiation could not be seen very distinctly.

4.2. COINCIDENCE SPECTRA

The coincidence relations of the transitions were investigated by gating the gamma spectrum produced in a $1\frac{3}{4}'' \times 2''$ NaI(Tl) crystal either with the conversion lines of the 80.2 and 182 keV transitions in the β-spectrometer or with various photopeaks detected by a second $1\frac{3}{4}'' \times 2''$ NaI(Tl) crystal. The

coincidence spectra were registered on a 70 channel pulse height analyzer. The coincidence relations are summarized in table 6.

TABLE 6

Coincidence relationships of lines in ^{166}Tm decay

Gamma energies (keV)	710	790	1180	1270	2000
80.2	+	+	+	+	+
182	+	−	+	−	+
710	−	−	+	−	−
790	−	−	−	+	−
1180	+	−	−	−	−
1270	−	+	−	−	−
2000	−	−	−	−	−

All gamma rays with energies larger than 500 keV are coincident with the 80.2 keV transition. All lines, except the 710 and 1180 keV photopeaks, can be seen in the spectrum coincident with the K 183 conversion line. No more conversion electron-gamma coincidence spectra were measured because of the small intensity of the conversion lines of the higher energy gamma rays. A series of gamma-gamma coincidence spectra were recorded, gating on the 710, 790, 1180, 1270 and even the 2000 keV photopeaks. The coincidence relationship of the 710 and 1180 and of the 790 and 1270 keV lines is shown in fig. 7.

No coincidences were recorded between the high energy lines and the 2000 keV line. No reliable coincidence results could be obtained with the 1550 keV gamma, because of its low intensity.

4.3. LEVEL SCHEME

This can be given for the most intensive transitions on the basis of the previous measurements. It is shown in fig. 8.

The two levels at 80 and 262 keV are also found in the Ho-decay. They are interpreted as rotational states, in agreement with their E2 character, which is evidenced by the L/(M+N) ratio of the 80 keV and the K/L-ratio of the 182 keV line. Assignments are accordingly (0, 0+), (0, 2+) and (0, 4+). A suggestion for spin and parity of the ground state of ^{166}Tm can be made from Nilsson's calculations of single particle levels in deformed nuclei, according to which the 69th proton should populate a state $\frac{1}{2}+$ or $\frac{7}{2}-$. The $\frac{1}{2}+$ assignment is in accordance with the ground state spin $\frac{1}{2}$ of ^{169}Tm. Comparing ^{166}Tm with ^{163}Dy, which nucleus also has 97 neutrons, one expects the neutron to be in a $\frac{5}{2}$ state. The coupling of the two unpaired nucleons in ^{166}Tm should result in a spin 2 or 3 and negative parity. The

strong capture branche to the 80 keV level and the very small intensity of the component to the 262 keV level favour the assignment 2−.

The two levels at 870 and 970 keV in ^{166}Er can be interpreted as a vibrational level with the first member of a rotational band on top of it. A calculation of the intensity ratio of the electron capture components to these levels gives equal intensities if the quantum numbers are (2, 2+) and

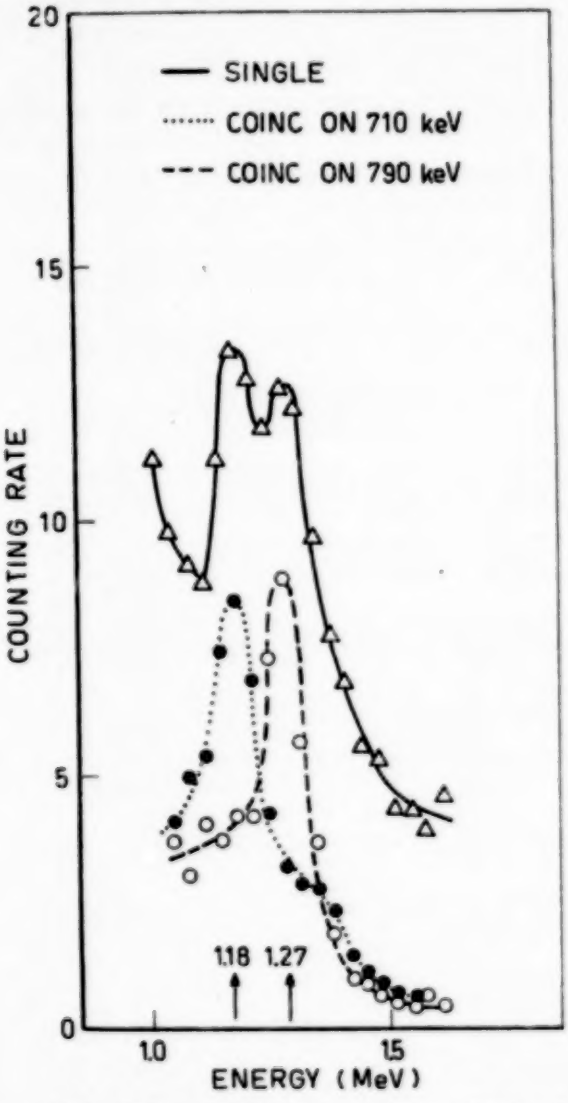

Fig. 7. $\gamma-\gamma$ coincidences of the 710 and 790 keV transitions with the 1.18 and 1.27 MeV lines in ^{166}Tm.

(2, 3+) for these states. This is in good agreement with the experimental values. A similar calculation with a 3− initial state for ^{166}Tm gives a ratio of about 5, so here we have a second argument for a 2− assignment of the ground state of ^{166}Tm. The energy difference between the ground states of ^{166}Tm and ^{166}Er was roughly estimated at 2600±200 keV, supposing the β^+-branches to go to the 870 and 80 keV states. This supposition is reasonable on the basis

of the energy difference between these states. Also, if the β^+-branches would feed higher energy states, there should be more intensive β^+-components to the lower states, since the β^+ to capture ratio increases strongly with decay energy.

Log *ft* values calculated for the electron capture branches on the basis of this total decay energy are given in table 7.

All values, except those of the components to the 2150 and 2260 keV states

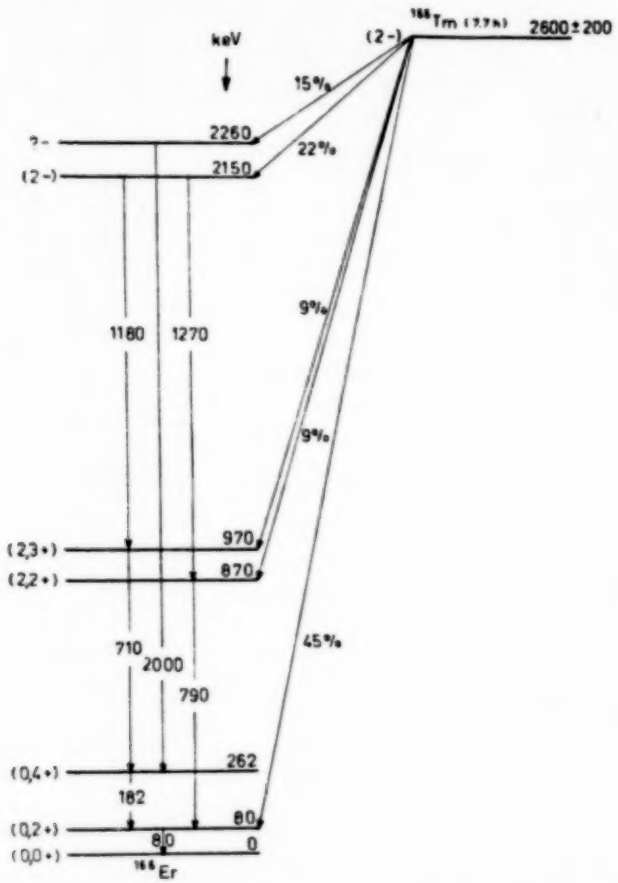

Fig. 8. Decay scheme of ^{166}Tm(7.7h).

TABLE 7.

Electron capture branches in the decay of ^{166}Tm

Transition energy (keV)	Intensity (%)	log *ft*	Classification
370	15	5.5	allowed
450	22	5.3	allowed
1630	9	6.9	first forbidden
1730	9	6.9	first forbidden
2520	45	6.6	first forbidden

indicate first forbidden transitions. The exceptions must be regarded as allowed transitions; therefore, the levels fed by these components should have negative parity.

The branching ratio of the 1180 and 1270 keV transitions from the 2150 keV level to the members of a rotational band agrees very well with the theoretical value 1, supposing a spin value 2 for the 2150 keV state. A spin value 3— does not fulfil this conditions.

The absence of transitions between the 970 and 80 keV levels and between the 870 keV level and the ground state reveals an inconsistency. The energy of these transitions would be about the same and the total intensity should be sufficiently large to be observed in the gamma spectrum.

Very little can be said about the weak transitions, because no coincidence measurements could be carried out here. The too large half width of the 1550 keV line suggests that this line consists of two components. The position of the 460 keV gamma-ray could not be ascertained.

5. Discussion of the Nuclear Levels in ^{166}Er

A discussion of the nuclear level spectrum of ^{166}Er can be given on the basis of the measurements described in this article and the results of the investigations of the 27h decay of ^{166}Ho. All results are summarized in fig. 9.

A rotational band on the ground state with quantum numbers (0, 0+), (0, 2+), (0, 4+), (0, 6+) and (0, 8+) is found very explicitly in the decay of ^{166}Ho*(> 30y). The levels in the ^{166}Tm decay at 870 and 970 keV with quantum numbers (2, 2+) and (2, 3+) can very well be interpreted as a rotational band on a vibrational level. A second vibrational level (0, 0+) is probably present at 1458 keV in the 27h decay. No rotational structure is found on this level, the 0-ground state spin of ^{166}Ho probably excludes population of rotational states built on this level.

All the states mentioned above can be described in terms of the collective motion associated with a quadrupole deformation of the nuclear shape.

The level at 940 keV in the > 30y Ho* decay has been assigned a spin and parity 5—, the level at 1760 keV spin and parity 6—. These levels cannot be interpreted in terms of collective motions of rather simple structure. The much too large K conversion coefficients of the 700 and 817 keV transitions seem to indicate that these transitions are accompanied by rather large changes in the deformation of the nucleus. The gamma transition may then be hindered, while the conversion transition probabilities will be unaffected. It is not clear yet if these levels can best be interpreted as particle excitations or as collective excitations of a more complex structure. The other levels could not be investigated so well, due to the small intensities of the corresponding transitions.

In conclusion it can be said that the level structure of ^{166}Er shows very distinctly the properties of the spectrum of a strongly deformed nucleus and

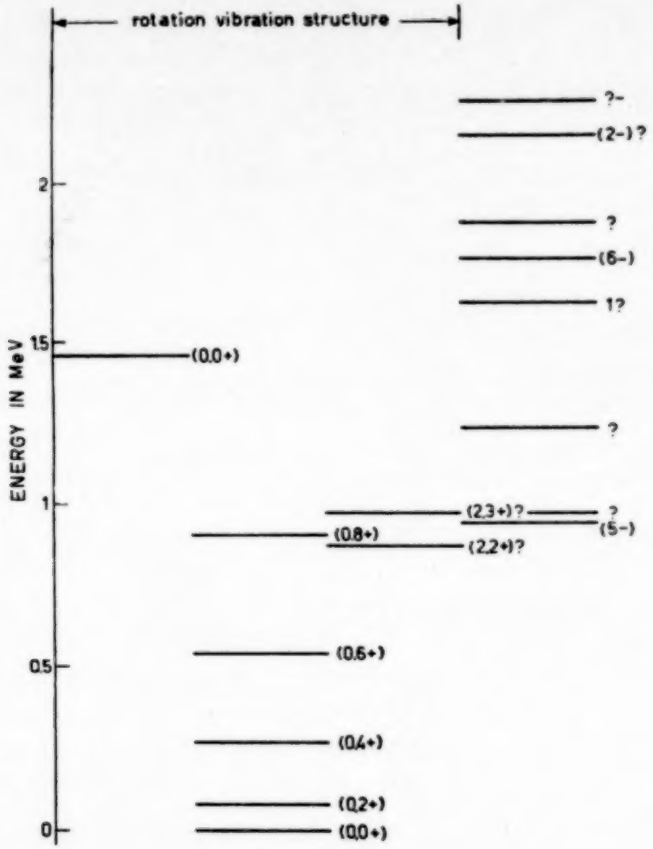

Fig. 9. Level scheme of ^{166}Er, from the decays of ^{166}Ho (27h), ^{166}Ho* (> 30y) and ^{166}Tm (7.7h).

provides therefore a good test for calculations in the strong coupling region of the Bohr-Mottelson model.

The authors wish to thank Professor H. Brinkman for providing them with excellent facilities for performing these experiments. Sincere thanks are also due to the personnel of the Amsterdam cyclotron for their unrelenting effort in making all the irradiations of the Ho and Er-targets. Thanks are further due to Mr. K. G. Dik and Mr. H. Beekhuis for their able assistance during the measurements and to Mr. A. J. Wagner, Mr. E. Houtman and Mr. W. G. Mook for making the ion exchange column separations.

References

1) J. M. Hollander, I. Pearlman and G. T. Seaborg, Revs. Mod. Phys. **25** (1953) 469
2) A. W. Sunyar, Phys. Rev. **93** (1954) 1345
3) R. L. Graham, J. L. Wolfson and M. A. Clark, Phys. Rev. **98** (1955) 1173A

4) J. S. Fraser and J. C. D. Milton, Phys. Rev. **98** (1955) 1173A
5) J. M. Cork, M. K. Brice, R. G. Helmer and R. M. Woods, Phys. Rev. **110** (1958) 526
6) F. D. S. Butement, Proc. Phys. Soc. A **65** (1952) 254
7) J. C. D. Milton, J. S. Fraser and G. M. Milton, Phys. Rev. **98** (1955) 1173A
8) J. C. D. Milton, J. S. Fraser and G. M. Milton, private communication
9) M. A. Grace, R. T. Taylor and P. B. Trecay, Phil. Mag. **3** (1958) 90
10) G. Wilkinson and H. G. Hicks, Phys. Rev. **75** (1949) 1370
11) W. E. Nervik and G. T. Seaborg, Phys. Rev. **97** (1955) 1092
12) G. M. Gorodinskii, A. N. Murin, V. N. Pokrovskii, B. K. Preobrazhenskii and N. E. Titov, Doklady **2** (1957) 39
13) J. W. Mihelich, B. Harmatz and T. H. Handley, Phys. Rev. **108** (1957) 989
14) A. Bohr and B. Mottelson, Mat. Fys. Medd. Dan. Vid. Selsk. **27**, No. 16 (1953)
15) M. E. Rose, Internal conversion coefficients (Amsterdam, 1958)
16) H. Postma *et al.*, to be published
17) E. L. Church and J. Wesener, Phys. Rev. **104** (1956) 1382
18) S. G. Nilsson and J. O. Rasmussen, Nuclear Physics **5** (1958) 617
19) S. G. Nilsson, Mat. Fys. Medd. Dan. Vid. Selsk. **29**, No. 16 (1955)

2.C *Nuclear Physics* **12** (1959) 552—562; © *North-Holland Publishing Co., Amsterdam*
Not to be reproduced by photoprint or microfilm without written permission from the publisher

THE DETERMINATION OF NEUTRON RESONANCE PARAMETERS OF TUNGSTEN BY THE TRANSMISSION METHOD

F. W. K. FIRK and M. C. MOXON

Atomic Energy Research Establishment, Harwell, Didcot, Berks.

Received 4 May 1959

Abstract: The neutron transmission of tungsten from 25 to 200 eV has been measured with a resolution of 0.01 μsec · m^{-1} using the Harwell 15 MeV linear accelerator and time-of-flight spectrometer. "Area" and, in some cases, "shape" analyses of the data were made to determine values of the peak total cross sections σ_0 and the total widths Γ of twelve resonances. Assuming a constant radiation width of approximately 0.07 eV the following values were obtained for the spins J of resonances formed in the compound nucleus W^{183}+n: $J = 1$ for the 27.17 and 46.08 eV resonances and $J = 0$ for the 47.74, 100.8, 144 and 174 eV resonances. Estimates of the neutron strength functions for the two spin states 0 and 1 are given. Resonances observed at 100.8, 101.5, 103.7, 154.5, 155.2, 156.7 and 192 eV have not been resolved previously.

1. Introduction

Although neutron resonances in tungsten have been studied by many workers [1,2,3]) there has been no satisfactory agreement on the values of the spins for resonances at 46.08, 47.74 and 100.8 eV. Extensive measurements of the neutron transmission, scattering yield and capture γ-ray yield from tungsten have been made by the Harwell 15 MeV linear accelerator group. This paper reports the transmission measurements.

In favourable conditions, the spin J can be determined from the transmission data assuming a constant value for the radiation width. The conditions required follow immediately from the expression

$$\frac{2J+1}{2(2I+1)} = \frac{\sigma_0 \Gamma}{4\pi\lambda\!\!\!^{-}_{\mathrm{R}}{}^2 \Gamma_{\mathrm{n}}} = \frac{\sigma_0}{4\pi\lambda\!\!\!^{-}_{\mathrm{R}}{}^2}\left(1+\frac{\Gamma_\gamma}{\Gamma_{\mathrm{n}}}\right) \qquad (1)$$

where I is the spin of the target nucleus in the ground state, Γ_{n} the neutron width, Γ_γ the radiation width, $2\pi\lambda\!\!\!^{-}_{\mathrm{R}}$ the de Broglie wavelength, in the centre-of-mass system, of the incident neutron of energy E_{R} and $J = I \pm \frac{1}{2}$. Eq. (1) has been used widely to determine values of J for resonances in the energy region above 1 keV. In this region $\Gamma_{\mathrm{n}} \gg \Gamma_\gamma$ so that an accurate determination of σ_0 is sufficient to determine J [4]). For an energy below 1 keV the method may still be used if Γ_γ is known with reasonable accuracy, for then, provided $\Gamma_{\mathrm{n}} \approx \Gamma_\gamma$, we can determine J from values of σ_0 and $\Gamma (= \Gamma_{\mathrm{n}} + \Gamma_\gamma)$ obtained from transmission measurements [2,5]). The method is particularly useful if

$I = \frac{1}{2}$, since this case gives the largest difference for the two possible values of J.

The transmission data are used to determine the radiation widths Γ_γ for the resonances at 40.60 and 66.70 eV, since $\Gamma_n \ll \Gamma_\gamma$, so that $\Gamma \approx \Gamma_\gamma$. This value of Γ_γ is then assumed to be constant throughout the rest of the analysis. A more accurate measurement of $\langle \Gamma_\gamma \rangle$ for resonances in $W^{183}+n$ is given by Waters *et al.* in the following paper [17]) and may be used in eq. (1) if such accuracy is required.

2. Experimental Procedure

Transmission measurements were made using the Harwell 15 MeV linear accelerator and time-of-flight spectrometer. This machine produces a pulse of moderated photo-neutrons of duration 0.25 μsec at a repetition rate of 400 p.p.s. Using timing channels of 0.2 μsec duration and a flight path of 32 m a nominal resolution of 0.01 μsec $\cdot$ m^{-1} is obtained [6]). Details of the detector (B^{10}—NaI) and measurements of the machine dependent background have been given previously [4]).

3. Methods of Analysis

Typical experimental transmission curves for natural tungsten are shown in figs. 1 and 2. The "measured" total cross section from 44—49 eV is shown in fig. 3a and from 50 to 200 eV in fig. 4.

3.1. THE STANDARD AREA METHOD

The standard method of thick (area $\propto \sqrt{\sigma_0 \Gamma^2}$) and thin (area $\propto \sigma_0 \Gamma$) sample area analysis [7]) is used to determine values of σ_0 and Γ for resonances from 27 to 200 eV. Corrections for the effect of Doppler broadening and finite sample thickness are made using curves due to Hughes [8]).

Even with good resolution the area method of analysis is not, by itself, a reliable technique for determining accurate values of σ_0 and Γ for the two resonances at 46.08 and 47.74 eV. This is due to the fact that for thick samples ($n\sigma_0 > 10$ where n is the number of W^{183} nuclei $\cdot$ cm^{-2}) the resonances overlap to such an extent that the measurement of the two areas is not possible (see fig. 1).

3.2. ANOTHER AREA METHOD

Another area technique is used to provide, in effect, a true thin sample measurement for the 46.08 and 47.74 eV resonances [9]). The cross section curve in fig. 3b is composed of the data from samples of different thicknesses: each thickness is used in the range where it has least error i.e. the thinnest sample around the peak and the thickest sample on the wings. The area A

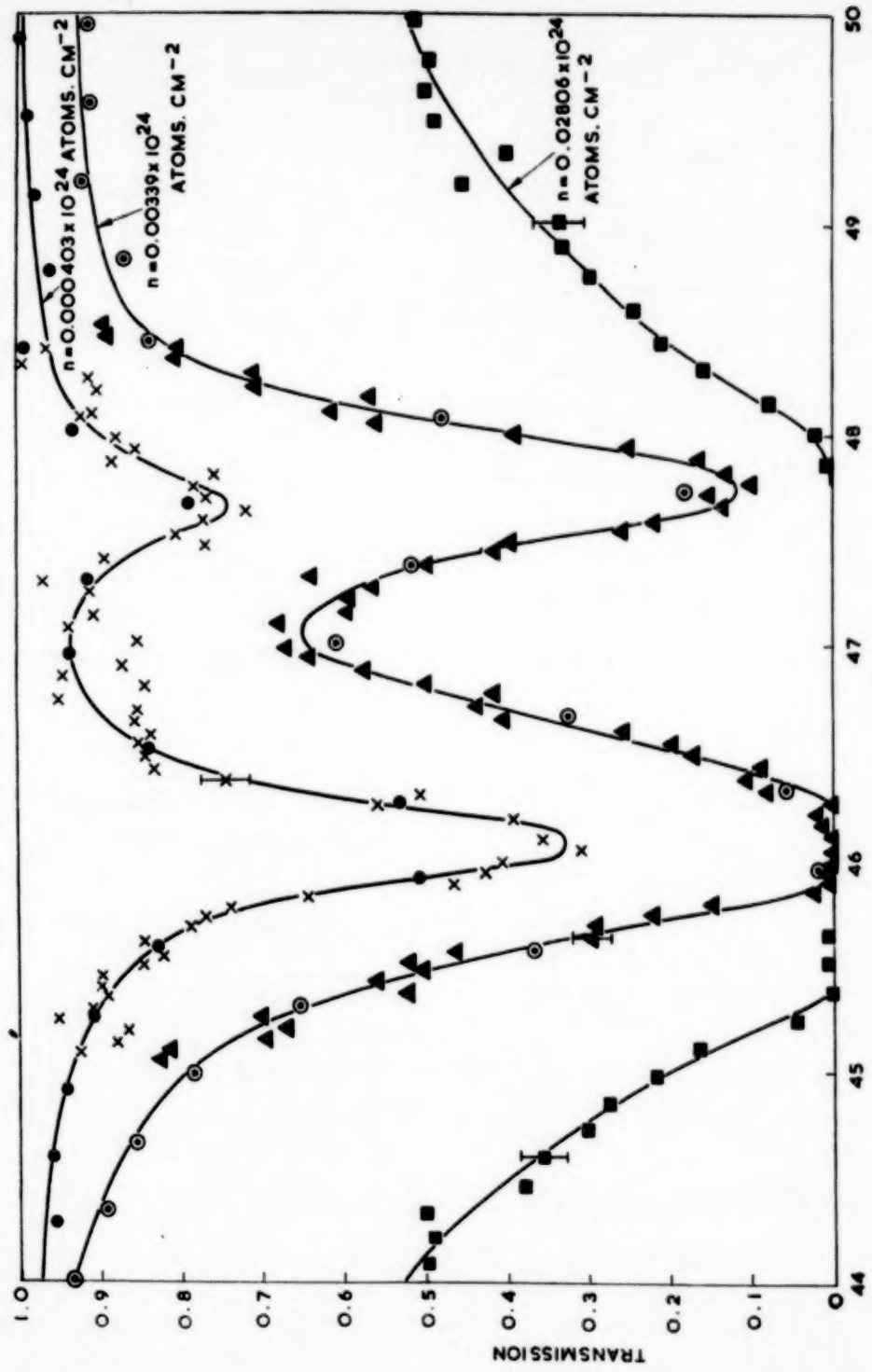

Fig. 1. The transmission of natural tungsten from 44 to 50 eV.

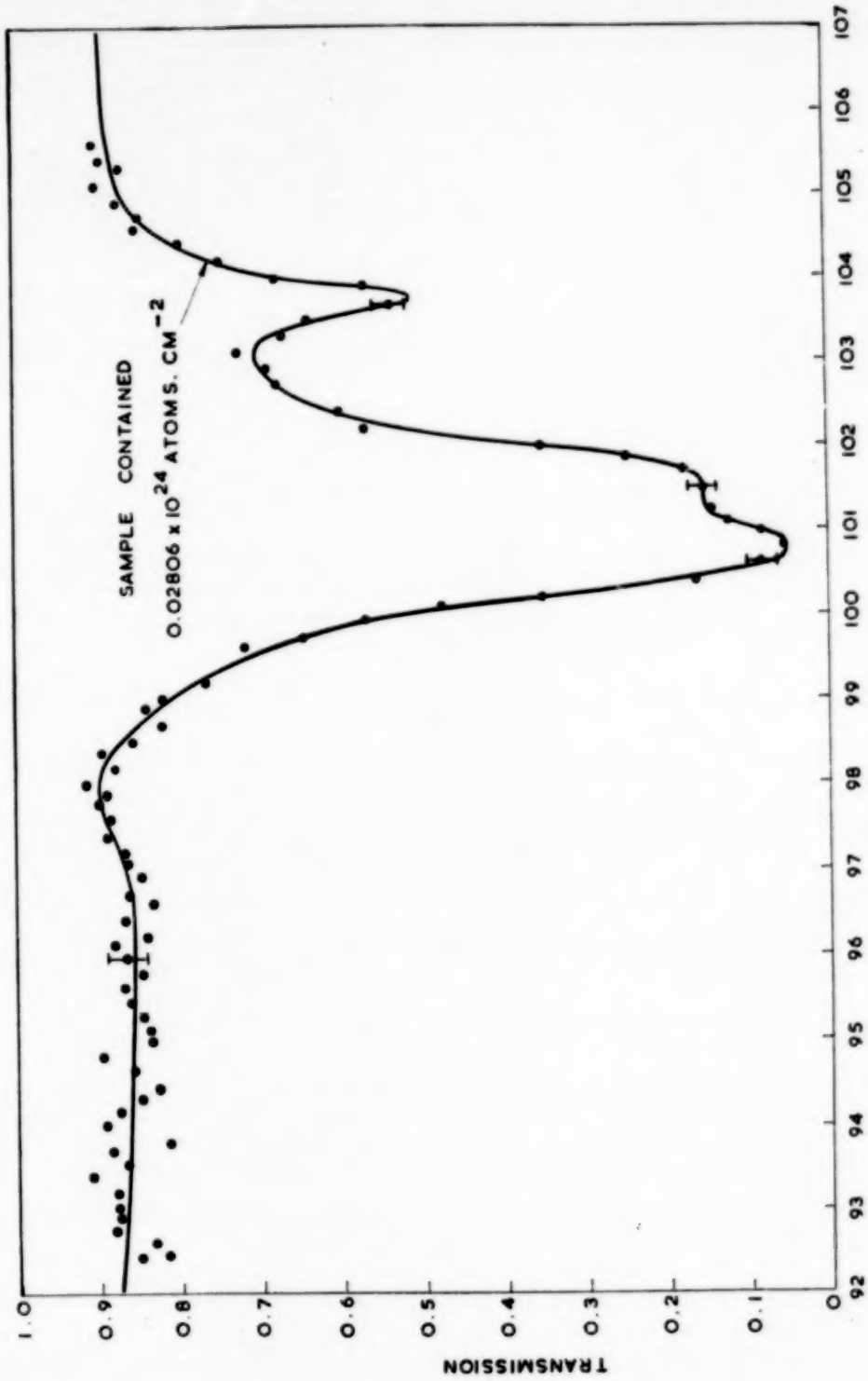

Fig. 2. The transmission of natural tungsten from 92 to 107 eV.

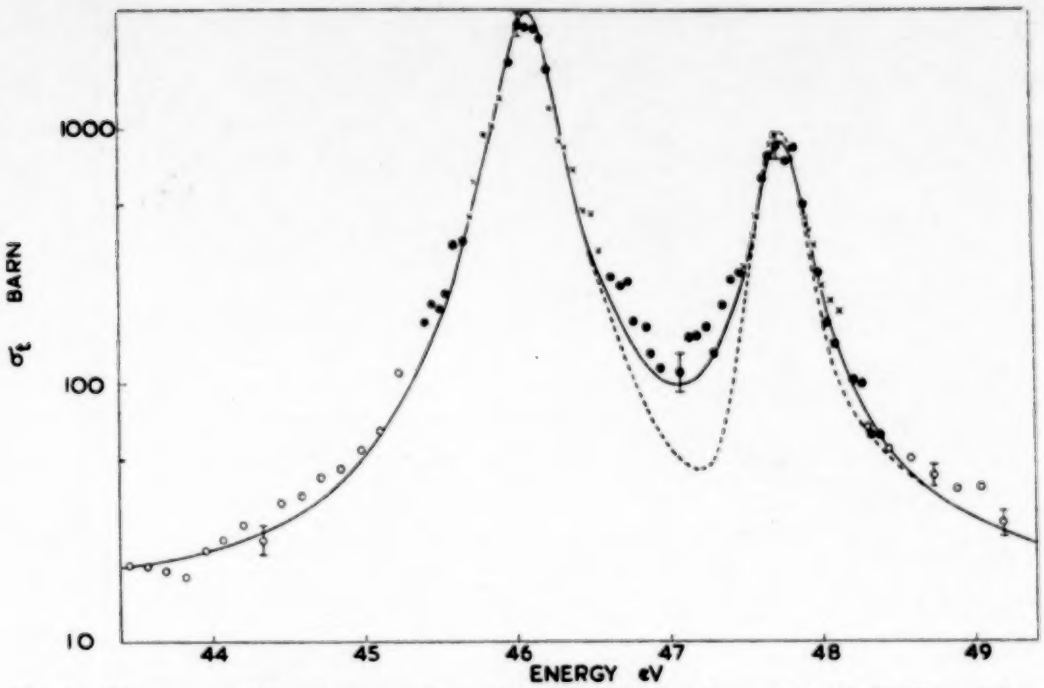

Fig. 3a. The measured total cross section of natural tungsten from 44 to 49 eV. The solid curve is the sum of two Doppler broadened Breit-Wigner expressions using the prarameters given in table 2 (opposite spins). The broken curve is a two-level theoretical fit using the parameters given in table 1 (same spins).

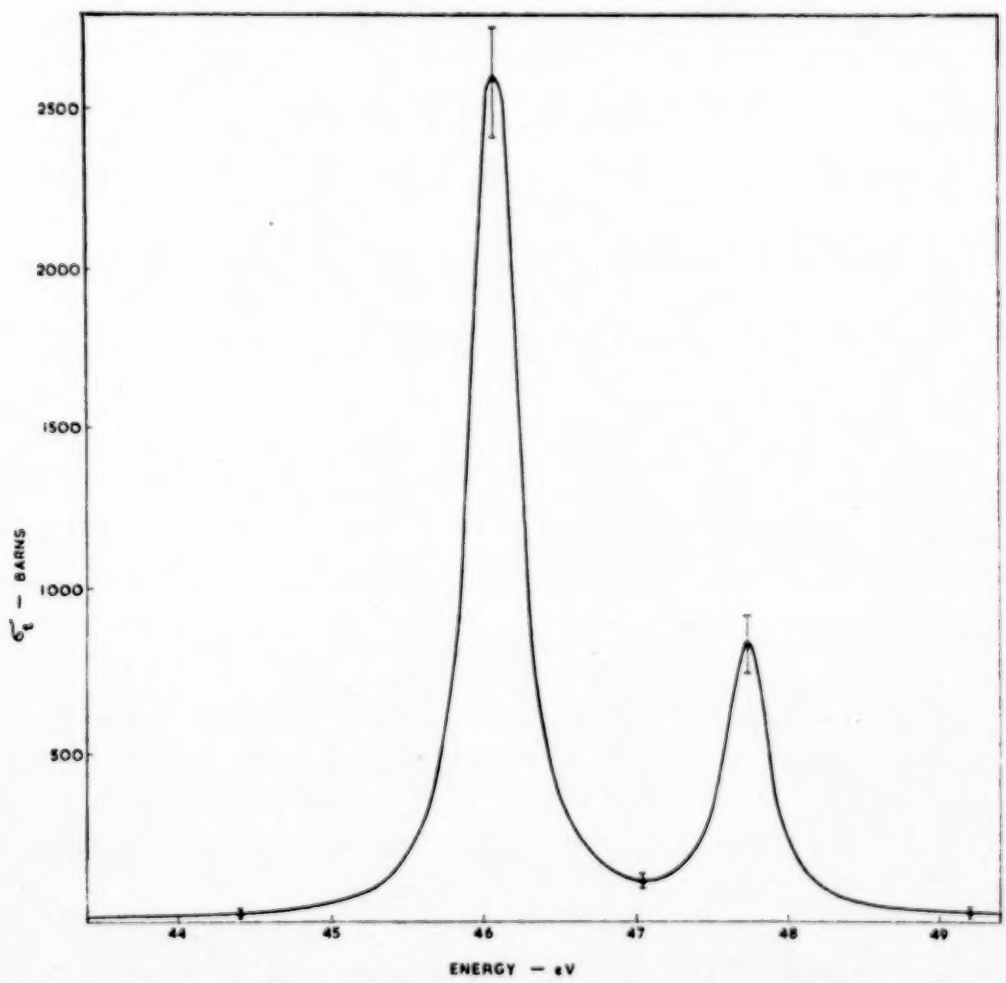

Fig. 3b. The measured total cross section of natural tungsten from 44 to 49 eV used to determine $\sigma_0\Gamma$: this is an effective thin sample measurement.

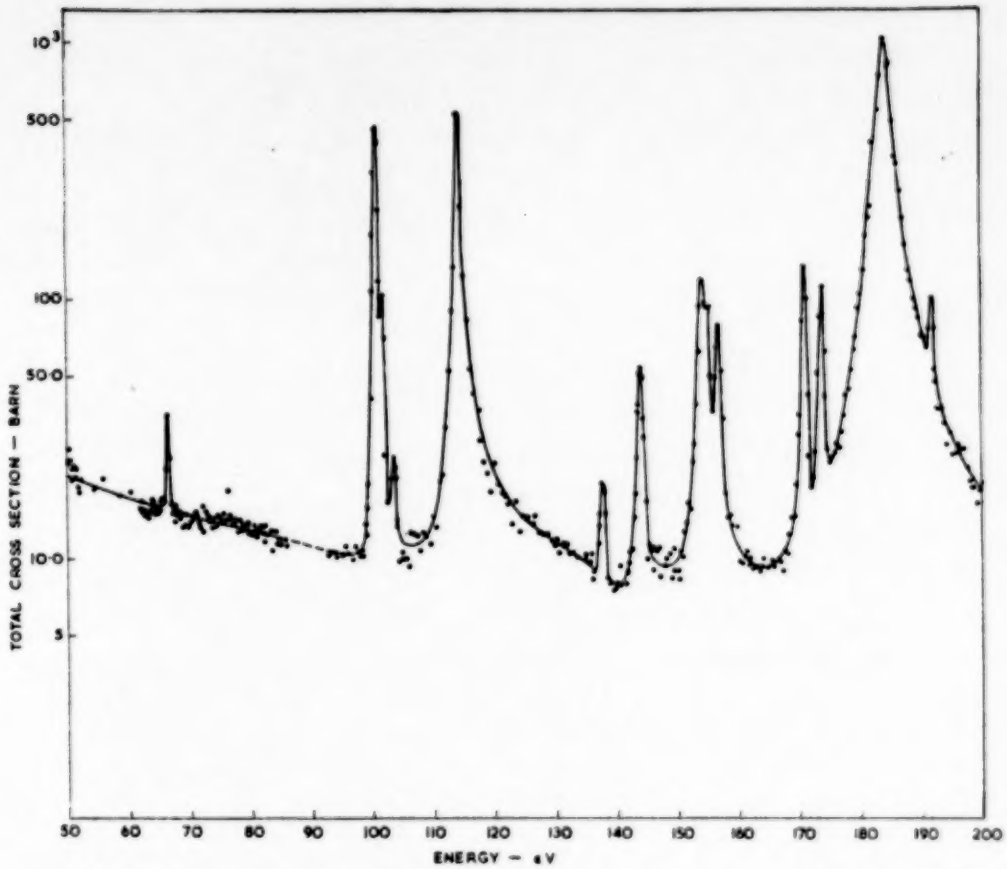

Fig. 4. The measured total cross section of natural tungsten from 50 to 200 eV.

under the cross section curve is then given by

$$A = \int_{-\infty}^{\infty} \sigma_{\text{obs}} \mathrm{d}E = \tfrac{1}{2}\pi\sigma_0\Gamma. \qquad (2)$$

This assumes perfect resolution (see sec. 3.4). The value of $\sigma_0\Gamma$ obtained from eq. (2) is then used in conjunction with the area data from the transmission curves.

3.3. THE MINIMUM TRANSMISSION METHOD

The "minimum transmission" method of Lynn and Rae [10]) is used to give $\sigma_0 = f(\Gamma)$ for each of the resonances being analysed: these measurements are also used with the (σ_0, Γ) curves obtained from the area data. This method assumes that the shape of the resolution function can be approximated by a Gaussian curve of full width R at $1/\sqrt{e}$ of the maximum: this is found to be a valid assumption in the present measurements with $R = 0.3$ μsec.

3.4. SHAPE ANALYSIS OF CROSS SECTION

A second set of parameters for the 46.08 and 47.74 eV resonances is obtained from the experimental data by a shape analysis of the cross section in the region 43—50 eV. The width of the resolution function at 47 eV is 0.07 eV. This has only a small and calculable effect on the observed widths

($\approx 2\,\%$) and peak cross sections. A direct measurement from the cross section curve thus gives values of Γ_Δ and σ_Δ, the Doppler broadened width and peak cross section respectively. Using curves of Γ/Γ_Δ and σ_0/σ_Δ versus Δ/Γ_Δ given by Melkonian [11]) the true parameters σ_0 and Γ are determined (here, $\Delta = 0.316\sqrt{(E_R/183)}$eV).

Since the thick sample area method is not applicable to these two resonances, values of $\sigma_0\Gamma^2$ are obtained from the cross section σ_W on the wings of the resonances. We have

$$\sigma_W = \frac{\sigma_0\Gamma^2}{4(E-E_R)^2} \pm \frac{ka\sigma_0\Gamma}{E-E_R} + \bar{\sigma}_{pot}. \tag{3}$$

In eq. (3) $\sigma_0\Gamma$ is known from the thin sample area analysis and the shape analysis; $\bar{\sigma}_{pot}$ is the "effective" potential scattering and is calculated from the parameters of distant levels plus the true potential scattering cross section.

The parameters for the 46.08 and 47.74 eV resonances given in table 2 are used to compute

$$\sigma_t = \sigma_0\psi(\beta x) + \frac{2ka\sigma_0 x}{1+x^2} + \bar{\sigma}_{pot}, \tag{4}$$

where $\psi(\beta x)$ is the well-known Doppler broadening correction to the resonance term [7]), k is the neutron wave number, a is the potential scattering length and $x = 2(E-E_R)/\Gamma$. The effect of Doppler broadening on the interference term is negligible [12]). Contributions to the cross section from resonances at 18.8, 27.17 and 40.60 eV are calculated from their measured parameters (the effect of resonances above 50 eV is negligible). When added to the potential scattering cross section the above contributions give a value of $\bar{\sigma}_{pot} = 15$b at 43.4 eV and 13.5b at 49.4 eV.

The theoretical fit is shown by the solid curve in fig. 3a.

The broken curve in fig. 3a is obtained using the following two-level expression which includes resonance-resonance interference [13]). If $|E_1-E_2| > \Gamma$ we have

$$\begin{aligned}\sigma_t = {} & \sigma_{01}\psi(\beta_1 x_1) + \sigma_{02}\psi(\beta_2 x_2) + \frac{2k_1a_1\sigma_{01}x_1}{1+x_1^2} + \frac{2k_2a_2\sigma_{02}x_2}{1+x_2^2} \\ & + \frac{k_1k_2\sigma_{01}\sigma_{02}(1+x_1x_2)}{2\pi g(1+x_1^2)(1+x_2^2)} + \bar{\sigma}_{pot},\end{aligned} \tag{5}$$

where 1 and 2 refer to the 46.08 and 47.74 eV resonances respectively and $g = (2J+1)/2(2I+1) = \frac{3}{4}$. The parameters used to compute eq. (5) are given in table 1. The effect of Doppler broadening on the interference minimum is calculated to be 6b. The value of $\sigma_{02}\Gamma_2$ used for the 47.74 eV resonance in eq. (5) is the same as that used in the single-level calculation for the $J = 0$ case.

TABLE 1

Resonance parameters for the 46.08 and 47.74 eV resonances assuming the same spins

E_R (eV)	σ_{0R} (b)	Γ_R (eV)	J	$\bar{\sigma}_{pot}$ (b)
46.08	29 500	0.20	1	15 at 43.4 eV
47.74	15 000	0.11	1	13.5 at 49.4 eV

It is clear from fig. 3a that the better fit is given by the solid curve, corresponding to opposite spins. The assignment of $J = 1$ to the 46.08 eV resonance is unambiguous (see table 2 and also Waters *et al.* [17])) so that the assignment $J = 0$ to the 47.74 eV resonance is no longer dependent upon any assumptions about the value of the radiation width.

The final parameters of 12 resonances obtained from area analyses, minimum transmissions and shape analyses are listed in table 2. The experimental areas include wing corrections (functions of the final parameters) but do not include corrections for Doppler broadening or finite sample thickness. The preferred values of the spins J for resonances in W^{183}+n are given in heavy type. The spin assignments of the resonances at 40.60 and 66.70 eV are those given by Bird [14]) from measurements of the γ-ray spectra of the resonances. There is also agreement between the present assignments and those given by Bird for the resonances at 27.17, 46.08 and 100.8 eV.

Resonances observed at 100.8, 101.5, 103.7, 154.5, 155.2, 156.7, 171, 174 and 192 eV have not been resolved previously in natural tungsten, although the two at 171 and 174 eV have been reported by the Brookhaven fast chopper group using separated isotopes [15]). It is interesting to note that the two resonances at 154.5 and 156.7 eV were not resolved by the Brookhaven group which suggests that they both belong to the same target isotope, W^{183}. An estimate of the radiation width (approximately equal to the total width) of the resonance at 101.5 eV obtained from an area and minimum transmission measurement indicates that it is also formed from W^{183}.

From the parameters of the resonances in W^{183}+n listed in table 2 we obtain the following estimates of the neutron strength functions for the two spin states:

$$\frac{\langle \Gamma_n^0 \rangle_{J=1}}{D_{J=1}} = (2.8 \pm 1.5) \times 10^{-4} \quad \text{and} \quad \frac{\langle \Gamma_n^0 \rangle_{J=0}}{D_{J=0}} = (3.0 \pm 1.9) \times 10^{-4}$$

where the large errors are due to the small number of levels investigated; $D_{J=1}(= 18$ eV) is the average level spacing for spin 1 resonances and $D_{J=0}(= 46$ eV) is the average level spacing for spin 0 resonances in the energy region covered by these measurements, $\langle \Gamma_n^0 \rangle_J$ is the average reduced

TABLE 2

Neutron resonance parameteters of tungsten from 27 to 200 eV

Resonance Energy (eV)	Target Isotope	Sample Thickness (atoms × cm^{-2} × 10^{24})	Experimental Area (eV)	σ_0 (b)	Γ (eV)
27.17 ± 0.05	183	0.001 337 0.001 337 0.000 243 0.000 058	1.29 ± 0.05 1.30 ± 0.03 0.560 ± 0.073 0.223 ± 0.021	22 000 ± 2200	0.124 ± 0.025
40.60 ± 0.06	183	0.004 01 0.000 485	0.331 ± 0.016 0.074 ± 0.022	1 100 ± 400	0.07 ± 0.03
46.08	183	0.000 243 0.000 0577	1.01 ± 0.05 0.44 ± 0.02	29 500 ± 3000	0.204 ± 0.022
47.74	183	0.000 485 0.000 0577	0.66 ± 0.06 0.10 ± 0.02	9 000 ± 1200	0.184 ± 0.03
66.70	183	0.004 01	0.25 ± 0.02	560 ± 120	0.08 ± 0.02
100.8	183	0.000 243	0.509 ± 0.031	6 200 ± 1800	0.27 ± 0.07
114	182	0.007 27 0.000 867 0.000 106	6.33 ± 0.22 2.30 ± 0.20 0.83 ± 0.08	19 500 ± 4000	0.31 ± 0.03
137.7	183	0.004 01	0.258 ± 0.042	650 ± 200	0.075 ± 0.020
144	183	0.004 01 0.003 97 0.001 34	1.131 ± 0.030 1.06 ± 0.08 0.61 ± 0.06	2 300 ± 850	0.18 ± 0.06
171	186	0.008 05 0.002 68	1.25 ± 0.07 0.81 ± 0.04	4 500 ± 1200	0.08 ± 0.02
174	183	0.004 01 0.001 33	1.41 ± 0.11 0.73 ± 0.06	2 100 ± 200	0.24 ± 0.02
185	184	0.002 98 0.000 498 0.000 121	12.7 ± 1.0 5.14 ± 0.17 2.03 ± 0.2	13 400 ± 2000	1.09 ± 0.15

Spin J	Γ_n (eV)	Γ_γ (eV)	Methods of analysis	General Remarks
0 1	0.126±0.027 0.039±0.004	— 0.085±0.025	Area+min. trans.	
0 1	0.005±0.002 0.002±0.001	0.065±0.031 0.068±0.031	Area+min. trans.	Spin 1 assignment due to Bird [14]).
0 1	0.36 ±0.02 0.148±0.007	— 0.056±0.025	Area+shape analysis	These parameters are the "best" values obtained from area and shape analyses.
0 1	0.100±0.007 0.030±0.002	0.084±0.032 0.154±0.031	Area+shape analysis	As for the 46.08 eV resonance. The spin 0 assignment is determined from the curve fitting.
0 1	0.005±0.003 0.002±0.001	0.075±0.021 0.078±0.021	Area+min. trans.	Spin 1 assignment due to Bird [14]).
0 1	0.25 ±0.10 0.09 ±0.04	0.02 ±0.13 0.20 ±0.08	Area+min. trans.	The ambiguity in spin assignment is reduced in following paper of Waters *et al.* [17]).
$\frac{1}{2}$	0.26 ±0.06	0.05 ±0.04	Area	
0 1	0.010±0.004 0.003±0.002	0.065±0.021 0.072±0.020	Area+min. trans.	Assumed to be spin 1 for the strength function calculation.
0 1	0.09 ±0.04 0.03 ±0.02	0.09 ±0.07 0.15 ±0.06	Area+min. trans.	Slight evidence in favour of the spin 0 assignment.
$\frac{1}{2}$	0.024±0.010	0.056±0.022	Area+min. trans.	
0 1	0.13 ±0.02 0.04 ±0.01	0.11 ±0.03 0.20 ±0.02	Area+min. trans.	
$\frac{1}{2}$	1.04 ±0.21	0.05 ±0.25	Area	

neutron width for resonances of spin J. We have used the assignment $J = 1$ for the 7.6 eV resonance given by Waters *et al.* [17]) and Fox *et al.* [3]).

There appears to be no significant difference for the two values of the strength functions which is in agreement with the evidence from strength function measurements on isotopes in the region of mass number 233 to 238. In this region the strength function is only slowly varying [16]) although the spins of the target nuclei differ considerably (e.g. $I = \frac{7}{2}$ for U^{235} and $I = 0$ for U^{238}). The errors on the above two values of the strength functions are large and clearly show the need for more work on this subject if possible small differences are to be observed.

The results obtained in this paper for resonances up to 100.8 eV are combined with neutron scattering and capture γ-ray yields in the following paper of Waters *et al.* where the combined data are discussed.

The authors wish to thank Drs. E. Melkonian and R. B. Schwartz for many helpful discussions concerning the analysis of the data. They are also grateful to the other members of the linear accelerator group for their interest in the tungsten programme and for their efficient operation of the machine.

References

1) F. B. Simpson and R. G. Fluharty, Bull. A.P.S. **3** (1958) 176
2) R. E. Chrien and R. L. Zimmerman, Bull. A.P.S. **3** (1958) 19
3) J. D. Fox, R. L. Zimmerman, D. J. Hughes, H. Palevsky, M. K. Brussel and R. E. Chrien, Phys. Rev. **110** (1958) 1472 (L)
4) J. E. Lynn, F. W. K. Firk and M. C. Moxon, Nuclear Physics **5** (1958) 603
5) J. R. Bird, M. C. Moxon and F. W. K. Firk, Bull. A.P.S. **4** (1959) 34
6) F. W. K. Firk, G. W. Reid and J. F. Gallagher, Nuclear Instruments **3** (1958) 309
7) E. Melkonian, W. W. Havens Jr. and L. J. Rainwater, Phys. Rev. **92** (1953) 702
8) D. J. Hughes, Journal of Nuclear En. **1** (1955) 237
9) E. Melkonian, private communication
10) J. E. Lynn and E. R. Rae, Journal of Nuclear En. **4** (1957) 418
11) E. Melkonian, Geneva Conference **4** (1955)
12) J. E. Lynn, private communication
13) H. Bethe, Revs. Mod. Phys. **9** (1937) 115
14) J. R. Bird, Geneva Conference A/Conf. 15/P/35(1958) (to be published)
15) D. J. Hughes and R. B. Schwartz, BNL-325, 2nd ed. (1958)
16) D. J. Hughes, R. L. Zimmerman and R. E. Chrien, Phys. Rev. Letters **1** (1958) 416
17) J. R. Waters, J. E. Evans, B. B. Kinsey and G. H. Williams, Nuclear Physics **12** (1959) 563

2.C *Nuclear Physics* **12** (1959) 563—578; © *North-Holland Publishing Co., Amsterdam*
Not to be reproduced by photoprint or microfilm without written permission from the publisher

SPINS AND RADIATION WIDTHS OF THE LOW ENERGY NEUTRON RESONANCES IN TUNGSTEN

J. R. WATERS, J. E. EVANS, B. B. KINSEY † and G. H. WILLIAMS
Atomic Energy Research Establishment, Harwell, Didcot, Berks.

Received 4 May 1959

Abstract: Measurements have been made of the parameters of nine low energy neutron resonances in tungsten. The results from neutron transmission, elastic scattering and capture γ-ray experiments were combined to obtain accurate values for the neutron and radiation widths, and, for W^{183}, of the spins of the excited levels. For W^{183} the resonances at 7.62, 27.1, 46.1, 47.7 and 100.8 eV were found to have spin 1, 1, 1, 0 and 0, respectively. The average value for the radiation widths for the levels with spin 0 and spin 1 were the same within the experimental error. For the three tungsten isotopes 182, 183 and 186 the average radiation widths were 50 ± 4 meV, 73 ± 4 meV and 45 ± 6 meV respectively. These values do not agree with the observation that the average radiation widths are roughly proportional to the fourth power of the binding energy.

1. Introduction

The low energy cross-section for heavy elements exhibits a series of resonances whose shape (in the absence of fission) is described by the Breit-Wigner single level formula [1]). The parameters which describe the shape of a resonance are the resonance energy E_R, the spin J, and the partial widths Γ_n (the neutron width) and Γ_γ (the γ-ray width). From neutron transmission experiments it is possible to determine E_R, Γ and $g\Gamma_n$ and, in favourable circumstances, J, Γ_n and Γ_γ. With measurements of neutron elastic scattering and the yield of capture γ-rays it is possible to derive other combinations of these parameters [2]). On being combined with the results of a transmission experiment, the parameters are overdetermined, so that the experimental uncertainties can be reduced. Silver [2]) and tantalum [3]) have been studied by this method. Results are given here for a similar investigation of the low energy resonances in tungsten. Preliminary results have already been reported [4]).

Tungsten resonances have been studied by several groups. The lowest energy resonance at 4.14 eV has been analysed by Landon [5]) using a crystal spectrometer. Transmission measurements at Brookhaven with a fast chopper (summarised in ref. [6])) have been made for resonances up to about 300 eV. Simpson and Fluharty [7]) have given values for the statistical weight factor $g = \frac{1}{2}[1\pm1/(2I+1)]$ (where I is the spin of the target nucleus) for the

† Now at the University of Texas, Austin, Texas, U.S.A.

27, 46 and 101 eV resonances using a combination of scattering and transmission measurements. Harvey [8]) has preliminary values for g, using a similar method, for W^{183} resonances up to 101 eV. These measurements give consistent spin value assignments for the 7.6 and 27 eV resonances of W^{183} but do not resolve the resonances at 46.1 and 47.7 eV. The radiation widths of all the levels (except that at 4.12 eV) are quite uncertain. In this paper we present the final results of the measurements of the resonance parameters of the stronger levels in tungsten up to 115 eV, obtained at Harwell using the 15 MeV electron linear accelerator as a pulsed neutron source. The resolution used for these measurements (and those reported in the preceding paper) has been improved to the extent that it has been possible to obtain the parameters of both the 46.1 and the 47.7 levels.

2. Method

2.1. GENERAL

The details of the three experimental methods (transmission, scattering and capture) have been reported elsewhere [2, 3]). Briefly, neutron detectors were used for the observation of scattering (BF_3 counters) and transmission (γ-rays from a B^{10} slab) and γ-ray detectors (NaI(Tl) scintillation counters) for resonance capture.

The area under the scattering or capture yield curve was measured for a number of targets of different thickness. A plot was made of the area per unit target thickness against target thickness. To eliminate the effects of self screening and multiple scattering the final result was obtained by extrapolating this plot to zero thickness. The quantities derived from these two experiments were $S \equiv g\Gamma_n^2/\Gamma$ from the scattering experiment and $C \equiv$ $\equiv g\Gamma_n(1-\Gamma_n/\Gamma)$ from the capture. The transmission gives the quantity $T \equiv g\Gamma_n \Gamma^p$ where p lies between 0 and 1. By combining these three quantities values for g, Γ_n and Γ can be found.

The values of C, S and T can be represented as a plot of neutron width against the total width. If the experimental values were precise, the curves so obtained would pass through the same point for one value of g, but not for the other. In practice these curves are never concurrent; it is therefore not possible to determine the value of g unambiguously but only the relative probabilities of the two possible solutions. This was done by a least squares method [2, 9]) coded for machine calculation. For tungsten only one isotope, W^{183}, has two possible values for g, viz. $\frac{1}{4}$ or $\frac{3}{4}$; all the others have $g = 1$. The more probable value of g for a W^{183} resonance is given by the solution with the lower value of χ^2_{min}, the sum of the squares of the weighted deviations of the experimental values of the neutron width from the mean. χ^2_{min} is shown in column 8 of table 2.

2.2. CAPTURE

As described elsewhere [2, 3, 10]), the areas obtained with the capture γ-ray detector were calibrated by a separate measurement of a suitable low energy resonance, and a determination of the neutron spectrum. For W^{182} the 4.14 eV resonance was used, the calibration being performed by inserting a 0.020″ tungsten foil normal to the neutron beam. For this resonance $\Gamma_n/\Gamma = 0.03$ so that nearly all the incident neutrons are captured. The correction to be applied for those neutrons being scattered out of this "black" sample was less than 1 % and was ignored. The neutron spectrum was measured by counting the 480 keV γ-rays from a thick slab of B^{10} in the beam as a function of time of flight of the neutrons. This spectrum was then normalised to the "black" sample capture yield at 4.14 eV. The shape of the spectrum agreed with that obtained with the lead calibration [3]) of the scattering experiment.

For the W^{183} resonances a slightly different procedure was used. Initially the capture areas were calibrated against the neutron spectrum normalised at 4.14 eV, a W^{182} resonance, as described above. This procedure, however, would introduce a systematic error into the measured value of C if the γ-ray spectra from the two isotopes are not identical. To estimate this error, a comparison was made between the observed counting rates for "black" samples at the 4.14 and 7.62 eV resonances, taking into account the neutron spectrum. The difficulty with this measurement was that the higher energy resonance is much weaker and needed a very thick sample (0.18″) to absorb all the neutrons. This would lead to a large fraction of the emergent γ-rays being absorbed in the target. To minimise this effect the 7.62 eV resonance was remeasured with the targets at 45° to the beam direction, the calibration being made against a "black" sample at the same energy. Details of this measurement are given in the appendix. It was found that the new value of C for this resonance differed by a factor of (0.825 ± 0.08) from the previous one. This implies that there is, indeed, a difference between the γ-ray spectra of the two isotopes. Since all the W^{183} resonances should have been calibrated against that at 7.62 eV, this correction factor was applied to all measured values of C for the W^{183} isotope.

The calibration of the capture areas involved the assumption that the efficiency for the detection of γ-rays was the same for each resonance, or, in effect, that the energy spectra of the capture radiation did not differ from resonance to resonance in the same isotope. The validity of this assumption has been discussed before [2, 3]). Bird [11]) has found that differences do exist between the spectra of γ-rays emitted from resonances of different spin in the same isotope. For resonances of like spin, the spectra are similar. For W^{182} all the resonances have the same spin; for W^{183} the 7.62, 27.1 and 46.1 eV were found to have spin 1, the 47.7 and 100.8 spin 0. The value of C

for the 100.8 level was not used because of inaccuracies due to poor resolution (see section 3.4). The value of C for the 47.7 eV resonance was consistent with the transmission and scattering results showing that any error in the calibration due to the change of spin was small.

A typical experimental yield curve is shown in fig. 1A. This is for the energy region containing the 46.1 and 47.7 eV levels. It was taken with a 0.002″ thick tungsten target with 0.5 μsec timing channels using a flight path of 11.5 metres. Several such runs were combined for each target.

The measured values of C' which are proportional to the capture area divided by the target thickness) were plotted against target thickness and extrapolated to zero thickness. The extrapolated value of $C'(= C)$ was used for combination with S and T. The values of C are given in column 4 of table 2; the figures in parenthesis are the standard deviations expressed as percentages.

2.3. SCATTERING

Scattering measurements were made from thin samples of natural tungsten and from very thin deposited targets of tungsten sulphide. The thinnest target was equivalent to about 0.0001″ of tungsten metal. The detector consisted of 18 two inch diameter BF_3 counters arranged in an annulus with the sample at the centre [2]). This detector was calibrated by observing the number of neutrons scattered from a pure lead target, assuming a cross-section of 11.4 barns for lead. Area measurements were made on at least three tungsten sample thicknesses for each resonance. Hughes' curves[12]) were used [3]) to obtain a correction to be applied to the areas which took account of the attenuation of the incident beam. The corrected values of S' (which are proportional to the area divided by the target thickness) were plotted as a function of target thickness. The result obtained when the corrected values were extrapolated to zero target thickness was used in the least squares fitting with C and T. This value is shown in column 3 of table 2.

Owing to the improvement in resolution brought about by reduction of the accelerator pulse length and the use of narrower detector gates [13]), it was possible to obtain values of S for both 46.1 and 47.7 eV resonances. A typical experimental result is shown in fig. 1B. Several such runs were combined. Four targets were used to give values of S for both resonances. The resolution was not good enough to enable the resonances above 120 eV to be analysed. However, at this energy the neutron width is so much larger than the radiation width that great accuracy in the measurement of S would be needed to give the same information as a rather poor measurement of C, the capture area.

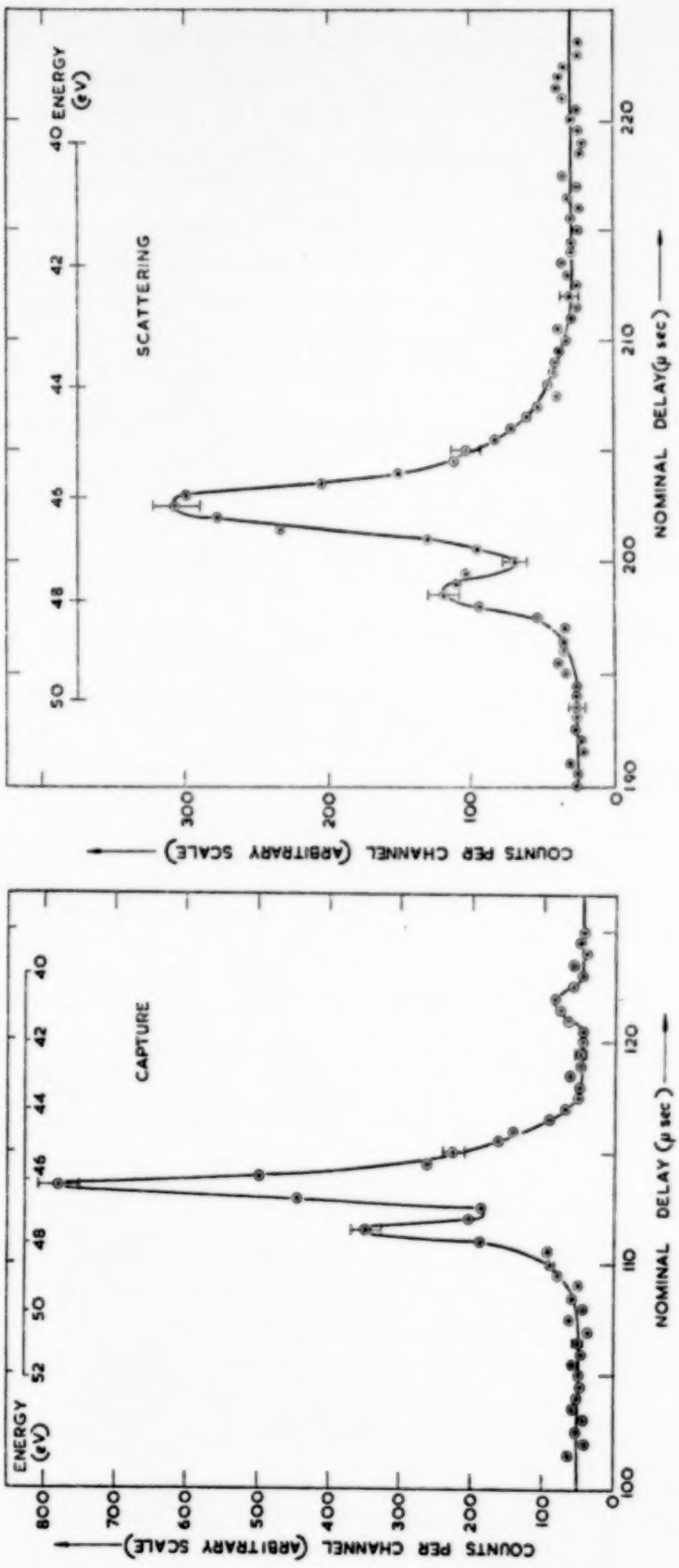

Fig. 1. Capture and scattering yield from a 0.002″ sample of natural tungsten. Timing channels 0.5μsec. Path lengths were 11.5 and 20 metres respectively.

2.4. TRANSMISSION

For the resonances of energy greater than 25 eV the results of the experiments described in the previous paper by Firk and Moxon [14]) were used.

For the resonances below 25 eV transmission areas were measured using the 11.5 metre flight path. The experimental arrangement was the same as that used for measuring the neutron spectrum. A thick slab of B^{10} was placed in the beam stopping all the neutrons up to a few hundred volts. The 480 keV γ-rays were observed with the NaI scintillation counters. Various thicknesses of tungsten metal were placed in the beam as transmission samples. The areas obtained are given in table 1, the figures in

TABLE 1

Transmission areas measured at 11.5 metres for tungsten resonances

Energy (eV)	Isotope	Sample thickness (atoms per cm²)	Area (eV)
4.14	182	8.69×10^{20}	0.386 (10)
		16.11	0.503 (10)
7.62	183	4.74	0.24 (15)
		80.1	0.925 (3)
18.8	186	0.116	0.59 (20)
		0.168	0.784 (19)
		0.478	1.20 (10)
21.1	182	0.446	0.229 (13)
		4.25	0.80 (19)

The quantities in brackets are percentage standard deviations.

parentheses being their standard deviations expressed as percentages. These areas include wing corrections but do not include corrections for sample thickness or Doppler effect. The areas were corrected using the Hughes' curve [12]) and put into a suitable form for handling by the digital computer for combination with the scattering and capture experiments.

3. Results

The results are collected in table 2. The experimental quantities S and C are given in columns 3 and 4. The figures in brackets are the standard deviations expressed as percentages. These take into account the consistency of the several measurements of S' and C' when extrapolating to zero thickness as well as the fluctuations in the number of counts observed. Column 5 gives, in bold face type, the preferred value of J, the spin of the compound nucleus formed by the addition of a neutron to the target nucleus. Columns 6 and 7 list the values of Γ_n and Γ_γ derived from the least squares combination of T, S and C. For W^{183}, Γ_n and Γ_γ are given for both values of J, the

TABLE 2

Parameters of the tungsten resonances

Energy (eV)	Isotope	S (meV)	C (meV)	J	Γ_n (meV)	Γ_γ (meV)	Number of experiments	χ^2_{min}
4.14	182	0.043 (11)	1.436 (5)	½	1.48 ± 0.06	49.3 ± 4.7	4	0.23
7.62	183	0.030 (25)	1.32 (7)	0	5.1 ± 0.3	72.1 ± 6.9	4	8.1
				1	1.8 ± 0.1	68.9 ± 6.0	4	0.7
18.8	186	207 (5)	37.0 (12)	½	251 ± 10	45.3 ± 6.0	5	4.1
21.2	182	14.2 (12)	23.6 (10)	½	36.6 ± 2.6	58.8 ± 11.5	4	0.2
27.1	183	10.3 (6)	17.8 (15)	0	97.5 ± 2.8	91.6 ± 8.9	5	19.7
				1	40.1 ± 1.1	76.9 ± 5.9	5	2.3
46.1	183	80 (10)	39.9 (15)	0	410 ± 20	179 ± 32	4	16
				1	147 ± 7	71 ± 12	4	1.7
47.7	183	19 (20)	10.8 (20)	0	121 ± 7	68 ± 17	4	0.02
				1	45 ± 3	46 ± 11	4	16
100.8	183	54 (20)	—	0	255 ± 12	30 ± 35	4	0.4
				1	95 ± 5	100 ± 22	4	15
114	182	220 (10)	46.2 (10)	½	263.5 ± 5.1	55.6 ± 6.5	7	1.5

For W^{183} the preferred J value is in heavy type.

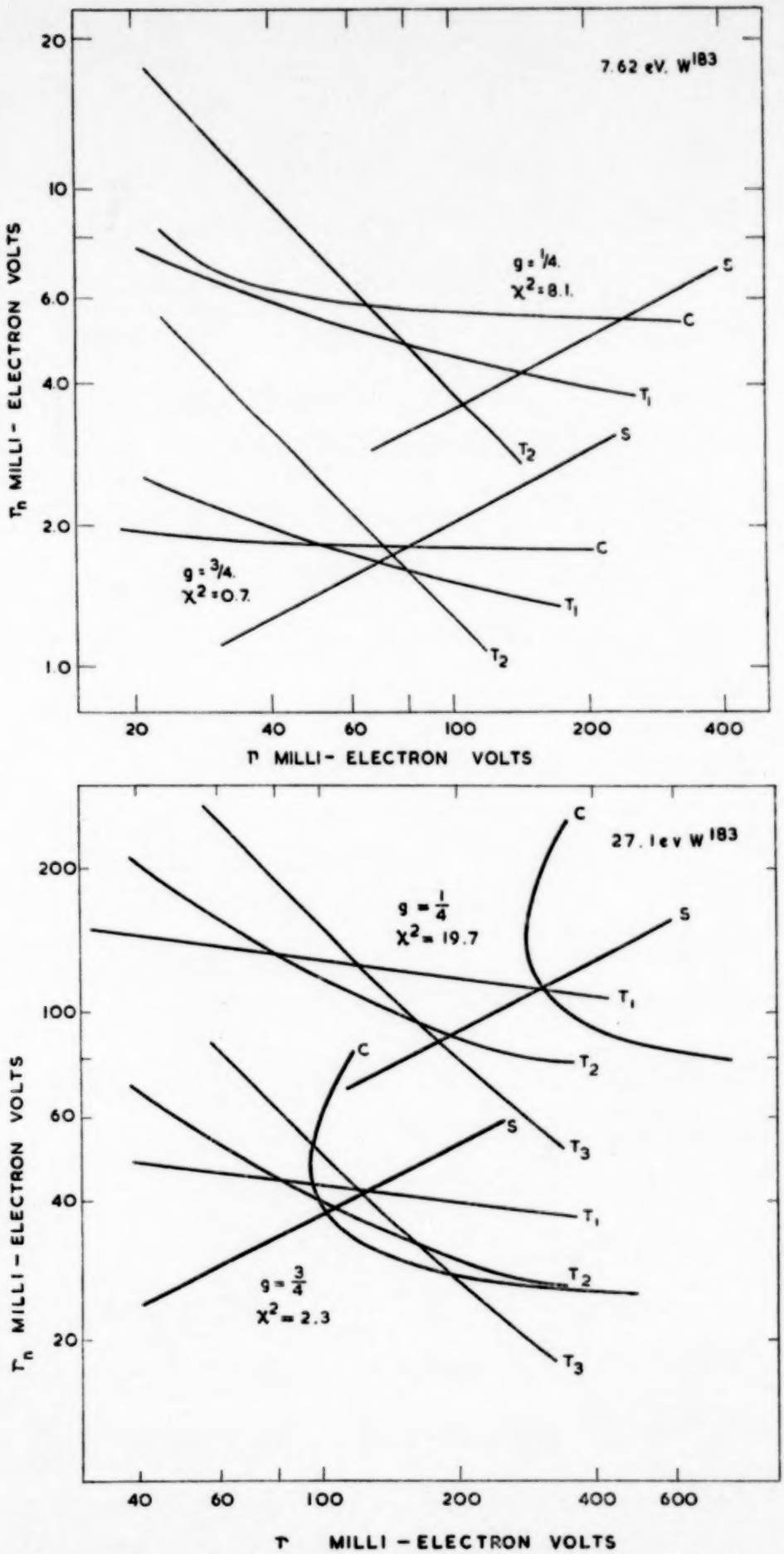

Fig. 2. Experimentally derived plots of Γ_n against Γ for the resonances observed in W^{183} for both values of g, the statistical weighting factor. The preferred g value has the lower χ^2_{min}.

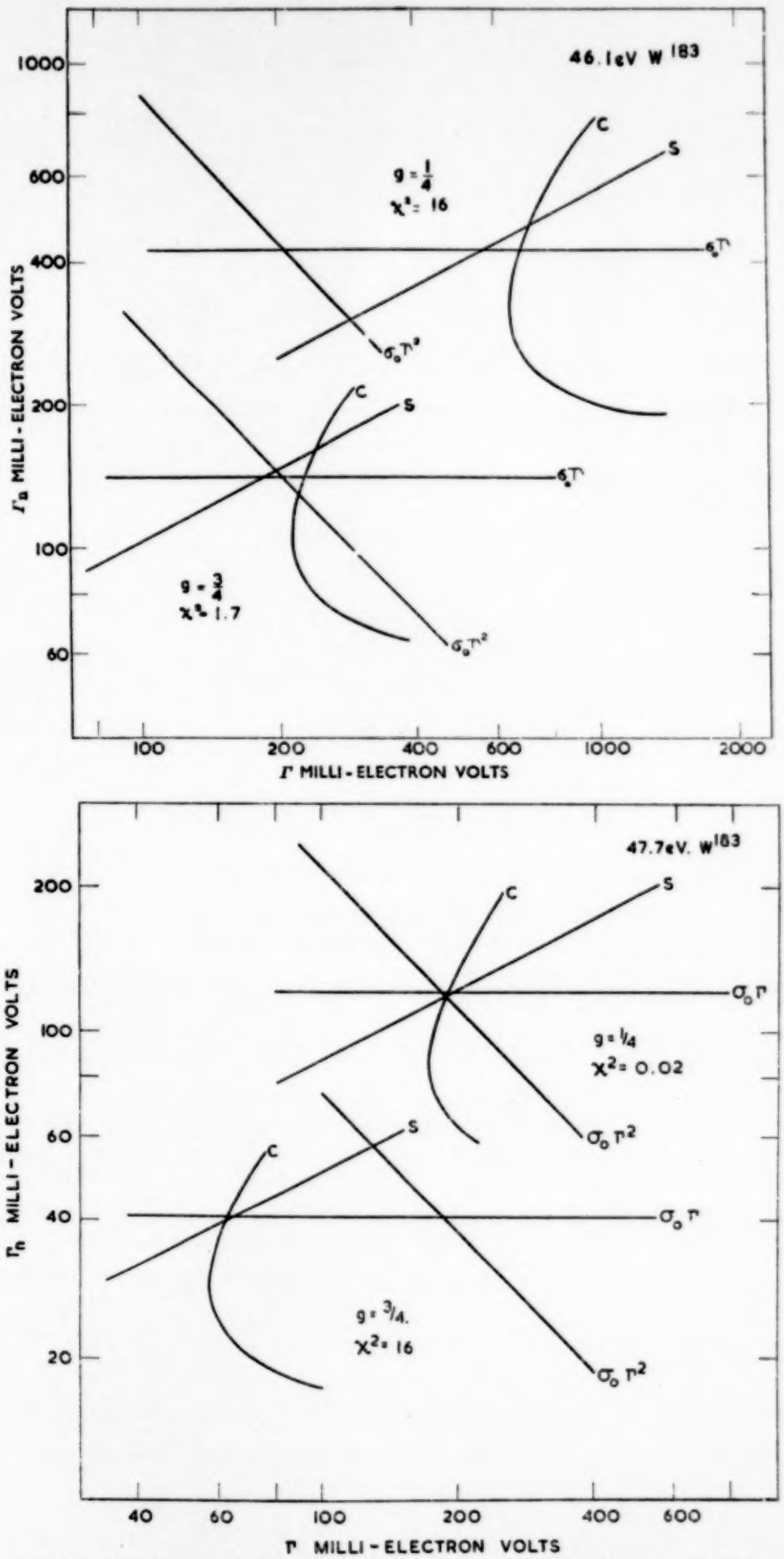

Fig. 2 (continued). Experimentally derived plots of Γ_n against Γ for the resonances observed in W^{183} for both values of g, the statistical weighting factor. The preferred g value has the lower χ^2_{min}.

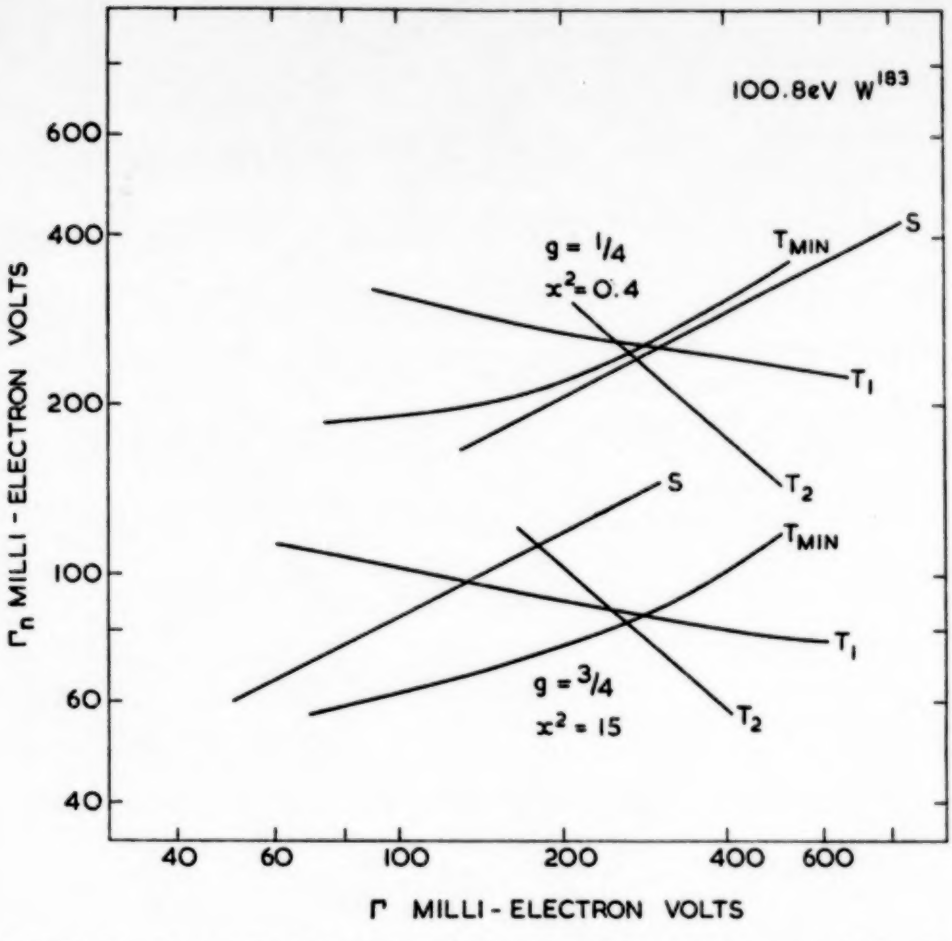

Fig. 2. (end). Experimentally derived plots of Γ_n against Γ for the resonances observed in W^{183} for both values of g, the statistical weighting factor. The preferred g value has the lower χ^2_{min}.

preferred set having the lower value of χ^2_{min} in column 9. The errors on Γ_n and Γ_γ are standard deviations. The number of experiments combined are listed in column 8; the number of degrees of freedom is two less than the number of experiments. Fig. 2 shows the plots of Γ_n against Γ for the resonances in W^{183} for both values of the weighting factor g. The preferred value of g is the one which gives the best intersection of the lines representing T, S and C. Some of the items in this table deserve special comment.

3.1. THE 4.14 AND THE 7.62 eV RESONANCES

The parameters of these two resonances have been measured previously. Landon [5]) used a crystal spectrometer to analyse the lower energy one. His values were $\Gamma_\gamma = 46 \pm 2$ meV and $\Gamma_n = 1.43 \pm 0.03$ meV which agree with our values. Schwartz, Pilcher and Schectman [6, 15]) have made transmission measurements on the 7.62 eV level by a "thick-thin" area method. Their values were $\Gamma_n = 2.2 \pm 0.2$ meV and $\Gamma_\gamma = 53 \pm 11$ meV, assuming $J = 1$ from the γ-ray spectra measurements of Fox *et al.*[16]). These values are slightly lower than those we obtained for Γ_n and Γ_γ.

3.2. ENERGY RANGE FROM 20 TO 30 eV

Apart from those at 21.2 and 27.1 eV no other resonances were observed in this energy region. Simpson and Fluharty [7]) report observing a resonance at 22.8 eV both in scattering and in self-indication transmission experiments. Our resolution was such (0.05 μsec/m) that this would have been observed (especially in the transmission experiment with a 0.010'' W sample) unless it was very much smaller than they reported.

3.3. THE 46.1 AND THE 47.7 eV RESONANCES

The resolution used by Firk and Moxon [14]) when measuring the transmission of tungsten for neutrons of this energy was good enough to enable them to fit the shape of their experimentally measured curves with two single level Breit-Wigner formulae. They were also able to determine the spins of the levels by measuring the values of σ_Δ and Γ_Δ, the Doppler broadened peak cross-section and width respectively and assuming an average radiation width for W^{183}. Several target thicknesses were used to derive the experimental cross-section. It was possible to get estimates of the quantities $\sigma_0\Gamma$ and $\sigma_0\Gamma^2$ with greater accuracy from the curve fitting than by combining the individual values of σ_0 and Γ [14]). Moreover, these combinations are also more accurate than the areas of the resonances since it was possible to use thicker samples in getting them; the samples had to be kept thin when measuring areas otherwise the two resonances could not be resolved. For these reasons values of $\sigma_0\Gamma$ and $\sigma_0\Gamma^2$ were used in the least squares combination with S and C rather than the areas. The values used were, for the 46.1 eV level, $\sigma_0\Gamma = 6020 \pm 450$ b · eV, $\sigma_0\Gamma^2 = 1230 \pm 123$ b · eV^2, and, for the 47.7 level, $\sigma_0\Gamma = 1660 \pm 100$ b · eV, $\sigma_0\Gamma^2 = 305 \pm 40$ b · eV^2. These values are shown in fig. 2 with S and C. It is clear from the way these lines intersect that the spin values are unambiguously fixed. This is shown quantitatively by the large differences in the values for $\chi^3_{\min}$ for the two spin values.

3.4. ENERGY RANGE 100 TO 105 eV

Firk and Moxon have found three levels in this energy range. They are at 100.8, 101.5 and 103.8 eV. The lowest energy resonance is the strongest and has been reported previously [6]); the other two levels are small by comparison. These levels could not be resolved in the scattering and capture experiments. By using 0.11 μsec timing channels and thin target it was just possible to separate the 103.8 eV resonance with the capture apparatus. However, this is the weakest level. Since the capture area, C, is proportional to $(\Gamma_n\Gamma_\gamma)/\Gamma$, and Γ_γ is expected to be roughly the same for all the levels, it was not found possible to estimate a correction to be applied to the value of C for the large level (100.8 eV). This value was not therefore used to obtain the best parameters.

For the scattering area, S, a correction could be estimated since S is proportional to Γ_n^2/Γ. A thin target transmission experiment at 32 metres gave a rough value for $g\Gamma_n$ for the three levels. Although the isotopic allocation of the two small levels was not known, it was possible to estimate the contribution to S by considering the various possibilities. The correction varied between about 5 and 12 %. Hence the measured value of S for the 100.8 eV level was multiplied by a factor of (0.90 ± 0.05), to take into account the contribution from both small levels.

As well as the thick and thin sample transmission areas, Firk and Moxon used the method of Lynn [17]) to get a value for the minimum transmission at the peak of the resonance. This gives a line, T_{min}, on fig. 2E. It will be seen that the value of $g = \frac{1}{4}$ is to be preferred. This is in contrast to the result of $g = \frac{3}{4}$ which is obtained if the three resonances are not resolved and the uncorrected values of T, S and C used for the least squares combination [4]). The radiation width obtained in table 2 has a large error due to the lack of an accurate value of C.

It is interesting to note that this spin allocation of $J = 0$ for the 100.8 eV resonance agrees with that obtained by Bird [11]) from a study of the high energy part of the capture γ-ray spectra from the three unresolved resonances at this energy. He finds a lack of γ-rays corresponding to the binding energy of the W^{184} nucleus. This suggests that the direct transition to the ground state is forbidden because both the capturing state and the ground state have spin 0. However, the lack of γ-rays corresponding to the ground state transition is no more than an indication that the excited state has spin 0, for the transition might be a weak one for some other reason. Taken in conjunction with our experimental result, however, it does seem very probable that the 100.8 eV level has spin 0.

3.5. RESONANCES OF ENERGY GREATER THAN 120 eV

These could not be resolved with the present scattering and capture apparatus. Longer flight paths, shorter timing channels, and, for the scattering experiment, reduction in the time jitter in the BF_3 counters are needed. For energies greater than 100 eV, to get information on Γ_γ, it is more important to measure C rather thans S due to the near equality of Γ_n and Γ. For example, a value of S with a standard deviation of 6 % was obtained for the 185 eV resonance which is so much bigger than its neighbours. This has not been listed in table 2 since it gave a value of $\Gamma_\gamma = 51 \pm 79$ meV on being combined with the transmission areas. It was not possible to measure C due to the poor resolution at these energies.

4. Conclusions

The values for the neutron width Γ_n, the radiation width Γ_γ and the spin of the compound nucleus have been measured for nine resonances in tung-

sten. As usual the values of the neutron width fluctuate considerably from resonance to resonance but the radiation widths are nearly constant. The radiation widths for the three isotopes are summarised in table 3; the weighted averages are also given.

TABLE 3

The radiation widths (in meV) of the resonances in tungsten

W^{182}	W^{183}		W^{186}
$J = \frac{1}{2}$	$J = 0$	$J = 1$	$J = \frac{1}{2}$
49± 5 (4.14)	68±17 (47.7)	69± 6 (7.62)	45±6 (18.8)
59±12 (21.2)	30±35 (100.8)	77± 6 (27.1)	
56± 7 (114)		71±12 (46.1)	
50± 4	61±15	73± 4	45± 6

Resonance energies are in brackets. The last line gives the average values.

For W^{183} there is no significant difference between the widths for the two values of the spin J. This may be due to the small number of levels observed, of course. However, it agrees with the observation by Rae *et al.* [2]) that the widths for the two values of J for the same isotope in silver, another spin $\frac{1}{2}$ target nucleus, are the same. This equality of the radiation widths for the two spin values is to be expected if the density of levels with spin J is proportional to $(2J+1)$ [2]). The actual number of levels measured is too small to show that there are more levels with $J = 1$ than $J = 0$.

Unfortunately, our knowledge of the radiation widths of the resonances of W^{186} is confined to that of the resonance at 18.8 eV. Within the experimental limits, this quantity is equal to the average of the radiation widths of the three resonances in W^{182}. Since the neutron binding energy of the product W^{187} is less than that of W^{183} by 0.5 MeV [18,19]) we should expect the radiation width in the former to be lower than that of the latter. According to the semi-empirical formula of Stolovy and Harvey [19]), the total radiation widths vary roughly as the fourth power of the binding energy. We should expect, therefore, a radiation width for the 18.8 eV level of about 32 meV. This is much lower than we have found. The comparison between the radiation widths in these two isotopes, then, seems to confirm what was found for silver [2]), namely, that the widths of successive isotopes do not vary with the mass number in the expected manner.

Table 3 shows that the mean width for W^{183} is appreciably larger than that of W^{182}. If the effective excitation energy is to be calculated by subtracting the pairing energy from the neutron binding energy, we should expect the radiation width for the W^{183} resonances to differ from those of W^{182} only by the contribution of the γ-rays at the top end of the spectrum. The total

contribution of these γ-rays does not amount to more than 10 % of the total width [18]); this seems inadequate to account for the 40 % difference observed (table 3). Not enough is yet known about the widths of adjacent even charge number isotopes to be sure that this difference is statistically significant.

We are indebted to Drs. R. B. Schwartz and R. E. Chrien, of Brookhaven National Laboratory, for sending us their tungsten transmission results. We are grateful for the assistance of the other members of the Electron Linear Accelerator Group at Harwell both for their continued operation of the accelerator and for many fruitful discussions. In particular we should like to thank Messrs. F. W. K. Firk and M. C. Moxon for assistance in analysing our transmission experiments.

Appendix

CAPTURE AREA MEASUREMENTS FOR W^{183}

Three NaI(Tl) scintillation counters were arranged at right angles to one another in a plane normal to the neutron beam. The elliptical tungsten sample was placed at 45° to the beam line and oriented so that the counter axes were at 45° to its surface. Two of the counters saw the front face of the target, the third one saw the back of it (at 45°). This geometry was chosen so as to reduce the γ-ray absorption to a minimum without losing too many counts. The neutron beam was filtered through cadmium to cut out low energy neutrons from the previous machine burst.

The "black" sample counting rate was measured using several targets made up of 0.020" sheets of tungsten. The counting rate at the top of the flat peak was noted, the normalisation being against one of three independent monitors of the integrated neutron output from the accelerator. The correct background to be subtracted was determined by observing the energy range 4 to 16 eV with wide time channels and drawing in smooth curves. Account had to be taken of the wings of the 18.8 and 4.14 eV resonances in estimating this quantity, since, with the thick targets used, these were appreciable. By this means the "black" sample counting rate could be measured to about 5 % accuracy, of which the uncertainty in the background contributed about 1 %. These rates are plotted in fig. 3 as a function of the target thickness. The correction to be applied for the absorption of the emitted γ-rays in escaping from the target was calculated. The corrected rates are indicated in the figure; it will be seen that they agree with that estimated by extrapolating the experimental data to zero thickness.

The thin samples used for the capture area measurements were placed in the same location as the calibration sample, the counts being normalised against the same monitor.

A total of five target thicknesses were used, the thinnest being 0.001". On extrapolating to zero thickness a value of $C = 1.32 \pm 0.09$ meV was obtained. This compared with $C = 1.60 \pm 0.11$ meV from the previous

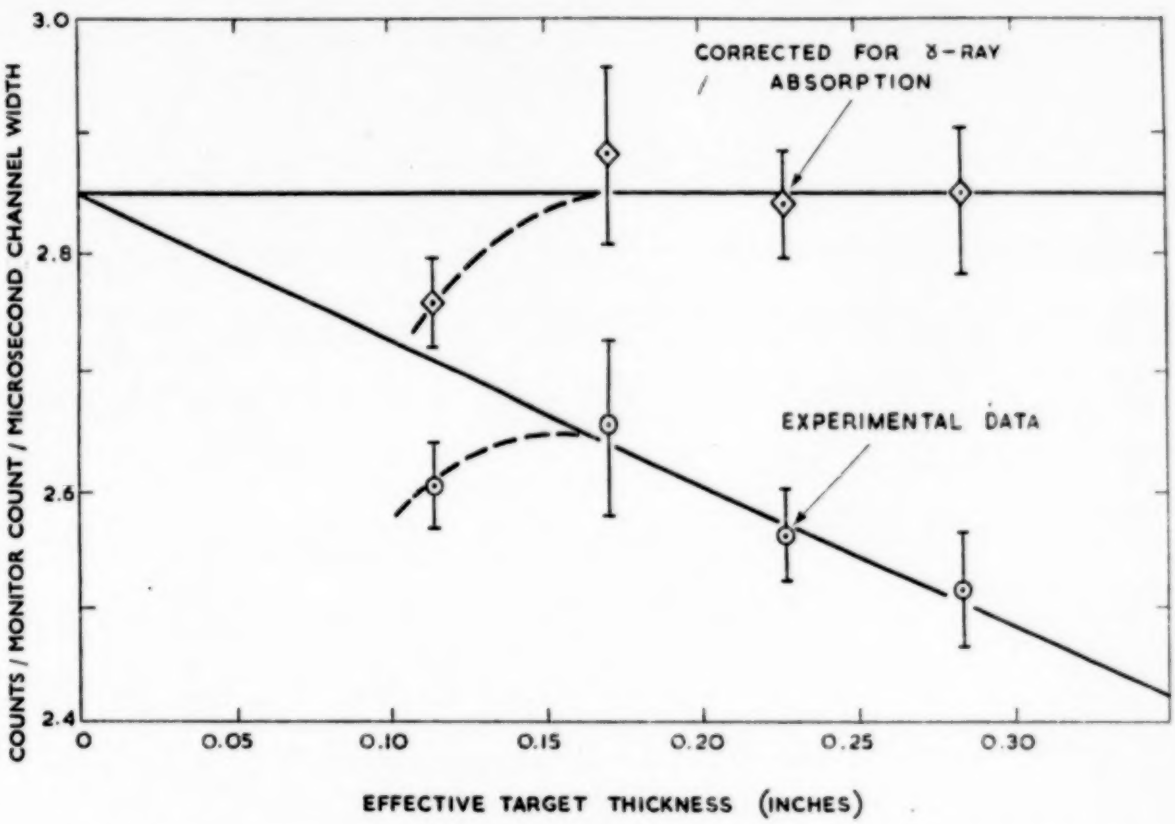

Fig. 3. Capture counting rates at the peak of the 7.62 eV resonance as a function of target thickness for thick targets. Only the three thickest targets are "black" i.e. absorb all incident neutrons. The broken line shows the fall off in counting rate when the targets are no longer "black". Rates corrected for γ-ray absorption are also shown.

measurement with the spectrum normalised at the 4.14 eV level. The values for C for all the W^{183} resonances were multiplied by the factor (0.825 ± 0.08) since they all had been measured in the same way.

References

1) G. Breit, E. U. Condon and R. D. Present, Phys. Rev. **50** (1936) 825
2) E. R. Rae, E. R. Collins, B. B. Kinsey, J. E. Lynn and E. R. Wiblin, Nuclear Physics **5** (1958) 89
3) J. E. Evans, B. B. Kinsey, J. R. Waters and G. H. Williams, Nuclear Physics **9** (1958) 205
4) J. E. Evans, F. W. K. Firk, B. B. Kinsey, M. C. Moxon, J. R. Waters and G. H. Williams, Bull. Amer. Phys. Soc. **4** (1959) 270 (A)
5) H. Landon, Phys. Rev. **100** (1955) 1414
6) D. J. Hughes and R. B. Schwartz, Brookhaven National Laboratory, BNL-325, 2nd Edition (1958)
7) F. B. Simpson and R. G. Fluharty, Bull. Amer. Phys. Soc. **3** (1958) 176 (A)
8) Private communication to Dr. E. R. Rae (1958)

9) E. R. Cohen and J. W. M. DuMond, Handbuch der Physik **35** (Springer-Verlag, Berlin, 1957) p. 63
10) E. R. Rae and E. M. Bowey, J. Nuc. Energy **4** (1957) 179
11) J. R. Bird, Proc. 2nd Int. Conf. Peaceful Uses of Atomic Energy A/CONF 15/P/35 (to be published)
12) D. J. Hughes, J. Nuc. Energy **1** (1955) 237
13) F. W. K. Firk, G. W. Reid and J. F. Gallagher, Nuclear Instruments **3** (1958) 309
14) F. W. K. Firk and M. C. Moxon, Nuclear Physics **12** (1959) 552
15) R. B. Schwartz, V. L. Pilcher and R. M. Schectman, Bull. Amer. Phys. Soc. **1** (1956) 187 (A)
16) J. D. Fox, R. L. Zimmerman, D. J. Hughes, H. Palevsky, M. K. Brussel and R. E. Chrien, Phys. Rev. **110** (1958) 1472 (L)
17) J. E. Lynn and E. R. Rae, J. Nuc. Energy **4** (1957) 418
18) L. V. Groshev, A. M. Demidov, V. N. Lutsenko and V. I. Pelekhov, Atlas of γ-ray Spectra (Pergamon Press, London 1959)
19) A. Stolovy and J. A. Harvey, Phys. Rev. **108** (1957) 353

1.E.1:
3.A:4.E

Nuclear Physics **12** (1959) 579—588; © *North-Holland Publishing Co., Amsterdam*

Not to be reproduced by photoprint or microfilm without written permission from the publisher

Fe^{59} DECAY SCHEME

J. M. FERGUSON

U.S. Naval Radiological Defense Laboratory, San Francisco 24, California

Received 1 June 1959

Abstract: The gamma-ray spectrum of 45-day Fe^{59} was investigated with scintillation detectors. In addition to the previously reported gamma rays at 0.19, 1.10, and 1.29 MeV, gamma rays at 0.14 and 0.33 MeV were observed. The positions of these gamma rays in the decay scheme are established from the gamma-ray energies and coincidence measurements. It is concluded that a level in Co^{59} at 1.43 MeV with a character of $\frac{1}{2}-$ is weakly excited by the Fe^{59} beta decay.

1. Introduction

Two recent developments prompted this reinvestigation of the Fe^{59} decay scheme. The first is the result of a study of the Co^{59} energy level spectrum, by Mazari, Sperduto and Buechner [1]), using the $Co^{59}(p, p')$ reaction. Their results indicate that there are six excited levels in Co^{59} low enough to be reached by negaton decay from Fe^{59} (see fig. 7). Only two excited levels have been observed from the Fe^{59} decay [2]).

The second development is the Centre-of-Gravity Theorem in Nuclear Spectroscopy reported by Lawson and Uretsky [3]). This theorem gives a relationship among the excited levels of certain neighbouring nucleides. Specifically, it indicates that for each level in ${}_{28}Ni^{60}_{32}$ there is a set of levels in ${}_{27}Co^{59}_{32}$ corresponding to the coupling of the angular momentum of the unpaired proton to the neutron angular momentum. Thus a set of five excited levels in Co^{59} are predicted corresponding to the first excited level of Ni^{60}, at 1.3325 MeV [4]). These levels would have characters of $\frac{3}{2}-$, $\frac{5}{2}-$, $\frac{7}{2}-$, $\frac{9}{2}-$, and $\frac{11}{2}-$. Their "centre of gravity" (mean excitation energy weighted according to their angular momentum) would be 1.33 MeV.

Metzger's work on the Fe^{59} decay scheme [2]) has established the characters of the 1.10 and 1.29 MeV levels to be $\frac{5}{2}-$ and $\frac{3}{2}-$, respectively. Of the remaining four levels in this energy region, three would presumably be the $\frac{7}{2}-$, $\frac{9}{2}-$, and $\frac{11}{2}-$ levels predicted by Lawson and Uretsky. The remaining one must be due to some other type of excitation.

In the present work a search was made for weak components in the Fe^{59} gamma-ray spectrum, in the hope of gaining more information about these Co^{59} levels.

2. Source and Equipment

Two Fe^{59} sources were available for this study. Both were made by the $Fe^{58}(n, \gamma)$ reaction at the Oak Ridge National Laboratory. One was obtained in January 1959, and the other was obtained in early 1958. All the spectra were taken with the new source, and then the results were checked with the old source to see if contaminants with different half-periods were responsible for the results.

Two four-inch diameter, four-inch high NaI(Tl) crystals were used to study the gamma-ray spectrum. These crystals have been calibrated for counting efficiency in a standard geometry by Mr. William Thompson of this laboratory. A 100-channel analyzer was used for recording the pulse-height spectrum.

The following arrangement was used for the coincidence work. After amplification, the output of one crystal was fed through a differential discriminator, and then into a slow (one microsecond resolving time) coincidence unit. The output of the other crystal was amplified and fed through an integral discriminator into the coincidence unit. The output of this crystal was also fed into a 20-channel analyzer which was triggered by the output of the coincidence unit. The operation of the coincidence circuit was checked with the annihilation radiation from a Na^{22} source and the cascade gamma rays from a Co^{60} source.

3. Singles Spectra

The singles pulse-height spectrum taken with a 4-in. by 4-in. NaI(Tl) crystal and a 100-channel analyzer is shown in fig. 1. The previously reported gamma rays at 0.19, 1.10, and 1.29 MeV [2]) are evident. The energies and relative intensities of these gamma rays, estimated from this spectrum, are given in table 1. In addition to these, there are gamma-ray, full-energy peaks at 0.14 and 0.33 MeV.

Fig. 2 shows an expanded view of the low-energy pulse-height spectrum. The two new gamma rays are evident. The energies and relative intensities are given in table 1.

The presence of the 0.14 and 0.33 MeV gamma rays indicates that one or more of the higher levels in Co^{59} is excited. Hence a careful search was made in the 1.4 MeV region. An expanded view of the pulse-height spectrum around 1.4 MeV is shown in fig. 3. The solid line is a Gaussian curve fitted to the 1.29 MeV peak. The data fit the Gaussian curve down to 0.4 percent of the 1.29 MeV peak height. The surplus counts can be accounted for as pile-up due to random coincidences between lower energy pulses. From these data an upper limit of 0.5 percent is put on the intensity of any gamma ray in the region from 1.40 to 1.60 MeV.

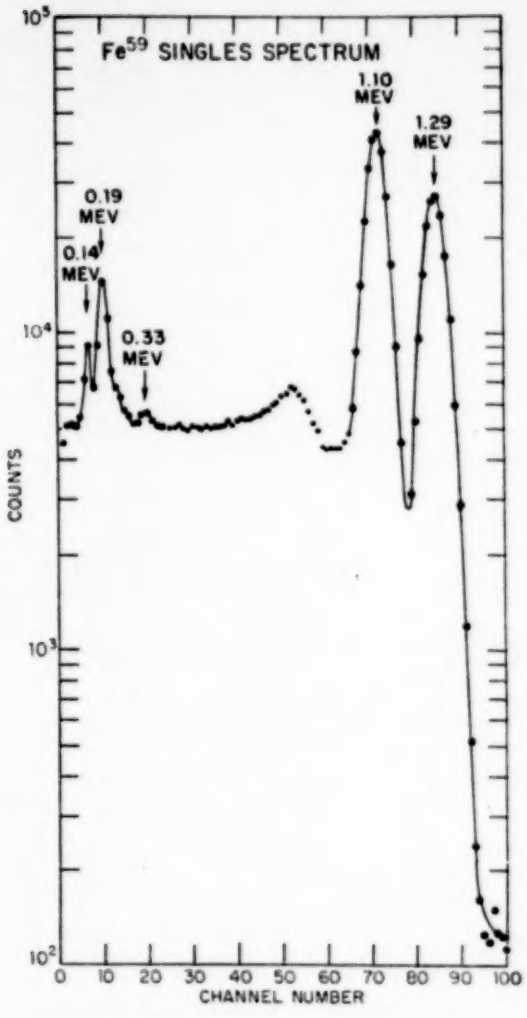

Fig. 1. The Fe^{59} gamma-ray pulse-height spectrum. This spectrum was taken with a 4″×4″ NaI(Tl) crystal and a 100-channel pulse-height analyzer. The crystal was surrounded by four inches of lead, with a ½-inch diameter hole in the top of the lead shield. The source was placed 20 inches above the top of the collimator.

TABLE I

Summary of results

E_γ(MeV)	Relative intensity
0.140±0.005	0.85±0.15
0.190±0.005	2.4 ±0.4
0.340±0.008	0.34±0.07
1.10 ±0.01	56 ±3
1.29 ±0.01	44 ±3
no 1.4 gamma	<0.5

The numbers in the first column are the observed gamma-ray energies and their probable errors, in MeV. The numbers in the second column are the numbers of gamma rays per 100 disintegrations, with their probable errors.

4. Coincidence Spectra

The spectra in coincidence with the 1.10 and 1.29 MeV peaks were taken with two 4-in. by 4-in. NaI(Tl) crystals. The differential discriminator on one side of the coincidence circuit selected pulses from the appropriate peak, while the pulse-height spectrum from the other crystal was taken in the 20-channel analyzer.

Fig. 4 shows the spectrum in the 100—200 keV region in coincidence with the 1.29 MeV gamma ray. The 0.14 MeV gamma ray observed in the singles spectrum appears, while the 0.19 MeV gamma ray is absent.

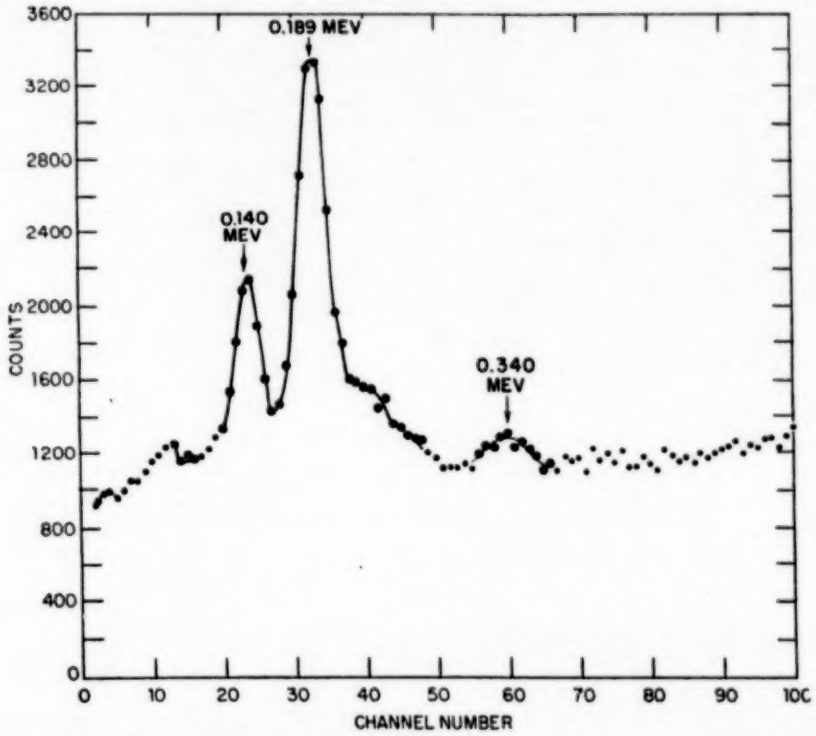

Fig. 2. The low energy end of the Fe^{59} gamma-ray pulse-height spectrum. This spectrum was taken under the same conditions as those in fig. 1, except that the amplifier gain was increased to expand the low-energy end of the spectrum. The peak at 0.075 MeV is due to the lead X-ray.

Portions of the spectrum in coincidence with the 1.10 MeV gamma rays are shown in fig. 5 and fig. 6. The 0.19 gamma ray (fig. 5) appears, as previously reported. [2]) Another gamma ray at 0.33 MeV is also in coincidence with the 1.10 MeV gamma ray (fig. 6).

5. Results

The experimental results are summarized in table 1. All these data may be fitted into a decay scheme consistent with the energy levels reported by Mazari, Sperduto and Buechner. The proposed decay scheme is shown in fig. 7. The assignments of the 0.190, 1.10, and 1.29 MeV gamma rays have

been previously established. The energy and coincidence data for the 0.144 and 0.33 MeV gamma rays make their assignment to the 1.43 MeV level obvious.

Since this work was completed, R. L. Heath, D. G. Proctor and C. W. Reich have independently reported similar results in an investigation of the Fe^{59} decay scheme[10]). The observed gamma rays, relative intensities, and assignment to a level at 1.43 MeV reported here are in good agreement with their results.

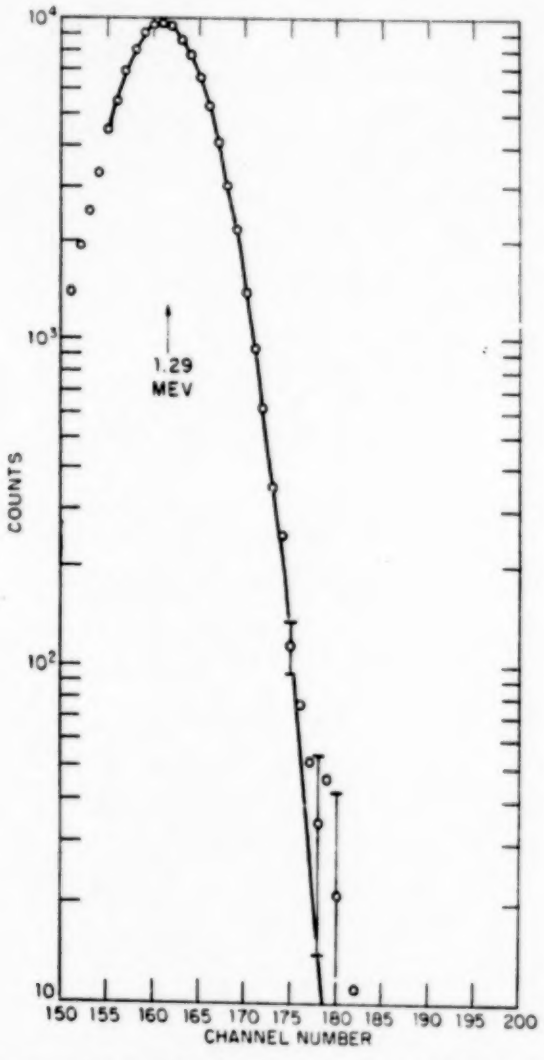

Fig. 3. The Fe^{59} gamma-ray pulse-height spectrum in the 1.4 MeV region. This curve was taken under the same conditions as that in fig. 1, except that the amplifier gain was increased and the first channel was set at 50 volts (0.5 volts per channel) in order to expand the high energy end of the spectrum. The solid line is a Gaussian curve fitted to the 1.29 MeV peak. The background has been subtracted.

6. Discussion

The proposed decay scheme is shown in fig. 7. The Co^{59} energy level spectrum is taken directly from the work of the MIT group. [1]) The character

assignments to the Co^{59} ground level, 1.10 and 1.29 MeV excited levels and the Fe^{59} ground level are taken from the work of Metzger.

Of the remaining four Co^{59} levels, we assume three are the $\frac{7}{2}-$, $\frac{9}{2}-$, and $\frac{11}{2}-$ levels predicted by Lawson and Uretsky, and the fourth is due to some other mode of excitation. Since the three predicted levels would each be at least second forbidden and thus not formed directly by the decay of Fe^{59}, the 1.43 MeV level must be the one not belonging to the set.

From these data we cannot positively establish that the Fe^{59} beta decay goes directly to the 1.43 MeV level, rather than the 1.46 or 1.48 MeV levels. The observed gamma rays from the 1.43 MeV level could possibly be in

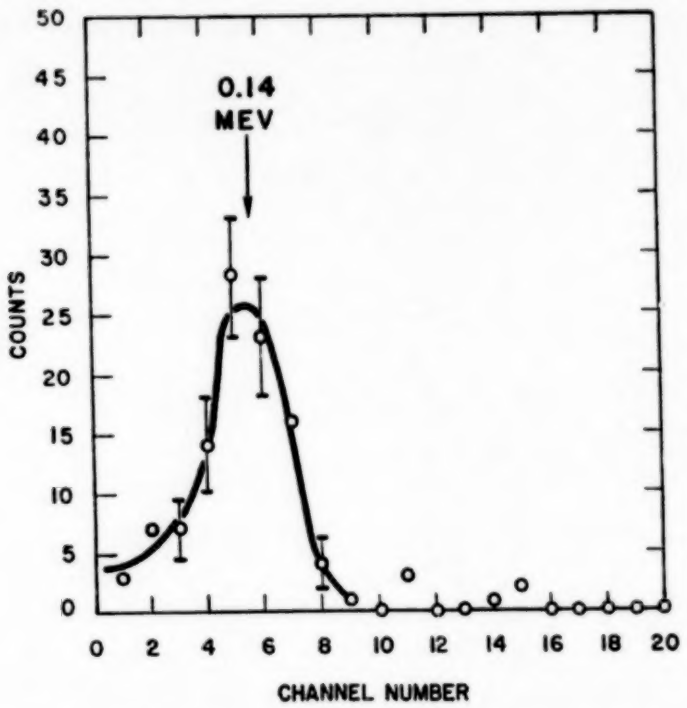

Fig. 4. A portion of the Fe^{59} gamma-ray pulse-height spectrum run in coincidence with the 1.29 MeV full-energy peak. Pulses from the 1.29 MeV peak in the other crystal were selected with a differential discriminator. A $4'' \times 4''$ NaI(Tl) crystal was used in each channel. Only a fraction of the original source was used, in order to reduce the background due to chance coincidences.

cascade with gamma rays of 26 or 47 keV from the higher levels. A search was made for gamma rys in the 20 to 50 keV region, and none were found. However, a gamma ray in this region could be missed because of the continuous background in the pulse-height spectrum and a reduced intensity due to internal conversion. If the 1.46 or 1.48 MeV levels were excited, however, one would expect to see gamma rays going directly to the lower Co^{59} levels. It is not possible to make a set of character assignments consistent with all the data without assuming the 1.43 MeV level is directly excited by beta decay.

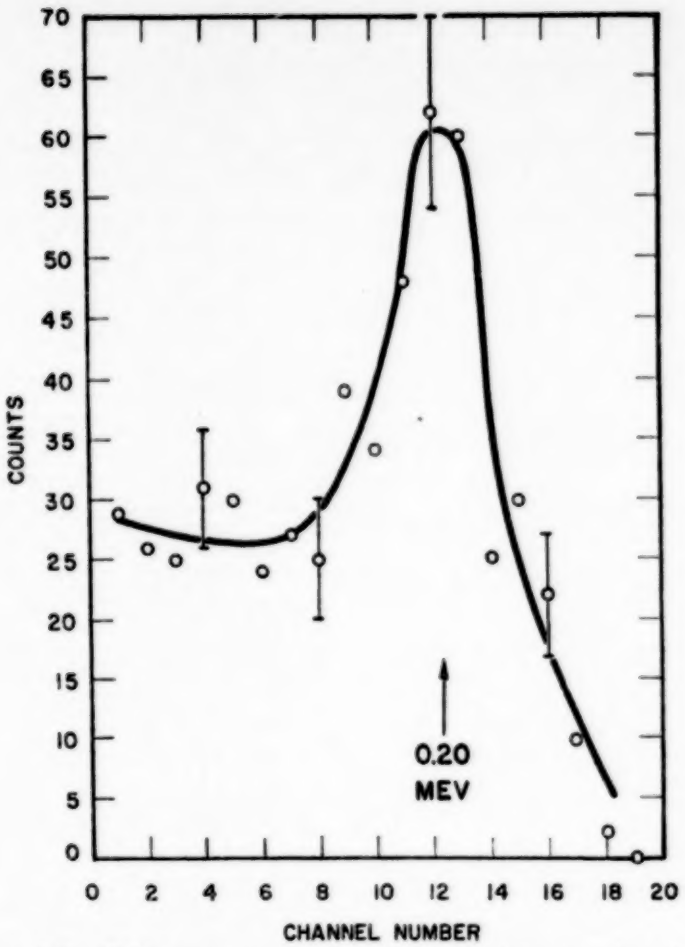

Fig. 5. A portion of the Fe^{59} gamma-ray pulse-height spectrum run in coincidence with the 1.10 MeV full-energy peak. This spectrum was taken under the same conditions as those in fig. 4, except that the differential discriminator was set on the 1.10 MeV peak.

TABLE 2

Gamma rays	Experimental intensity ratios	Single-particle model predictions	
$\frac{(1.43)}{(0.35)}$	< 2	$\frac{(M3)}{(E2)} = 1.6$	$\frac{(E2)}{(M1)} = 1000$
$\frac{(1.43)}{(0.14)}$	< 1	$\frac{(M3)}{(M1)} = 8$	$\frac{(E2)}{(M1)} = 5000$
$\frac{(0.33)}{(0.14)}$	0.4	$\frac{(E2)}{(M1)} = 4.5$	$\frac{(E1)}{(M1)} = 15$

The numbers in the experimental column are the observed values for the ratio of the intensities of the two gamma rays whose energies are listed in the column at the left. In the other two columns are listed the ratios predicted from Weisskopf's model for single-particle transitions[5]), assuming the multipolarities indicated. The multipolarities in the third column are what would be expected if the character of the 1.43 MeV level were $\frac{1}{2}-$, and those in the fourth column for $\frac{3}{2}-$.

Assuming then that the 1.43 MeV level is formed directly by the decay of Fe^{59}, we obtain a log *ft* value of 6.6 for the beta transition to this level. Hence it is an allowed transition, so the 1.43 MeV level must have a character of $\frac{1}{2}-$, $\frac{3}{2}-$, or $\frac{5}{2}-$. We chose among these by comparing the branching ratios of the various gamma rays with those predicted for single-particle transitions. [5]) Although the predicted single-particle transition rates often differ from the observed ones by a factor of 10 or 100 [6]), they give some indication of the expected transition rates.

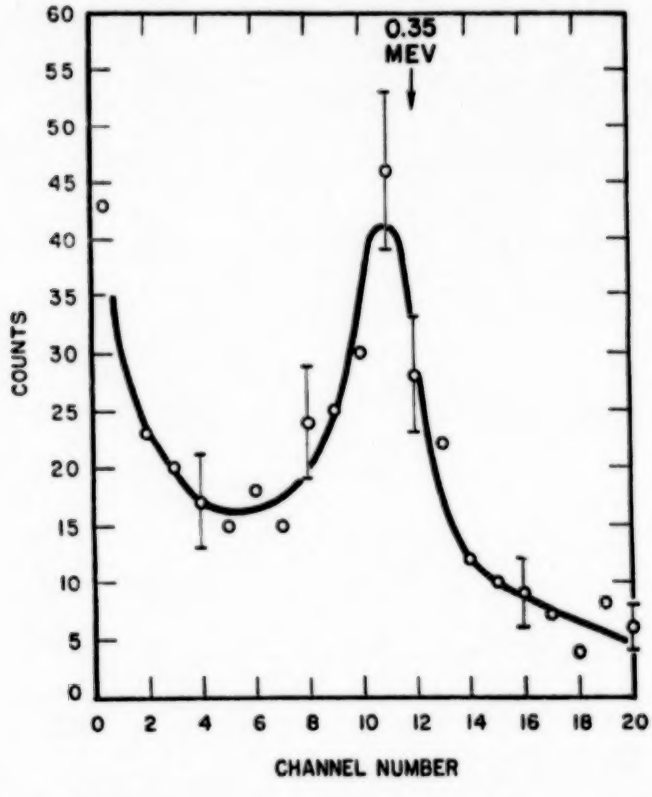

Fig. 6. A portion of the Fe^{59} gamma-ray pulse-height spectrum run in coincidence with the 1.10 MeV gamma ray. This spectrum was taken under the same conditions as those in fig. 5, with the 20-channel analyzer set to cover a different portion of the pulse-height spectrum.

A comparison between the observed and predicted branching ratios is made in table 2. A character assignment of $\frac{1}{2}-$ is chosen for the 1.432 MeV level, largely on the basis of the relatively-strong transition to the $\frac{3}{2}-$ level at 1.29 MeV. A $\frac{3}{2}-$ or $\frac{5}{2}-$ level would be expected to decay directly to the ground level.

The Co^{59} level spectrum may be expected to be similar to the Co^{57} level spectrum. Using Lawson and Uretsky's technique, one would again expect a set of five levels with characters of $\frac{3}{2}-$, $\frac{5}{2}-$, $\frac{7}{2}-$, $\frac{9}{2}-$, and $\frac{11}{2}-$, corresponding to the 1.45 MeV level in Ni^{58}. The Ni^{57} decay scheme has recently been investigated by Konijn, Hagedoorn and Van Nooijen. [7]) They found a

$\frac{1}{2}-$ level at 1.44 MeV in the Co^{57} level spectrum, in addition to a $\frac{3}{2}-$ level and a $\frac{5}{2}-$ level.

The levels at 1.19, 1.46, and 1.48 MeV are expected to have characters of $\frac{7}{2}-$, $\frac{9}{2}-$, and $\frac{11}{2}-$, not necessarily in that order. It seems unlikely that the 1.19 MeV level has a spin of $\frac{7}{2}-$, since one would expect to see a relatively-strong 100 keV transition from the 1.29 MeV level in that case. If we take

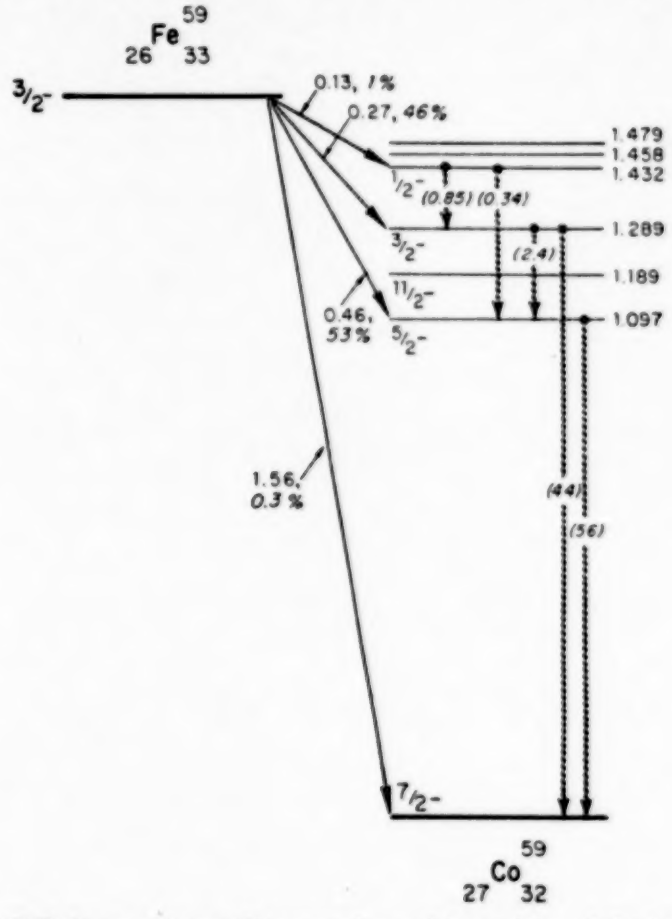

Fig. 7. Proposed Fe^{59} decay scheme. The energies and intensities of the beta transitions are indicated in the figure. The intensities of the gamma transitions are given in parentheses on the lines representing the transitions. The beta-ray energies and intensities to the 1.097 and 1.289 MeV levels are taken from Metzger's work [2]). The energies of the Co^{59} levels are taken from the Co^{59}(p, p′) measurements by the MIT group [1]). The character of the Co^{59} ground level is taken from the work of Bleaney and Ingram [8]) and Proctor and Yu [9]). The characters of the Fe^{59} ground level and 1.10 and 1.29 MeV levels in Co^{59} are based on the work of Metzger [2]). The intensities and positions of the gamma rays in the decay scheme, and the character assignment to the 1.432 MeV level are based on the current work.

the 1.19 MeV level to be $\frac{11}{2}-$, we obtain a value of 1.33 MeV for the Ni^{60} 2+ level. If we assume the 1.19 MeV level is $\frac{9}{2}-$, we obtain a value of 1.31 MeV for the Ni^{60} 2+ level. Since 1.33 MeV is closer to the measured value (all the energies are known to ± 5 keV) we chose $\frac{11}{2}-$ for the 1.189 MeV level. The levels at 1.458 MeV and 1.479 MeV are too close together to make a decision as to which is $\frac{7}{2}-$ and which is $\frac{9}{2}-$.

The author wishes to express his gratitude to Dr. C. S. Cook for many discussions during the course of this experiment, to Dr. D. L. Love for preparation of the sources, to Dr. R. L. Uretsky for reading a draft of the manuscript and making some very helpful suggestions, and to Mr. R. A. Taylor for his help with the electronic equipment.

References

1) M. Mazari, A. Sperduto and W. W. Buechner, MIT-LNS Annual Progress Report (May, 1957) p. 134
2) F. R. Metzger, Phys. Rev. **88** (1952) 1360
3) R. D. Lawson and J. L. Uretsky, Phys. Rev. **108** (1957) 1300
4) G. Lindstrom, A. Hedgran and D. E. Alburger, Phys. Rev. **89** (1953) 1303
5) V. F. Weisskopf, Phys. Rev. **83** (1950) 1073
6) M. Goldhaber and A. W. Sunyar, Beta- and Gamma-Ray Spectroscopy (North Holland Publishing Co., 1955) Ch. XVI
7) J. Konijn, H. L. Hagedoorn and B. Van Nooijen, Physica **24** (1958) 129
8) B. Bleaney and D. J. E. Ingram, Proc. Roy. Soc. A **208** (1951) 143
9) W. G. Proctor and F. C. Yu, Phys. Rev. **81** (1951) 20
10) R. L. Heath, D. G. Proctor and C. W. Reich, Bull. Am. Phys. Soc. **9** (1959) 278 (Washington meeting)

8.B *Nuclear Physics* **12** (1959) 589—595; © *North-Holland Publishing Co., Amsterdam*
Not to be reproduced by photoprint or microfilm without written permission from the publisher

REMARKS ON THE DECAY INTERACTIONS IN THE K_{e3} PROCESS

MINORU YONEZAWA
Department of Physics, Hiroshima University, Hiroshima

Received 11 May 1959

Abstract: In this note the following two points are discussed with respect to the decay interaction of K_{e3}.

a) The possibility of Konopinski-Uhlenbeck type interaction (rather than Fermi type interaction) is examined. It is shown that there exists a certain equivalence theorem between Fermi type interaction and Konopinski-Uhlenbeck type interaction and that owing to this theorem it is impossible to discriminate between them.

b) The present experimental data concerning the secondary electron energy spectrum in K^+_{e3} are analysed from the standpoint of primary weak Fermi interaction in order to discuss the type of decay interaction. It is suggested that the existence of scalar and tensor interactions is necessary to explain the experimental K^+_{e3} electron energy spectrum, while the vector interaction gives a fit with χ^2-probability $\lesssim 0.07$.

1. Introduction

We have given a study of the electron spectrum of the K_{e3} decay process ($K_{e3} \to e+\nu+\pi$) based only on physically reasonable assumptions [1]) (this work is referred to as A). In this analysis, as a model of the weak interaction participating in this process we have taken a Fermi type interaction: the K-meson decays through a virtual baryon and antibaryon pair into leptons by a weak local Fermi interaction. The purpose of this note is to supplement the previous analysis and give more a detailed discussion of some problems which were then only briefly touched. The first problem concerns the "Fermi type" hypothesis for the lepton coupling, i.e. the assumption that the decay interaction does not contain derivatives of the lepton wave functions. Another possibility to examine is the interaction which contains the derivative of the neutrino field (Konopinski-Uhlenbeck type interaction) [2]). Apart from the desirability of extending the discussion of the K_{e3} process to more general types of interaction, there is a special interest in investigating the Konopinski-Uhlenbeck type interaction in this case: it is expected that if the weak interaction has non-local character, non-local effects may be prominent in the K_{e3} process, since the momentum transfer is very large; and a non-local effect of the lepton coupling may be represented in the effective interaction by a derivative of a lepton field.

This possibility was once discussed by Y. Miyachi [3]) and he obtained some interesting results. However, his analysis was carried out under the assumption that the effective coupling constants may be replaced by momentum independent constants. In this note the problem is discussed without making this approximation. The analysis shows that owing to the existence of a certain equivalence theorem between these two kinds of interaction the discrimination will be practically impossible. Next, we shall discuss the present experimental data on K_{e3}^{+} decay for each type of decay interaction. The analysis of the experimental results indicates that both scalar and tensor interactions are necessary.

2. The Possibility of Konopinski-Uhlenbeck Type Interaction

We start from the assumption that *the leptons are created at a vertex by a weak interaction which contains the derivative of the neutrino field*, while still keeping the assumption that the electromagnetic radiative correction which may violate the locality of neutrino and electron coupling may be omitted. With these assumptions the transition matrix element for K_{e3} decay can be written as follows:

$$\begin{aligned} M \propto\ & G^{V1}(l_0)\bar{\psi}^{(e)}(p)\psi^{(\nu)}(q)q_\rho k_\rho \varphi^*(l)\Phi(k) \\ & +G^{V2}(l_0)\bar{\psi}^{(e)}(p)\psi^{(\nu)}(q)q_\rho l_\rho \varphi^*(l)\Phi(k) \\ & +G^{T}(l_0)\bar{\psi}^{(e)}(p)(\gamma_\rho q_\sigma-\gamma_\sigma q_\rho)\psi^{(\nu)}(q)k_\rho l_\sigma \varphi^*(l)\Phi(k), \end{aligned} \tag{1}$$

where the notations are those of the previous articles [1,3]). We shall prove a certain equivalence between the Fermi type interaction and the Konopinski-Uhlenbeck type interaction with respect to the electron energy spectrum. The pion-electron energy correlation function derived from (1) is

$$\begin{aligned} \mathscr{D}^{K-U}(p_0, l_0) \propto\ & |G^{V1}(l_0)|^2(W_\pi-l_0)(m_K-l_0-p_0)^2 \\ & +|G^{V2}(l_0)|^2(W_\pi-l_0)(W_e-p_0)^2 \\ & +|G^{T}(l_0)|^2(W_\pi-l_0)^2 m_K\{2p_0(m_K-l_0-p_0)-m_K(W_\pi-l_0)\} \\ & +2\,\mathrm{Re}[G^{V1}(l_0)G^{V2*}(l_0)](W_\pi-l_0)(m_K-l_0-p_0)(W_e-p_0); \end{aligned} \tag{2}$$

here l_0 denotes the pion energy, p_0 the electron energy, m_K the mass of the K-meson, W_π the maximum available energy of the pion, and W_e the maximum available energy of electron; the mass of the electron is neglected.

A remarkable result is obtained if we compare this with the electron-pion energy correlation function for the Fermi type interaction (A—1):

$$\begin{aligned} \mathscr{D}^{F}(p_0, l_0) \propto\ & |F^{S}(l_0)|^2(W_\pi-l_0)+|F^{V}(l_0)|^2 m_K\{2p_0(m_K-l_0-p_0)-m_K(W_\pi-l_0)\} \\ & +|F^{T}(l_0)|^2 m_K{}^2(W_\pi-l_0)(m_K-l_0-2p_0)^2 \\ & +2\mathrm{Re}\,[F^{S}(l_0)F^{T*}(l_0)]m_K(W_\pi-l_0)(m_K-l_0-2p_0). \end{aligned} \tag{A—1}$$

In spite of the apparent difference between the structure of Fermi interaction and Konopinski-Uhlenbeck interaction, there is a certain correspondence between the spectra arising from them. As is easily seen from the expressions (2) and (A−1), an appropriate choice of G^{V1} and G^{V2} leads to the same spectrum as that given by F^S and F^T, and vice versa. The same relation exists between G^T and F^V. So long as we have no information on the effective coupling constants, which would require information about the strong interaction of the strange particles, we cannot distinguish one type interaction from the other with the help of the experimental data on the electron-pion energy spectrum. This equivalence can be more directly established between the matrix elements, and the proof is given in the appendix. It must be noted that this correspondence will no longer hold if the time reversal invariance is violated in the weak interaction participating in the K_{e3} decay process. In the case of maximum violation, for example, an electron energy spectrum with $R < 1$, where R is the ratio between high energy and low energy secondary electrons [1]), cannot be obtained for the Fermi type interaction, while such a spectrum is given by the Konopinski-Uhlenbeck type interaction.

These circumstances show that from the consideration of the K_{e3} and $K_{\mu 3}$ processes alone, the question whether the decay interaction is of the Fermi type or of the K−U type cannot be answered. The information obtained about one type of interaction can immediately be translated into the other type of interaction.

In the following analysis, we accordingly discuss only the case of Fermi interaction, since the hypothesis of a primary weak Fermi interaction seems to be successful to explain various weak processes such as the beta decay of the neutron or the muon-electron decay.

3. Comparison of the Fermi Type Interaction with the Experimental Data on K^+_{e3}

In this section we shall analyse the experimental data so far reported † and attempt to obtain information on the type of Fermi interaction without making any particular assumption about the effective coupling constants. We shall first examine the case of energy independent coupling constants in order to see the quantitative change resulting from the removal of restrictions on the effective coupling constants. The argument is always referred to sets of interactions rather than to pure interactions. We take S+T+(P) and V+(A) combinations to be in agreement with the sets often used in the analysis of the nuclear beta decay. It will be noted that for the V+A set the K_{e2} mode of decay is nearly forbidden. The nomenclature of the interactions

† These data are summarized in ref. [1]).

adopted here is the same as if the pseudoscalar K-meson would decay through parity conserving interaction; and the analysis of the K_{e3} decay process gives information only about the scalar, vector and tensor interactions. The results of the comparison of the theoretical values with the experimental data are given in table 1 and fig. 1. As is seen in table 1 and

TABLE 1

χ^2-probability of the theoretical electron energy spectrum in $K^{\pm}_{e3}$

Type of interaction		V+(A)	S+T+(P)
Energy dependence of effective coupling constant	F = const.	pure V: 0.004	pure S: < 0.0001 pure T: 0.03 mixed (S+T) †† 0.86
	F arbitrary	$F \approx \delta(W_\pi - l_0)$ †; 0.07	better fit than for constant F may be achieved

† Probably very close to the best fit when arbitrary choice is allowed for F. Curve V in fig. 1.
†† The ratio of effective coupling constants $F^S/F^T m_\pi^2 \approx 0.6$. Curve S+T in fig. 1.

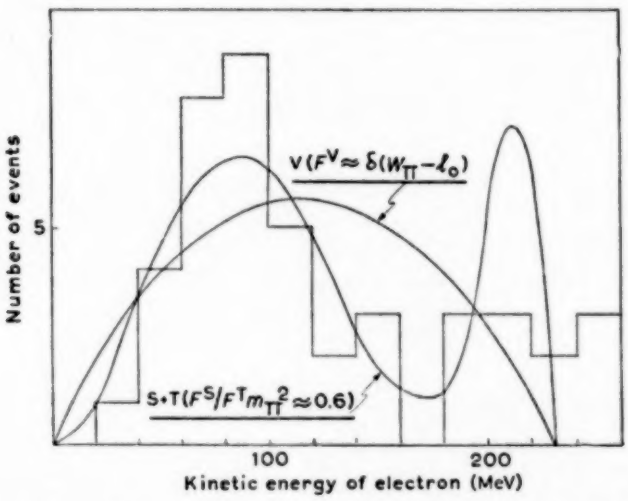

Fig. 1. The experimental and theoretical energy spectrum of electrons in the $K^{\pm}_{e3}$ decay process. The histogram indicates the experimental data (43 events). The theoretical curves are those of table 1.

fig. 1, if we make the approximation that the effective coupling constants are energy-independent, the pure vector and scalar interactions are almost excluded. The mixing of the scalar interaction with the tensor interaction gives a unique solution which is consistent with experiment. Other combinations of interactions do not give better fits. Thus, in this approximation, the S+T+(P) set is much more probable than the V+(A) set. It is difficult to estimate the amount of vector interaction which might be present besides S+T+(P); we give only an example. A curve for S+T probably very close to the best fit is obtained with $F^S/F^T m_\pi^2 \approx 0.6$. In this case, if we mix a

vector interaction with the coupling constant $F^V/F^T m_\pi \approx 1$ (the contribution from the vector interaction to the total transition probability is then nearly equal to that of S+T), the fit is reduced to a χ^2-probability 0.22.

Before we discuss the case of arbitrary effective coupling constants, it will be useful to refer to some simple features of the electron energy spectrum for fixed pion energy given by (A—1). The curves for pure interactions are given in fig. 2. The mutual relations among various types of interaction are

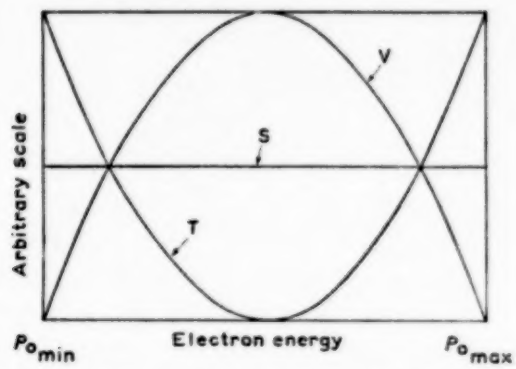

Fig. 2. Electron energy spectrum for fixed pion energy in K_{e3}. The maximum and minimum electron energies are given by $p_{o\,\mathrm{min}}^{\mathrm{max}} = \frac{1}{2}(m_K - l_0 \pm 1)$.

independent of the pion energy. It can be easily understood that a bimodal distribution is a feature which is characteristic for the tensor interaction even when F^T is not constant, if F^S and F^V have no singular energy dependence. (If F^S and F^V were singular, the bimodal feature would be very different from that indicated by the experiments: the second peak would be at 180 MeV.)

The main feature of the present data is the preponderance of low energy electrons over high energy ones. To obtain better agreement with the experimental data, it is necessary to shift the maximum towards the low energy side. This is possible if we choose a $F(l_0)$ that is large at high pion energy. The extreme case will be $F(l_0) \approx \delta(W_\pi - l_0)$.

When the assumption of energy independence of the coupling constants is removed, it is interesting to examine the vector interaction, since the S+T+(P) set can explain the experimental spectrum well on the assumption of energy independence of the effective coupling constants. However, even without this assumption, the fit of the vector interaction with the experimental data is never so much improved as to surpass that of the S+T combination. It gives at best a curve with χ^2-probability 0.07. Summarizing the results of this section, we may say that the chance of the S+T+(P) set is high, while the V+(A) set is rather improbable.

The present analysis cannot exclude the possibility of an V—A theory, since the χ^2 probability of the best fit, 0.07, is not small. However, it is

emphasized that the S+T interaction can give a good fit with the experimental data in the approximation of energy-independent constants while a strong energy dependence is required for the effective vector coupling constant to improve the fit at any rate with the present data. Although the theory of the universal V−A Fermi interaction [4]) is successful in explaining the strangeness-conserving weak processes, it is not clear whether all the strangeness non-conserving weak processes can be explained by the V−A Fermi interaction [5]). In this section we have found that the K_{e3} decay interaction provides some evidence against the V−A theory. Although the experimental data reported so far are scanty and unknown experimental biases which suppress the detection of the high energy electrons † may affect these data, this evidence against the V−A theory should be noticed and it is hoped that further experimental investigation will give a more definite answer. Finally, it is suggested that one possibility to explain the present features of the electron spectrum by the V−A theory would be to introduce a non-local Fermi interaction, in which both e−ν coupling and baryon-baryon coupling are non-local.

The author wishes to express his gratitude to S. Furuichi and S. Sawada for their kind co-operation. He also thanks Prof. H. Yukawa, Prof. K. Sakuma and Dr. S. Ogawa for the interest shown in this work. He is indebted to a Fellowship of the Yukawa Memorial Foundation for financial aid.

Appendix

EQUIVALENCE OF FERMI TYPE INTERACTION AND KONOPINSKI-UHLENBECK TYPE INTERACTION IN THE K_{e3} DECAY PROCESS.

The matrix elements for which equivalence is to be proved are ††

$$M^{F} \propto F^{S}\bar{\psi}^{(e)}(p)\psi^{(\nu)}(q)+F^{V}\bar{\psi}^{(e)}(p)\gamma_{\rho}\psi^{(\nu)}(q)k_{\rho} +F^{T}\bar{\psi}^{(e)}(p)\tfrac{1}{2}(\gamma_{\rho}\gamma_{\sigma}-\gamma_{\sigma}\gamma_{\rho})\psi^{(\nu)}(q)k_{\rho}l_{\sigma} \quad \text{(I)}$$

for Fermi type interaction, and

$$M^{K-U} \propto G^{V1}\bar{\psi}^{(e)}(p)\psi^{(\nu)}(q)k_{\rho}q_{\rho}+G^{V2}\bar{\psi}^{(e)}(p)\psi^{(\nu)}(q)l_{\rho}q_{\rho} +G^{T}\bar{\psi}^{(e)}(p)[\gamma_{\rho}q_{\sigma}-\gamma_{\sigma}q_{\rho}]\psi^{(\nu)}(q)k_{\rho}l_{\sigma}. \quad \text{(II)}$$

for K−U type interaction. In the K-meson rest system the energy dependence of the effective coupling constants $F^{S}\ldots$ and $G^{V1}\ldots$ is expressed in terms of the pion energy only. In this system, the equivalence can be easily verified by making use of the equations of motion for the electron and the neutrino in order to reduce (I) and (II):

† Even if we use the "unbiased" spectrum of the re-analysed data [6]) the discussion of this section will not suffer essential change.

†† In eq. (I), F^{T} differs in sign from the F^{T} of eq. (A−1).

$$M^{F} \propto [F^{S}-m_{K}(m_{K}-l_{0})F^{T}]\bar{\psi}^{(e)}\psi^{(\nu)}+2m_{K}\not{p}_{0}F^{T}\bar{\psi}^{(e)}\psi^{(\nu)} + [F^{V}+im_{e}F^{T}]\bar{\psi}^{(e)}\gamma_{\rho}\psi^{(\nu)}k_{\rho}, \tag{I'}$$

$$M^{K-U} \propto [-m_{K}(m_{K}-l_{0})(G^{V1}+im_{e}G^{T})-m_{K}W_{e}G^{V2}]\bar{\psi}^{(e)}\psi^{(\nu)} + [G^{V1}+G^{V2}+im_{e}G^{T}]m_{K}\not{p}_{0}\bar{\psi}^{(e)}\psi^{(\nu)} + m_{K}(W_{\pi}-l_{0})G^{T}\bar{\psi}^{(e)}\gamma_{\rho}\psi^{(\nu)}k_{\rho}. \tag{II'}$$

Comparison of (I') and (II') leads to the following necessary and sufficient conditions that Fermi type interaction should give the same physical effect as the K−U type interaction in the K_{e3} process:

$$\begin{aligned} (m_{K}-l_{0})(G^{V1}+im_{e}G^{T})+W_{e}G^{V2} &= (m_{K}-l_{0})F^{T}-F^{S}/m_{K}, \\ G^{V1}+G^{V2}+im_{e}G^{T} &= 2F^{T}, \\ m_{K}(W_{\pi}-l_{0})G^{T} &= F^{V}+im_{e}F^{T}. \end{aligned} \tag{III}$$

There always exist G^{V1} . . . satisfying (III) for given F^{S} . . ., and vice versa. A similar correspondence can be established for the case when parity violating interaction exists. These correspondences no longer hold if the weak interaction is non-invariant for time-reversal. It must be observed that these correspondences are superficial, in the sense that in reality $G^{T} \approx F^{T}$, $G^{V1} \approx F^{V}$, since they are the contributions from the baryon loops of the Feynman diagram.

References

1) S. Furuichi, S. Sawada and M. Yonezawa, Nuovo Cimento **10** (1958) 541
2) E. J. Konopinski and G. E. Uhlenbeck, Phys. Rev. **48** (1935) 7; see also H. A. Bethe and R. F. Bacher, Revs. Mod. Phys. **8** (1936) 82
3) Y. Miyachi, Prog. Theor. Phys. **19** (1958) 112
4) R. P. Feynman and M. Gell-Mann, Phys. Rev. **109** (1958) 193
5) S. Okubo *et al.*, Phys. Rev. **112** (1958) 665
6) M. Bruin *et al.*, Nuovo Cimento **9** (1958) 422

2.L *Nuclear Physics* **12** (1959) 596—605; © *North-Holland Publishing Co., Amsterdam*
Not to be reproduced by photoprint or microfilm without written permission from the publisher

INELASTIC SCATTERING OF HIGH ENERGY PROTONS BY HELIUM: AN EXCITED LEVEL?

PETER HILLMAN †, ARNE JOHANSSON, GUNNAR TIBELL†† and HELGE TYRÉN
The Gustaf Werner Institute for Nuclear Chemistry, University of Uppsala

and

H. S. KÖHLER
Theoretical Division, CERN, Geneva

Received 1 May 1959

Abstract: No clear evidence for the existence of an excited level has been found in an investigation of the energy spectra and polarizations of 185 MeV protons inelastically scattered by He^4 in the angular region $6.5°$—$43.5°_{lab}$. An upper limit of 0.02 mb · $sr^{-1}_{c.m.}$ has been obtained for the excitation of an excited level in the region 4—17 MeV excitation energy in $33.5°_{lab}$ scattering of these protons. A peak in the energy spectra is seen at all angles at 22.5 ± 0.4 MeV excitation energy, which is quite well fitted with a simple model of quasi-free nucleon-nucleon scattering with a final state interaction for which the parameter values required, however, seem anomalous.

1. Introduction

There have been many attempts to establish the existence of excited bound or virtual states in He^4, none apparently completely incontrovertible. The evidence from reactions at low energies has recently been summarized [1]), and seems to indicate the presence of at least one virtual level near the nucleon separation energies. However, no level was found when the energy spectra of inelastically scattered 32 and 40 MeV protons from He^4 were recorded at various angles [2,3,4]), the higher energy corresponding to a search up to 28 MeV excitation energy. If the excited level should correspond to some kind of single particle state, the probability of exciting it might be greater with nucleons of higher energy, for which the wavelength is short compared with the internucleon distance, and in any case the upper-limit cross sections for excitations below 28 MeV are not yet very low. For this reason the experiment on 185 MeV proton scattering, reported earlier [5]), has been repeated with improved techniques, the energy spectra have been recorded for a larger range of angles, and in addition the polarizations of the scattered protons have been measured at selected energies and angles.

† CERN (European Organization for Nuclear Research, Theoretical Study Division). Now at SC Division, CERN, Geneva.
†† Now at SC Division, CERN, Geneva.

2. Method and Apparatus

In order to improve the earlier preliminary measurements [5]), performed with a pressure gas target, a cryostatic target was built. Its greater helium density and thinner walls made possible measurements at larger and at smaller angles, background being minimized.

The cryostat was conventional in design. Starting at liquid air temperature about 5 litres of liquid helium poured into the cryostat filled the $3\frac{1}{2}$ litre reservoir, which then lasted 48 hours. The level was monitored with carbon resistor thermometers. The target container was a 33 mm diameter horizontal cylinder of 0.02 mm nickel with its axis always perpendicular to the bisector of the scattering angle.

The proton energies were analysed in a 90° magnetic spectrometer [6]), giving a resolution of 1.8 MeV full width at half height (increasing at the larger angles to 2.5 MeV at 33.5° and 3.0 MeV at 43.5°). At selected energies and angles the protons emerging from the magnet were rescattered by carbon into two symmetrically placed counters, to determine their polarization [7]). The equipment is described in ref. [6]).

The counting rate with empty target container was measured at a few selected points, and generally was a large fraction of the counting rate between the elastic and inelastic helium peaks with filled target container. The residue might be due to elastically scattered particles slowed down in slits, etc. Contamination of the helium was minimized by careful filling procedures and should be negligible.

The methods of converting the spectra to energy and cross section scales, of calibrating the polarization analyser, and of correcting and estimating errors on all data were essentially as described in ref. [6]) and [7]), except that absolute cross sections were obtained by normalizing to the gas chamber data [5]).

3. Results

The energy spectra are shown in fig. 1. Except for the case of 6.5° no background subtraction has been made. Statistical errors are indicated on typical points, and should be the total relative errors within each spectrum. Absolute errors should be less than 20 %, and the relative errors among the spectra somewhat less. The position of the inelastic peak at all angles is 22.5 ± 0.4 MeV. The proton and neutron separation energies, 19.8 and 20.6 MeV respectively, are indicated on all spectra, as are the energies which the scattered protons would have had from free nucleon-nucleon collisions. Fig. 2 shows the height of the inelastic peak near 22 MeV *versus* scattering angle, as taken directly from fig. 1. The angle at which protons from free nucleon-nucleon collisions would have lost 22 MeV is indicated.

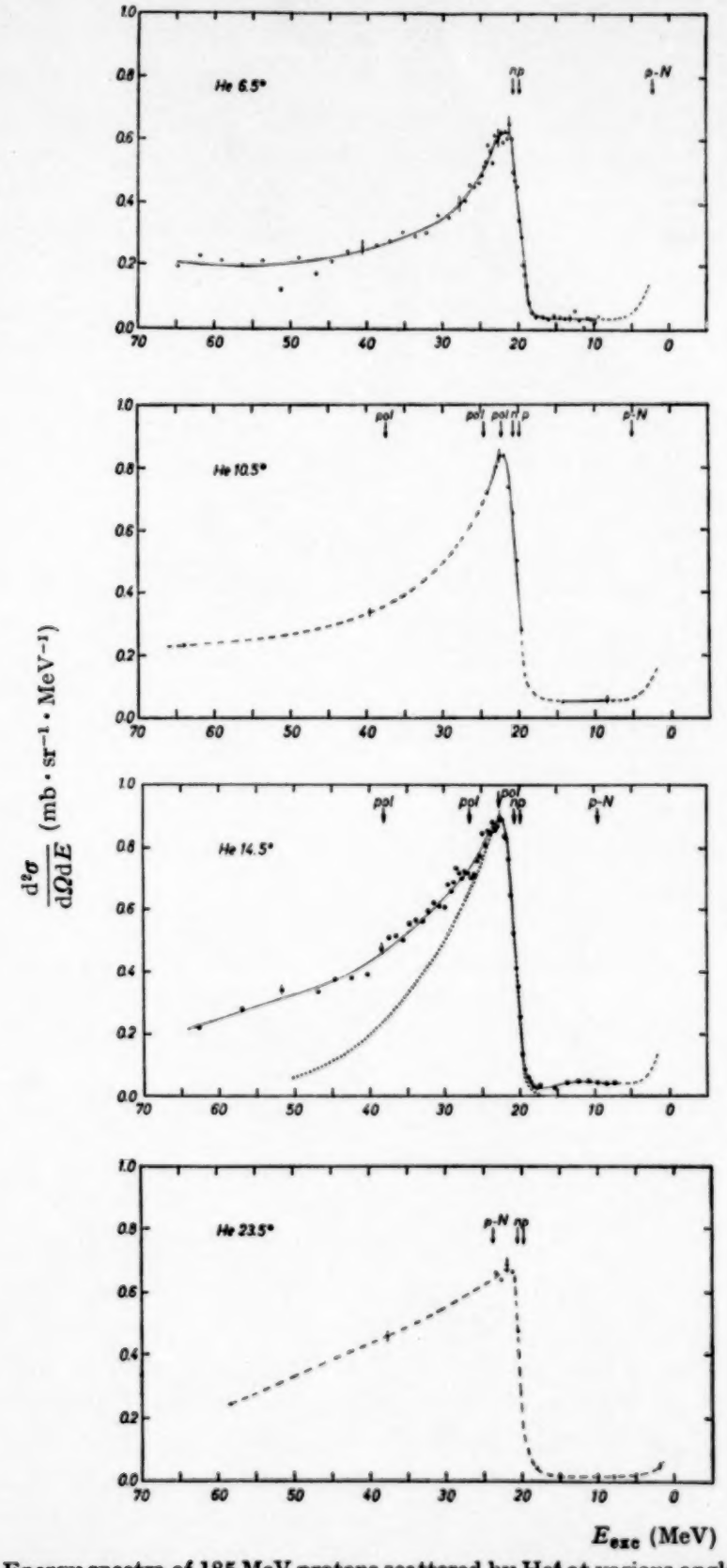

Fig. 1. Energy spectra of 185 MeV protons scattered by He^4 at various angles. Note the change in cross section scale in the last two diagrams. Arrows indicate neutron and proton separation energies (labelled 'n' and 'p'), the energy the scattered proton would have had from a collision with a free nucleon (marked 'p-N'), and the positions at which polarizations were measured (labelled 'pol'). Dotted curves are theoretical, with experimental energy resolution folded in.

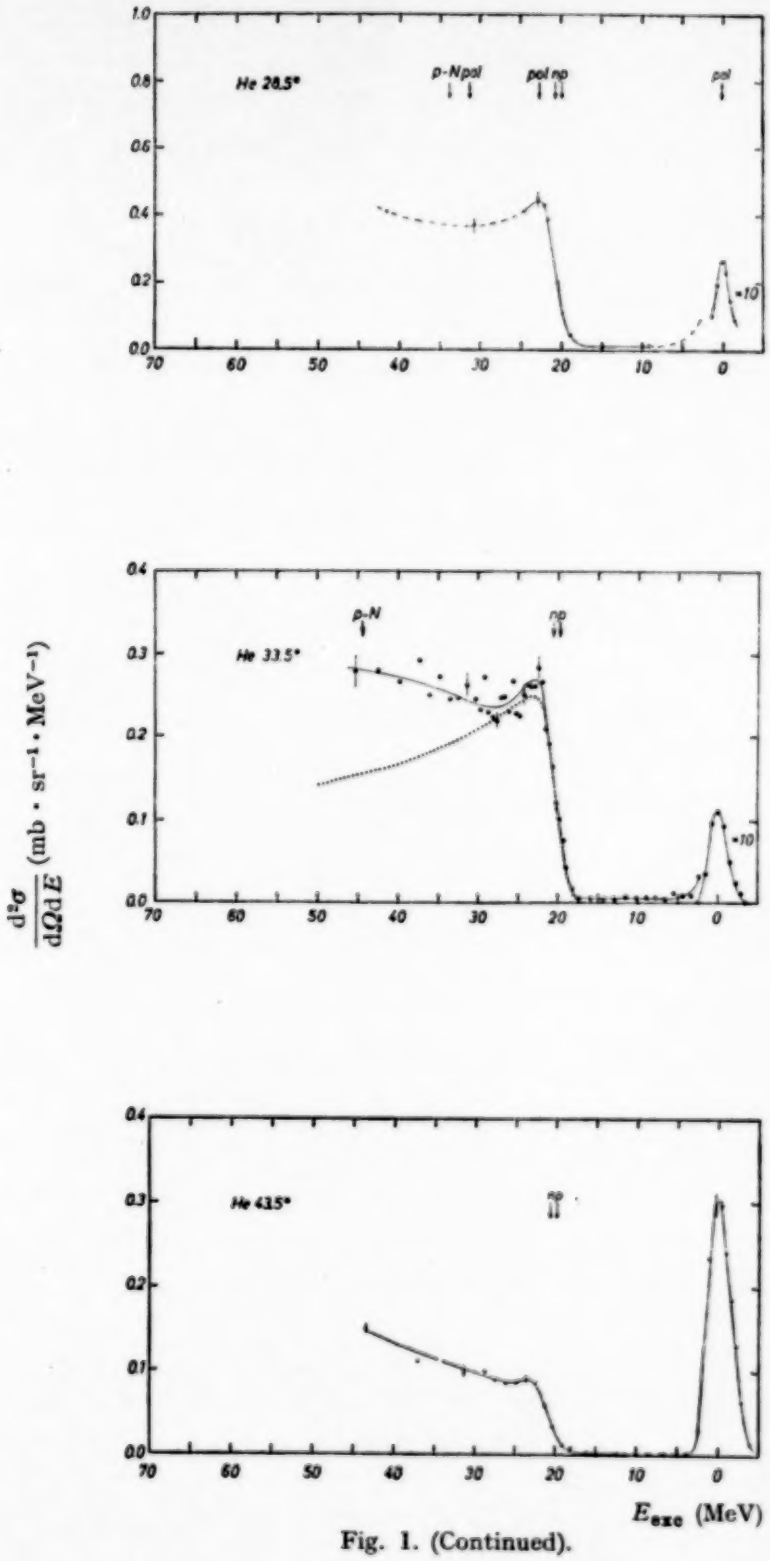

Fig. 1. (Continued).

Measurements of the polarizations of the scattered protons were made at 9.0°, 18.2°, and 28.5°, at points indicated by arrows on the nearest spectra, 10.5°, 14.5° and 28.5° respectively of fig. 1. The results are given in table 1 with only statistical errors indicated; other errors should be small. Also shown in table 1 are values of the elastic helium polarization (taken from Wilson [8]) where not measured) and weighted means of published p-n and p-p polarizations.

From fig. 1 we estimate that a sharp peak with an excitation cross section of 0.02 mb · $sr^{-1}_{c.m.}$ between 4 and 17 MeV excitation energies would have had a 90 % probability of being seen in the 33.5°$_{lab}$ spectrum. (The c.m.

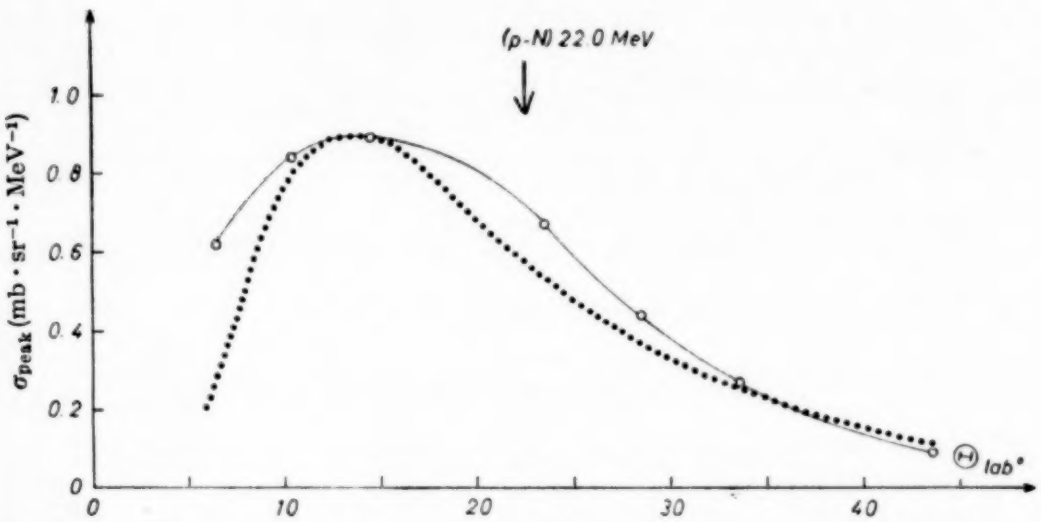

Fig. 2. The height of the inelastic peak near 22 MeV excitation energy in 185 MeV proton scattering from He^4. Arrow indicates angle at which 185 MeV protons would lose 22 MeV in collisions with free nucleons. Dotted curve is theoretical, with experimental energy resolution folded in.

angle corresponding to this lab angle varies from 42.6° to 43.2° as the excitation energy goes from 0 to 22 MeV.) For comparison, Benveniste and Cork [2])

TABLE 1

Polarizations in percent of 185 MeV protons scattered by He^4 at various angles and energy losses.

Energy Group	Laboratory Angle		
	9.5°	18.5°	28.5°
Peak	15±15	28±13	17±20
Slope or dip	11±21	37±14	–
Continuum	36±27	1±21	4±23
Elastic	(40)	(80)	61±12
Free p-N	(14)	(29)	(33)

Bracketed values are from experiments by other workers.

obtained an upper limit of 0.1 mb · $sr^{-1}_{c.m.}$ for excitations up to 23.3 MeV in 32 MeV proton scattering at $45°_{c.m.}$, and Eisberg [4]) obtained 0.25 mb · $sr^{-1}_{c.m.}$ for 23—28 MeV excitations in 40 MeV proton scattering at $65°_{c.m.}$.

We might note also that, taking background into account, we set an upper limit of 0.003 mb · $sr^{-1}_{c.m.}$ · MeV^{-1} on the average cross section at $33.5°_{lab}$ in the region 4—17 MeV.

4. Theory and Discussion

In inelastic scattering of 20—40 MeV protons one generally expects collective levels to be preferentially excited because of the long wave lengths of the protons [9]). Protons of 180 MeV have much shorter wavelengths and greater mean free paths in nuclear matter, and are therefore more likely to undergo single nucleon-nucleon collisions inside nuclei, and thus to excite single-particle levels. The fact that no inelastic scattering is observed below 17 MeV in either our experiment or in the lower energy ones makes the existence of any kind of level up to at least 17 MeV very unlikely. (Our experiment is sensitive to peaks 1 % of the size typically found in other elements [10])).

It is of great interest to know whether or not the peak which persists at all angles at 22.5 MeV in the energy spectra might indicate the presence of a virtual level. For this purpose we have calculated the spectrum of protons to be expected from the following simple model.

We consider the inelastic scattering to be a free nucleon-nucleon collision with the struck nucleon having a certain momentum distribution at the time of the collision due to its binding in the nucleus, and having a final state interaction with the residual (assumed unexcited) H^3 or He^3 nucleus. We neglect the distortion of the high energy proton wave by the nucleus before and after the localized elementary collision.

If the indices 0, 1, 2, 3, and 4 label respectively the high energy proton, the knocked out nucleon, and the residual nucleons, and $\mathbf{p}$ and $\mathbf{k}$ are the laboratory system momenta before and after the elementary collision, the transition matrix element becomes

$$T = \langle \phi_f(\mathbf{k}_1\mathbf{k}_2\mathbf{k}_3\mathbf{k}_4)\mathbf{k}_0|t(\mathbf{q})|\phi_i(\mathbf{p}_1\mathbf{p}_2\mathbf{p}_3\mathbf{p}_4)\mathbf{p}_0\rangle$$

where as usual we have approximated t as a function of momentum transfer $\mathbf{q} = \mathbf{k}_0 - \mathbf{p}_0$. We also assume the wave functions of particles 2, 3 and 4 to be unaffected by the elementary collision (impulse approximation), so that integration over their momenta just gives a normalization constant. Integration over $\mathbf{p}_1$ gives, assuming momentum conservation in the elementary scattering,

$$T \propto \int \phi_f^*(\mathbf{k}_1)t(\mathbf{q})\phi_i(\mathbf{q}+\mathbf{k}_1)d\mathbf{k}_1.$$

Because of the final state interaction, $\mathbf{k}_1$ does not have a sharp value. We now make the approximation that $\mathbf{k}_1$ has an average value $\mathbf{K}$, the wave number that would result if the scattering took place in an infinite medium. If we assume that $t(\mathbf{q})\phi_1(\mathbf{q}+\mathbf{k}_1)$ varies slowly with $\mathbf{k}_1$, we can write

$$T \propto t(\mathbf{q})\phi_1(\mathbf{q}+\mathbf{K})\int \phi_f^*(\mathbf{k}_1)\mathrm{d}\mathbf{k}_1$$
$$\propto t(\mathbf{q})\phi_1(\mathbf{q}+\mathbf{K})\phi_f^*(r=0)$$

where $\phi(r)$ is the Fourier transform of $\phi(\mathbf{k})$.

We now represent the final state interaction as an s-state interaction with a square well of radius r_0 and depth V. Then

$$\phi_f(r) = \frac{K}{s}\frac{\sin(sr_0+\delta)}{\sin Kr_0}\frac{\sin Kr}{Kr} \quad (r<r_0),$$

where δ is the s-wave phase-shift and $\mathbf{s}$ the final relative momentum of the struck nucleon. We also neglect Coulomb effects in setting equal the p—H^3 and n—He^3 interactions, which should be satisfactory above 1—2 MeV. Assuming for simplicity the struck and residual nuclei to be infinitely heavy, and summing over final states consistent with final energy E of the high energy proton with initial energy E_0, we obtain for the cross section

$$\frac{\mathrm{d}^2\sigma}{\mathrm{d}\Omega\,\mathrm{d}E} \propto \left(\frac{E}{E_0}\right)^{\frac{1}{2}} |\phi_f(r=0)|^2\bar{\sigma}(\vartheta)\int \mathrm{d}\mathbf{s}\delta\left(p_0^2-k_0^2-s^2-\frac{2MB}{\hbar^2}\right)|\phi_1(\mathbf{k}_0-\mathbf{p}_0+\mathbf{K})|^2$$

where B is the binding energy of a nucleon in He^4 (assumed equal for neutron and proton $=\frac{1}{2}(19.8+20.6)=20.2$ MeV), M is the nucleon mass, and $\bar{\sigma} \propto \sum_{n=1}^{4}|t_n(\mathbf{q})|^2$ is the average of the proton-proton and proton-neutron cross sections at energy E_0+V, where the sum is taken over the nucleons in He^4. Note that the magnitude of $\mathbf{s}$ is fixed by the δ-function.

We now set $\mathbf{s}/s = \mathbf{K}/K$, neglecting refraction at the edge of the potential. We also neglect $V-B$ in the δ-function and integrate over K as in Wolff's paper [11]), obtaining

$$\frac{\mathrm{d}^2\sigma}{\mathrm{d}\Omega\,\mathrm{d}E} \propto A\left(\frac{E}{E_0}\right)^{\frac{1}{2}}\bar{\sigma}(\vartheta)\int_{p_{\min}}^{\infty}\frac{N(p)p\mathrm{d}p}{q}$$

where

$$A = \frac{K}{s}\frac{\sin^2(sr_0+\delta)}{\sin^2 Kr_0}, \quad p_{\min} = (k_0-p_0\cos\vartheta)\cot\vartheta$$

(laboratory angles), and $N(p) = |\phi_1(\mathbf{k}_0-\mathbf{p}_0+\mathbf{K})|^2$ is the nucleon momentum distribution in He^4. Fitting the wave function at the nuclear surface gives $s\cot(sr_0+\delta) = K\cot Kr_0$ so that

$$A = \frac{Ks}{s^2+K_0^2\cos^2 Kr_0}$$

where $K^2-s^2 = K_0^2 = 2MV/\hbar^2$. For small s, we can expand K about K_0, and if we introduce the concept of a scattering length a, which for a square well is given by [12]) $aK_0 = r_0K_0 - \tan r_0K_0$, the s-dependence of A can be written as

$$A \propto \frac{s}{s^2+\gamma^2}$$

where $\gamma^{-2} = a(a-r_0)+(1/2K_0^2)$. For zero-range final state interaction, $r_0 \to 0$ and $K_0 \to \infty$, so that we would have

$$A \propto \frac{s}{s^2+a^{-2}}$$

which is the form given by Watson [13]).

Our final equation is then

$$\frac{\mathrm{d}^2\sigma}{\mathrm{d}\Omega \mathrm{d}E} \propto \frac{s}{s^2+\gamma^2}\left(\frac{E}{E_0}\right)^{\frac{1}{2}} \bar{\sigma}(\vartheta) \int_{p_{\min}}^{\infty} \frac{N(p)p\mathrm{d}p}{q}.$$

The cross section is calculated from this formula for the experimental angles with $V = 40$ MeV, $r_0 = 2\times 10^{-13}$ cm, and for Gaussian momentum distributions $N(p) = 8\pi^{\frac{3}{2}}\beta^{-\frac{1}{2}} \exp(-p^2/\beta^2)$ with values of $\beta^2\hbar^2/2M$ of 18 MeV and 5 MeV, the former being typical of heavier elements including carbon [14]), while there is some indication that the latter value is better for helium [15]). The free parameter γ is fixed by fitting to the experimental peak energy after the experimental resolution is roughly folded into the theoretical curves, and, for the momentum distribution with $\beta^2\hbar^2/2M = 18$ MeV, gives values of the scattering length $a = 4.6$ or -2.6 in units of 10^{-13} cm with an error of about 20 %. Finally the curves are normalized by fitting the peak heights at 14.5 °.

Examples of the resultant curves for $a = 4.6\times 10^{-13}$ cm and a 1/e value of 18 MeV for the Gaussian momentum distribution of the struck nucleon are shown in fig. 1 for 14.5 °and 33.5°, and the angular distribution of the peak height is shown in fig. 2. The results for a 1/e value of 5 MeV taken as a whole are not clearly better or worse. The peak height drops off much more rapidly at small angles but does not strongly change at larger angles. The energy spectra at small angles also become worse, the theoretical curves falling off even more rapidly with increasing excitation energy, but at large angles a steeper rise brings the theoretical curves closer to the experimental.

Considering the simplicity of the model, the theoretical curves fit the experimental results quite well, and the remaining appreciable discrepancies seem to have simple explanations. Firstly, the too rapid fall-off of the theoretical peak height angular distribution at small angles may be explainable by our omission of the distortion of the incident and scattered high-energy proton waves in the nucleus. Similar effects have been predicted for

carbon by MacCauley [16]), for example. With regard to the too rapid experimental rise of the cross section with increasing excitation energy at the large angles, it is quite likely that this is due to the onset of the (p, pd), (p, 2pn) and complete breakup reactions between 24 and 28 MeV. The cross sections for these reactions should be more isotropic than those of the (p, 2p) and (p, pn) reactions, so that their relative contributions to the small-angle results will be smaller. In addition, the scattering length concept, as well as the approximations we have made, should not be valid for kinetic energies of the knocked-out nucleon of more than a few MeV, especially if the scattering length is not allowed to vary with energy.

The fact that we have obtained a reasonable fit with experiment from our simple theory does not necessarily imply the absence of an excited level in He^4 near 22 MeV. The values of the scattering lengths we have obtained for the nucleon — H^3 or —He^3 interaction differ from that to be expected from the square well parameters we have assumed, which is 2.4×10^{-13} cm, or from interpolation among neighbouring light elements [17]). It is not clear without further calculation what effect the large He^3(n, p) cross section or an appreciable p-wave interaction for instance could have on changing the effective scattering length. However, we simply note that an equally good fit with the experimental results could have been obtained with a value of the scattering length near 2.4×10^{-13} cm and a small superposed resonance ($\lesssim 30\,\%$) at 22 MeV corresponding to an excited He^4 state. The good angular distribution fit of the peak height might not be affected, since the angular distributions of most excited state resonances are similar [10]). The upper limit we can put on excitation (in 33.5 ° scattering) of an excited level in He^4 in the region from 17 MeV to the breakup energy grades from 0.02 mb · $sr^{-1}_{c.m.}$ at 17 MeV to about 0.3 mb · $sr^{-1}_{c.m.}$ at 22 MeV, then decreases slowly towards the breakup energy of 28 MeV.

Our polarization measurements do not resolve the problem. The polarizations of protons inelastically scattered from various light elements leaving them in specific levels frequently are very high, and in fact at small angles follow the trend of the elastic polarizations [7]). For helium, we see from table 1 that the polarizations of the various inelastic groups (on and off the peak) are consistent with each other and with the appropriately averaged free proton-nucleon values, as might be expected for a free final state of the struck nucleon [18]), and are definitely smaller than the elastic polarizations. However, a 30 % contribution of the elastic polarizations is not excluded.

5. Conclusion

No clear evidence for the existence of an excited level in He^4 has been found from cross section and polarization measurements on inelastic high

energy proton scattering up to the break-up energy. It is very unlikely that there is any level below 17 MeV, but a level near 22 MeV is not excluded pending further calculations †.

We thank Prof. The Svedberg for encouragement. We are very grateful to Prof. J. Linde and Mr. C. Svensson of the Royal Institute of Technology for liquefying the helium and for providing much technical aid and advice. Dr. Th. A. J. Maris contributed many helpful discussions. Thanks are also due to Prof. R. Wilson for informing us about his results on proton scattering by helium before publication. The work was supported by the Swedish Atomic Energy Commission.

† After the above paper was completed, an article on 95 MeV proton scattering from helium by Selove and Teem [19]) was received. They present inelastic spectra at three angles, and reach qualitative conclusions that are similar to some of ours.

References

1) Bergman, Isakov, Popov and Shapiro, Soviet Physics JETP **6** (1958) 6;
Vlasov, Kalinin, Oglobin, Samoilov, Sidorov and Chuev, Soviet Physics JETP **1** (1955) 500
2) J. Benveniste and B. Cork, Phys. Rev. **89** (1953) 422
3) A. F. Wickersham, UCRL-2662 (1954) unpublished
4) R. M. Eisberg, Phys. Rev. **102** (1956) 1104
5) Tyrén, Tibell and Maris, Nuclear Physics **4** (1957) 277
6) H. Tyrén and Th. A. J. Maris, Arkiv för Fysik **13** (1957) 609
7) Hillman, Johansson and Tyrén, Nuclear Physics **4** (1957) 648
8) R. Wilson, Proceedings of the 1958 Annual International Conference on High Energy Physics at CERN (Geneva 1958) 57
9) B. L. Cohen and A. G. Rubin, Phys. Rev. **111** (1958) 1568
10) H. Tyrén and Th. A. J. Maris, Nuclear Physics **4** (1957) 637
11) P. A. Wolff, Phys. Rev. **87** (1952) 434
12) R. G. Sachs, Nuclear Theory (Addison-Wesley 1953) p. 71
13) K. Watson, Phys. Rev. **88** (1953) 1163
14) Cladis, Hess and Moyer, Phys. Rev. **87** (1952) 425;
J. M. Wilcox and B. Moyer, Phys. Rev. **99** (1955) 875
15) W. F. Stubbins, UCRL-8501 (1958) unpublished
16) G. P. MacCauley, Proc. Phys. Soc. **73** (1959) 309
17) R. K. Adair, Phys. Rev. **94** (1954) 737
18) H. S. Köhler, Nuclear Physics **9** (1958/59) 49;
L. Marshall, Phys. Rev. **99** (1955) 1033
19) W. Selove and J. M. Teem, Phys. Rev. **112** (1959) 1658

1.B:6.D *Nuclear Physics* **12** (1959) 606—611; © *North-Holland Publishing Co., Amsterdam*
Not to be reproduced by photoprint or microfilm without written permission from the publisher

PHENOMENOLOGICAL TWO-NUCLEON POTENTIALS AND THE DEUTERON, II

K. V. LAURIKAINEN and O. VARHO †
Institute of Physics, University of Turku, Turku, Finland

Received 25 April 1959

Abstract: The ground state of the deuteron corresponding to Gammel and Thaler's potential has been investigated by numerical integration. There exists no exact ground state in the neighbourhood of the right binding energy. An approximate ground state wave function has been tabulated and the corresponding electromagnetic properties of the deuteron have been studied, including the correction to the magnetic moment due to the LS-potential.

In a previous paper [1]) one of us (K. V. L.) tried to estimate the properties of the ground state of the deuteron corresponding to the phenomenological two-nucleon potential proposed by Gammel and Thaler [2]). Because of the simplifications made in this estimate, only some preliminary results could be obtained. Later, more exact calculations have been done by using the same variational procedure [3]), but the trial functions used so far have not given quite satisfactory convergence in this case. Therefore, we have carried out the calculation by using numerical integration and employing the IBM 650 machine. We have paid special attention to the influence of the LS-term in Gammel and Thaler's potential (called "GT-potential" in the following) upon the properties of the ground state of the deuteron.

1. The Ground State of the Deuteron Corresponding to the GT-Potential

The radial components of the ground state wave function of the deuteron (ϕ_0 and ϕ_2) are in the following considered as functions of the dimensionless quantity

$$x = \frac{r}{\alpha}, \tag{1}$$

α being some unit of length. The equation system which determines the functions $\phi_0(x)$ and $\phi_2(x)$ in the case of the GT-potential can be written in the form

† The Finnish Board for Computing Machinery.

$$\frac{d^2\phi_0}{dx^2} = \left(k^2 - b_1 \frac{e^{-\mu_1 x}}{\mu_1 x}\right)\phi_0 - 2\sqrt{2} b_2 \frac{e^{-\mu_2 x}}{\mu_2 x}\phi_2,$$
$$\frac{d^2\phi_2}{dx^2} = \left(k^2 + \frac{6}{x^2} - b_1 \frac{e^{-\mu_1 x}}{\mu_1 x} + 2b_2 \frac{e^{-\mu_2 x}}{\mu_2 x} + 3\chi \frac{e^{-\mu_3 x}}{\mu_3 x}\right)\phi_2 - 2\sqrt{2} b_2 \frac{e^{-\mu_2 x}}{\mu_2 x}\phi_0. \tag{2}$$

where all quantities are dimensionless and where the constants can be expressed by using the constants of the potential, the reduced mass m, and the binding energy B of the deuteron as follows:

$$\mu_1 = \alpha^3 \mu_C^+, \qquad \mu_2 = \alpha^3 \mu_T^+, \qquad \mu_3 = \alpha^3 \mu_{LS}^+,$$
$$b_1 = \frac{2m\alpha^2}{\hbar^2} {}^3V_C^+, \qquad b_2 = \frac{2m\alpha^2}{\hbar^2} {}^3V_T^+, \qquad \chi = \frac{2m\alpha^2}{\hbar^2} {}^3V_{LS}^+, \tag{3}$$
$$k^2 = \frac{2m\alpha^2}{\hbar^2} B.$$

In our calculations we have chosen $\alpha = 10^{-13}$ cm. The cut off radius expressed on the x-scale is then

$$x_0 = \frac{{}^3\gamma_0^+}{\alpha} = 0.4. \tag{4}$$

Above a given limit M, the wave functions have been approximated by the asymptotic expressions

$$\phi_0 = de^{-kx}, \quad \phi_2 = e^{-kx}\left(k^2 + \frac{3k}{x} + \frac{3}{x^2}\right), \tag{5}$$

where d is the "mixing parameter" closely related to the quadrupole moment Q. The value $M = 10$ was found sufficiently large, and beginning from this upper limit the functions ϕ_0 and ϕ_2 were calculated by using the Runge-Kutta-Gill numerical integration method [4]). The parameters k and d have then to be chosen so as to satisfy the boundary conditions

$$\phi_0 = \phi_2 = 0 \quad \text{at} \quad x = x_0. \tag{6}$$

When using the GT-potential it was found, however, that it is impossible to satisfy both conditions (6) simultaneously, at least if the energy parameter k is not exceedingly far from the value $k = 0.232$ corresponding to the correct binding energy. *Thus no ground state of the deuteron would exist, if the* n—p-*interaction exactly corresponded to the* GT-*potential* †. If, instead, the conditions (6) are only approximately satisfied, it is possible to construct *approximate* wave functions for the deuteron, and then the energy parameter can be varied within a rather large interval around the value $k = 0.232$. In fact, the Jacobian $\partial(\phi_0, \phi_2)/\partial(k, d)$ vanishes almost exactly for the values in question, and therefore ϕ_0 (0.4) and ϕ_2 (0.4) are dependent on each other;

† A possible ground state corresponding to a quite wrong binding energy has no physical meaning.

TABLE 1

Approximate wave function for the ground state of the deuteron corresponding to the GT-potential

$$\Psi = \sqrt{\frac{\alpha}{4\pi}} \frac{\Phi_0 + \frac{1}{\sqrt{8}} \Phi_2 S_{12}}{r} \chi_1^m.$$

x	Φ_0	Φ_2	x	Φ_0	Φ_2
Hard core radius: $x_0 = 0.4$			5.1	0.697	0.0919
			5.2	0.681	0.0879
			5.3	0.666	0.0841
0.4	−0.0033	0.552	5.4	0.650	0.0805
0.5	0.293	0.325	5.5	0.636	0.0771
0.6	0.528	0.279	5.6	0.621	0.0739
0.7	0.721	0.291	5.7	0.607	0.0708
0.8	0.880	0.322	5.8	0.593	0.0679
0.9	1.009	0.356	5.9	0.579	0.0652
1.0	1.111	0.386	6.0	0.566	0.0625
1.1	1.191	0.411	6.1	0.553	0.0600
1.2	1.251	0.428	6.2	0.540	0.0576
1.3	1.295	0.439	6.3	0.528	0.0554
1.4	1.325	0.445	6.4	0.516	0.0532
1.5	1.344	0.445	6.5	0.504	0.0512
1.6	1.354	0.541	6.6	0.493	0.0492
1.7	1.357	0.433	6.7	0.481	0.0473
1.8	1.353	0.423	6.8	0.470	0.0455
1.9	1.345	0.411	6.9	0.459	0.0438
2.0	1.332	0.398	7.0	0.449	0.0422
2.1	1.317	0.384	7.1	0.439	0.0406
2.2	1.299	0.369	7.2	0.429	0.0392
2.3	1.280	0.354	7.3	0.419	0.0377
2.4	1.259	0.339	7.4	0.409	0.0364
2.5	1.237	0.323	7.5	0.400	0.0351
2.6	1.214	0.309	7.6	0.391	0.0338
2.7	1.191	0.294	7.7	0.382	0.0326
2.8	1.168	0.280	7.8	0.373	0.0315
2.9	1.144	0.267	7.9	0.364	0.0304
3.0	1.120	0.254	8.0	01356	0.0293
3.1	1.097	0.241	8.1	0.348	0.0283
3.2	1.074	0.230	8.2	0.340	0.0273
3.3	1.050	0.218	8.3	0.332	0.0264
3.4	1.028	0.208	8.4	0.324	0.0255
3.5	1.005	0.197	8.5	0.317	0.0247
3.6	0.983	0.188	8.6	0.310	0.0238
3.7	0.961	0.179	8.7	0.303	0.0230
3.8	0.940	0.170	8.8	0.296	0.0223
3.9	0.919	0.162	8.9	0.289	0.0215
4.0	0.898	0.154	9.0	0.282	0.0208
4.1	0.878	0.147	9.1	0.276	0.0202
4.2	0.858	0.140	9.2	0.269	0.0195
4.3	0.838	0.133	9.3	0.263	0.0189
4.4	0.819	0.127	9.4	0.257	0.0183
4.5	0.801	0.121	9.5	0.251	0.0177
4.6	0.783	0.116	9.6	0.246	0.0171
4.7	0.765	0.110	9.7	0.240	0.0166
4.8	0.747	0.105	9.8	0.234	0.0161
4.9	0.730	0.101	9.9	0.229	0.0156
5.0	0.714	0.0961	10.0	0.224	0.0151

For $x > 10$ use asymptotic expressions (5) with $k = 0.232$, $d = 2.2776$. The wave function given in this table is not normalized. For normalization divide Φ_0 and Φ_2 by $N^{\frac{1}{2}}$, where

$$N = \int_0^\infty (\Phi_0^2 + \Phi_2^2) dx = 6.76.$$

and, on the other hand, every change in the value of k can be compensated for by a suitable variation of d. The smallest *common* value of ϕ_0 and ϕ_2 at $x = 0.4$ is $+0.11$. Detailed calculations have been carried out for $k = 0.232$ and $d = 2.2776$. For this choice ϕ_0 satisfies condition (6) ($\phi_0(0.4) = -0.0033$), while $\phi_2(0.4) = +0.552$. The corresponding functions, $\phi_0(x)$

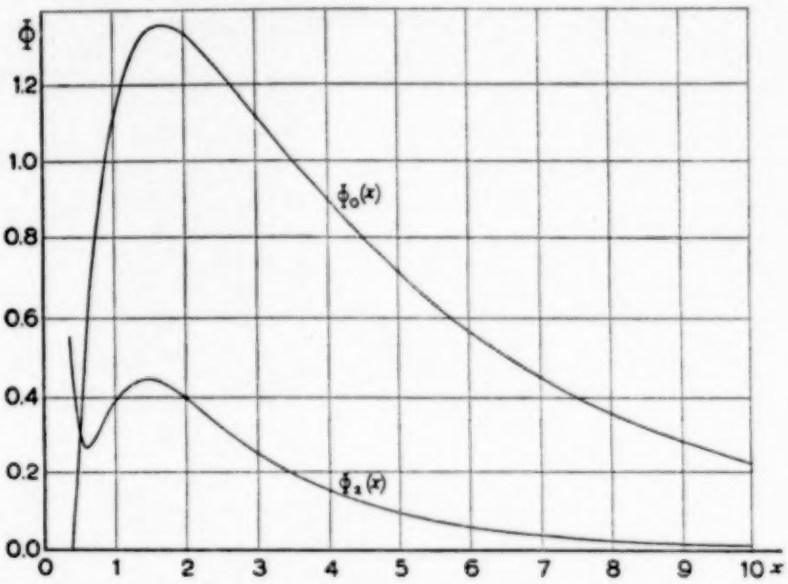

Fig. 1. Approximate wave function for the ground state of the deuteron corresponding to the GT-potential (see table 1).

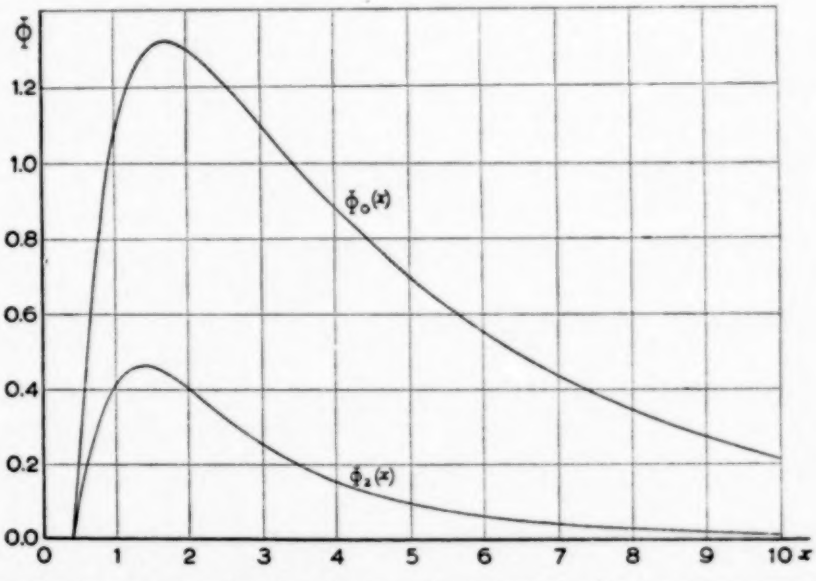

Fig. 2. Approximate wave function for the ground state of the deuteron corresponding to the "abridged" GT-potential (without the LS-term).

and $\phi_2(x)$, are given in table 1 and also graphically in fig. 1. The corresponding values of the quadrupole moment Q and the D-state probability p_D are

$$Q = 2.63 \times 10^{-27}\ \text{cm}^2, \quad p_D = 6.3\ \%. \tag{7}$$

Hence the quadrupole moment is 4.1 % smaller than the experimental value, and this illustrates the accuracy of the GT-potential as applied to the deuteron.

It should be mentioned that the conditions (6) can be satisfied for $x_0 = 0.345$ by choosing, for instance, $k = 0.2315$, $d = 2.288$.

2. The Influence of the Spin-Orbit Interaction upon the Deuteron

As contradictory estimates have been published of the influence of a spin-orbit force upon the binding energy of the deuteron [5,6]), we have done some calculations by dropping the LS-term of the GT-potential and leaving the other terms unchanged. If k is taken $= 0.232$, both functions, ϕ_0 and ϕ_2, can be brought to vanish simultaneously at $x = 0.4$ by choosing $d = 2.2263$. In this case the following results are obtained:

Given quantities: $k = 0.232$, $d = 2.2263$, $\alpha = 10^{-13}$ cm.

Values of ϕ_0 and ϕ_2 at $x = 0.4$:

$$\phi_0(0.4) = -0.00057, \quad \phi_0(0.4) = +0.00236.$$

The quadrupole moment corresponding to this wave function:

$$Q = 2.93 \times 10^{-27} \text{ cm}^2.$$

From the point of view of the deuteron the potential thus becomes more satisfactory when the LS-term is dropped. This is not quite unexpected, when we consider how the potential has been constructed (ref. [2]), p. 1337).

Even the "abridged" potential (without the LS-term) does not uniquely determine the ground state of the deuteron: a change in the energy parameter k can be compensated for, at least within a rather wide interval, by changing the mixing parameter d. Thus, it is impossible to say how much the LS-term changes, say, the binding energy. But if the energy parameter is taken as fixed, one can determine how much the quadrupole moment is changed by dropping the LS-term:

The value of the deuteron quadrupole moment corresponding to $k = 0.232$ when applying the GT-potential without the LS-term:

$$Q = 2.93 \times 10^{-27} \text{ cm}^2.$$

The same value when applying the whole GT-potential:

$$Q = 2.63 \times 10^{-27} \text{ cm}^2.$$

The experimental value of the quadrupole moment:

$$Q = 2.74 \times 10^{-27} \text{ cm}^2.$$

Hence it has been shown by this example that even a very strong spin-orbit force does not essentially change the properties of the deuteron, in every case not so much as one could expect on the grounds of some estimates.

Feshbach has, however, pointed out [7]) that an LS-force can cause trouble when considering the *magnetic moment* of the deuteron. We have calculated the correction to the magnetic moment due to the LS-term of the GT-potential by using the wave function given in the attached table:

$$\begin{aligned} \Delta\mu_{LS} &= -(0.0069-0.0019-0.0016)\ \text{n.m.} \\ &= -0.0034\ \text{n.m.} \end{aligned} \tag{8}$$

(The first term is the pure S-term, the last one is the pure D-term and the second one is the SD-interference term.) This result shows that Feshbach has much overestimated the correction in question (Feshbach gives the value $\Delta\mu_{LS} = -0.036$ n.m.), the right correction being even smaller than the value obtained by Swart, Marshak and Signell [8]). Considering the large D-state probability implied by the GT-potential it seems, however, that a discrepancy remains between the theoretical and the experimental values.

It is noteworthy that the GT-potential causes difficulties in the theory of the deuteron. When constructing the potential, the properties of the deuteron were not directly taken into consideration. Hence we have here an example of the fact that a phenomenological potential is always only an interpolation formula referring to a given experimental material. When used in other cases, involving different material, it is always possible that it will turn out to be unsatisfactory.

We are obliged to the Finnish Atomic Energy Commission and to the State Commission for Natural Sciences for financial support. We also like to thank Miss Seija Lyytikäinen, Phil. Mag., for help in numerical calculations.

References

1) K. V. Laurikainen, Nuclear Physics **8** (1958) 210
2) J. L. Gammel and R. M. Thaler, Phys. Rev. **107** (1957) 201; 1337
3) K. V. Laurikainen, Ann. Acad. Sci. Fenn. A **6** (1959) no. 27
4) S. Gill, Proc. Camb. Phil. Soc. **47** (1951) 96
5) G. Abraham, Nuclear Physics **1** (1956) 415
6) L. C. Biedenharn, J. M. Blatt and M. H. Kalos, Nuclear Physics **6** (1958) 359
7) H. Feshbach, Phys. Rev. **107** (1957) 1626
8) J. J. Swart, R. E. Marshak and P. S. Signell, Nuovo Cimento **6** (1957) 1189

1.E.1:
3.B

Nuclear Physics **12** (1959) 612—618; © *North-Holland Publishing Co., Amsterdam*
Not to be reproduced by photoprint or microfilm without written permission from the publisher

MULTIPOLARITIES OF U^{233} TRANSITIONS

K. MAACK BISGÅRD, P. DAHL and K. OLESEN
The Physical Institute, University of Aarhus, Denmark

Received 15 May 1959

Abstract: Multipolarities for twelve gamma transitions in the beta decay of Pa^{233} have been determined on the basis of relative conversion coefficients measured with a six gap spectrometer. Spin and parity have been assigned to all corresponding levels in U^{233}. Some conversion line interpretations differ from those of previous authors and a few formerly unreported electron lines have been observed.

1. Introduction

The previous measurements [1]) on the beta decay of Pa^{233} indicate U^{233} energy levels which with a single exception are well established, but quantitative information on the multipolarities are restricted to three out of fourteen transitions reported as being well-known. Recent work on Coulomb excitation [2]) has further shown that the lowest level (40 keV) is a member of a rotational band, the transition to the ground state being a mixture of magnetic dipole and electric quadrupole radiation.

On the basis of the present data it is possible to assign multipolarities to nearly all of the transitions allowing spin determinations to be made for all levels confirmed.

2. Experimental Method

The beta decay of Pa^{233} was studied by means of a single channel gamma spectrometer and a recently built six gap beta spectrometer [3]) of the same type [4]) as those built at Institute for Theoretical Physics, Copenhagen. It consists of six identical gaps placed symmetrically around the axis through source and focus. Each gap is symmetrical around the central plane perpendicular to the axis, and the angle between its pole faces is 20°. The diameter of the magnet system is 100 cm in the central plane, and the distance between source and focus is 34 cm. The dispersion is about 600 mm and the maximum $B\rho$ value exceeds 18 000 G · cm. In the present investigation the electron counter was furnished with an EMI multiplier tube, type 9536B allowing a counting efficiency of more than 90 % for 25 keV electrons. Several runs were performed with the spectrometer adjusted to transmissions ranging

from about 10 % to 1 % corresponding to a resolution of 0.8 % and 0.4 % respectively.

The sources were prepared by the Pa^{233} activity extracted from neutron irradiated thorium metal, the irradiations being made in the Saclay pile, France. The sources used had areas from 4 to 10 mm^2 with activities ranging from a few μC to about 100 μC placed on foils of VYNS and polyethylene (thickness 10—25 $\mu g/cm^2$) or on aluminium foils (0.2 mg/cm^2).

3. Results

More than 60 conversion lines were found in the energy region from 15 to 500 keV. These lines are in agreement with the level scheme suggested by Brodie [1]), and the relative intensities make possible an assignment of multipolarities for nearly all of the transitions involved.

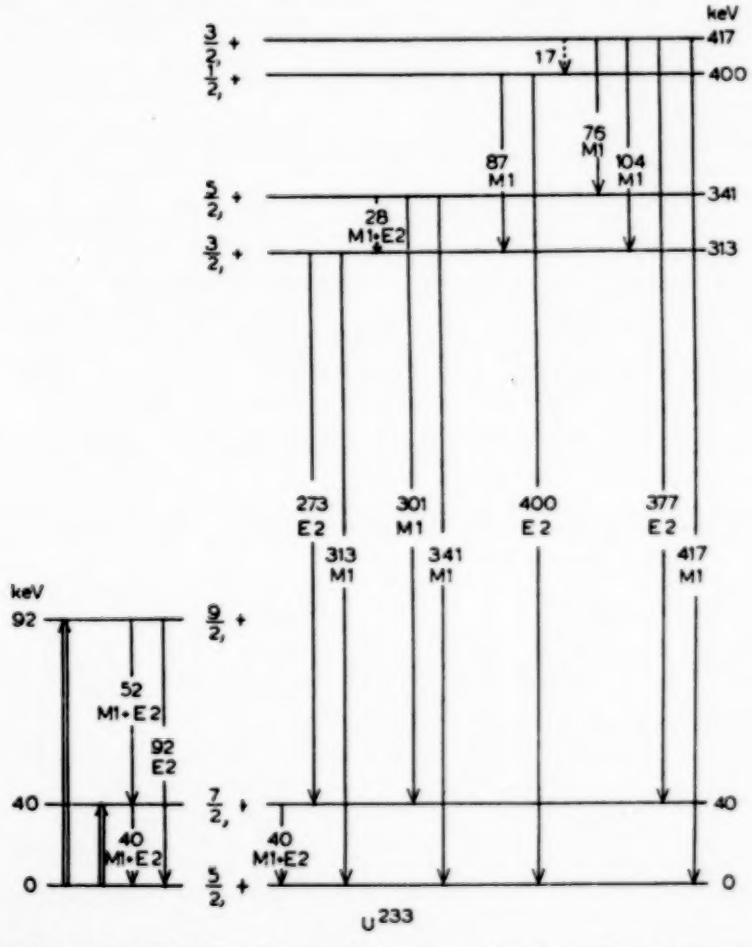

Fig. 1. Spin, parity and multipole assignments for energy levels and transitions in U^{233} from the beta decay of Pa^{233}. Coulomb excitation data from the work of Newton [2]) are also shown.

In the table are listed the transitions in question, and all the experimentally determined relative conversion coefficients which are conclusive or

TABLE 1

Relative conversion coefficients

E_γ (keV)	Conversion ratio	Experimental values	Theoretical values			Assignment
			E1	E2	M1	
28	$\frac{M_I+M_{II}}{M_{III}}$	$\approx$ 9	2.2	0.7	170	M1+E2 [b]
	$\frac{M_{III}}{M_{IV}}$	> 20	1.9	62	7.6	
	(M_I+M_{II}) [a]					
40	$\frac{L_I+L_{II}}{L_{III}}$	1.0	1.1	1.1	$\approx$ 230	M1+E2 [b]
	$\frac{L_I}{L_{II}}$	$\approx$ 0.4	0.7	0.03	13	
	$\frac{M_I+M_{II}}{M_{III}}$	1.7	2.0	1.1	200	
	$\frac{M_{III}}{M_{IV}}$	$\gtrsim$ 50	2.8	46	7.3	
	(L_{III})					
76	$\frac{L_I+L_{II}}{L_{III}}$	> 130	2.2	1.3	223	M1
	$\frac{L_I}{L_{II}}$	$\approx$ 13	1.4	0.06	12	
87	$\frac{L_I+L_{II}}{L_{III}}$	> 20	2.4	1.3	207	M1
	$\frac{L_I}{L_{II}}$	$\approx$ 9	1.5	0.06	11	
	(L_{III})					
104	$\frac{L_I+L_{II}}{L_{III}}$	> 30	1.9	1.6	229	M1
	$\frac{L_I}{L_{II}}$	$\approx$ 9	0.9	0.06	11	
	(L_{III})					
273	$\frac{K}{L}$	0.55	5.2	0.67	4.6	E2
	$\frac{L_I+L_{II}}{L_{III}}$	2.8	6.7	3.3	274	

TABLE 1 (continued)

E_γ (keV)	Conversion ratio	Experimental values	Theoretical values			Assignment
			E1	E2	M1	
301	$\frac{K}{L}$ (L_{III})	5.0	5.2	0.84	4.5	M1 [b]
313	$\frac{K}{L}$ (L_{III})	5.1	5.1	0.9	4.5	M1 [b]
341	$\frac{K}{L}$	5.0	5.2	1.1	4.5	M1
	$\frac{L_I+L_{II}}{L_{III}}$	> 100	8.2	4.2	277	
377	$\frac{K}{L}$	1.2	5.1	1.2	4.6	E2
	$\frac{L_I+L_{II}}{L_{III}}$	3.1	9.0	4.9	287	
400	$\frac{K}{L}$	≈ 2.4	5.2	1.3	4.5	E2
	$\frac{L_I+L_{II}}{L_{III}}$	4.0	9.2	5.1	294	
417	$\frac{K}{L}$	3.9	5.1	1.5	4.4	M1
	$\frac{L_I+L_{II}}{L_{III}}$ (K, L_I+L_{II}, L_{III})	> 20	9.9	5.5	297	

[a]) The letters in parentheses denote conversion groups which are energetically coincident with other electron lines.

[b]) See text as regards the 28, 40, 301 and 313 keV transitions.

indicative for the multipolarity assignment. Further are tabulated some corresponding theoretical conversion ratios according to Rose [5]) and the assignments made by us. The experimental data refer to a single complete run. The results from the other measurements are in agreement with the conclusions mentioned. The intensities have not been corrected for discrimi-

nator cut off, which might have some influence on the low energy ratios.

The letters in parentheses in column 2 of the table denote conversion groups energetically coincident with other groups of possibly comparable intensities. In all important cases significant limits on the mixing ratio can be determined based upon theoretical and experimental data.

In fig. 1 is shown the level scheme and our spin and parity assignments. Referring to the level scheme the following comments should be made on the multipole assignments in the table:

40 keV: The L_I/L_{II} ratio and the M_{III}/M_{IV} ratio from this and the other runs seem to exclude a pure electric quadrupole radiation in agreement with Coulomb excitation data. Further, the gamma ray intensity indicates that the transition is not E1.

28, 301 and 313 keV: Electric dipole transitions are excluded by parity considerations.

4. Remarks

The present experimental data indicate the existence of three rotational bands in U^{233} and are consistent with the previously reported [1]) multi-

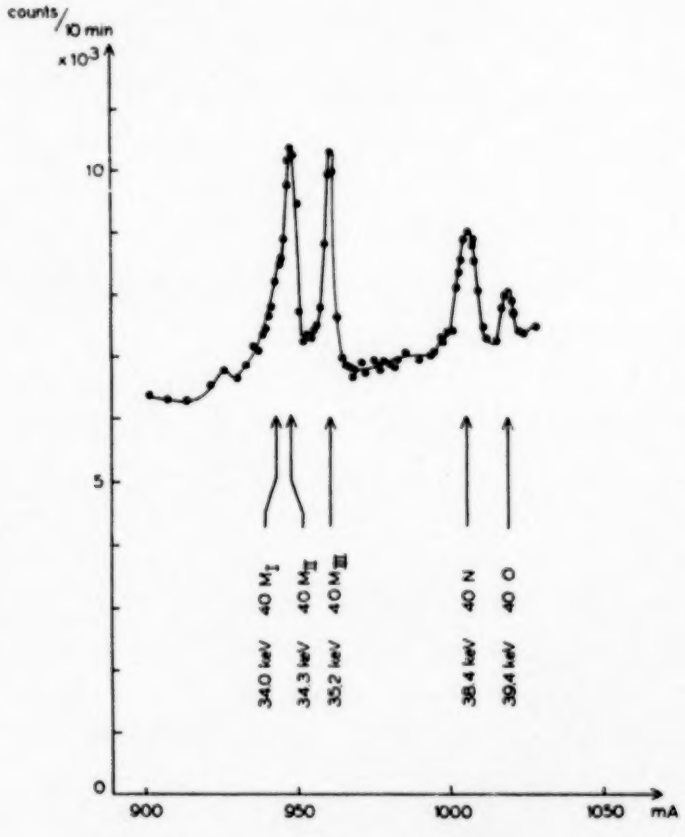

Fig. 2. Part of the conversion line spectrum showing the present interpretation of the 40 keV M, N and O lines. The spectrometer was adjusted to secure maximum of resolution in this energy region: 0.45 %, transmission $\gtrsim$ 1 %.

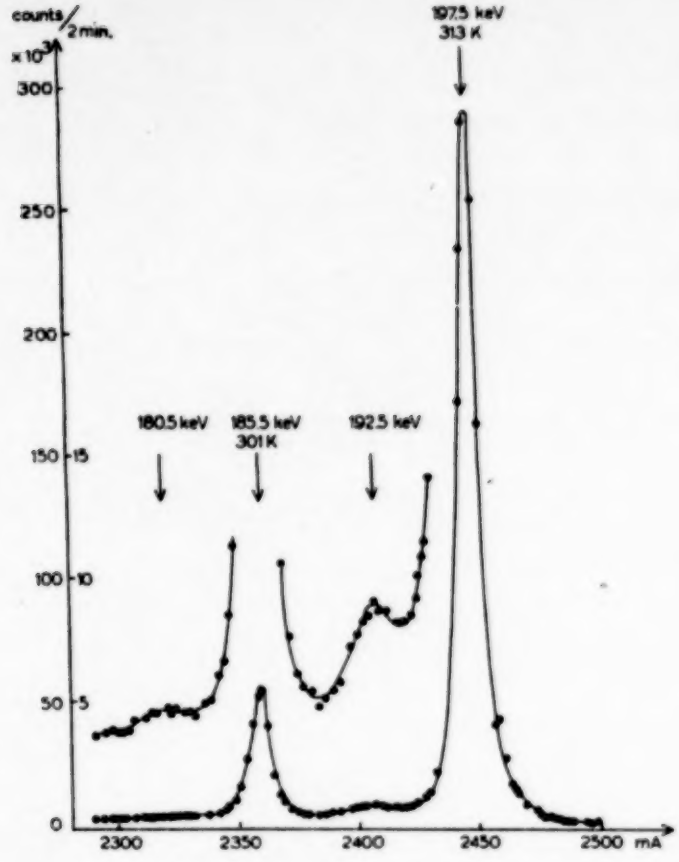

Fig. 3. Part of the conversion line spectrum showing the 301 K and 313 K lines and two of the previously unreported electron lines mentioned in the text. Resolution 0.50 %, transmission 2—3 %.

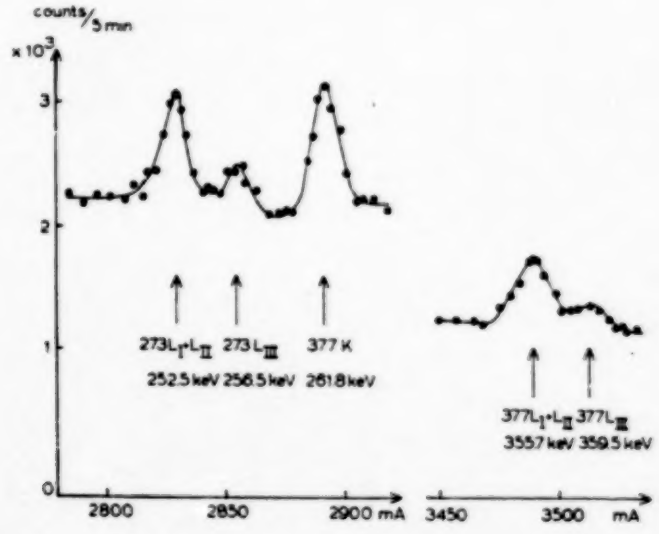

Fig. 4. Parts of the conversion line spectrum showing the 273 L lines and the 377 K and L lines. Resolution 0.45 %, transmission 2—3 %.

polarities for the three strongest transitions. They agree with the assignments suggested by Newton [2]) on the basis of less informative results.

Conversion lines which with certainty confirm a transition from the 400 keV to the 341 keV level were not observed. A 58 L conversion line with an intensity comparable with that reported by other authors [1]) is not compatible with the present interpretation of lines in this energy region as shown on fig 2.

It should be mentioned that besides a few groups at low energies, new electron lines are observed 5 keV below the 301 K, 313 K and 341 K lines with intensities of a few percent of the neighbouring peaks. Two of these groups are shown on fig. 3.

The 476 keV transition reported by some authors [1]) was observed neither in the gamma nor in the beta spectrum. The 360 keV electron line which is tentatively ascribed to this transition by Ong and Kramer fits the experimental data quantitatively when interpreted as the 377 L_{III} conversion line (cf. fig. 4).

The beta spectrum and the relative intensity measurements which cover nearly all the lines observed provide data for a more detailed analysis and for a comparison with theory. The questions raised by the new electron lines will be discussed in this connection.

We are indebted to Mr. O. B. Nielsen, Institute for Theoretical Physics, Copenhagen, for invaluable advice and to the Radiochemical Group at Institute for Theoretical Physics for preparing the sources. We wish to thank Mr. S. A. Nielsen for his careful assistance during the measurements.

References

1) H. B. Keller and J. M. Cork, Phys. Rev. **79** (1950) 1030;
L. G. Elliott and A. B. Underhill, A.E.R.E.L., Harwell, Report HAR 761 (1952);
W. D. Brodie, Proc. Phys. Soc. **67** (1954) 397;
Ong Ping Hok and P. Kramer, Physica **21** (1955) 676

2) J. O. Newton, Nuclear Physics **5** (1958) 218

3) To be published

4) O. Kofoed-Hansen, J. Lindhard and O. B. Nielsen, Mat. Fys. Medd. Dan. Vid. Selsk. **25**, No. 16 (1950);
O. B. Nielsen and O. Kofoed-Hansen, Mat. Fys. Medd. Dan. Vid. Selsk. **29**, No. 6 (1955)

5) M. E. Rose, Internal Conversion Coefficients (Amsterdam, 1958)

2.E *Nuclear Physics* **12** (1959) 619—624; © *North-Holland Publishing Co., Amsterdam*
Not to be reproduced by photoprint or microfilm without written permission from the publisher

ON THE IMAGINARY OPTICAL POTENTIAL

R. H. LEMMER, Th. A. J. MARIS and Y. C. TANG
Department of Physics, Florida State University, Tallahassee, Florida, U.S.A. †

Received 19 May 1959

Abstract: The imaginary part of the nuclear optical potential for nucleons is investigated in a semi-quantitative way. For simplicity, harmonic oscillator wave functions have been used to perform calculations for O^{16} and Ca^{40}. Results indicate that surface absorption is quite important for incident energies up to about 60 MeV.

The purpose of this note is to give a semi-quantitative discussion of the shape and magnitude of the imaginary part of the optical potential for a shell model nucleus. Under the assumptions to be made, this calculation is hoped to give reasonable results for incident nucleons with energies larger than about 20 MeV. The essential difference between the present treatment and those of Harada and Oda [1]) and of Kikuchi [2]) is that the concept of a Fermi energy dependent on the local density in a nucleus is not used. Instead, we employ the fact that the root mean square radii of nuclear shells on the average increase with decreasing binding energy.

The classical expression for the mean free path of a nucleon in nuclear matter of density ρ is

$$l = \frac{1}{\rho\bar{\sigma}}, \tag{1}$$

$\bar{\sigma}$ being the average of the free cross-sections for the incident particle with the nucleons in the nucleus. In this formula the influence of neighbouring particles on a nucleon-nucleon collision is neglected, and therefore, λ of the incident nucleon should be small compared to the average distance between neighbouring particles. This restriction, and also assumptions to be made later, limits us to energies of about 20 MeV or more. At these energies, many-particle excitations and compound nucleus formation can be considered as multiple scattering processes; hence, they are included in this treatment.

The imaginary optical potential is related to the mean free path by the relation

$$W = \frac{\hbar}{\sqrt{2m\,l}}\sqrt{E}, \tag{2}$$

† This work was partially supported by the Air Force Office of the Scientific Research, ARDC, and the Atomic Energy Commission.

in which E is the kinetic energy of the incoming nucleon.

Expression (1) can be corrected in the following respects:

(a) At relatively low energies the exclusion principle forbids many collisions in the nucleus [3]), thus reducing the value of $\bar{\sigma}$ to be taken in (1). At this stage, we only treat the simple case of doubly closed-shell nuclei. In the energy range considered, we may then neglect the contributions from bound excited single particle states, so that a collision is forbidden if the incoming particle has an energy less than the binding energy of the particle with which it collides. It is therefore convenient to write $\sum_i \rho_i \bar{\sigma}_i$ instead of $\rho\bar{\sigma}$ in (1), with the summation going over the various occupied single particle states of the nucleons in the ground state of the nucleus; $\bar{\sigma}_i = 0$, if the bombarding energy is lower than the binding E_i of the i^{th} single particle state.

(b) When the bombarding energy is sufficient to eject a particle, the cross-section for this process will still be reduced in comparison with that of a free collision because of the smaller available phase space. An estimate of this effect is obtained by taking as final states the continuum states of the nuclear potential which are plane waves at infinity. Considering the result of the collision as only differing from that with a free particle at rest insofar as the total available kinetic energy of the final particles is reduced by the binding energy B_i of the struck particle, one finds a reduction factor $\sqrt{[(E-B_i)/E]}$. This factor yields correct values for the extreme cases when the collision is forbidden by the exclusion principle, and when, in the high energy limit, the cross-section becomes roughly equal to the free one. While this estimate is certainly crude, we believe that it is sufficiently accurate for the present purpose.

(c) As in ref. [1]) and [2]), one further improvement is introduced by realizing the fact that the effective kinetic energy of the approximately localizable incoming particle is dependent on the location at which the collision occurs. We take the value $E' = E+V(r, E)$, in which V is the absolute value of the real optical corresponding to the energy of the incident particle.

With these modifications,

$$\bar{\sigma}_i = \bar{\sigma}_{\text{free}}(E') \sqrt{\frac{E-B_i}{E'}}, \tag{3}$$

and we may finally write (2) as

$$W = \frac{\hbar}{\sqrt{2m}} \bar{\sigma}_{\text{free}}(E') \sum_i \rho_i \sqrt{E-B_i}. \tag{4}$$

Results for O^{16} and Ca^{40} are shown in figs. 1—5. For the calculation of ρ_i and B_i, we have used a harmonic oscillator potential of depth 50 MeV and spacing $\hbar\omega = 41\, A^{-\frac{1}{3}}$ MeV [4]) with no spin-orbit force. A Woods-Saxon form

with parameters as compiled by Glassgold [5]) is taken for $V(r, E)$. The free cross-sections are from the article by Beretta *et al.* [6])

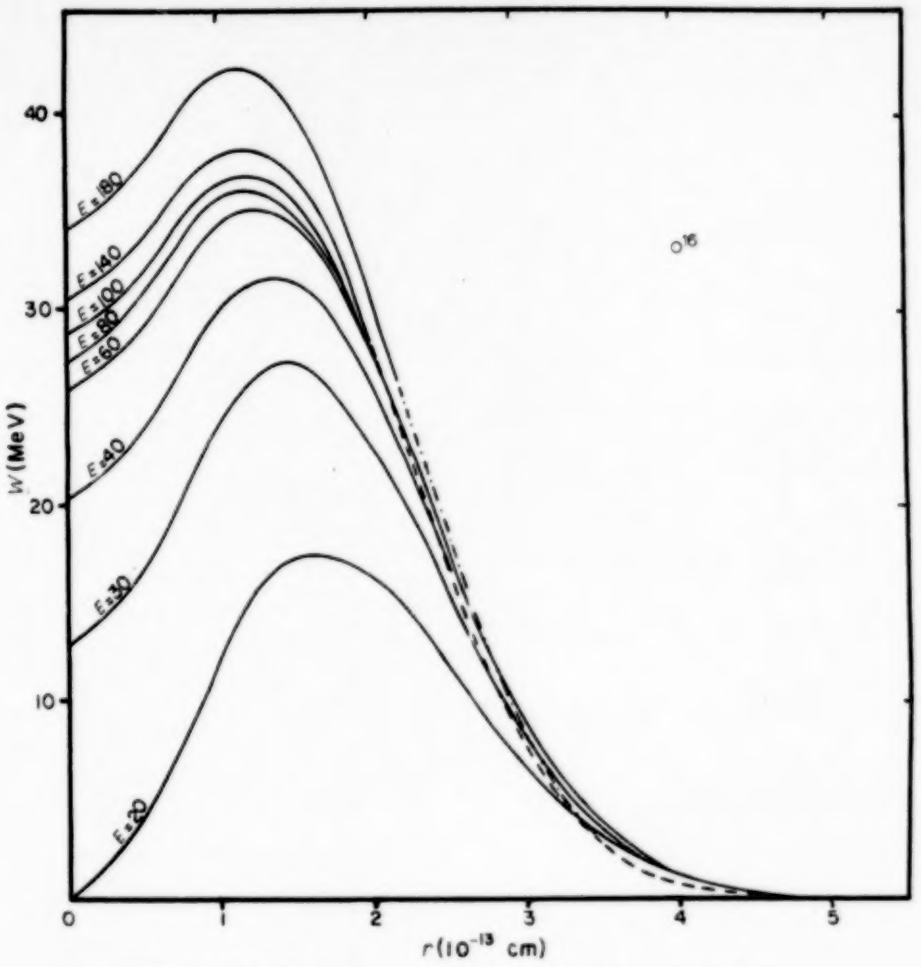

Fig. 1. Imaginary potential for O^{16} at various energies.

For O^{16}, the surface absorption is evident from fig. 1 for energies below 60 MeV. However, for Ca^{40}, this effect is not clearly visible from the shape of the imaginary part directly. This is due to the fact that harmonic oscillator wave functions give too high a density at the centre of this nucleus. This tends to overshadow the surface absorption, and will not be present for calculations with more realistic densities to be done at a later time. A more indicative measure of the radial dependence of the absorption is given by the ratio W/ρ. At low energies, this ratio does indeed increase quite rapidly with r, while at high energies (> 100 MeV), it approaches a constant value (normalized to unity) indicating pure volume absorption.

In the present calculation, the surface absorption is caused by two effects of about equal importance:

(a) The r.m.s. radii, $\sqrt{\langle r_i^2 \rangle}$, of the nuclear orbits increase with decreasing binding energies. (In a harmonic oscillator well, $\langle r_i^2 \rangle$ is proportional to the

average kinetic energy of the state in question, and a similar tendency is also true for a more realistic well.) The reduction factor $\sqrt{[(E-B_i)/E']}$ for the

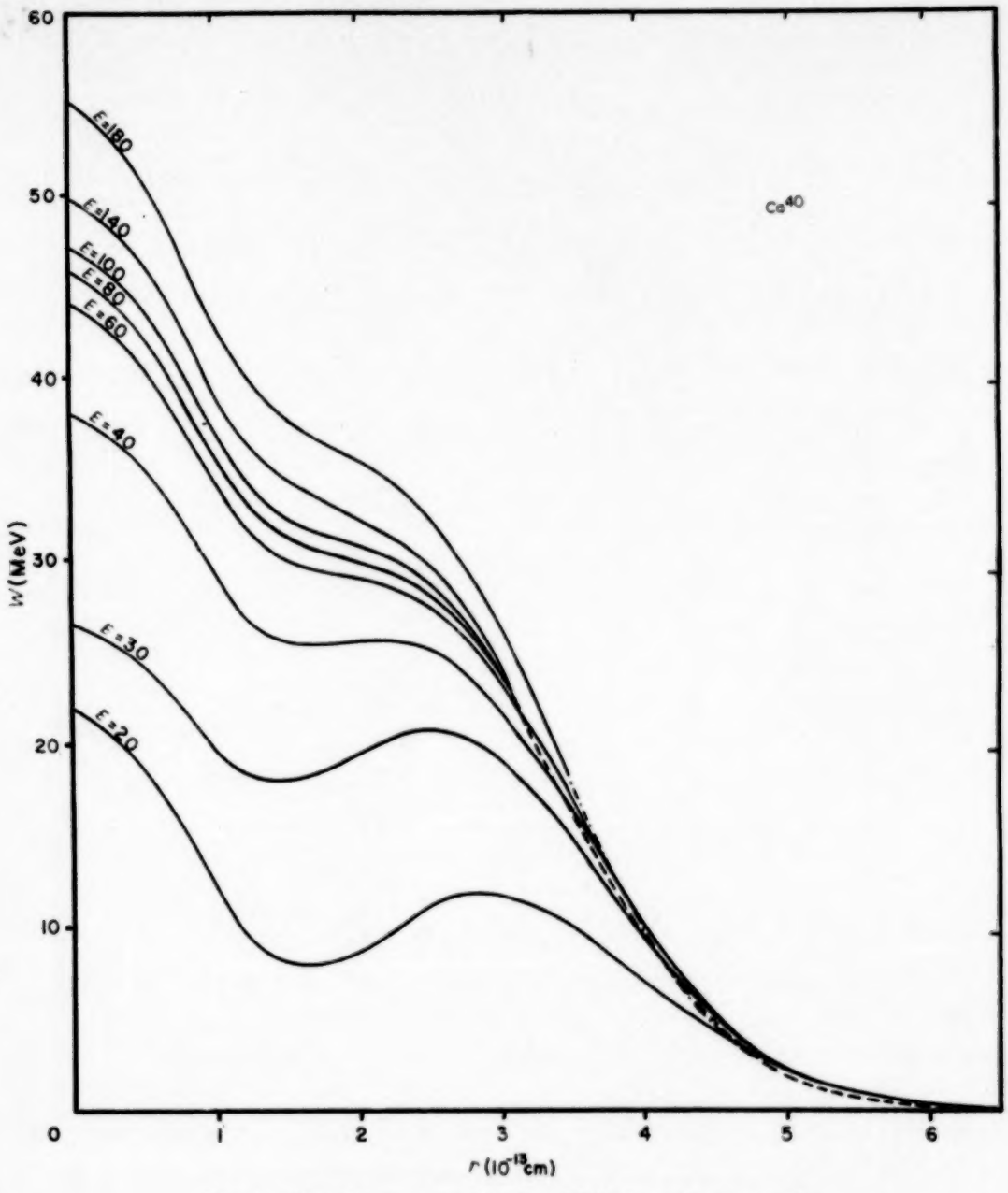

Fig. 2. Imaginary potential for Ca^{40} at various energies.

cross-section gives shells with smaller binding energies (larger $\langle r_i^2 \rangle$) larger weights than those with larger binding energies (smaller $\langle r_i^2 \rangle$).

(b) $\bar{\sigma}_i$ increases with radius. This comes from the energy dependence of the free cross-section and the fact that we take $E' = E+V(r, E)$ as the effective collision energy.

To make a comparison of the calculated magnitude for W inferred from

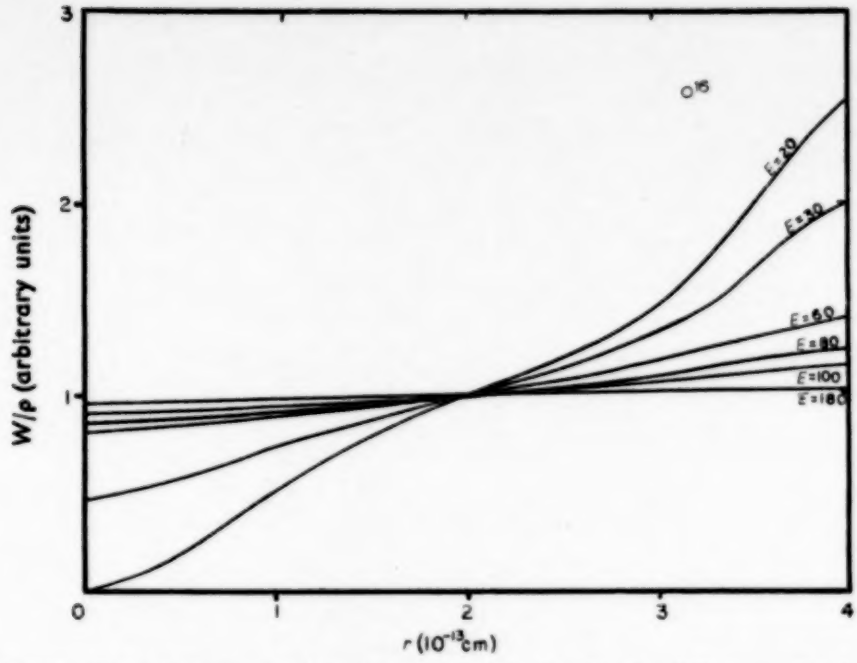

Fig. 3. Ratio of imaginary potential to total particle density for O^{16}, normalized to unity at $r = 2\times10^{-13}$ cm.

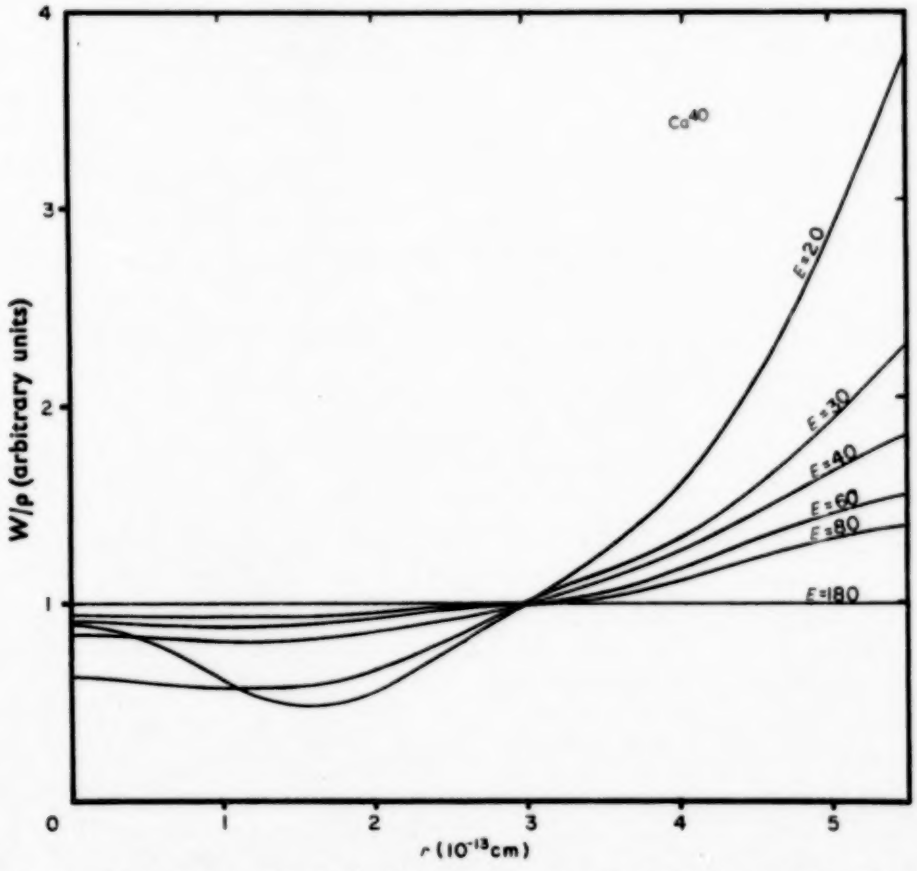

Fig. 4. Ratio of imaginary potential to total particle density for Ca^{40}, normalized to unity at $r = 3\times10^{-13}$ cm.

scattering experiments [5]), we plot in fig. 5. the equivalent absorptive Woods-Saxon potential, equivalent being defined as having the same volume

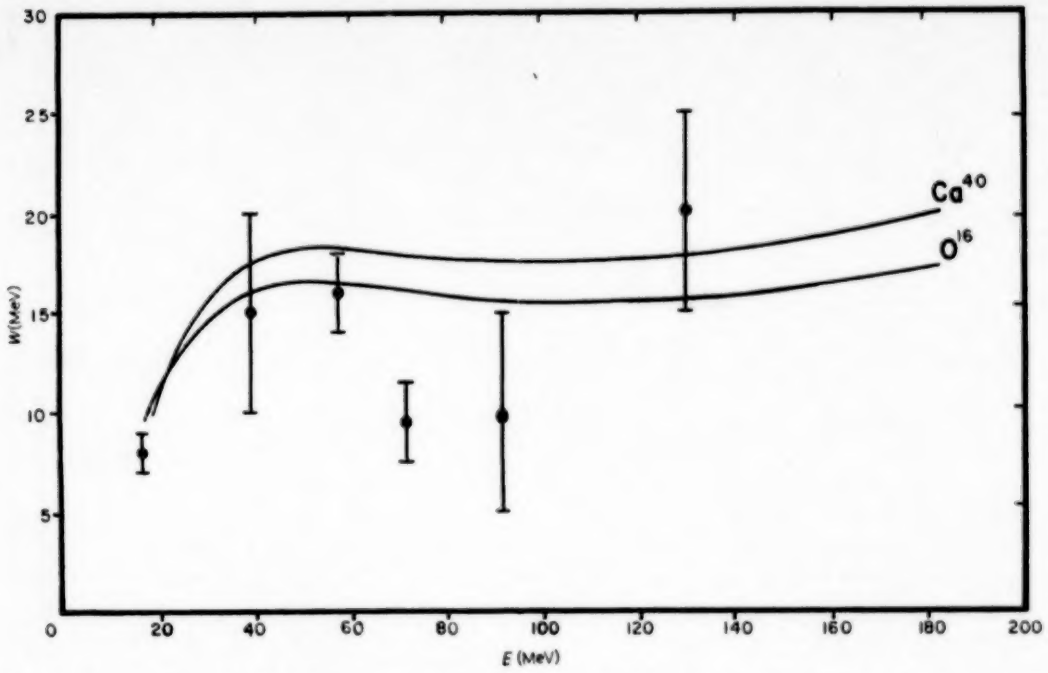

Fig. 5. Equivalent Woods-Saxon potential depth as a function of incident nucieon energy. The empirical points are from ref. [5]).

integral as the potentials in figs. 1 and 2. The general trend of the empirical data seems to be fairly well represented over a wide energy range.

Finally, it may be remarked that if the velocity dependence of the potential for the bound states is taken into account, the binding energies of the deep lying states increase [7]). From (4), it therefore follows that the surface absorption effect will become even more prominent in this case.

References

1) K. Harada and N. Oda, Prog. Theor. Phys. **21** (1959) 260
2) K. Kikuchi, preprint
3) R. Serber, Phys. Rev. **72** (1947) 1114
4) S. G. Nilsson, Mat. Fys. Medd. Dan. Vid. Selsk. **29**, (1955) 16
5) A. E. Glassgold, Revs. Mod. Phys. **30** (1958) 419
6) L. Beretta, C. Villi and F. Ferrari, Nuovo Cimento Supp. **12** (1954) 499
7) W. E. Frahn and R. H. Lemmer, Nuovo Cimento **5** (1957) 1564

1.D.3:
7.C

Nuclear Physics **12** (1959) 625—628; © *North-Holland Publishing Co., Amsterdam*
Not to be reproduced by photoprint or microfilm without written permission from the publisher

NATURE OF NUCLEAR MATTER IN THE FREE-MESON LATTICE MODEL

L. E. H. TRAINOR and P. C. SOOD
University of Alberta, Edmonton, Canada

Received 11 May 1959

Abstract: Possible types of structure of nuclear matter arising from the "atomic" model for the physical nucleons are considered and some of their properties discussed.

In the present note we should like to extend the considerations made in a previous paper [1]) concerning the nature of nuclear matter. We suggested that in the independent particle approximation nuclear matter exhibits a periodic structure, reminiscent, perhaps, of the structure of a normal liquid. We termed this model the quasi-lattice model and showed, in Wigner-Seitz approximation, that good agreement with the accepted values of the nuclear density and the binding energy per nucleon is obtained with the two-body potentials of Gammel and Thaler [2]). We now wish to point out that more fundamental considerations could lead quite naturally to a periodic model of nuclear matter.

For simplicity, let us assume an atomic model for the physical nucleons with one or more real π-mesons bound to a nucleon core. With a simple form of such a model, in which the ground state of the physical nucleon corresponds to a single π-meson moving in a p-orbit about the core, Feld [3]) has been able to account for the static properties of the nucleons. The binding energy of the single meson on this model is appropriate to the experimentally measured threshold for meson production in centre of mass (about 139.6 MeV, the rest energy of the π-meson).

Consider now the interior of a heavy nucleus in such an atomic model. In the usual interpretation of nuclear matter, which we shall refer to as Case A, each real meson must be pictured as being tightly bound to a single nucleon core, so that the system of core plus meson moves as a single entity, the physical nucleon. It is possible, however, that the interaction between cores and mesons is such that the mesons have a limited mobility for moving from core to core. We associate this situation with the quasi-lattice model of our previous paper [1]) and refer to it as Case B. The extreme situation, Case C, in which the mesons possess almost complete mobility, we refer to as the "free-meson lattice model" in loose analogy with the free-electron model of a

metallic lattice. In this extreme, the internal kinetic energy of nuclear matter is due largely to the circulating mesons, and one may consider in some approximation that the nucleon cores form a lattice.

Cases A, B, and C are illustrated in fig. 1 for a hypothetical meson nucleon-core interaction. The potential energy of a π-meson is plotted as a function of its position along a line joining two nucleon cores, the presence of other cores and mesons being neglected. When the distance $2a$ between cores is large, the π-mesons are trapped on individual cores (see fig. 1a). As this distance is reduced, however, the barrier height between cores is also reduced, and the binding energy of the meson altered in a manner which depends on the potential shape. The change in the mobility of the mesons is determined by

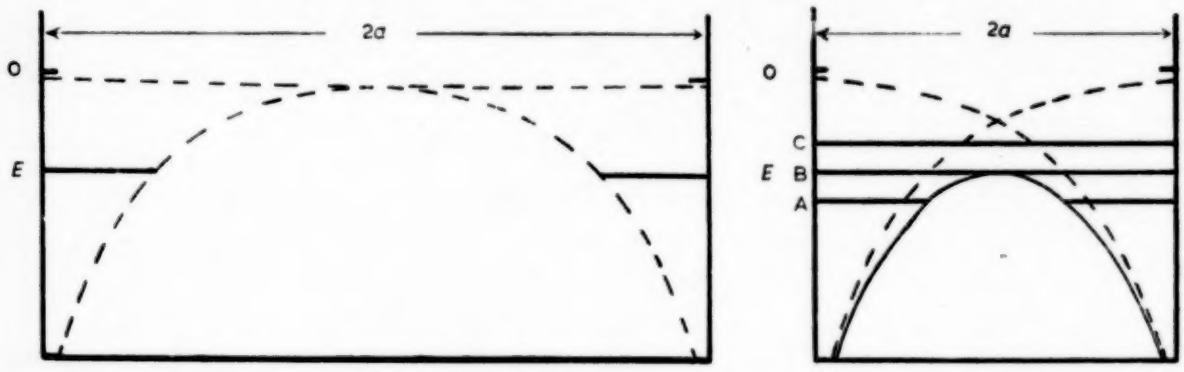

Fig. 1a Fig. 1b

Fig. 1. Hypothetical potential $V(r)$ for a π-meson between two nucleon cores. The solid curve represents the addition of the separate potentials (dotted curves) due to each core. Fig. 1a corresponds to a large core separation, such as one finds in the deuteron. Fig. 1b corresponds to the average separation of cores in a heavy nucleus. Energies E_A, E_B and E_C depict the lowest states appropriate to cases A, B and C respectively.

the competition between decreased barrier height, which increases the mobility, and increased (decreased) meson binding, which decreases (increases) the mobility. Cases A, B and C of the previous paragraph are illustrated in fig. 1b, where E_A typifies the energy of the lowest state assuming Case A to hold, E_B typifies the energy of the lowest state assuming Case B to hold, and E_C typifies the energy of the lowest state assuming Case C to hold.

The possibility that Case C, the free-meson lattice model, actually obtains in the interior of heavy nuclei is enhanced by two fundamental considerations. First, the meson nucleon-core interaction has to be very strong to account for the various nucleon properties (see Feld [3])); second, the intranucleonic spacing inside a heavy nucleus is relatively small. From an oversimplified point of view, one can say that the packing is too tight for high mobility of the physical nucleons so that there is a tendency for the cores to remain immobile and for the π-mesons to account for the greater portion of the internal motion.

The question arises whether such a model leads to observable consequences. One possibility is that the Bohr-Mottelson rotational states [4]) correspond in first approximation to collective motions of the free mesons in the lattice of nucleon cores, rather than to collective motions involving the physical nucleons themselves. Presumably, one would then expect the effective moments of inertia to be smaller due to the smaller mass of the mesons as compared to the nucleons. This consideration may bear some relation to the experimental fact that the effective moment of a deformed nucleus is smaller by a factor of two to three from that calculated for rigid rotation of the nucleus as a whole.

The free-meson lattice model predicts diffraction phenomena, both in the electromagnetic scattering of electrons and μ-mesons and in the nuclear scattering of π-mesons and nucleons. The situation is complicated, however, by the strong geometrical diffraction produced by the sharp surface boundaries of actual nuclei. The two types of diffraction would not be easy to distinguish in practice, since the characteristic diffraction lengths are not very different (the intra-nucleonic spacing in heavy nuclei is about 1.7×10^{-13} cm, compared with nuclear radii of 6 or 7×10^{-13} cm). Moreover, the model applies only to the nuclear interior, so that a characteristic lattice diffraction would be obscured by surface effects in all but the heaviest nuclei.

The deuteron represents an extreme where the free-meson lattice model has a vanishing validity. Since the neutron-proton separation is large and the total binding energy of 2 MeV is negligible compared to the binding energies of the π-mesons, it can be inferred that the π-mesons of the atomic model are bound firmly to the individual nucleon cores. Hence, the threshold for meson production in deuterium should correspond closely with that for meson production in hydrogen, aside from centre of mass effects. In heavier nuclei, however, the average separation between nucleons decreases and the average binding energy of the mesons is altered. The mesons become mobile and one has to consider the problem of the momentum distribution of the free mesons in the lattice of nucleon cores. It might be interesting to investigate in detail the variation of the threshold for meson production with increasing mass number A. Unfortunately, most meson production seems to occur at the nuclear surface where the free-meson lattice model is least valid.

Although the arguments presented above have been based explicitly on an atomic model of the physical nucleons, they are not necessarily invalidated from the point of view of field theory. As Feld [3]) points out, the atomic model may be regarded, in so far as it proves successful, as a useful approximation derivable from a complete treatment using the methods of field theory. Unfortunately, it is not possible in practice to proceed in this manner, since no satisfactory field theory exists. It may still be useful to consider

phenomenologically atomic models of the physical nucleons which lead to predictions that can be checked experimentally. For example, we are investigating a model in which nucleonic cores possess "like mesonic charge" and the π-mesons possess the "opposite mesonic charge". Binding of physical nucleons then arises from the attraction of opposite mesonic charges, much in the same way as binding occurs for atoms and molecules under electromagnetic forces. Such a model is beset with difficulties, but it also has some attractive features. For example, one can speculate that the basic core-meson interaction force has a simple inverse square radial dependence and that the short range of the nucleon-nucleon force is due to the screening of the nucleon cores by the orbital π-mesons. From this point of view, the deuteron can be regarded as the analogue of the hydrogen molecule in atomic physics. Such a model also could account for the observed strong, short-range, repulsive forces between nucleons [2]). Ignoring serious relativistic complications, a rough estimate of the "mesonic charge" g can be made by replacing the electronic mass and charge in Bohr's formula for hydrogen by the π-mesonic mass and "charge". The requirement that the binding energy of the π-meson equal its rest energy then yields a value of $g^2/\hbar c = \sqrt{2}$.

We are indebted to the National Research Council of Canada for a post-doctorate fellowship for one of us (P. C. S.)

References

1) L. E. H. Trainor, A. B. Bhatia and P. C. Sood, Nuclear Physics **9** (1958) 287
2) J. Gammel and R. M. Thaler, Phys. Rev. **107** (1957) 291; 107 (1957) 1337
3) B. T. Feld, Ann. of Phys. **1** (1957) 58; **4** (1958) 189
4) A. Bohr and B. R. Mottelson, Mat. Fys. Medd. Dan. Vid. Selsk. **27**, No. 16 (1953)

1.B:7.A *Nuclear Physics* **12** (1959) 629—646; © *North-Holland Publishing Co., Amsterdam*
Not to be reproduced by photoprint or microfilm without written permission from the publisher

ELASTIC NEUTRON-DEUTERON SCATTERING

RICHARD BLANKENBECLER, MARVIN L. GOLDBERGER
and FRANCIS R. HALPERN
Palmer Physical Laboratory, Princeton University, Princeton, New Jersey †

Received 19 May 1959

Abstract: The process of elastic neutron-deuteron scattering is discussed from the standpoint of dispersion theory. Aside from the appearance of anomalous thresholds, there seems to be no difficulties in principle, although no derivation of the relations is attempted. Certain features of the process, such as the pick-up peak in the backward direction, appear quite neatly and the general occurrence of such phenomona is discussed. The theory is developed for the general case, but our only application is to forward scattering at low energies where phase shift analyses are available. The agreement with experiment is quite good.

1. Introduction

It is of some interest to apply dispersion techniques to problems involving composite particles. One example is the elastic scattering of neutrons by deuterons, which will be treated here. This process has been extensively treated in terms of potentials; however, the calculations are quite complicated and detailed comparison with experiment is difficult [1]).

We wish to examine this problem using the techniques of dispersion theory, to see if a tractable computation scheme results. This would seem to be the case, although a complete dynamical calculation would be very hard. It should be stated that to our knowledge, dispersion relations for nucleon-deuteron scattering have not been proved by anyone. Aside from a difficulty to be mentioned later, they would seem to hold in perturbation theory. Another motivation for examining this problem is the wealth of experimental data available, which makes it possible to see whether dispersion theory is at all meaningful in this case [2]).

As in the case of nucleon-nucleon scattering, one will be confronted with a large unphysical region [3]). It might be expected that this unphysical region will make a significant contribution to the scattering amplitude. As we shall see, there are two discrete poles in this region which, for low energy scattering, seem to be the dominant terms. These are the poles due to the proton

† Supported in part by the Air Force Office of Scientific Research, Air Research and Development Command.

and triton intermediate states. The proton pole will be of particular importance to us.

In the earlier treatments of elastic neutron-deuteron scattering, particularly those employing the impulse approximation, the peak in the backward direction had its explanation in terms of a so-called pick-up process; the incident neutron would pick up the proton and the resultant deuteron moved forward, leaving the originally bound neutron behind. There is no difficulty in isolating this contribution to the scattering amplitude in a conventional description in terms of potentials. The quantitative agreement with experiment is not very good, the theoretical values being quite a bit too large. There are many possible reasons for this which we will not go into here.

The pick-up term in the elastic scattering amplitude may be isolated quite neatly using the formalism of quantum field theory (provided that theory includes a description of composite particles). Let the neutron four momenta before and after the collision be n, n' while those of the deuteron are d, d'. We select from all possible Feynman diagrams the one in which the deuteron, after suffering its last internal collision, dissociates into the final neutron n' and an intermediate proton, $p = d-n'$; the incident neutron collides with the proton and in doing so becomes the final deuteron d'. See fig. 1(a). This is the diagram that gives rise to the proton pole in the dispersion relations.

Even this one diagram is far too complicated to evaluate exactly, since we require the vertex functions describing $\mathrm{d} \to \mathrm{n}'+\mathrm{p}$ and $\mathrm{p}+\mathrm{n} \to \mathrm{d}'$, as well as the complete propagation function for the virtual proton p. In the immediate neighbourhood of the singularity described by $(d-n')^2+$ $+m^2 = 0$ (i.e., where the intermediate proton becomes real), the evaluation becomes quite easy. The dispersion treatment used here requires only the evaluation of these quantities at the singularity, thus yielding a considerable simplification.

If we retain only the contribution of the proton pole to the scattering amplitude, the cross section takes the form

$$\mathrm{d}\sigma/\mathrm{d}n' = R^2[(d-n')^2+m^2]^{-2}, \tag{1}$$

where R is a function of the total centre of mass energy alone. The denominator vanishes when the final neutron energy in the laboratory system is equal to half the deuteron mass. This corresponds to a slightly negative kinetic energy. In the backward direction the denominator is smallest and thus one again finds the explanation for the backward peaking in this exchange diagram.

Let us digress here slightly to consider a general elastic scattering process between two composite particles of mass M and m. If the masses are not equal, the scattering amplitude will in general have a pole which tends to

produce peaking in the backward direction. If selection rules permit the heavier particle M to dissociate virtually into the lighter one m and a

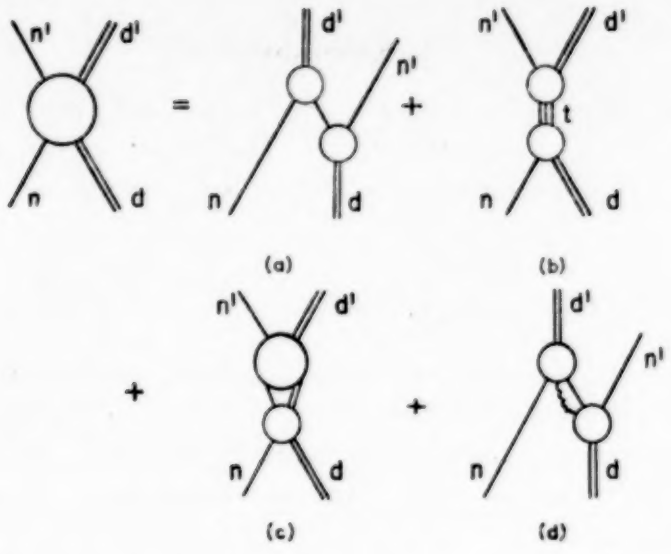

Fig. 1. Some of the simple diagrams in neutron deuteron scattering.

fragment of mass μ, this pole occurs at a final laboratory-system kinetic energy of the lighter particle (assumed to be the projectile) given by

$$T_t = -\frac{\mu}{M}(m+\mu-M) \tag{2}$$

to lowest order in $(m+\mu-M)/M$. This corresponds to the proton pole in the present problem. This pole seems to explain the observed backward peaking in nucleon-deuteron and nucleon-alpha elastic scattering [4]), and is probably of general importance in the elastic scattering of non-identical composite particles.

There is also the pole generated by the "uncrossed" diagram, fig. 1(b). In this process, the two particles virtually fuse into a "compound nucleus" of mass K. The initial kinetic energy of the lighter particle at this pole is given by

$$T_i = -\frac{M+m}{M}(K-M-m). \tag{3}$$

The triton intermediate state gives rise to this pole in the present problem.

In section 2, we discuss the kinematics of neutron-deuteron scattering and the decomposition of the scattering amplitude into invariant matrices. In section 3, the dispersion relations are written down and the absorptive part of the amplitude is examined. In section 4, the evaluation of the discrete contributions to the absorptive amplitude is undertaken. Finally,

in section 5, numerical results and conclusions are presented. The possibility of extending this work is briefly discussed. We turn now to the rather involved kinematic aspects of the problem.

2. Kinematics

The momenta of neutron and deuteron, before and after the collision, are denoted by n, d and n', d' respectively. These four vectors are related by $n+d = n'+d'$. It is possible to form two independent scalars. These are taken to be

$$\nu = -\frac{(n+n')(d+d')}{4M_d}, \qquad \Delta^2 = (d'-d)^2. \tag{4}$$

In addition to their momenta, it is necessary to describe the internal coordinates of the particles. The neutron is, of course, described by the conventional four component spinor $u(n)$. The deuteron spin polarization is described by the complex space-like pseudo-vector ξ, that satisfies the following relations:

$$\xi \cdot d = 0, \ \xi^* \cdot \xi = 1. \tag{5}$$

The physical meaning of ξ will be clarified in section 4.

The three vectors listed below will also prove useful in the description of the scattering:

$$N = \tfrac{1}{2}(n+n'), \quad D = \tfrac{1}{2}(d+d'), \quad \Delta = d'-d = n-n'. \tag{6}$$

To form a basis in four-dimensional momentum space, it is necessary to add a fourth vector. We chose this to be the pseudo-vector

$$L_\alpha = \varepsilon_{\alpha\beta\gamma\delta} N_\beta D_\gamma \Delta_\delta. \tag{7}$$

The invariant scattering amplitude M must be linear in the initial and final neutron spins and the initial and final deuteron polarizations. To show this dependence explicitly the quantity $M_{\alpha\beta}$ is introduced such that

$$M = \bar{u}(n')\xi'^*_\alpha M_{\alpha\beta}\xi_\beta u(n); \tag{8}$$

$M_{\alpha\beta}$ has the tensor properties indicated by its subscripts and is also a matrix in the spin space of the neutron. That is, $M_{\alpha\beta}$ has the form

$$M_{\alpha\beta} = A_{\alpha\beta}\mathbf{1} + iB_{\alpha\beta,\mu}\gamma^\mu + C_{\alpha\beta,\mu\nu}\sigma^{\mu\nu} + D_{\alpha\beta,\mu}\gamma^\mu\gamma_5 + E_{\alpha\beta}\gamma_5. \tag{9}$$

The quantities A to E are to be constructed from the four vectors defined in (6) and (7) times scalar functions of ν and Δ.

Because of the restrictions imposed by the Dirac equation and the first condition of (5), there are only twelve suitable tensors possible. For example, for $A_{\alpha\beta}$ any quantity bilinear in the vectors N, D, Δ and L is possible. There are four choices made from only one vector:

$$D_\alpha D_\beta, \quad N_\alpha N_\beta, \quad \Delta_\alpha \Delta_\beta, \quad L_\alpha L_\beta,$$

but because of (5), $\Delta_\alpha\Delta_\beta$ is equivalent to $D_\alpha D_\beta$. Since L is a pseudo-vector, no terms linear in L are acceptable; thus, the possible mixed quantities are $N_\alpha D_\beta \pm N_\beta D_\alpha$, $N_\alpha\Delta_\beta \pm N_\beta\Delta_\alpha$, and $D_\alpha\Delta \pm_\beta D_\beta\Delta_\alpha$. Of these the first two are equivalent by (3), while the third reduces to one of the earlier terms. Thus, there are four possible terms for $A_{\alpha\beta}$:

$$D_\alpha D_\beta, \quad N_\alpha N_\beta, \quad L_\alpha L_\beta, \quad D_\alpha N_\beta + D_\beta N_\alpha. \tag{10}$$

The possibility of a minus sign in the last term is removed by the condition that

$$M_{\alpha\beta}(N, D, \Delta) = CM^{\mathrm{T}}_{\beta\alpha}(-N, -D, \Delta)C^{-1}, \tag{11}$$

where the transposition is in the spin space and C is the charge conjugation matrix. This follows from considering the invariance properties of the six point vacuum expectation function and its relation to the S matrix. Requiring invariance under inversion of motion leads to a similar reduction of terms. Finally, one may observe that there exist scalar functions $C_1 \ldots C_4$ such that

$$\xi'^*_\alpha[C_1 D_\alpha D_\beta + C_2 N_\alpha N_\beta + C_3 L_\alpha L_\beta + C_4(D_\alpha N_\beta + D_\beta N_\alpha)]\xi_\beta = \xi'^*_\alpha \delta_{\alpha\beta}\xi_\beta. \tag{12}$$

This permits the replacement of $L_\alpha L_\beta$ by $\delta_{\alpha\beta}$, so that the final set of tensors $A_{\alpha\beta}$ is

$$\delta_{\alpha\beta}, \quad D_\alpha D_\beta, \quad N_\alpha N_\beta, \quad D_\alpha N_\beta + N_\alpha D_\beta. \tag{13}$$

In the $B_{\alpha\beta,\mu}$ the μ dependence can only be supplied by L_μ or D_μ, since the Δ and N terms are reducible by the Dirac equation to A type terms. The L_μ terms can also be eliminated by use of the identity

$$\gamma \cdot L = \tfrac{1}{4}[\gamma \cdot N, \{\gamma \cdot D, \gamma \cdot \Delta\}]\gamma_5. \tag{14}$$

Systematic application of (14) reduced all terms of the form $b_{\alpha\beta}L_\mu\gamma^\mu$ to the form $D_{\alpha\beta,\mu}\gamma^\mu\gamma_5$. The remaining γ_μ terms are given by $b_{\alpha\beta}D_\mu\gamma^\mu$. It is easy to show that the set of permissible $b_{\alpha\beta}$ is identical with the set $A_{\alpha\beta}$ treated above.

The $\mu\nu$ dependence of $C_{\alpha\beta,\mu\nu}$ must be antisymmetric because of $\sigma_{\mu\nu}$. Neither N nor Δ may enter because of the Dirac equation. There is one term that remains, $(D_\mu L_\nu - D_\nu L_\mu)$. But by arguments similar to those for the $L_\mu\gamma^\mu$ term, this is reducible to D and E type terms.

$D_{\alpha\beta,\mu}$ can have either D_μ or L_μ supply the μ dependence, but L_μ may be eliminated in the standard way in favor of $b_{\alpha\beta}D_\mu$. Thus, $D_{\alpha\beta,\mu}$ becomes $d_{\alpha\beta}D_\mu$ where $d_{\alpha\beta}$ must be a pseudo-tensor and thus, linear in L. The available combinations are

$$D_\alpha L_\beta \pm D_\beta L_\alpha \quad \text{and} \quad N_\alpha L_\beta \pm N_\beta L_\alpha. \tag{15}$$

The Δ terms are not distinct from the D terms. The minus sign is ruled out by eq. (11).

Finally, $E_{\alpha\beta}$ is a pseudo-tensor and, therefore, must be linear in L.

The combinations (15) are again possible and the minus sign is indicated by (11).

The four invariants involving L may be replaced by the four combinations

$$\begin{aligned} &D_\alpha\gamma_\beta+D_\beta\gamma_\alpha, \quad D_\alpha[\gamma_\beta, D_\mu\gamma^\mu]-D_\beta[\gamma_\alpha, D_\mu\gamma^\mu], \\ &N_\alpha\gamma_\beta+N_\beta\gamma_\alpha, \quad N_\alpha[\gamma_\beta, D_\mu\gamma^\mu]-N_\beta[\gamma_\alpha, D_\mu\gamma^\mu]. \end{aligned} \tag{16}$$

The replacement proceeds using the identity (14).

For convenience the twelve invariants are listed below. Each of them is multiplied by an invariant function of ν and Δ in the tabulation. In the future the invariants and the functions shall be indiscriminately labelled by the same symbol:

$$\begin{gathered} a_1\delta_{\alpha\beta}, \quad a_2N_\alpha N_\beta, \quad a_3D_\alpha D_\beta, \quad a_4(D_\alpha N_\beta+D_\beta N_\alpha); \\ ib_1\delta_{\alpha\beta}D_\mu\gamma^\mu, \quad ib_2N_\alpha N_\beta D_\mu\gamma^\mu, \quad ib_3D_\alpha D_\beta D_\mu\gamma^\mu, \quad ib_4(D_\alpha N_\beta+D_\beta N_\alpha)D_\mu; \\ \tfrac{1}{2}ic_1(N_\alpha\gamma_\beta+N_\beta\gamma_\alpha), \quad \tfrac{1}{2}ic_2(D_\alpha\gamma_\beta+D_\beta\gamma_\alpha); \\ id_1\{D_\alpha[\gamma_\beta, D_\mu\gamma^\mu]-D_\beta[\gamma_\alpha, D_\mu\gamma^\mu]\}, \quad id_2\{N_\alpha[\gamma_\beta, D_\mu\gamma^\mu]-N_\beta[\gamma_\alpha, D_\mu\gamma^\mu]\}. \end{gathered} \tag{17}$$

The invariant amplitude M is related to matrix elements of the conventional transition operator by

$$T_{fi} = \left(\frac{m^2}{n_0n'_04d_0d'_0}\right)^{\frac{1}{2}} M_{fi}, \tag{18}$$

where we have used box normalization, which is implied by (21).

In terms of T, the optical theorem is

$$\sigma_{ii} = 2 \operatorname{Im} T_{ii}/V,$$

where σ_{ii} is the total cross section for an initial state i to any final state and V is the relative velocity of the colliding particles. The unpolarized cross section σ_u is the average of σ_{ii} over initial spin states. Thus, σ_u can be expressed in terms of our invariants:

$$\sigma_u = \tfrac{1}{6}\sum_i \sigma_{ii} = \frac{1}{3V}\frac{m}{2n_0d_0}\sum_i \operatorname{Im} M_{ii}.$$

The expression of the forward amplitude M_{ii} in terms of the invariants is considerably simpler than the general expression, since six of them, namely, a_3, a_4, b_3, b_4, c_2 and d_1, do not contribute. To find the required spin averages, it is necessary to sum over the neutron spin and the deuteron polarization. The eutron spin sum leads to a simple trace.

Finally, the sum over α and β must be carried out. Recalling that the fourth component of ξ vanishes in the rest frame, we find $\sum\xi^*\cdot\xi = 3$ by the normalization of ξ, and

$$\tfrac{1}{3}\sum(\xi^*\cdot N)(N\cdot\xi) = N^2-\frac{(N\cdot D)^2}{D^2}.$$

Thus, we find

$$\sigma_u = \frac{1}{3V}\frac{m}{2n_0 d_0}\left[6\,\mathrm{Im}\,a_1 + 6\frac{N\cdot D}{m}\,\mathrm{Im}\,b_1 + 2\left(N^2 - \frac{(N\cdot D)^2}{D^2}\right)\times\left(\mathrm{Im}\,a_2 + \frac{N\cdot D}{m}\,\mathrm{Im}\,b_2 + \frac{2}{m}\,\mathrm{Im}\,c_1\right)\right].$$

It is convenient to introduce an amplitude $\tilde{\alpha}$, whose imaginary part will be simply related to σ_u, that is

$$\tilde{\alpha} = a_1 + \frac{N\cdot D}{m}b_1 + \tfrac{1}{3}\left(N^2 - \frac{(N\cdot D)^2}{D^2}\right)\left(a_2 + \frac{N\cdot D}{m}b_2 + \frac{1}{m}c_1\right). \quad (20)$$

With this definition, the total cross-section is given by

$$\sigma_u = \frac{m}{V n_0 d_0}\,\mathrm{Im}\,\tilde{\alpha}.$$

It is of interest to compare the amplitude $\tilde{\alpha}$ with the forward scattering amplitude f. There are no cross terms between the invariants that are present in f which are not present in $\tilde{\alpha}$. The only invariant in f that is not in $\tilde{\alpha}$ is d_2, and the trace of the cross terms between d_2 and the other invariants vanish in the forward direction. Hence, $|f|^2$ is greater than $|\tilde{\alpha}|^2$, as it has an additional positive contribution from $|d_2|^2$. Therefore, $|\tilde{\alpha}|^2$ is a lower bound on the forward scattering cross section.

We consider now the normalization of the one, two, and three body amplitudes which will enter into our later discussion. Since we are forced by reasons of ignorance to consider the two and three body amplitudes in their non-relativistic limit, we shall assume the following normalization conventions, which have the property of reducing to the correct non-relativistic limit. The deuteron shall be treated as a boson and the triton as a fermion.

Defining the amplitudes

$$\chi_N = \langle 0|\psi|N\rangle = (m/n_0)^{\frac{1}{2}}u(N),$$
$$\chi_D = \langle 0|\mathrm{T}(\psi\psi)|D\rangle = (2d_0)^{-\frac{1}{2}}\Phi_D,$$
$$\chi_t = \langle 0|\mathrm{T}(\psi\psi\psi)|t\rangle,$$

the normalization conventions are

$$\int \mathrm{d}^3x\,\bar{\chi}_N\beta\chi_N = m/n_0,$$
$$\int \mathrm{d}^3x_1\mathrm{d}^3x_2\,\bar{\chi}_D\beta^{(1)}\beta^{(2)}\chi_D\big|_{t_1=t_2} = 1, \quad (21)$$
$$\int \mathrm{d}^3x_1\mathrm{d}^3x_2\mathrm{d}^3x_3\,\bar{\chi}_t\beta^{(1)}\beta^{(2)}\beta^{(3)}\chi_t\big|_{t_1=t_2=t_3} = M_t/t_0.$$

3. The Dispersion Relations

We now use the standard procedures for writing the S-matrix as a retarded commutator of the neutron fields. The result is

$$M(\nu, \Delta^2) = i(4d'_0 d_0)^{\frac{1}{2}} \int \mathrm{d}^4x \bar{u}(n') \langle d' | \{ f(0), \bar{f}(x) \} \theta(-x) | 0 \rangle u(n) \mathrm{e}^{inx}. \quad (22)$$

The equal-time commutator contribution vanishes identically because of isobaric spin considerations. The physical reason for this is that it represents the exchange of one pion between the neutron and deuteron. Since the deuteron cannot absorb a single pion (with isobaric spin one) and remain bound, this term must vanish.

The imposition of the causality requirement makes plausible the statement that M is an analytic function in the upper half plane, and hence, the invariant functions, to be called M_i, might be expected to satisfy a dispersion relation of the form

$$\mathrm{Re}\, M_i(\nu, \Delta^2) = \frac{1}{\pi} \int_{-\infty}^{+\infty} \frac{\mathrm{Im}\, M_i(\nu', \Delta^2)}{\nu' - \nu} \mathrm{d}\nu'. \quad (23)$$

The question of subtractions is a difficult one. It is intuitively clear that the number of subtractions should be no greater than the number required in nucleon-nucleon scattering. This follows from the observation that the elastic scattering amplitude certainly falls off faster with increasing energy than the inelastic scattering amplitude.

This latter amplitude should approach a sum of nucleon-nucleon scattering amplitudes, since the initial binding produces a momentum distribution which plays no role in the limit. Thus, it might be expected that no more subtractions are required here than in nucleon-nucleon scattering. We shall be somewhat optimistic and perform one subtraction when we attempt a quantitative evaluation of the dispersion relation.

There is also the problem of choosing the particular set of invariant matrices into which the causal amplitude is expanded. One criterion for choosing this set is the requirement that the discrete contributions to the absorptive part of the amplitude yield what might be called the renormalized Born approximation. In our case, the Born approximation, i.e., the contribution from the diagram (a) in fig. 1, is very complicated and contains certain "form factors" describing the bound state nature of the scattering problem. For simplicity, we will choose a set of invariants such that the imaginary part of one of the invariant functions, say $\bar{\alpha}$, is proportional to the total scattering cross-section if evaluated in the forward direction. The discrte contribution in this case turns out to be the renormalized. Born approximation but with the residues evaluated at the pole.

There is a third problem associated with the dispersion approach, and that involves the question of the so-called "anomalous" thresholds [5]). Even if one knows that an "anomalous" region exists, which is the case here, the dispersion relations cannot be evaluated because the absorptive part of the amplitude is unknown in this region. One might use the absorptive amplitude determined from an ordinary dispersion relation and attempt to continue it analytically to the anomalous threshold, but it certainly is not clear that this is the correct procedure. We will ignore this problem here since it can be shown that the anomalous threshold disappears in the limit of infinite nucleon mass. We are aware that such a cavalier procedure may be dangerous, since the cross-section varies rapidly near threshold.

We turn now to a qualitative discussion of the absorptive amplitude. The absorptive amplitude is obtained from the causal amplitude in the usual manner, and upon insertion of a complete set of physical states and performance of the space-time integral, we find

$$A = \pi(4d'_0 d_0)^{\frac{1}{2}} \sum_s \bar{u}(n')[\langle d'|f(0)|s\rangle\langle s|\bar{f}(0)|d\rangle\delta(n+d-s) + \langle d'|\bar{f}(0)|s\rangle\langle s|f(0)|d\rangle\delta(n-d'+s)]u(n). \quad (24)$$

The lowest mass states present in this sum are represented in fig. 1.

Of particular interest as intermediate states are the discrete 1 proton and 1 triton states:

$$A_p = \pi(4d'_0 d_0)^{\frac{1}{2}} \sum_{\text{p-spin}} \langle d'|\bar{f}(0)|p\rangle u(n)\bar{u}(n')\langle p|f(0)|d\rangle\delta(n-d'+p) \quad (25)$$

$$A_t = \pi(4d'_0 d_0)^{\frac{1}{2}} \sum_{\text{t-spin}} \bar{u}(n')\langle d'|f(0)|t\rangle\langle t|f(0)|d\rangle u(n)\delta(n+d-t). \quad (26)$$

We are here using the fact that the triton appears to possess no excited (bound) states. It is interesting to note that there appears here what one might term generalized vertex functions, describing a coupling between composite particles and nucleons. The evaluation of these functions is extremely complex in general, but we see that the dispersion approach requires a knowledge of them only on the mass shell. It will be seen later that it is this fact which allows us to effect an evaluation in a relatively simple manner.

The threshold for a state of minimum mass M is

$$\nu_M = (M^2 - M_d^2 - m^2)/2M_d - \Delta^2/4M_d,$$

and the arguments of the relevant delta functions are $(\nu \pm \nu_M)$, where the plus (minus) sign is associated with a crossed (uncrossed) graph. The spectrum will now be discussed in more detail.

There are the continuum states related to the uncrossed diagrams with their lowest threshold at $D = M - (\Delta^2/4M_d)$, corresponding to an intermediate neutron and deuteron. The three nucleon intermediate state

3. The Dispersion Relations

We now use the standard procedures for writing the S-matrix as a retarded commutator of the neutron fields. The result is

$$M(\nu, \Delta^2) = i(4d'_0 d_0)^{\frac{1}{2}} \int \mathrm{d}^4x \bar{u}(n') \langle d' | \{ f(0), \bar{f}(x) \} \theta(-x) | 0 \rangle u(n) \mathrm{e}^{inx}. \quad (22)$$

The equal-time commutator contribution vanishes identically because of isobaric spin considerations. The physical reason for this is that it represents the exchange of one pion between the neutron and deuteron. Since the deuteron cannot absorb a single pion (with isobaric spin one) and remain bound, this term must vanish.

The imposition of the causality requirement makes plausible the statement that M is an analytic function in the upper half plane, and hence, the invariant functions, to be called M_i, might be expected to satisfy a dispersion relation of the form

$$\mathrm{Re}\, M_i(\nu, \Delta^2) = \frac{1}{\pi} \int_{-\infty}^{+\infty} \frac{\mathrm{Im}\, M_i(\nu', \Delta^2)}{\nu' - \nu} \mathrm{d}\nu'. \quad (23)$$

The question of subtractions is a difficult one. It is intuitively clear that the number of subtractions should be no greater than the number required in nucleon-nucleon scattering. This follows from the observation that the elastic scattering amplitude certainly falls off faster with increasing energy than the inelastic scattering amplitude.

This latter amplitude should approach a sum of nucleon-nucleon scattering amplitudes, since the initial binding produces a momentum distribution which plays no role in the limit. Thus, it might be expected that no more subtractions are required here than in nucleon-nucleon scattering. We shall be somewhat optimistic and perform one subtraction when we attempt a quantitative evaluation of the dispersion relation.

There is also the problem of choosing the particular set of invariant matrices into which the causal amplitude is expanded. One criterion for choosing this set is the requirement that the discrete contributions to the absorptive part of the amplitude yield what might be called the renormalized Born approximation. In our case, the Born approximation, i.e., the contribution from the diagram (a) in fig. 1, is very complicated and contains certain "form factors" describing the bound state nature of the scattering problem. For simplicity, we will choose a set of invariants such that the imaginary part of one of the invariant functions, say $\bar{\alpha}$, is proportional to the total scattering cross-section if evaluated in the forward direction. The discrte contribution in this case turns out to be the renormalized. Born approximation but with the residues evaluated at the pole.

There is a third problem associated with the dispersion approach, and that involves the question of the so-called "anomalous" thresholds [5]). Even if one knows that an "anomalous" region exists, which is the case here, the dispersion relations cannot be evaluated because the absorptive part of the amplitude is unknown in this region. One might use the absorptive amplitude determined from an ordinary dispersion relation and attempt to continue it analytically to the anomalous threshold, but it certainly is not clear that this is the correct procedure. We will ignore this problem here since it can be shown that the anomalous threshold disappears in the limit of infinite nucleon mass. We are aware that such a cavalier procedure may be dangerous, since the cross-section varies rapidly near threshold.

We turn now to a qualitative discussion of the absorptive amplitude. The absorptive amplitude is obtained from the causal amplitude in the usual manner, and upon insertion of a complete set of physical states and performance of the space-time integral, we find

$$A = \pi(4d'_0 d_0)^{\frac{1}{2}} \sum_s \bar{u}(n')[\langle d'|f(0)|s\rangle\langle s|\bar{f}(0)|d\rangle\delta(n+d-s) + \langle d'|\bar{f}(0)|s\rangle\langle s|f(0)|d\rangle\delta(n-d'+s)]u(n). \quad (24)$$

The lowest mass states present in this sum are represented in fig. 1.

Of particular interest as intermediate states are the discrete 1 proton and 1 triton states:

$$A_p = \pi(4d'_0 d_0)^{\frac{1}{2}} \sum_{\text{p-spin}} \langle d'|\bar{f}(0)|p\rangle u(n)\bar{u}(n')\langle p|f(0)|d\rangle\delta(n-d'+p) \quad (25)$$

$$A_t = \pi(4d'_0 d_0)^{\frac{1}{2}} \sum_{\text{t-spin}} \bar{u}(n')\langle d'|f(0)|t\rangle\langle t|f(0)|d\rangle u(n)\delta(n+d-t). \quad (26)$$

We are here using the fact that the triton appears to possess no excited (bound) states. It is interesting to note that there appears here what one might term generalized vertex functions, describing a coupling between composite particles and nucleons. The evaluation of these functions is extremely complex in general, but we see that the dispersion approach requires a knowledge of them only on the mass shell. It will be seen later that it is this fact which allows us to effect an evaluation in a relatively simple manner.

The threshold for a state of minimum mass M is

$$\nu_M = (M^2 - M_d{}^2 - m^2)/2M_d - \Delta^2/4M_d,$$

and the arguments of the relevant delta functions are $(\nu \pm \nu_M)$, where the plus (minus) sign is associated with a crossed (uncrossed) graph. The spectrum will now be discussed in more detail.

There are the continuum states related to the uncrossed diagrams with their lowest threshold at $D = M - (\Delta^2/4M_d)$, corresponding to an intermediate neutron and deuteron. The three nucleon intermediate state

threshold is only $\frac{3}{2}\varepsilon$ higher, where ε is the deuteron binding energy. Incidently, because of this low inelastic threshold, one might expect that any "one neutron" approximation, made in analogy with the corresponding treatment of meson-nucleon scattering, should be quite poor if the inelastic cross section were comparable to the elastic. This seems not the case if the energy is low enough [1]).

The continuum states corresponding to the crossed diagrams have their highest threshold at

$$\nu = -\nu_\pi = (M_d{}^2 - 2m_\mu - \mu^2)/2M_d + \Delta^2/4M_d = m - \tfrac{1}{2}(\mu+\varepsilon) + \Delta^2/4M_d,$$

and are continuous to minus infinity. For values of ν less than $-M+\Delta^2/4M_d$, one is in the physical region again, corresponding to elastic neutron-antideuteron scattering. There are many thresholds in the unphysical region corresponding to additional pions in the intermediate state.

In order to discuss the contribution to the absorptive amplitude from the state consisting of one nucleon and one pion, it is convenient to formulate the required matrix elements in terms of meso-disintegration of the deuteron. This process is of interest in its own right and will be treated in a separate paper. It occurs also in the problem of photo-disintegration of the deuteron. We have attempted an estimate of the contribution of this state to the problem at hand, and find that it seems to be small for low neutron energies. Since a subtraction will be performed in the dispersion relations, we expect that this state will negligibly effect the scattering amplitude except insofar as it determines the precise value of the subtraction constants. We plan further study of the meso-disintegration process and its contribution to the unphysical region.

4. Discrete Contributions

4.1. PROTON POLE

In evaluating the contribution of the proton intermediate state to the absorptive amplitude, it is convenient to introduce the following amplitude:

$$K = -2\pi i\delta(d-p-n')\left(\frac{p_0 2d_0}{m}\right)^{\frac{1}{2}} \bar{u}(n')\langle p|f(0)|d\rangle. \tag{27}$$

As will become apparent during the evaluation, it is the presence of the delta function which allows us to calculate this quantity in a simple manner. If we write the delta function as a spatial integral and contract the proton, we find

$$K = (2d_0)^{\frac{1}{2}} \int \mathrm{d}^4x \mathrm{d}^4y \mathrm{e}^{-in'x - iPy} \bar{u}(n')\bar{u}(p) G_n{}^{-1} G_p{}^{-1} \langle 0|\mathrm{T}(\psi(y)\psi(x))|d\rangle.$$

It should not be surprising that we have generated the Bethe-Salpeter (B. S.) amplitude describing the deuteron. It is now convenient to introduce

relative and centre-of-mass coordinates. The integration over the centre-of-mass coordinate can be performed, and the initial delta function is regained.

If the Fourier transform with respect to the relative coordinate of the two-body amplitude is introduced, according to

$$\int \mathrm{d}^4 r e^{-ikr} \Phi(r, d) = 2\pi \Phi(k, d),$$

the auxiliary amplitude becomes

$$K = (2\pi)^2 \delta(d-p-n') \bar{u}(p) \bar{u}(n') G_p^{-1} G_n^{-1} \Phi(\tfrac{1}{2}(p-n'), d). \tag{28}$$

We must now construct the function $\Phi(k, d)$. It satisfies the well known equation

$$G_p^{-1} G_n^{-1} \Phi(k, d) = i(2\pi)^{-4} \int V(k, k') \Phi(k', d) \mathrm{d}^4 k. \tag{29}$$

Since all that one really understands about the deuteron is its description by means of the Schrödinger equation, the B. S. amplitude must be expressed in such terms. This problem has been solved by Salpeter [1]). The answer is that one introduces an equal-time amplitude $\phi(\mathbf{k}, d)$ as the integral over k_0 of $\Phi(k, d)$. In the non-relativistic limit $\phi(\mathbf{k}, d)$ reduces to the Schrödinger wave function. If we use the Schrödinger equation in conjunction with an instantaneous potential in eq. (29), then,

$$G_p^{-1} G_{n'}^{-1} \Phi(k, d) = (2\pi i m)^{-1} (k^2 + \alpha^2) \phi(\mathbf{k}, d),$$

where $\alpha^2 = m\varepsilon$. The amplitude of interest is then readily found in terms of the Schrödinger wave function. Before this can be done explicitly, the matrix function ϕ must be constructed and normalized.

The sixteen component amplitude ϕ is represented in terms of the Dirac matrices. Since the spin and momentum functions separate in the required limit, we can write

$$\phi_{ab} = \int \mathrm{d}k_0 \langle 0 | \mathrm{T}(\psi_a \psi_b) | d \rangle = \phi(\mathbf{k}, d) S_{ab}(\mathbf{k}, d); \tag{30}$$

S is a matrix which yields the correct combination of nucleon spin states to form a triplet state. If the small components of the spinors are neglected, a suitable representation for a triplet S state is

$$S_0 = \frac{1}{\sqrt{2}} \begin{pmatrix} \boldsymbol{\sigma} \cdot \boldsymbol{\xi} \sigma_y & 0 \\ 0 & 0 \end{pmatrix},$$

where the σ's are the usual Pauli matrices; $\boldsymbol{\xi}$ is a unit vector and we see that the three possible values of $\boldsymbol{\xi}$ yield linear combinations of the usual magnetic substates. Notice also that this combination forbids a σ_y in the upper left element, a form which would represent a singlet state. If S is written in

terms of gamma matrices, we see that the matrix

$$S_0 = \frac{1}{2\sqrt{2}} \frac{M_d - i\gamma d}{M_d} (\gamma\xi)C$$

reduces to the correct form in the deuteron rest frame.

It is a simple matter to introduce the effect of the D-state. Near the pole of interest, the S- and D-states have the same momentum dependence. The desired spin function, written in terms of the usual tensor operator S_{12}, is of the form

$$S = \left(1 + \frac{\rho}{\sqrt{8}} S_{12}\right) S_0,$$

where ρ is a measure of the D-state admixture. In the rest frame, the spin function is found to be

$$S = [(1+\rho/\sqrt{2})(1+\beta)\gamma\xi/(2\sqrt{2}) - (3\rho/8k^2)(1+\beta)(\gamma k)(\xi k)]C. \quad (31)$$

It is a simple matter to generalize this to an arbitrary frame.

The momentum function $\phi(\mathbf{k}, d)$ must now be constructed in the neighbourhood of $\mathbf{k}^2 = -\alpha^2$, which is required by the delta function in k. Using elementary methods, this is easily shown to be

$$\phi(\mathbf{k}, d) = N(\mathbf{k}^2 + \alpha^2)^{-1}, \quad (32)$$

where

$$N = 16\, M_D \pi\alpha(1 - \alpha r_e)^{-1}(1+\rho^2)^{-1},$$

and r_e is the usual effective range [3]). Collecting this information, we find

$$K = -2\pi\delta(d - p - n')(n/m)\bar{u}(p)[(1+\tfrac{1}{2}\rho)i\gamma\xi/\sqrt{2} + (\xi N')((3p/2\varepsilon) + (1+\rho/\sqrt{2})/\sqrt{2}M_d)]C\bar{u}(n'). \quad (33)$$

This can be substituted into the form of A_p and the proton spin sums can be trivially performed. The answer is

$$A_p = \frac{\pi}{2M_d} \delta(v + v_p) C^{-1} u(n)[Fi\gamma\xi'^* + G(n'\xi'^*)](m - i\gamma p)[Fi(\gamma\xi) + G(n\xi)]C\bar{u}(n') \quad (34)$$

where

$$F = 16\pi\alpha(1+\tfrac{1}{2}\rho)^2[m(1-\alpha r_e)(1+\rho^2)]^{-1},$$
$$G = 72\pi\alpha\rho^2[m\varepsilon^2(1-\alpha r_e)(1+\rho^2)]^{-1},$$
$$v_p = -\tfrac{1}{2}M_d - \Delta^2/4M_d.$$

It should be pointed out that this is actually the most general form for this matrix element. We have evaluated F and G in their non-relativistic limit.

It is possible to eliminate the charge conjugation matrices from this expression by transposing the neutron spinors into their normal order. It is then possible to rewrite the result in terms of the invariant functions

introduced in sec. 2. We find

$$\begin{aligned} \text{Im } a_1^{\text{p}} &= 0, \quad \text{Im } a_2^{\text{p}} = 2mG^2; \\ \text{Im } b_1^{\text{p}} &= F^2, \quad \text{Im } b_2^{\text{p}} = G^2; \\ \text{Im } C_1^{\text{p}} &= F^2 - 4mFG. \end{aligned}$$

The contribution to Im $\tilde{a}$ from the proton pole is

$$-\pi\delta(\nu+\nu_{\text{p}})\Gamma_{\text{p}}, \text{ with } \Gamma_{\text{p}} = 8\pi\alpha/m(1-\alpha r_{\text{e}}). \tag{35}$$

4.2. TRITON INTERMEDIATE STATE

The matrix elements necessary to calculate the contribution of the triton intermediate state will be evaluated in close analogy to the method used for the proton state. It is also possible to evaluate this contribution by using a formulation of the scattering amplitude in terms of potentials. This latter approach has been carried out in detail and agrees with the results of the field-theory discussion to be presented below. We prefer the field-theory approach because it simplifies discussion of the Pauli principle, formal relativistic invariance, and problems associated with the centre-of-mass motion of many body systems. This method may also be extended to the evaluation of the proton vertex function for more general nuclear systems. The vertex function of interest is

$$L = -2\pi\delta(t-d-n')(2d_0)^{\frac{1}{2}}\bar{u}(n')\langle d|f(0)|t\rangle. \tag{36}$$

In order to proceed further, it is necessary to know how to contract the deuteron. This problem has been solved by Haag [7]), Nishijima [8]) and Zimmerman [9]). Their form of the contraction rule does not seem to be as convenient in the problem at hand as one which involves the B. S. amplitude and the two-body Green's function directly [10]). If the delta function in L is written as a space-time integration and the deuteron is contracted, the vertex function becomes

$$\begin{aligned} L = \int \frac{\mathrm{d}^4x\mathrm{d}^4y\mathrm{d}^4z}{(2\pi)^3} \bar{\Phi}(k, d)\bar{u}(n')G_{\text{n}'}{}^{-1}G_{\text{d}}{}^{-1}\langle 0|\mathrm{T}(\psi_{\text{n}'}(x)\psi_{\text{n}}(y)\psi_{\text{p}}(z))|t\rangle \\ \times\exp\{-i[n'x+\tfrac{1}{2}d(y+z)+k(z-y)]\}. \end{aligned} \tag{37}$$

The matrix element in this expression is immediately recognized as the B. S. amplitude describing a triton; $\bar{\Phi}(k, d)$ is the B. S. amplitude describing a deuteron of total momentum d and relative momentum k. The inverse two-body Green's function has been defined in the previous section, eq. (29).

The centre-of-mass and relative coordinates of the triton are introduced as

$$x = X+r, \; y = X+s, \; z = X-r-s.$$

Lorentz invariance of the triton amplitude implies that

$$\chi_t(s, y, z) = \chi_t(r, s, -r-s)\mathrm{e}^{itX}.$$

Introducing the Fourier transform of this function and the momentum variables

$$l = n'-k-\tfrac{1}{2}d = n'-p, \quad K = -2k = p-n,$$

the integration over the centre-of-mass coordinate can be performed; L becomes

$$L = 2\pi\delta(t-n'-d)3^4 \int \frac{\mathrm{d}^4k}{(2\pi)} \bar{u}(n')\bar{\Phi}(k, d)G_{n'}{}^{-1}G_{d}{}^{-1}\Theta(t, l, K).$$

Our problem is now to construct the triton amplitude $\Theta(t, l, K)$. It satisfies an equation of the form

$$G_{n'}{}^{-1}G_{n}{}^{-1}G_{p}{}^{-1}\Theta(t, l, K) = A\int V_{t}\Theta(t, \bar{l}, \bar{K})\mathrm{d}^4\bar{l}\mathrm{d}^4\bar{K}, \tag{38}$$

where

$$V_{t} = G_{p}{}^{-1}V_{n'n}\delta(p-\bar{p})+G_{n}{}^{-1}V_{n'p}\delta(n-\bar{n})+G_{n'}{}^{-1}V_{np}\delta(n'-\bar{n}'),$$

and A is a constant. Direct three body forces have been neglected, but can be included with no trouble.

This equation must be reduced to an equal-time or Schrödinger equation. This can be done exactly as in the two-body case. An equal-time amplitude is introduced and defined as

$$\vartheta(t, \mathbf{l}, \mathbf{K}) = \int \mathrm{d}l_0\mathrm{d}K_0\Theta(t, l, K).$$

Use is also made of the formula

$$\int \mathrm{d}l_0\mathrm{d}K_0G_pG_nG_{n'} = 3(2\pi i)^2(H_p+H_n+H_{n'}-t_0)^{-1}, \tag{39}$$

where the H_1 are the Dirac Hamiltonians for the respective particles and t_0 is the triton binding energy. Negative energy components have been neglected, and this has been evaluated in the rest frame of the triton.

If it is assumed that V_t is independent of l_0 and K_0, it can be shown that the defining equation for Θ preserves this property. The equation satisfied by the equal-time amplitude is then found to be

$$(H_p+H_n+H_{n'}-t_0)\vartheta(t, \mathbf{l}, \mathbf{K}) = 3A(2\pi i)^2\int V_t\vartheta(t, \bar{\mathbf{l}}, \bar{\mathbf{K}})\mathrm{d}^3\bar{\mathbf{l}}\mathrm{d}^3\bar{\mathbf{K}},$$

which reduces to the Schrödinger equation if the constant A is chosen properly. Thus, the equal-time amplitude reduces to the Schrödinger wave function in the non-relativistic limit.

The equation for $\Theta(t, l, K)$ can be rearranged to read

$$G_{n'}{}^{-1}G_{d}{}^{-1}\Theta(t, l, K) = A\int V_{dn'}\Theta(t, \bar{l}, \bar{K})\mathrm{d}^4\bar{l}\mathrm{d}^4\bar{K}, \tag{41}$$

where

$$V_{dn'} = G_{p}{}^{-1}V_{nn'}\delta(p-\bar{p})+G_{n}{}^{-1}V_{pn'}\delta(n-\bar{n}).$$

Using the equations that have been developed, one can show that

$$G_{n'}^{-1}G_d^{-1}\Theta(t, l, K) = [3(2\pi i)^2]^{-1}(H_d+H_{n'}-t_0)\vartheta(t, \mathbf{l}, \mathbf{K}),$$

where

$$H_d = H_p+H_n-V_{pn}.$$

If this expression is inserted into L, the k_0 integration can be carried out trivially, and

$$L = -2\pi\delta(t-n'-d)\frac{3^3}{(2\pi)^3}[n'_0+d_0-t_0]\int d^3k\bar{u}(n')\phi(\mathbf{k}, d)\vartheta(t, \mathbf{l}, \mathbf{k}),$$

an expression involving only equal-time or Schrödinger wave functions. We must now construct the triton wave function. Since our knowledge of the triton ground state is quite limited, the D state of deuteron will be neglected in the evaluation of L.

The triton amplitude is characterized by three spinor labels. Since Θ must be antisymmetric in the two neutrons, it is reasonable to assume that it is space symmetric and spin antisymmetric. The triton spin function S must then satisfy

$$S_{\alpha\beta\gamma} = -S_{\beta\alpha\gamma},$$

where γ is the proton spinor label. The neutrons will be in a relative singlet spin state and the triton spin will then be labelled with the spin of the proton. A suitable form for S in the triton rest frame is found to be

$$S_{\alpha\beta\gamma} = \left[\frac{1+\beta}{2\sqrt{2}}iC\gamma_5\right]_{\alpha\beta}u_\gamma(t). \tag{42}$$

It is assumed from invariance arguments that the Dirac spinor has as its arguments the triton momentum t and the triton mass M_t. This is easily generalized to an arbitrary coordinate system.

The spin matrix element in L is therefore

$$\bar{u}_\alpha(n')\bar{S}_{\beta\gamma}(d)S_{\alpha\beta\gamma}(t) = \frac{i}{8M_tM_d}\bar{u}(n')[(M_t-i\gamma t)(M_d-i\gamma d)(\gamma\xi^*)]\gamma_5 u(t).$$

This can be reduced to the form

$$\bar{u}(n')[A_t i(\gamma\xi^*)+B_t(n'\xi^*)]\gamma_5 u(t),$$

where

$$A_t = [M_dM_t+\tfrac{1}{2}(M_t^2+M_d^2-m)]/4M_dM_t,$$
$$B_t = [M_t+M_d+m]/4M_dM_t.$$

It should be noted that since ξ^* is a pseudo-vector, this is the matrix element of a scalar. This is the most general possible form for the matrix element. Our approximations are in evaluating A_t and B_t.

We turn now to the problem of the triton momentum wave function. The triton model, which must possess the correct asymptotic behaviour, is chosen to be

$$= 2N_t\{[\mathbf{P}^2+\mathbf{N}^2+\mathbf{N}'^2-\alpha_t^2]^{-1}-[\mathbf{P}^2+\mathbf{N}^2+\mathbf{N}'^2-\beta_t^2]^{-1}\},$$

where $\beta_t \gg \alpha_t$, $\mathbf{P}+\mathbf{N}+\mathbf{N}' = \mathbf{t}$, and $\alpha_t^2 = mt_0$. The constant N_t is determined by the normalization condition, eq. (21), which is

$$\int d^3p\, d^3n |\vartheta(p, n)|^2 = M_t(2\pi)^6/(t_0 3^6).$$

The momentum integral in L is easily evaluated at the point demanded by the delta function. The result is

$$L = \delta(t-n'-d)[3^3 N_d N_t \alpha_0 A_t/M]\bar{u}(n')i(\gamma\xi^*)\gamma_5 u(t),$$

where B_t has been neglected in comparison with A_t.

This allows a simple evaluation of the triton pole. The result is

$$A_t = \frac{\pi}{2M_d}\delta(\nu-\nu_t)R_t\bar{u}(n')(\gamma\xi_t^*)(M_t+i\gamma t)(\gamma\xi_1)u(n),$$

where

$$\nu_t = (M_t^2-M_d^2-m^2-\tfrac{1}{2}\Delta^2)/2M_d, \tag{44}$$

and

$$R_t = 24(2\pi)^2\sqrt{3}\left\{(1-\alpha r_e)(1+\beta_t^2/\alpha_t^2)\left[1-\frac{4\alpha_t^2}{\beta_t^2}\ln\frac{\beta_t}{\alpha_t}\right]\right\}^{-1}(\varepsilon/t_0)\sqrt{\varepsilon/m}.$$

The contribution to the amplitude $\mathrm{Im}\,\bar{\alpha}$ is easily computed to be

$$\pi\delta(\nu-\nu_t)5R_t/4 = -\pi\delta(\nu-\nu_t)\Gamma_t. \tag{45}$$

5. Numerical Results and Conclusions

The large size and complexity of the unphysical region precludes any detailed evaluation of its contributions to the dispersion relations. In the preceding section the evaluation of the contributions of the two discrete poles was effected. The next lowest state after these is the state of one π meson and a nucleon. A preliminary effort at evaluating this contribution suggests that it is not large for small incident neutron energies and is not strongly dependent on this energy. In a singly subtracted dispersion relation it may be permissible to neglect the one meson and all more massive negative energy states. At sufficiently low energies we are thus led to suggest a dispersion relation of the type

$$\mathrm{Re}\,\bar{\alpha}(\nu)-\mathrm{Re}\,\bar{\alpha}(0) = \frac{-\nu\Gamma_p}{(\nu+\nu_p)\nu_p}+\frac{\nu\Gamma_t}{(\nu-\nu_t)\nu_t}+\frac{\nu}{\pi}\mathrm{P}\int_M^\infty \frac{\mathrm{Im}\,\bar{\alpha}(\nu')}{(\nu'-\nu)\nu'}d\nu'. \tag{46}$$

In fig. 2, the $\mathrm{Re}\,\bar{\alpha}$ computed from (46) is plotted in which $\mathrm{Im}\,\bar{\alpha}$ has been replaced by the total cross section. This may be compared with the real part of the forward scattering amplitude calculated from the experimental phase shifts. At zero kinetic energy these agree because of the subtraction. At 9.6 MeV $\mathrm{Re}\bar{\alpha}$ has been calculated using the phase shifts of Gammel and

Christian[11]). The two calculations are in quite good agreement. This comparison is shown in fig. 2. Presumably at low energies the dispersion relation (46) is valid, and it is sufficient to include only the pole contributions to the unphysical region.

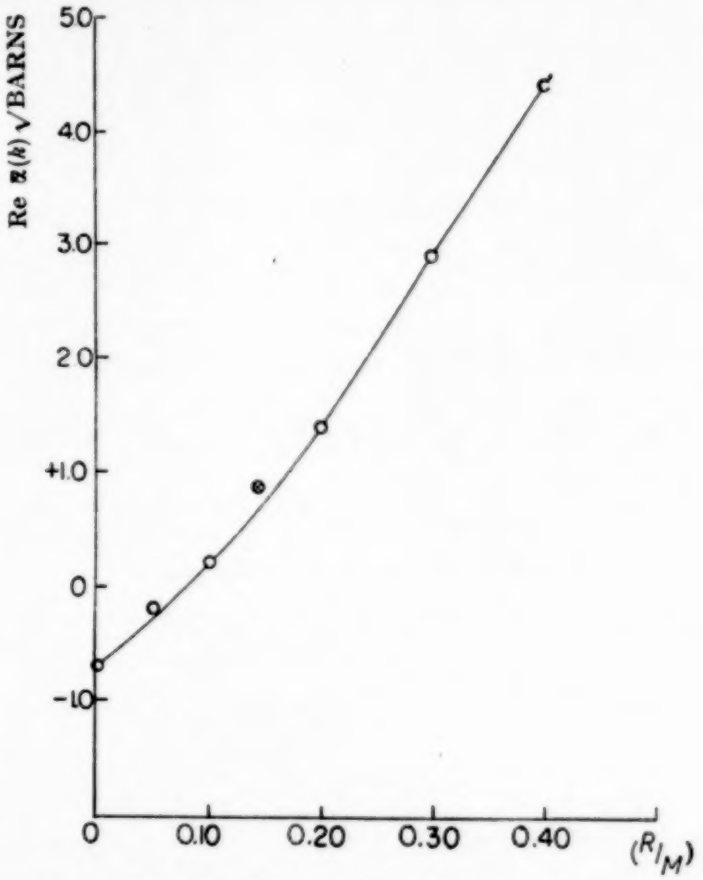

Fig. 2. A comparison of Re $\mathfrak{a}(k)$ calculated from dispersion theory and from phase shifts.
○ Re $\mathfrak{a}(k)$ calculated from dispersion relations.
⊗ Re $\mathfrak{a}(k)$ calculated with the Christian-Gammel phase shifts.

The amplitude involved in the proton pole may be expressed as was shown in sec. 3, in terms of the familiar parameters of the two nucleon system. It is of interest to see whether the relevant combination of parameters F and G may be obtained by some sort of extrapolation from neutron deuteron scattering. In the neighbourhood of the pole, the cross section $d\sigma/dn'_0$ is particularly suited for a discussion of this extrapolation. If a non-relativistic notation is employed, this cross section becomes, in the laboratory system,

$$\left(\frac{d\sigma}{d\tau'}\right)_L = 24\frac{\pi}{m}\frac{1}{\varepsilon\tau}\frac{h^2}{(1+2\tau')^2} = \frac{9\pi}{2\tau}\left(\frac{d\sigma}{d\Omega}\right)_C \qquad (47)$$

where $\tau = (n_0 - m)\varepsilon$, and τ' is similarly defined; ε is the deuteron binding energy and h is $(1-\alpha r_e)^{-1}$. The D state contribution has been neglected. The angular distribution $d\sigma/d\Omega$ is evaluated in the centre-of-mass system,

and τ and τ' are related by $\tau' = \tau(\frac{5}{9}+\frac{4}{9}\cos\theta)$. Due to the scarcity of accurate data at very large angles it is difficult to make a convincing extrapolation to determine h^2, although the qualitative agreement is satisfactory.

It may be possible that with suitable approximations the dispersion relations introduced here could be solved for the scattering amplitude at low energies. Assuming that dispersion relations hold for the quartet and doublet spin states separately, the dispersion relations can be solved if the S-state phase shift is the only one different from the Born approximation. This procedure is to be discussed in detail in a forthcoming paper [12]). In principle, this approximation can be improved by a well defined iteration scheme.

The use of dispersion methods in a discussion of deuteron reactions seems to provide a systematic way of treating these problems which is rather different from those used before. The manner in which the various contributions are classified seems attractive. There are, however, some theoretical difficulties to be overcome before the dispersion theory of composite particles can be regarded as complete. In particular, the problem of the anomalous thresholds must be studied further.

It is possible to write dispersion relations involving composite particles and achieve some quantitative success in treating experimental data. The reliability of our results would, of course, be greatly enhanced from a study of the matrix element for the process

$$\pi+\mathrm{d}\to\mathrm{n}+\mathrm{n},$$

which is the next most massive state in our expansion. A knowledge of this process and the total n—d cross section may be sufficient to predict the doublet and quartet scattering lengths, and thus, to resolve the present ambiguity in the experimental values [1]).

References

1) M. Verde, Handbuch der Physik **39** (1957);
L. Sartori and S. I. Rubinow, Phys. Rev. **112** (1958) 214
2) D. G. Hurst and J. Alcock, Can. J. Phys. **29** (1951) 36;
Wollan, Shull and Koehler, Phys. Rev. **83** (1951) 700;
R. Wilson, (to be published)
3) M. L. Goldberger, Y. Nambu and R. Oehme, Ann. Phys. **2** (1957) 226
4) P. E. Hodgson, Adv. Phys. **1** (1958) 1
5) Karplus, Sommerfeld and Wichmann, Phys. Rev. **111** (1958) 1187;
Y. Nambu, Nuovo Cimento **9** (1958) 610;
J. Bjorken, (to be published)
6) E. E. Salpeter, Phys. Rev. **87** (1952) 328
7) R. Haag, Phys. Rev. **112** (1958) 669
8) K. Nishijima, Phys. Rev. **111** (1958) 995
9) W. Zimmerman, Nuovo Cimento **10** (1958) 597
10) R. Blankenbecler, (to be published)
11) R. S. Christian and J. L. Gammel, Phys. Rev. **91** (1953) 100
12) S. Gartenhaus and R. Blankenbecler, (to be published)

1.D.1 *Nuclear Physics* **12** (1959) 647—656; © *North-Holland Publishing Co., Amsterdam*
Not to be reproduced by photoprint or microfilm without written permission from the publisher

ON SYMPLECTIC INVARIANCE OF THE ENERGY MATRIX IN A NUCLEAR j^N CONFIGURATION

K. HELMERS

Physikalisches Staatsinstitut, Hamburg

Received 15 May 1959

Abstract: The energy matrix of a nuclear j^N configuration of maximum isobaric spin is given a convenient form by methods of field theory, and its invariance under the symplectic transformations of Flowers and Edmonds is investigated. A δ-interaction of arbitrary exchange type is shown to lead to an energy matrix that is non-invariant in this sense.

1. Introduction

In the jj-coupling shell model, the transformation properties of the energy matrix and the state vectors under the unitary symplectic group $\mathrm{Sp}(2j+1)$ play a certain role. The most important problems in this connexion have been treated by Flowers and Edmonds [2,3]). In the following, we propose to enter into some questions that have not been answered in the literature in so explicit and elementary a manner as they deserve.

In sections 2 and 3 we shall give a compact form of the energy matrix for maximum isobaric spin (neutrons only or protons only) which enables us to formulate the condition for symplectic invariance † of the energy matrix explicitly as a condition on the Slater integrals (section 4). This serves us to prove that the δ-interaction does not lead to an energy matrix invariant under the symplectic group (section 5) as the criterion for invariance is clearly violated. In section 6 we give, for a shell strongly localized in space, that 2-particle interaction which would make the energy matrix invariant. For nearly invariant energy matrices, we give the Flowers-Edmonds approximation explicitly (section 7) with an application to the δ-potential.

2. The Energy Matrix in the Formalism of Field Theory

We consider the incompletely filled neutron †† shell in a nucleus, with one-particle wave-functions $\psi_m(\mathbf{r}, \zeta)$, $m = -j, -j+1, \ldots j$, m being the magnetic quantum number and j the half odd integer value of one-neutron

† This must not be confused with the "pairing property" of the interaction discussed by Racah and Talmi (ref. [5])).

†† Protons may be treated in a similar way.

angular momentum characterizing the shell; $\mathbf{r}$ is the position and ζ the spin variable (with possible values $\pm\frac{1}{2}$) of the neutron. Let the *residual interaction* between any pair (i, k) of neutrons in the shell be a Wigner † potential $v(\mathbf{r}_i, \mathbf{r}_k)$. If there are N neutrons in the shell, the total residual interaction is

$$H_{\text{int}}^{(N)} = \sum_{1 \leqq i < k} v(\mathbf{r}_i, \mathbf{r}_k). \tag{1}$$

We form the matrix of this operator with respect to the antisymmetric N-neutron states of our j^N configuration, which is the submatrix of

$$H_{\text{int}} = -\tfrac{1}{2} \sum_{m_1=-j}^{j} \sum_{m_2=-j}^{j} \sum_{m_3=-j}^{j} \sum_{m_4=-j}^{j} v_{m_1 m_2 m_3 m_4} a_{m_1}^* a_{m_2}^* a_{m_3} a_{m_4} \tag{2}$$

in the subspace of N neutrons. Here a_m^* and a_m are the creation and annihilation matrices, respectively, for a neutron in state ψ_m, satisfying the usual relations

$$\begin{aligned} &a_m^* a_{m'} + a_{m'} a_m^* = \delta_{mm'}, \\ &a_m a_{m'} + a_{m'} a_m = 0, \end{aligned} \qquad (m, m' = -j, -j+1, \ldots j). \tag{3}$$

The $v_{m_1 m_2 m_3 m_4}$ are matrix elements of the interaction potential:

$$v_{m_1 m_2 m_3 m_4} = \sum_{\zeta_1 \zeta_2} \int d\mathbf{r}_1 d\mathbf{r}_2 \psi_{m_1}^*(\mathbf{r}_1, \zeta_1) \psi_{m_2}^*(\mathbf{r}_2, \zeta_2) \cdot v(\mathbf{r}_1, \mathbf{r}_2) \psi_{m_3}(\mathbf{r}_1, \zeta_1) \psi_{m_4}(\mathbf{r}_2, \zeta_2). \tag{4}$$

The matrix

$$N_{\text{op}} = \sum_{m=-j}^{j} a_m^* a_m \tag{5}$$

has as its eigenvalues the possible numbers N of neutrons in the shell, which are $0, 1, 2, \ldots 2j+1$. In the following we consider the full energy matrix (2) and therefore leave N unspecified.

3. Reduction of the Energy Matrix by Rotational Invariance of the Two-Nucleon-Interaction

The interaction potential $v(\mathbf{r}_1, \mathbf{r}_2)$ is assumed to be symmetric in $\mathbf{r}_1$ and $\mathbf{r}_2$ and invariant under simultaneous rotation of $\mathbf{r}_1$ and $\mathbf{r}_2$. The coefficients $v_{m_1 m_2 m_3 m_4}$ are then expressible by a few fundamental interaction integrals. To show this, we introduce polar coordinates r, ϑ, φ and observe that $v(\mathbf{r}_1, \mathbf{r}_2)$ can only depend on r_1, r_2 and the angle ϑ_{12} between directions (ϑ_1, φ_1) and (ϑ_2, φ_2). As a function of $\cos \vartheta_{12}$ it can be expanded in Legendre polynomials as follows:

$$\begin{aligned} v(\mathbf{r}_1, \mathbf{r}_2) &= \sum_{k=0}^{\infty} v_k(r_1, r_2) P_k(\cos \vartheta_{12}) \\ &= \sum_{k=0}^{\infty} v_k(r_1, r_2) \frac{4\pi}{2k+1} \sum_{q=-k}^{k} Y_{kq}^*(\vartheta_1, \varphi_1) Y_{kq}(\vartheta_2, \varphi_2). \end{aligned} \tag{6}$$

† For a discussion of Majorana and Bartlett potentials see section 5.

The Y_{kq} are spherical harmonics in the normalization of Edmonds [1]). Let

$$\psi_m(\mathbf{r}, \zeta) = R(r)W_m(\vartheta, \varphi, \zeta) \tag{7}$$

with $R(r)$ real and normalized according to

$$\int_0^\infty R(r)^2 r^2 \mathrm{d}r = 1, \tag{8}$$

and let the ψ_m and W_m have a *definite* value l of *orbital angular momentum* and hence a *definite parity* $(-1)^l$.

By substituting (6) and (7) into (4) we obtain

$$v_{m_1 m_2 m_3 m_4} = \sum_{k=0}^{\infty} \sum_{q=-k}^{k} \frac{4\pi}{2k+1} F^{(k)} (jm_3|Y_{kq}|jm_1)^* (jm_2|Y_{kq}|jm_4), \tag{9}$$

where we have introduced the *Slater integrals*

$$F^{(k)} \equiv \int_0^\infty \int_0^\infty v_k(r_1, r_2) R(r_1)^2 R(r_2)^2 r_1^2 \mathrm{d}r_1 r_2^2 \mathrm{d}r_2, \tag{10}$$

and matrix elements of the type

$$(jm_2|Y_{kq}|jm_4) \equiv \sum_{\zeta} \int W^*_{m_2}(\vartheta, \varphi, \zeta) Y_{kq}(\vartheta, \varphi) W_{m_4}(\vartheta, \varphi, \zeta) \sin\vartheta \mathrm{d}\vartheta \mathrm{d}\varphi, \tag{11}$$

which by use of the Wigner-Eckart theorem (cf. ref. [1])) can be transformed into

$$(jm_2|Y_{kq}|jm_4) = (4\pi)^{-\frac{1}{2}} (-1)^{j-m_4} (jm_2 j - m_4|jjkq)(j||C_k||j). \tag{12}$$

Here $(jm_2 j - m_4|jjkq)$ is a Clebsch-Gordan coefficient which is real and vanishes for $k > 2j$. The value of the reduced matrix element $(j||C_k||j)$ is found from Edmonds' book (ref. [1]), eq. (7.1.9)) to be

$$(j||C_k||j) = \begin{cases} 0 & \text{for } k \text{ odd}, \\ 2(-1)^{\frac{1}{2}k} \left[\dfrac{(2j-k)!}{(2j+k+1)!}\right]^{\frac{1}{2}} \dfrac{k!}{(\frac{1}{2}k)!^2} \dfrac{(j+\frac{1}{2}k+\frac{1}{2})!}{(j-\frac{1}{2}k-\frac{1}{2})!} & \text{for } k \text{ even}. \end{cases} \tag{13}$$

Thus (9) goes into

$$v_{m_1 m_2 m_3 m_4} = \sum_{k=0}^{2j} \sum_{q=-k}^{k} F_k (-1)^{j-m_4} (jm_2 j - m_4|jjkq)(-1)^{j-m_1} (jm_3 j - m_1|jjkq) \tag{14}$$

with the abbreviation

$$F_k \equiv \frac{F^{(k)}}{2k+1} (j||C_k||j)^2. \tag{15}$$

By (14) the coefficients $v_{m_1 m_2 m_3 m_4}$ have indeed been *reduced to a few constants* $F_0, F_2, F_4, \ldots F_{2j-1}$. The F_k for odd k vanish by (13).

The result (14) can be used to simplify the energy matrix. We define the following expressions † which are bilinear in the a_m^*, $a_{m'}$:

† They are $(2k+1)^{\frac{1}{2}}$ times the tensor operators $U_q^{(k)}$ of ref. [3]).

$$u_{kq} = \sum_{m_2 m_4} (-1)^{j-m_4}(jm_2j-m_4|jjkq)a^*_{m_2}a_{m_4}, \quad \begin{pmatrix} k = 0, 1, 2, \ldots j \\ q = -k, -k+1, \ldots k \end{pmatrix}. \tag{16}$$

Then by inserting (14) into (2), by using the commutation relations (3) and the symmetry and orthogonality properties of the Clebsch-Gordan coefficients we obtain

$$H_{\text{int}} = \tfrac{1}{2}\sum_{k=0}^{2j} F_k \sum_{q=-k}^{k} u^*_{kq}u_{kq} - N_{\text{op}}\tfrac{1}{2}\sum_{k=0}^{2j} F_k \frac{2k+1}{2j+1}. \tag{17}$$

4. The Condition for Symplectic Invariance of the Energy Matrix

Let the infinitesimal parameters $\varepsilon_{mm'}$ form an antihermitean matrix:

$$\varepsilon_{mm'}+\varepsilon_{m'm}{}^* = 0 \qquad (m, m' = -j, -j+1, \ldots j). \tag{18}$$

Then the operator

$$U = 1+\sum_{m=-j}^{j}\sum_{m'=-j}^{j} \varepsilon_{mm'}a_m{}^*a_{m'} \tag{19}$$

is unitary to first order in the $\varepsilon_{mm'}$ and induces an infinitesimal unitary transformation of the a_m in the following sense:

$$U^{-1}a_mU = \sum_{m'} (\delta_{mm'}+\varepsilon_{mm'})a_{m'}. \tag{20}$$

Starting from this, we construct the group $U(2j+1)$ of finite *unitary transformations* of the a_m by defining the transform of a_m to be $U^{-1}a_mU$, the transform of $a_m{}^*$ to be $U^{-1}a_m{}^*U$, and the transform of any integral rational function A of the $a_m{}^*$ and $a_{m'}$ to be $U^{-1}AU$. It is easily proved that the $a_m{}^*$ are then transformed *contragrediently* † to the a_m, thus N_{op} is invariant. The unitary group contains as a subgroup the group $R(3)$ which represents *rotations* in 3-dimensional physical space with transformation matrices of the special form $\mathscr{D}^{(j)}_{mm'}$ (ref. [1]), p. 55). Flowers [2]) was led to consider another subgroup of $U(2j+1)$ which contains $R(3)$, the group $Sp(2j+1)$ of *symplectic* transformations in $2j+1$ dimensions. Its fininitesimal parameters $\varepsilon_{mm'}$ satisfy (18) as well as

$$(-1)^{j-m'}\varepsilon_{-m',-m}+(-1)^{j-m}\varepsilon_{mm'} = 0 \qquad (m, m' = -j, -j+1, \ldots j). \tag{21}$$

From this it follows that under symplectic transformations the $(-1)^{j-m}a_{-m}$ are transformed contragrediently to a_m, i.e. they are transformed as the $a_m{}^*$. Thus

$$Q_{00} \equiv (2j+1)^{-\frac{1}{2}}\sum_{m=-j}^{j}(-1)^{j-m}a_{-m}a_m = \sum_{m_1 m_2}(jm_1jm_2|jj00)a_{m_2}a_{m_1} \tag{22}$$

is *invariant* under $Sp(2j+1)$. Replacing m_4 by $-m_4$ and using $(-1)^{2m_4}$

† The transformation matrix of the $a_m{}^*$ is, therefore, the complex conjugate of the transformation matrix of the a_m.

$= -1$ we get from (16):

$$u_{kq} = -\sum_{m_2 m_4} (-1)^{j-m_4}(jm_2jm_4|jjkq)a^*_{m_2}a_{-m_4}, \tag{23}$$

which, under Sp(2j+1) (and, especially, under R(3)), is *transformed in the same way as*

$$Q^*_{kq} = \sum_{m_2 m_4} (jm_2jm_4|jjkq)a^*_{m_2}a^*_{m_4}. \tag{24}$$

The hermitean conjugate of this operator in the special case $k = 0$, $q = 0$, is the Q_{00} introduced above in (22).

Under R(3) the $a_m (m = -j, -j+1, \ldots j)$ form an irreducible tensor operator, and so do the $a_m{}^*$. Thus, for fixed k, the $Q^*_{kq} (q = -k, -k+1, \ldots k)$ form an *irreducible tensor operator under* R(3). This is also true for the u_{kq} $(q = -k, -k+1, \ldots k)$ because they are transformed as the Q^*_{kq}. Thus, the *rotational invariance of* H_{int} becomes especially evident from (17).

Under unitary symplectic transformations, $u_{00} = u^*_{00}$ is invariant, which follows from the symplectic invariance of Q_{00} or from

$$u_{00} = u^*_{00} = (2j+1)^{-\frac{1}{2}}N_{\text{op}}. \tag{25}$$

If we label the irreducible representations [2]) of Sp(2j+1) by $j+\frac{1}{2}$ integers $(\sigma_1, \sigma_2, \ldots \sigma_{j+\frac{1}{2}})$ such that $\sigma_1 \geqq \sigma_2 \geqq \ldots \geqq \sigma_{j+\frac{1}{2}} \geqq 0$, then u_{00} constitutes an irreducible representation of type (00 . . . 0). It may be shown [2, 3]) that the u_{kq} with *odd* k span an irreducible unitary representation (20 . . . 0) of Sp(2j+1), while the u_{kq} with k even and non-zero span an irreducible unitary representation (110 . . . 0) of Sp(2j+1) †. Clearly, the u^*_{kq} are transformed with corresponding complex conjugate matrices.

The operator H_{int} only depends on the u_{kq} from representations (00 . . . 0) and (110 . . . 0) as $F_k = 0$ for odd k. Assume now H_{int} to be invariant under Sp(2j+1), i.e.

$$S^{-1}H_{\text{int}}S = H_{\text{int}} \quad \text{for all } S \text{ from Sp}(2j+1), \tag{26}$$

which can be written

$$\tfrac{1}{2}\sum_{\substack{k>0\\ \text{even}}}\sum_q F_k(S^{-1}u^*_{kq}S)(S^{-1}u_{kq}S) = \tfrac{1}{2}\sum_{\substack{k>0\\ \text{even}}}\sum_q F_k u^*_{kq}u_{kq} \tag{27}$$

for all S from Sp(2j+1). On the left-hand side, the $S^{-1}u_{kq}S$ can be represented as linear combinations of the $u_{k'q'}$ with the help of the representative matrix of S in the representation (110 . . . 0) with the u_{kq} as a basis. The $S^{-1}u^*_{kq}S$ can be treated analogously. Integrating (27) over the full group S and using the orthogonality relations of the representative matrices, we

† This is the explicit result of the reduction process

$$(10\ldots0)\times(10\ldots0) = (0\ldots0)+(20\ldots0)+(110\ldots0),$$

applied to the Kronecker product of two representations (10 . . . 0) of Sp(2j+1) given by the $a_m{}^*$ and the a_m, respectively.

obtain from (27) after some reduction

$$\tfrac{1}{2}F \sum_{\substack{k>0\\ \text{even}}} \sum_{q} u^*_{kq} u_{kq} = \tfrac{1}{2} \sum_{\substack{k>0\\ \text{even}}} \sum_{q} F_k u^*_{kq} u_{kq}, \tag{28}$$

where F is some constant. Eq. (28) is thus a condition *necessary* for (26) to hold. Obviously, it is also *sufficient* as the left-hand side is invariant under Sp $(2j+1)$.

Thus a necessary and sufficient condition for *symplectic invariance* † *of* H_{int} is that the latter has the form

$$H_{\text{int}} = \tfrac{1}{2}F \sum_{\substack{k>0\\ \text{even}}} \sum_{q} u^*_{kq} u_{kq} + \tfrac{1}{2}F_0 u^*_{00} u_{00} - N_{\text{op}} \tfrac{1}{2} \sum_{k=0}^{2j} F_k \frac{2k+1}{2j+1}, \tag{29}$$

where F is some constant. The following *condition on the interaction integrals* F_k is *sufficient* for (29):

$$F_2 = F_4 = \ldots = F_{2j-1} = F, \tag{30}$$

and it may be shown to be also *necessary*. For $j = \frac{3}{2}$, (30) becomes trivial and is always satisfied.

By use of (25) and (30) we obtain

$$H_{\text{int}} = \tfrac{1}{2}F \sum_{\substack{k>0\\ \text{even}}} \sum_{q} u^*_{kq} u_{kq} - \tfrac{1}{2}F \frac{2j^2+j-1}{2j+1} N_{\text{op}} + \tfrac{1}{2}F_0 (2j+1)^{-1} (N^2_{\text{op}} - N_{\text{op}}) \tag{31}$$

if H_{int} is invariant under Sp$(2j+1)$,

and introducing (cf. ref. [3]) the operators

$$G(\text{U}) = \sum_{k=0}^{2j} \sum_{q} u^*_{kq} u_{kq}, \qquad G(\text{Sp}) = 2 \sum_{k \text{ odd}} \sum_{q} u^*_{kq} u_{kq}, \tag{32}$$

we have, again using (25),

$$H_{\text{int}} = \tfrac{1}{2}F[G(\text{U}) - \tfrac{1}{2}G(\text{Sp})] - \tfrac{1}{2}FjN_{\text{op}} + \tfrac{1}{2}(F_0 - F)(2j+1)^{-1}(N^2_{\text{op}} - N_{\text{op}}) \tag{33}$$

if H_{int} is invariant under Sp $(2j+1)$.

As can easily be verified by using the commutation relations (3) and the symmetry and orthogonality of the Clebsch-Gordan coefficients,

$$G(\text{U}) = (2j+2)N_{\text{op}} - N^2_{\text{op}}, \tag{34}$$

hence the problem of diagonalizing H_{int} is reduced to that of diagonalizing $G(\text{Sp})$, the solution of which is well known (ref. [3]): $G(\text{Sp})$ is Casimir's operator for the symplectic group and has eigenvalues $(2j+3)s - s^2$, where s is the (non-negative integer)*seniority* quantum number characterizing the transformation behaviour of the eigenfunction under the group Sp$(2j+1)$. The operator H_{int} has therefore the *eigenvalues*

$$\tfrac{1}{2}F[-(j+\tfrac{3}{2})s + \tfrac{1}{2}s^2 + (j+2)N - N^2] + \tfrac{1}{2}(F_0 - F)(2j+1)^{-1}(N^2 - N) \tag{35}$$

in the case of symplectic invariance.

† cf. footnote on p. 647.

5. The Non-Invariance of the Energy Matrix for δ-Interactions

Let us consider as a special but important case a δ-interaction of Wigner type:

$$v(\mathbf{r}_1, \mathbf{r}_2) = V\delta(\mathbf{r}_1 - \mathbf{r}_2), \tag{36}$$

V being a constant. The expansion coefficients in (6) are easily found to be

$$v_k(r_1, r_2) = (4\pi r_1^2)^{-1}\delta(r_1 - r_2)(2k+1)V, \tag{37}$$

so that the Slater integrals (10) are

$$F^{(k)} = (2k+1)F^{(0)}, \qquad F^{(0)} = (4\pi)^{-1}V\int_0^\infty \mathrm{d}r r^2 R(r)^4, \tag{38}$$

and the interaction constants (15) become, using (38) and (13)

$$F_k = F^{(0)}(j\|C_k\|j)^2 = \begin{cases} 0 & \text{for } k \text{ odd}, \\ 4\dfrac{(2j-k)!\,(k!)^2(j+\frac{1}{2}k+\frac{1}{2})!}{(2j+k+1)!\,(\frac{1}{2}k)!^4(j-\frac{1}{2}k-\frac{1}{2})!}F^{(0)} & \text{for } k \text{ even}; \end{cases} \tag{39}$$

thus, the condition (30) for symplectic invariance of H_{int} is *not* satisfied, which may be seen qualitatively from the approximate expression

$$(j\|C_k\|j)^2 \approx \frac{2}{\pi}\left[\left(\frac{2j+1}{k}\right)^2 - 1\right]^{\frac{1}{2}} \qquad (k = 2, 4, \ldots 2j-1), \tag{40}$$

which is obtained from (39) by use of Stirling's formula for the factorials.

Our above analysis has been confined, by the assumption (1), to interactions of *Wigner* type. A *Heisenberg* interaction $\Sigma v(\mathbf{r}_i, \mathbf{r}_k)P_r(i,k)P_\zeta(i,k)$ containing operators P_r for exchange of coordinates and P_ζ for exchange of spins is, within our j^N neutron configuration, equivalent to the Wigner interaction $-\Sigma v(\mathbf{r}_i, \mathbf{r}_k)$, which follows from the Pauli principle. For the same reason, a *Bartlett* interaction $\Sigma v(\mathbf{r}_i, \mathbf{r}_k)P_\zeta(i,k)$ reduces to a *Majorana* interaction $-\Sigma v(\mathbf{r}_i, \mathbf{r}_k)P_r(i,k)$. Thus there remains the Majorana type to be discussed, which for $v(\mathbf{r}_i, \mathbf{r}_k) = V\delta(\mathbf{r}_i - \mathbf{r}_k)$ reduces to the Wigner type. Thus, *our result on the non-invariance of* H_{int} under $\mathrm{Sp}(2j+1)$ *is true for* δ*-interactions with any mixture of exchange types.*

The reason for this is that the *Slater integrals* $F^{(k)}$ *for the* δ*-potential do not increase strongly enough with increasing* k, as, for symplectic invariance, the $F^{(k)}$, by (30), (15), and (40), would have to satisfy

$$F^{(k)} = (2k+1)(j\|C_k\|j)^{-2}F \approx \tfrac{1}{2}\pi F(2k+1)\left[\left(\frac{2j+1}{k}\right)^2 - 1\right]^{-\frac{1}{2}} \tag{41}$$

for $k = 2, 4, \ldots 2j-1$, with F independent of k. For the δ-potential, (38) holds instead of (41).

6. Application of the Invariance Condition to a Special Case

Let the 2-particle interaction be a function of the distance $|\mathbf{r}_1-\mathbf{r}_2|$ only:

$$v(\mathbf{r}_1, \mathbf{r}_2) = v(|\mathbf{r}_1-\mathbf{r}_2|), \tag{42}$$

and let in (7) the *radial part* $R(r)$ be *strongly localized* at some r-value r_s (the "shell radius") †:

$$R(r)^2 = r_s^{-2}\delta(r-r_s). \tag{43}$$

We introduce these specializations into the following general formula which is easily derived from (6) and (10):

$$\int_0^\infty \mathrm{d}r_1 r_1^2 R(r_1)^2 \int_0^\infty \mathrm{d}r_2 r_2^2 R(r_2)^2 v(\mathbf{r}_1, \mathbf{r}_2) = \sum_{k=0}^{\infty} F^{(k)} P_k(\cos\vartheta_{12}), \tag{44}$$

and obtain

$$v(2r_s \sin\tfrac{1}{2}\vartheta_{12}) = \sum_{k=0}^{\infty} F^{(k)} P_k(\cos\vartheta_{12}), \tag{45}$$

where the potential as a function of distance has become directly related to the Slater integrals. For interparticle distances $> 2r_s$ this result does *not* apply, as $\sin\frac{1}{2}\vartheta_{12} < 1$. It is reasonable for an outer shell of a heavy nucleus, such as we have in mind, to assume the range r_0 of the potential to be $\ll r_s$; then (45) covers all physically relevant values of distance.

Using the invariance condition (41), we get for the potential

$$\begin{aligned} v(2r_s \sin\tfrac{1}{2}\vartheta_{12}) &= F\sum_{n=1}^{j-\frac{1}{2}} (4n+1)(j||C_{2n}||j)^{-2} P_{2n}(\cos\vartheta_{12}) + \ldots \\ &\approx \tfrac{1}{2}\pi F \sum_{n=1}^{j-\frac{1}{2}} (4n+1)\left[\left(\frac{2j+1}{2n}\right)^2 - 1\right]^{-\frac{1}{2}} P_{2n}(\cos\vartheta_{12}) + \ldots, \end{aligned} \tag{46}$$

where terms in $P_k(\cos\vartheta_{12})$ with $k \neq 2, 4, \ldots 2j-1$, which are left *undetermined* by the invariance condition, have been replaced by dots.

The potential is thus determined to a certain extent by the invariance requirement.

7. Flowers' Expansion of a Non-Invariant H_{int}

Flowers and Edmonds [2,3]) have shown how H_{int} may be *approximately diagonalized* when it is only *approximately invariant* under $\mathrm{Sp}(2j+1)$, as is the case e.g. for the δ-potential (36). We wish to indicate briefly how their result is to be written in our more explicit notation.

We observed in section 4 that the u_{kq} ($k = 2, 4, \ldots 2j-1$) are transformed under $\mathrm{Sp}(2j+1)$ according to the irreducible representation $(110\ldots0)$.

† Note that (43) must not be used together with a δ-potential (36) as the $F^{(k)}$ would then be infinite.

The same is true for the u^*_{kq} ($k = 2, 4, \ldots 2j-1$), as (110 . . . 0) is equivalent to its conjugate complex representation †. The products

$$u^*_{k'q'}u_{kq} \qquad (k, k' = 2, 4, \ldots 2j-1) \tag{47}$$

are therefore transformed according to the product representation (110 . . .0) $\times$ (110 . . . 0) which is, in general, reducible and splits into a number of irreducible representations among which the identical representation (0 . . . 0) occurs just once, the corresponding (invariant) basis element being given, apart from a factor, by the left-hand side of (28). In place of the operators (47), we introduce certain linear combinations

$$v_\kappa \qquad (\kappa = 1, 2, \ldots (2j^2+j-1)^2) \tag{48}$$

which are transformed irreducibly under Sp($2j+1$) and R(3) *simultaneously*. The transformation coefficients between (47) and (48) form a unitary matrix. Any operator (47) can be written as a linear combination of the v_κ, thus

$$\tfrac{1}{2}\sum_{\substack{k>0\\ \text{even}}}\sum_q F_k u^*_{kq}u_{kq} = \sum_{\kappa=1}^{(2j^2+j-1)^2} G_\kappa v_\kappa, \tag{49}$$

with certain coefficients G_κ. Now, there exist exactly $j-\frac{1}{2}$ independent linear combinations of the operators (47) that are rotational invariants (e.g. the

$$\sum_q u^*_{kq}u_{kq} \qquad (k = 2, 4, \ldots 2j-1) \tag{50}$$

occurring on the left-hand side of (49)), and thus there are also $j-\frac{1}{2}$ rotational invariants among the v_κ, which we may assume to be $v_1, v_2, \ldots v_{j-\frac{1}{2}}$. Eq. (49) then reduces to

$$\tfrac{1}{2}\sum_{\substack{k>0\\ \text{even}}}\sum_q F_k u^*_{kq}u_{kq} = \sum_{\kappa=1}^{j-\frac{1}{2}} G_\kappa v_\kappa. \tag{51}$$

We may further assume that v_1 is the only existing symplectic invariant among the v_κ; one then finds, using the unitarity of the transformation between (47) and (48):

$$G_1 v_1 = \tfrac{1}{2}F\sum_{\substack{k>0\\ \text{even}}}\sum_q u^*_{kq}u_{kq} \tag{52}$$

with the definition

$$F \equiv (2j^2+j-1)^{-1}\sum_{\substack{k>0\\ \text{even}}}\sum_q F_k = (2j^2+j-1)^{-1}\sum_{\substack{k>0\\ \text{even}}}(2k+1)F_k, \tag{53}$$

which represents an *average* of the F_k formed in a plausible way. The numerator $2j^2+j-1$ is just the number of terms in the double sum.

Inserting (52) and (51) into (17), H_{int} is transformed into

† This follows from the fact that the irreducible characters of Sp($2j+1$) are real (ref. [4]).

$$H_{\text{int}} = \tfrac{1}{2}F \sum_{\substack{k>0 \\ \text{even}}} \sum_{q} u^*_{kq} u_{kq} - \tfrac{1}{2}F \frac{2j^2+j-1}{2j+1} N_{\text{op}} + \tfrac{1}{2}F_0(2j+1)^{-1}(N^2_{\text{op}} - N_{\text{op}}) + \sum_{\kappa=2}^{j-\frac{1}{2}} G_\kappa v_\kappa, \tag{54}$$

which is the desired *symplectic expansion of a non-invariant* H_{int}. The above-mentioned *approximation* consists in neglecting the non-invariant terms in $v_2, \ldots, v_{j-\frac{1}{2}}$, and diagonalizing the remaining expression which is of the form (31) and has thus the eigenvectors discussed in section 4, and the eigenvalues (35).

Especially for the δ-potential (36), eq. (53) together with (39) gives

$$F = F^{(0)} \frac{j+\frac{1}{2}}{j+1}, \tag{55}$$

which can be proved by calculating $\sum_{m_1 m_2} v_{m_1 m_2 m_2 m_1}$ in two ways (from (14) and from (4)) and equating the results. Further, by (39),

$$F_0 = F^{(0)}(2j+1). \tag{56}$$

Substituting these expressions into (35), we obtain as *approximate eigenvalues* of H_{int} for a δ-interaction

$$(j+\tfrac{1}{2})F^{(0)} \left[\frac{N-s}{2} + \frac{s(s-1)}{4(j+1)}\right]. \tag{57}$$

There are no terms in N^2 for this interaction; furthermore, for the lowest seniorities $s = 0$ and $s = 1$, the second term vanishes which leads one to interpret $(j+\frac{1}{2})F^{(0)}$ as the "pairing energy".

I am grateful to Professor Süssmann and Dr. Stichel for stimulating discussions.

References

1) A. R. Edmonds, Angular momentum in quantum mechanics (Princeton University Press, 1957)
2) B. H. Flowers, Proc. Roy. Soc. A **212** (1952) 248
3) A. R. Edmonds and B. H. Flowers, Proc. Roy. Soc. A **214** (1952) 515
4) H. Weyl, The classical groups (Princeton University Press, 1946)
5) G. Racah and I. Talmi, Physica **18** (1952) 1097

2.B *Nuclear Physics* **12** (1959) 657—661; © *North-Holland Publishing Co., Amsterdam*
Not to be reproduced by photoprint or microfilm without written permission from the publisher

ON THE DETECTION OF DEUTERON POLARIZATION

L. J. B. GOLDFARB
Department of Theoretical Physics, University of Manchester

Received 29 May 1959

Abstract: An investigation is made of the angular distributions and polarizations arising from the use of polarized deuteron beams in the d(H^3, He^4)n and d(He^3, He^4)p reactions.

It has recently been observed by Galonsky, Willard and Welton [1]) that the reactions H^3(d, n)He^4 and He^3(d, p)He^4, when proceeding through their resonances, serve as efficient detectors of deuteron polarization. The resonances occur at deuteron kinetic energies (as measured in the laboratory) of 107 and 430$\pm$30 keV, respectively. A particularly interesting feature of these processes is that only s-waves of the deuterons play a role so that the unpolarized angular distributions are isotropic; yet when polarized deuterons initiate the process, there is a non-isotropic angular distribution, which, in fact, provides a measure to the polarization. The presence of the polarization singles out preferred directions in space, and since the emergent products proceed through d-waves, non-isotropic angular distributions are to be expected.

The analysis of Galonsky *et al.* was made by assigning polarization to the deuterons through the expectation values of m_d and m_d^2, where m_d is the component of deuteron spin along the direction of propagation. If we are concerned with only aligned deuterons or deuterons with 'vector' polarization this is a sufficient description; however, it appears to be possible to produce beams of deuterons from several nuclear reactions with polarization which is not restricted to a single line of symmetry [2]). It is therefore of interest to recalculate the angular distributions using a more general description of the deuteron polarization †.

We may consider both of the above reactions together since they involve identical angular-momentum quantum numbers. Each reaction is assumed to be described by a single reaction matrix-element R corresponding to an intermediate state of spin $\frac{3}{2}$. These matrix-elements are each of the usual Breit-Wigner type. The deuteron polarization is characterized by the

† The fact that the calculation of Galonsky *et al.* is restricted to the special case of an alignment axis and that an alteration is required for the more complex type of deuteron polarization, in actual fact, was noted by the authors in a footnote to their paper.

statistical spin-tensors, $\rho_{k_{1s}\kappa_{1s}}(s_1)$, whose rank k_{1s} takes on values 0,1 and 2 and where κ_{1s} is an integer satisfying $-k_{1s} \leqq \kappa_{1s} \leqq +k_{1s}$. The zero rank corresponds to a scalar (no polarization), while first and second rank correspond, respectively, to a linear combination of the components of the vector $\mathbf{P}$ and of the tensor P_{ij}. Here, the subscripts i and j take on values 1, 2 and 3 corresponding the x, y and z coordinate axes. These spin tensors are mean values of tensor operators such that

$$\mathbf{P}(s) = \frac{\mathbf{1}}{s}\overline{\mathbf{s}}, \qquad P_{ij}(\mathbf{1}) = \tfrac{3}{2}[\overline{s_i s_j + s_j s_i}] - 2\delta_{ij}.$$

A general analysis of polarization [2]) shows that the added terms to the angular distribution, which owe their origin to incoming polarization of rank k_{1s}, involve the real or imaginary parts of RR'^*, according as k_{1s} is even or odd (R and R' designate two elements of the scattering matrix). Since in the reactions of interest we restrict ourselves to single-matrix elements, it is clear that only tensors of rank 2 lead to a non-isotropic distribution. This is equivalent to the result of ref. [1]), where it was observed that the polarization arising from m_d (i.e. $\mathbf{P}(\mathbf{1})$) does not affect the angular distribution.

On the other hand, vector polarization of the deuteron gives rise to polarization of the outgoing nucleons and there is no contribution from either unpolarized deuterons or deuterons having tensor polarization. This is a consequence of a more general result [3]) † that if the polarization of the outgoing beam, $\rho_{k_{2s}\kappa_{2s}}(s_2)$, is measured and there is an incoming polarization, this former polarization will involve Re (RR'^*) or Im (RR'^*) according as $k_{1s}+k_{2s}$ is even or odd. Since k_{2s} is restricted to be either 0 or 1 for spin-$\frac{1}{2}$ particles, it is clear that the outgoing polarization only arises from $k_{1s} = 1$.

The angular distribution as measured by polarization-insensitive detectors, $W(\Omega)\mathrm{d}\Omega$, where Ω typifies the angles, is found by reference to expressions given earlier [2]). Thus,

$$W(\Omega) = \tfrac{1}{6}\lambda\!\!\!^{-2}|R|^2[1 - \tfrac{1}{2}P_{33}P_2(\cos\theta) - \tfrac{1}{3}(P_{13}\cos\chi + P_{23}\sin\chi)P_2^1(\cos\theta) - \tfrac{1}{12}\{(P_{11}-P_{22})\cos 2\chi + 2P_{12}\sin 2\chi\}P_2^2(\cos\theta)],$$

where $\lambda\!\!\!^{-}$ is the reduced wave length and χ is the angle between the 2-axis describing the incident polarization and $\mathbf{n}$ the normal to the reaction plane. The unit vector $\mathbf{n}$ is defined as $(\mathbf{k}_1 \times \mathbf{k}_2)/|\mathbf{k}_1 \times \mathbf{k}_2|$, where $\mathbf{k}_1$ and $\mathbf{k}_2$ are initial and final propagation vectors. The 3-axis is along $\mathbf{k}_1$. All quantities refer to the centre-of-mass system of the reaction.

† This is shown in ref.[3]), using the channel-spin representation; however, it is possible to show that this result holds in any representation. In fact the result may be generalized still further so that if the polarizations of more than two radiations are measured in a single or multiple process, the contribution to the angular distribution involves $\mathrm{Re}(RR'^*)$ or $\mathrm{Im}(RR'^*)$ according as $\Sigma_n k_{ns}$ is even or odd.

If measurement is made using polarization-sensitive detectors, i.e. if the transverse components of nucleon polarization $P_1(\frac{1}{2})$ and $P_2(\frac{1}{2})$ are measured with efficiencies [2]), $P_1^{\mathrm{d}}(\frac{1}{2})$ and $P_2^{\mathrm{d}}(\frac{1}{2})$, respectively, we must add to $W(\Omega)$ the terms

$$\tfrac{1}{6}\lambda^2|R|^2[P_2(1)P_2^{\mathrm{d}}(\tfrac{1}{2})+P_1(1)P_1^{\mathrm{d}}(\tfrac{1}{2})\cos\theta+P_3(1)P_1^{\mathrm{d}}(\tfrac{1}{2})\sin\theta].$$

For reasons of simplicity it is assumed that the 2-axes for the two descriptions of polarization are along $\mathbf{n}$ and that the 3-axes are along either $\mathbf{k}_1$ or $\mathbf{k}_2$. The efficiency vector $\mathbf{P}^{\mathrm{d}}(\frac{1}{2})$ will, in turn, be related to the angular distribution of a subsequent process. Since the longitudinal polarization of the nucleon cannot be measured in this manner, we have ignored $P_3(\frac{1}{2})$.

The above results may be compared to the general expression for detection of deuteron polarization through an arbitrary process [2]).

$$W(1) = W_0[1+\tfrac{3}{2}\mathbf{P}\cdot\mathbf{P}^{\mathrm{d}}+\tfrac{1}{2}P_{33}P_{33}^{\mathrm{d}}+\tfrac{2}{3}(P_{13}P_{13}^{\mathrm{d}}+P_{23}P_{23}^{\mathrm{d}}+P_{12}P_{12}^{\mathrm{d}}) +\tfrac{1}{6}(P_{11}-P_{22})(P_{11}^{\mathrm{d}}-P_{22}^{\mathrm{d}})]$$

where P_{ij}^{d} represents the efficiency for detection of the polarization P_{ij} through the angular distribution of the process. If we let the 2-axes coincide with $\mathbf{n}$, then

$$\begin{aligned}
P_1^{\mathrm{d}}(1) &= \tfrac{2}{3}P_1^{\mathrm{d}}(\tfrac{1}{2})\cos\theta,\\
P_2^{\mathrm{d}}(1) &= \tfrac{2}{3}P_2^{\mathrm{d}}(\tfrac{1}{2}),\\
P_3^{\mathrm{d}}(1) &= \tfrac{2}{3}P_1^{\mathrm{d}}(\tfrac{1}{2})\sin\theta;\\
P_{33}^{\mathrm{d}} &= -P_2(\cos\theta) = \tfrac{1}{2}(1-3\cos^2\theta),\\
P_{13}^{\mathrm{d}} &= -\tfrac{1}{2}P_2^1(\cos\theta) = -\tfrac{3}{2}\sin 2\theta,\\
P_{11}^{\mathrm{d}}-P_{22}^{\mathrm{d}} &= -\tfrac{1}{2}P_2^2(\cos\theta) = -\tfrac{3}{2}\sin^2\theta,\\
P_{23}^{\mathrm{d}} &= P_{12}^{\mathrm{d}} = 0.
\end{aligned}$$

The maximum and minimum values of $\mathbf{P}^{\mathrm{d}}$ and P_{ij}^{d} which obtain for any process are as follows:

$$\begin{aligned}
(P_1^{\mathrm{d}})_{\substack{\max\\\min}} &= (P_2^{\mathrm{d}})_{\substack{\max\\\min}} = (P_3^{\mathrm{d}})_{\substack{\max\\\min}} = \pm 1,\\
(P_{13}^{\mathrm{d}})_{\substack{\max\\\min}} &= (P_{23}^{\mathrm{d}})_{\substack{\max\\\min}} = (P_{12}^{\mathrm{d}})_{\substack{\max\\\min}} = \pm\tfrac{3}{2},\\
(P_{11}^{\mathrm{d}}-P_{22}^{\mathrm{d}})_{\substack{\max\\\min}} &= \pm 3,\\
(P_{33}^{\mathrm{d}})_{\substack{\max\\\min}} &= \begin{matrix}+1\\-2\end{matrix}.
\end{aligned}$$

Identical results obtain for $\mathbf{P}$ and P_{ij}. Comparing the above equations, we note that P_{13}^{d} reaches the maximum possible magnitude at $\theta = \frac{1}{4}\pi$ and $\frac{3}{4}\pi$, while half the maximum values occur for P_{33}^{d} at $\theta = 0$ and π and for $P_{11}^{\mathrm{d}}-P_{22}^{\mathrm{d}}$ at $\theta = \frac{1}{2}\pi$. With appropriate choices of θ and $\mathbf{P}(\frac{1}{2})$, large values for $\mathbf{P}^{\mathrm{d}}(1)$ are also obtained.

We may also consider the reactions as sources of polarized nucleons by first writing the general expression for production and detection of spin-$\frac{1}{2}$ polarization:

$$W(\tfrac{1}{2}) = W_0[1+\mathbf{P}(\tfrac{1}{2}) \cdot \mathbf{P}^d(\tfrac{1}{2})].$$

Suppose the incoming beam of deuterons has polarization which is only of the vector kind. Then the outgoing beam has transverse polarization with

$$P_1(\tfrac{1}{2}) = P_1(1) \cos\theta + P_3(1) \sin\theta,$$
$$P_2(\tfrac{1}{2}) = P_2(1).$$

An incoming beam of fully polarized deuterons can give rise to fully polarized nucleons.

It thus appears that these reactions serve as highly efficient and selective detectors of deuteron polarization. Their feasibility from the point of view of experiment has already been discussed by Galonsky *et al.* and, for completeness, we repeat an enumeration of some of the attractive features [4]) displayed by these processes:

(1) The differential unpolarized cross sections are quite large, e.g. for the H^3(d, n)He^4 process, $W(\theta) \approx 0.4$ b/sr.

(2) The emergent particles are easily detected by virtue of their high energy: the nucleons have energies $\approx$ 14 MeV.

(3) The resonances are broad, so that the incident deuteron beam need not be too well-defined in energy. The widths at half-maximum are $\approx$ 140 keV for the H^3(d, n)He^4 process and $\approx$ 500 keV for the He^3(d, p) He^4 process.

An interesting aspect of the results is the independence of the efficiency of the reaction and the polarization of the nucleons on the specific parameters associated with the resonance. This is because of the neglect of the contributions from distant levels of the intermediate state. These levels are sufficiently separated in energy from the resonance level. Another feature of a process with a single effective matrix element is that in the neighbourhood of the resonances the results are insensitive to the energy of the deuteron beam. The effect of a spread in energy of the order of the width of the resonance is to alter the quantity R which is common to both the unpolarized and polarized angular distributions. There is a complication since the angle θ refers to the centre-of-mass system; however, this presents no serious difficulty inasmuch as the centre-of-mass system practically coincides with the laboratory system.

One practical use for these processes is the measurement of the polarization of the deuterons which are elastically scattered from He^4 through the resonance with incident deuteron energies of 1.07 MeV. It is anticipated [5]) that the quantity $P_{11}-P_{22}$ reaches a maximum value of $\approx$ 1.8 when the scattering is through an angle $\approx$ 120°. If these deuterons are now made to proceed through either He^3 or H^3 at near the resonance energies and meas-

urement is made of the particles which are emitted through $\theta = \frac{1}{2}\pi$, then the 'left-up' asymmetry, (L−U)/(L+U) should be 0.45. Here, L and U refer to the intensities corresponding to an angle between the two reaction planes equal to 0 and $\frac{1}{2}\pi$, respectively. A measurement of this kind would be a useful check on the assumptions made in the calculation of the d+He^4 process.

Another application is to deuteron 'pick-up' processes. As shown by Satchler [6]) if one includes the effect of distortion of the proton state by the optical potential representing the interaction between the proton and nucleus, and neglects the spin-orbit coupling, the polarization of the deuterons is found to be only of the vector kind. A similar result is that tensor polarization of deuterons, which are incident in a stripping process, does not alter the angular distributions. If one lets the deuterons from a 'pick-up' process initiate either of the resonances considered above, the detection of a non-isotropic angular distribution is direct proof of the importance of the spin-orbit interaction in the 'pick-up' reaction.

References

1) A. Galonsky, H. B. Willard and T. A. Welton, Phys. Rev. Lett. **2** (1959) 349
2) L. J. B. Goldfarb, Nuclear Physics **7** (1958) 622
3) A. Simon, Phys. Rev. **92** (1953) 1050
4) F. Ajzenberg and T. Lauritsen, Revs. Mod. Phys. **27** (1955) 77
5) L. J. B. Goldfarb and J. R. Rook, Nuclear Physics **12** (1959) 494
6) G. R. Satchler, Nuclear Physics **6** (1958) 543

1.E.7:
2.C

Nuclear Physics **12** (1959) 662—671; © *North-Holland Publishing Co., Amsterdam*
Not to be reproduced by photoprint or microfilm without written permission from the publisher

ENERGY LEVELS OF Na^{22} FROM THE $Mg^{24}(d, \alpha)Na^{22}$ AND $Mg^{25}(p, \alpha)Na^{22}$ REACTIONS

CORNELIUS P. BROWNE

University of Notre Dame, Notre Dame, Indiana †

Received 29 May 1959

Abstract: Energy levels of Na^{22} were observed with the $Mg^{24}(d, \alpha)Na^{22}$ and $Mg^{25}(p, \alpha)Na^{22}$ reactions. Bombarding energies in the range of 5.0 to 7.5 MeV were used, and the alpha particles were recorded with a broad-range spectrograph. Ground state Q-values are 1.954 ± 0.007 MeV for the first and $-3.153\ ^{+0.012}_{-0.006}$ MeV for the second reaction. Excited states, presumably with isobaric spin zero, were found at 0.585, 0.893, 1.533, 1.944, 1.990, 2.219, 2.576, 2.975, 3.066, 3.526, 3.713 ± 0.008, 3.949, 4.323 ± 0.008, (4.472 ± 0.008) MeV (all ± 0.005 except where shown otherwise) using the (d, α) reaction. The first and second of these were also seen through the (p, α) reaction and, in addition, a $T = 1$ state at 0.661 ± 0.008 MeV. The ground state Q-value for the $N^{14}(p, \alpha)C^{11}$ reaction was found to be $-2.928\ ^{+0.025}_{-0.005}$ MeV.

1. Introduction

This paper is a report of an experiment that was begun several years ago as one in a series of experiments to locate the low lying $T = 1$ levels in the light odd-nuclei [1]). A preliminary report of some of the data has been given [2]). Difficulties with target preparation delayed the work and meanwhile other nuclei proved more tractable for measurements of the validity of isobaric spin selection rules in (d, α) reactions [3]). A recent positive identification of the lowest $T = 1$ level [4]) in Na^{22} made it worthwhile to complete the analysis of the $Mg^{24}(d, \alpha)Na^{22}$ and $Mg^{25}(p, \alpha)Na^{22}$ data and present the results.

When this investigation was begun, little was known about the energy levels of Na^{22}. Later, a gamma ray from the first excited state was found using the $F^{19}(\alpha, n\gamma)Na^{22}$ reaction [5]). It was thought at the time that this might be the expected $T = 1$ level, as it occurred at about the right excitation. A strong yield from the $Mg^{24}(d, \alpha)$ reaction to this level, however, suggested that it was actually a $T = 0$ level. The recent experiment of Temmer and Heydenburg [4]) uses both the $F^{19}(\alpha, n\gamma)Na^{22}$ and $Ne^{20}(He^3, p\gamma)Na^{22}$ reactions. The work confirms the levels given in the preliminary

† This work was supported in part by the joint program of the Office of Naval Research and the United States Atomic Energy Commission.

The data of this experiment were recorded on nuclear track plates while the author was a member of the Physics Department at Massachusetts Institute of Technology.

report [2]) of the Mg^{24}(d, α)Na^{22} reaction, definitely shows the $T = 1$ level at 0.666 MeV, which was only suggested by one run in the previously analyzed Mg^{25}(p, α)Na^{22} data, and shows a new level at 3.75 MeV. An angular distribution of the tritons from the Na^{23}(d, t)Na^{22} reaction leading to the ground state and three excited states of Na^{22} has been measured [6]). Excitation energies agree with previous work, but no level is seen at 0.666 MeV.

The plan of the present experiment was to use the Mg^{24}(d, α)Na^{22} reaction to locate the $T = 0$ levels in Na^{22} and then to attempt to find the lowest $T = 1$ level through Mg^{25}(p, α)Na^{22}. Conservation of isobaric spin should prevent the first reaction, but not the second, from going to $T = 1$ states. No $T = 1$ states except the first would be reached with the bombarding energy available because of the rather large negative Q-value of the (p, α) reaction.

2. Experimental Method

A deuteron or proton beam from the MIT-ONR electrostatic accelerator was magnetically analyzed at a resolution of 0.1 percent, and bombarding energies from 5 to 7.5 MeV were used.

For the Mg^{24}(d, α)Na^{22} experiment targets were made by evaporating natural magnesium metal onto Formvar backings. Targets of 40 to 50 keV stopping power for the alpha-particles were used for the survey runs, and a target of about 20 keV stopping was used for later runs. The material enriched in Mg^{25} came in the form of the oxide †. All attempts to reduce this to the metal during vacuum evaporation or to evaporate it as the oxide failed. Electroplating from a pyridine solution onto thin nickle backings was also tried but no usuable targets were obtained. The method finally used was to deposit a salt from solution. No really satisfactory target was produced because non-uniformity of deposition resulted in a comparatively large stopping power for a small amount of Mg^{25}. This gave alpha-particle groups of low intensity and large energy spread, so that the resulting peaks on the nuclear track plates were low and broad. The target finally used was made by dissolving the $Mg^{25}O$ in acetic acid, evaporating the water, adding alcohol and ether and allowing successive drops of the solution to evaporate on a thin nickel-foil backing. On this target, nitrogen was found as a contaminant, probably coming from the ammonia solution used to dissolve the copper backing from the nickel foil. Reaction products and scattered particles emitted at angles of 30, 60 or 90 degrees were analyzed with the MIT broad-range spectrograph [7]). The length of track in the nuclear emulsion served to distinguish alpha-particles, protons and deuterons. The procedure used to

† Obtained from Oak Ridge National Laboratories, Isotopes Division.

obtain the particle energy from the measured position of a group on the nuclear track plate is discussed in ref. [7]).

Bombarding energies were accurately measured by using the spectrograph to find the energy of particles elastically scattered from target nuclei. Values obtained from groups scattered by the different magnesium isotopes and by oxygen agreed within 1 keV in most cases. This, plus the fact that a fresh target spot was used for each bombardment, suggested that errors from contaminating surface layers were small.

The target nucleus responsible for a given alpha group was ascertained by changing the bombarding energy and observation angle. When the group is correctly assigned such changes will, of course, have no effect on the calculated Q-values. This procedure served to identify the target nucleus to within one mass number. To be sure that none of the groups assigned to Mg^{24} actually arose from the Mg^{25} isotope in the natural targets, one of the runs was repeated on the Mg^{25} target. Although this target had approximately six times as much Mg^{25} as the natural target, no alpha groups other than those from $O^{16}(d, \alpha)N^{14}$ were seen.

3. Results

An alpha particle spectrum from one of the thinner natural magnesium targets is shown in fig. 1. Peak widths here are determined by energy loss in the target, as other peak broadening effects are negligible by comparison. The groups leading to states in Na^{22} are numbered in order of increasing excitation energy beginning with (0) for the ground state group. Excitation energies in Na^{22} may be read from the sloping line using the right hand ordinate scale.

Particle groups arising from the $O^{16}(d, \alpha)N^{14}$ reaction are labelled with the symbol N^{14}. Strong groups leading to the ground state and second excited state are seen; and a somewhat weaker group leading to the first excited state, in violation of the isobaric-spin selection rule, also appears. This group was first observed in the early part of the present work. An investigation of the selection rule violation has been made [3]).

The position of the second excited ($T = 1$)Na^{22} state is indicated by an arrow on the plot. It is seen that there is a suggestion of a weak group at this point. Upper limits for the intensity of a group corresponding to this excitation are given in table 1 for three bombarding energies and angles. At 7.0 MeV bombarding energy and an observation angle of 90° no other alpha groups appeared with an intensity greater than 5 percent of the ground state group. The small group seen in fig. 1 immediately below the position of the 0.661 MeV level failed to reappear at any other angle or bombarding energy and is therefore unidentified.

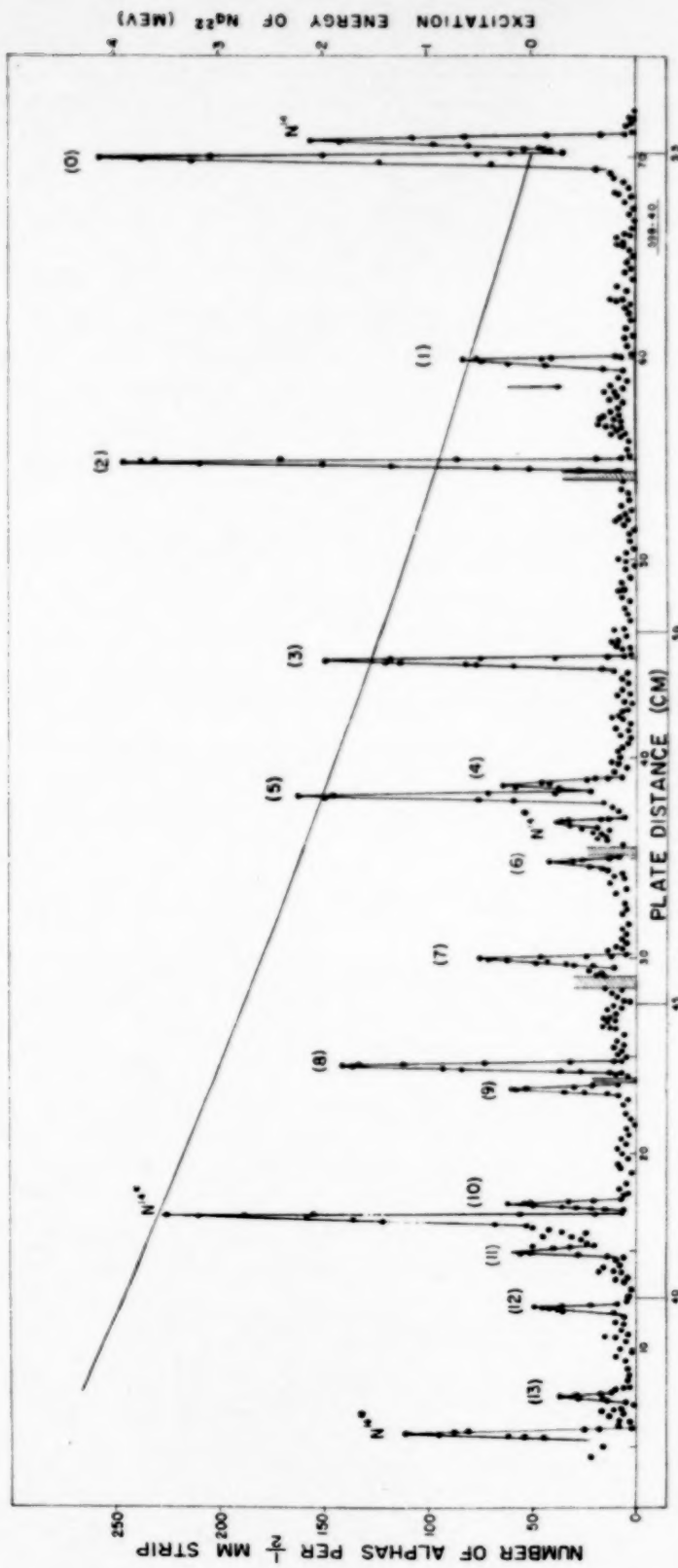

Fig. 1. Alpha particle groups from natural magnesium target bombarded with 7.0 MeV deuterons. Numbered groups arise from levels in Na^{22}. Other groups come from the $O^{16}(d, \alpha)N^{14}$ reactions. Cross hatching shows regions that were obscured by intense proton groups or by gaps between track plates. The arrow near group (1) indicates position for a group leading to the first $T = 1$ level.
Magnetic field: 6 950 gauss
Deuteron energy: 7.009 MeV
Angle of observation: 90°.

TABLE 1

Upper limit for yield of the $Mg^{24}(d, \alpha)Na^{22*}$ reaction to first $T = 1$ level

Deuteron energy (MeV)	Observation angle (Degrees)	Intensity ratio of $T = 1$ state to first $T = 0$ state
6.5	30	< 0.2
7.0	30	< 0.1
7.0	90	< 0.09

Fig. 2 is a plot of alpha particles from the Mg^{25} target under bombardment with protons. The peaks are rather wide and uneven because of the non-uniformity of the target. Counting of the tracks was difficult because of their shortness and so was carried only about halfway down the plate. Groups from $Mg^{25}(p, \alpha)Na^{22}$ are lettered beginning with (A) for the ground state. Groups B and D correspond to groups (1) and (2) respectively of

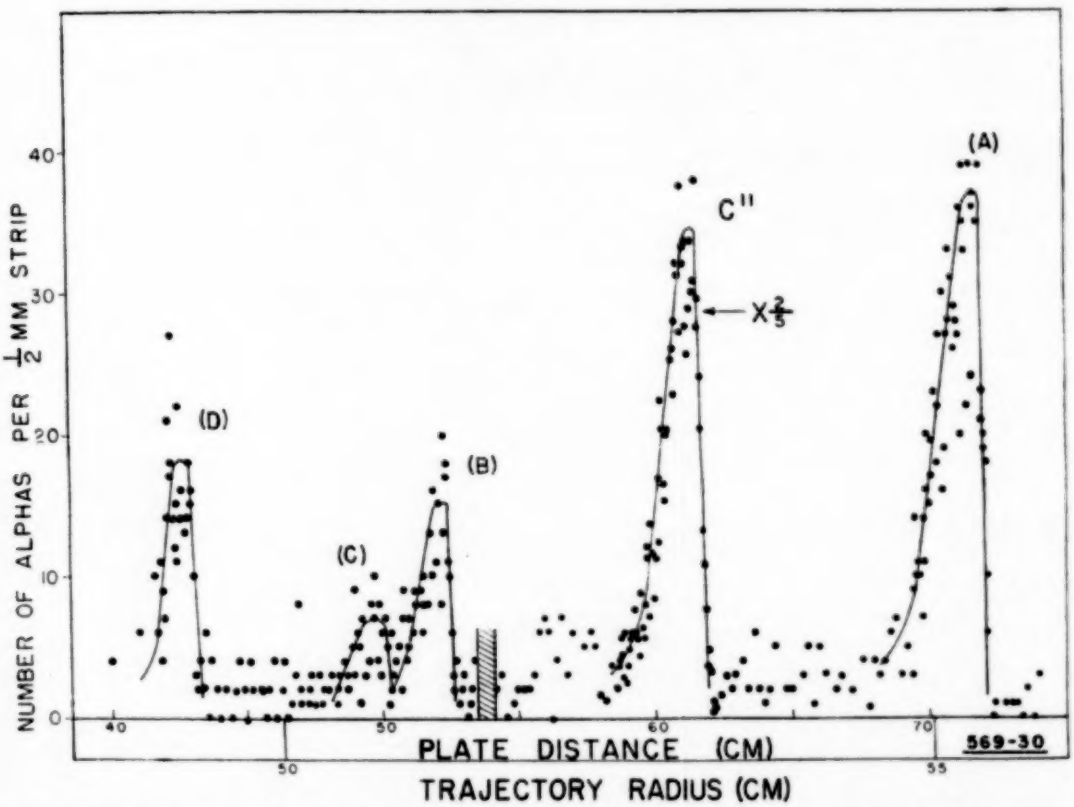

Fig. 2. Alpha particle groups from a target of enriched Mg^{25} bombarded with 7.5 MeV protons. Lettered groups arise from levels in Na^{22}. The most intense group comes from the $N^{14}(p, \alpha)C^{11}$ reaction. Group (C) leads to the first $T = 1$ level in Na^{22}.
$E_d = 7.516$ MeV, $B = 5.079$ gauss, $\theta = 60°$

fig. 1. In addition to these groups leading to the Na^{22} levels seen with the (d, α) reaction, a group (C) is found at the position corresponding to an excitation energy of 0.661 MeV. A comparatively strong group from the

$N^{14}(p, \alpha)C^{11}$ reaction on the nitrogen contaminant also appears in fig. 2.

The excitation energies measured in this experiment are listed in table 2. Excitations rather than Q-values are given because, as many groups were simultaneously observed on the nuclear track plate, the error in energy difference between levels is smaller than the errors in the Q-values themselves. In calculating the excitation energies from most of the runs, the

TABLE 2

Excitation Energies in Na^{22}

Group Label		Number of Observations	Excitation Energy (MeV)	
Fig. 1	Fig. 2		$Mg^{24}(d, \alpha)$ [a]	$Mg^{25}(p, \alpha)$ [b]
1	B	6	0.585 ± 0.005	0.582 ± 0.006
	C	3		0.661 ± 0.008
2	D	6	0.893 ± 0.005	0.891 ± 0.006
3		4	1.533 ± 0.005	
4		8	1.944 ± 0.005	
5		5	1.990 ± 0.005	
6		7	2.219 ± 0.005	
7		8	2.576 ± 0.005	
8		5	2.975 ± 0.005	
9		7	3.066 ± 0.005	
10		4	3.526 ± 0.005	
11		3	3.713 ± 0.008	
12		3	3.949 ± 0.005	
13		3	4.323 ± 0.008	
Not shown		1	$(4.472) \pm 0.008$	

[a]) Ground state Q-value 1.954 ± 0.007 MeV.

[b]) Ground state Q-value $-3.153^{+0.012}_{-0.006}$ MeV.

ground state Q-value determined in that run was used. In three of the (d, α) exposures, covering levels of higher excitation, the ground state group lay out of the energy range covered and hence no ground state Q-value was measured. For these runs the sum of the Q-values for five of the levels of intermediate excitations was compared with the average of the sum of the Q-values for the same levels obtained from the runs in which the ground state Q-value was measured. The small difference was used as a correction to adjust all excitations from the three runs. In other words runs not showing the ground state group were used simply to give the energy difference between those levels of already known excitation and the previously unmeasured higher levels. The number of observations made of each group is given in the third column of table 2. With the exception of one run at 30 degrees all the (d, α) exposures were taken at an observation angle of 90 degrees, whereas one (p, α) run was made at 90 degrees and two at 60 degrees.

In the (p, α) data, a group corresponding to an excitation energy of 0.661

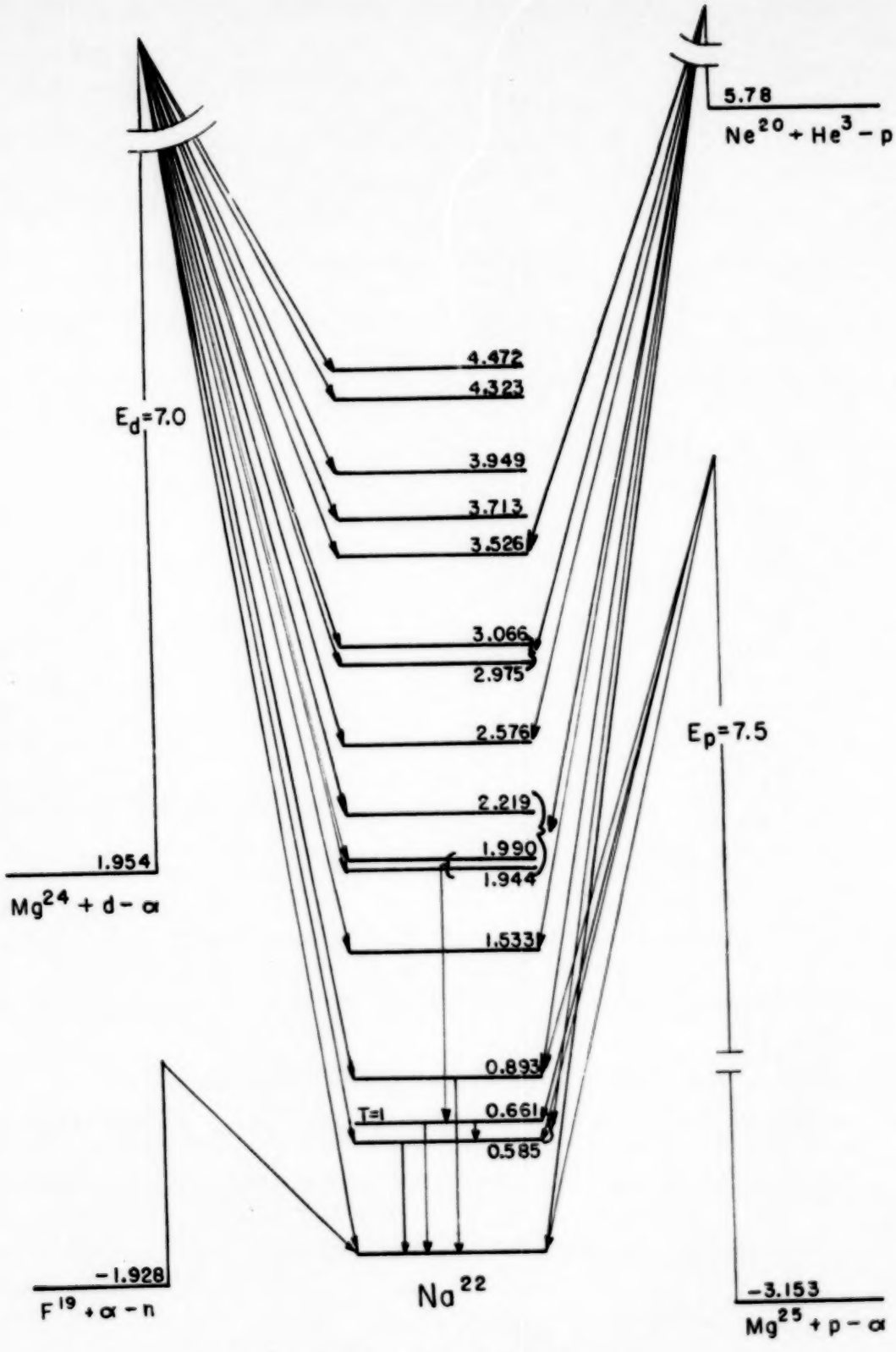

Fig. 3. Energy level diagram for Na^{22}.

MeV was seen in three runs at different angles and bombarding energies. The groups were so weak and so poorly resolved from the group leading to the first level, however, that one would hesitate to assign them definitely to $Mg^{25}(p, \alpha)Na^{22}$ without further evidence. This evidence is supplied with the observation by Temmer and Heydenburg [4]) of a gamma-ray transition going from a level at this position to the first excited state at 0.585 MeV. It is seen that excitation energies for the first and third excited states, measured with the (p, α) reaction are in excellent agreement with those from the (d, α) reaction. In view of this agreement, one has confidence in the value obtained for the energy of the second excited state in spite of the low intensity. Somewhat larger errors are attached to the (p, α) excitation energies because of the wide and weak groups arising from the poor target. Fig. 3 is an energy level diagram for Na^{22} summarizing the present results and results of other investigators.

For the $Mg^{24}(d, \alpha)Na^{22}$ ground state reaction a Q-value of 1.954 ± 0.007 MeV was found. The measured value for the ground state Q-value of the $Mg^{25}(p, \alpha)Na^{22}$ reaction is $-3.153^{+0.012}_{-0.006}$ MeV. The reason for giving a larger uncertainty in the positive direction is the extreme sensitivity of a (p, α) Q-value to contaminant surface layers on the target. A surface layer that makes an undetectable difference in the energy of elastically scattered protons offers sufficient stopping power for alpha-particles to cause a large error.

The $N^{14}(p, \alpha)C^{11}$ Q-value was found to be $-2.928^{+0.025}_{-0.005}$ MeV. As the nitrogen was an impurity in the target there is a question whether it was on the surface or under the magnesium acetate. To attempt to answer this question, the energy of protons elastically scattered from the nitrogen was measured as well as the energies of protons scattered from the Mg^{25} and O^{16}. The bombarding energies calculated from the three groups agreed to well within the uncertainties, but that from the N^{14} groups was one or two keV lower than that from the other two groups. Unfortunately the (p, α) Q-value is so sensitive that a surface layer causing one keV energy loss for protons would give as much as 30 keV error in the Q-value. For this reason the number given here must be regarded as a lower limit only.

4. Discussion

From the measured ground state Q-value for the (p, α) reaction the Mg^{25}—Na^{22} mass difference may be found. This plus the Na^{22} β-decay energy [8]) gives an accurate link between the masses of the neon isotopes and the magnesium isotopes. Table 3 lists the Mg^{25}—Ne^{22} mass difference (in terms of the difference in mass excesses) found in this fashion, and that found from the sum of the measured Q-value of three other reactions [9]),

and compares these values with the ones derived from four current tabulations of atomic masses [10]).

TABLE 3

$Mg^{25}-Ne^{22}$ Mass excess difference

$Mg^{25}(p, \alpha)Na^{22}$ $+Na^{22}\beta, \gamma\ Ne^{22}$	$Mg^{25}(d, \alpha)Na^{23}$ $+Na^{23}(d, \alpha)Ne^{21}$ $+Ne^{21}(d, p)Ne^{22}$	Li [a])	Wapstra[a])	Endt and Braams [a])	Mattauch *et al.* [a])
-4.292 ± 0.008	-4.320 ± 0.020	-4.295	-4.285	-4.277	-4.283

[a]) See ref. [11]).

By substracting the $Mg^{25}(p, \alpha)Na^{22}$ Q-value from the $Mg^{24}(d, \alpha)Na^{22}$ Q-value one gets a number for the $Mg^{24}(d, p)Mg^{25}$ Q-value. The result, using the present measurements is 5.107 ± 0.011 MeV. This agrees well with the figure of 5.097 ± 0.007 MeV reported for the direct measurement [11]), and exactly with the number 5.107 ± 0.007 obtained by subtracting the deuteron binding energy from the measured [12]) $Mg^{24}(n, \gamma)Mg^{25}$ reaction energy.

The $N^{14}(p, \alpha)C^{11}$ Q-value given above agrees with the accepted value [9]) from reaction chains of -2.916 ± 0.008 MeV. To make an accurate determination of the $N^{14}(p, \alpha)$ Q-value greater pains must be taken to correct for possible surface layers on the target. This might be done, for example, by observing the Q-value as a function of the α-particle energy for different angles of observation and bombarding energies.

The excitation energy determined for the first excited state of Na^{22} is 0.585 ± 0.005 MeV which agrees within the errors with 0.592 ± 0.003 MeV found for the gamma ray energy [4]). A value of 76 ± 8 keV is found from the (p, α) reaction for the spacing between the first and second excited states. This may be compared with 73 ± 4 keV found [4]) for the energy of the gamma ray emitted in the transition between these states. If a weighted average of these two numbers is added to the presently measured value for the first excited state the result is an excitation energy of 0.659 ± 0.006 MeV for the second excited state. This is a slightly better value for the excitation than that found directly from the (p, α) reaction.

The absence of a (d, α) reaction leading to the second excited state is in accord with the isobaric spin selection rule which forbids a (d, α) reaction leading from a $T = 0$ initial state to a $T = 1$ final state. Some violation of the selection rule is to be expected both on theoretical grounds and in view of experimental results with (d, α) reactions leading to other self-conjugate nuclei [3, 13]). To observe the violation for the present reaction it would be necessary to take angular distributions at a number of bombarding energies. The upper limits on the yield of the forbidden group given here in table 1 are an indication of the $T = 1$ character of the second excited state but

furnish no indication of the extent of the validity of the selection rule.

It is interesting to note that level 5 (peak (4) in fig. 1) is just at the position where the second $T = 1$ level would be expected judging from the excitation energy of the first level in the neighbouring isobar Ne^{22}. It is probable that there is another level close to level 5, but there is the possibility that this is the second $T = 1$ level and the selection rule breaks down.

If the suggestion of Alford [13]) that the inhibition of all the (d, α) reactions to the first $T = 1$ states that have so far been observed is actually caused to a large extent by the statistical weighting factor for reactions where both initial and final states are 0+ is correct, it may be that the isobaric spin selection rule is grossly violated in (d, α) reactions. It would be instructive to examine the Na^{22} level structure around levels 5 and 6 with some reaction not affected by isobaric spin.

The author wishes to thank W. W. Buechner and other members of the MIT-ONR generator group especially Lt. W. C. Cobb who helped take and analyze a good deal of the early (d, α) data and Mr. W. A. Tripp and Miss Sylvia Darrow who did much of the plate counting for the (d, α) data; also Mr. George Pogue of Notre Dame who helped with counting and plotting.

References

1) Browne, Bockelman, Buechner and Sperduto, Phys. Rev. **92** (1953) 665;
Browne and Bockelman, Phys. Rev. **105** (1957) 1301
2) Browne and Cobb, Phys. Rev. **99** (1955) 644(A)
3) C. P. Browne, Phys. Rev. **104** (1956) 1598;
C. P. Browne, Phys. Rev. (to be published)
4) Temmer and Heydenburg, Phys. Rev. **111** (1958) 1303
5) Heydenburg and Temmer, Phys. Rev. **94** (1954) 1252
6) W. F. Vogelsang and J. N. McGruer, Phys. Rev. **109** (1958) 1663
7) C. P. Browne and W. W. Buechner, Revs. Scient. Inst. **27** (1956) 899
8) Macklin, Lidofsky and Wu, Phys. Rev. **78** (1950) 318;
Wright, Phys. Rev. **90** (1953) 159(L);
Alburger, Phys. Rev. **76** (1949) 435(L);
P. Marmier, private communication to Lauritsen and Ajzenberg-Selove
9) D. M. Van Patter and W. Whaling, Revs. Mod. Phys. **26** (1954) 402
10) C. W. Li, Phys. Rev. **88** (1952) 1038;
A. H. Wapstra, Physica **21** (1955) 367;
Endt and Braams, Revs. Mod. Phys. **29** (1957) 683;
Mattauch, Waldman, Bieri and Everling, Z. Naturforsch. **11a** (1956) 525
11) VanPatter, Sperduto, Endt, Buechner and Enge, Phys. Rev. **85** (1952) 142
12) B. B. Kinsey and G. A. Bartholomew, Can. J. Phys. **31** (1953) 901
13) W. P. Alford (to be published)

1.E.1:
3.A

Nuclear Physics **12** (1959) 672—688; © *North-Holland Publishing Co., Amsterdam*
Not to be reproduced by photoprint or microfilm without written permission from the publisher

THE LEVEL SCHEME OF ^{134}Ba

SOME FEATURES OF THE NaI SUMMING SPECTROMETER

R. K. GIRGIS † and R. VAN LIESHOUT

Instituut voor kernphysisch Onderzoek, Amsterdam

Received 8 June 1959

Abstract: A detailed analysis of the gamma ray spectrum from ^{134}Cs was performed. The results are in agreement with previous measurements, but two additional weak gamma rays of 960 and 1570 keV were found. Summing peaks of 1.17, 1.40, 1.57, 1.64, 1.77 and 1.97 MeV were observed, establishing the presence of levels of these energies in ^{134}Ba. The gamma ray spectrum from the decay of ^{134}La was also examined. Only one gamma ray of 605 keV was observed, thus confirming that the first 2^+ level in ^{134}Ba has this energy.

Some features of the NaI summing spectrometer are demonstrated and discussed in an appendix to this report.

1. Introduction

As part of a general study of the properties of the second excited state of even nucleides, undertaken at this Institute, the level scheme of ^{134}Ba was investigated through the decay of ^{134}Cs and ^{134}La.

The disintegration of the 2.2 year ^{134}Cs which leads to levels in ^{134}Ba, has already been extensively investigated by several groups [1]) using a variety of methods. The complexity of both its beta and gamma ray spectrum makes the construction of a definite decay scheme for this isotope rather difficult. Levels at 605, 1168, 1401 and 1971 keV have been established with the help of gamma-gamma coincidence [2,3]) and summing measurements [4]). Additional levels at 1641 and 1773 keV are suggested by the presence of weak beta ray branches which may feed such levels [1]). The level at 1773 keV is still the most doubtful one among these levels, since the gamma rays which deexcite it, if present, should have exactly the same energy as some other gamma rays, which deexcite the well established 605 and 1168 keV levels. Due to this accidental degeneracy, the intensity ratio between the cross-over and the stop-over transitions, deexciting the 1168 keV level is not known with sufficient accuracy to decide whether this level can be the second 2^+ level in ^{134}Ba.

In the aim of clearing up this situation, a detailed analysis of the gamma ray spectrum from ^{134}Cs and an examination of its summing spectrum were undertaken. The gamma ray spectrum of ^{134}La, which leads to levels in ^{134}Ba, was also studied.

† On leave of absence from the Faculty of Science, University of Cairo, Giza, Egypt, U.A.R.

2. Production and Chemical Procedure

Sources of ^{134}Cs were produced by a (d, p) reaction on caesium. Caesium chloride was irradiated with $\approx$ 18 MeV deuterons for $\approx$ 100 μAh in the synchrocyclotron of this Institute. Targets were left to cool off for $\approx$ 2 months until all possible short lived activities had died out, in particular the 6 day ^{132}Cs which is produced by the accompanying (d, dn) reaction. The target was thereafter dissolved in dilute hydrochloric acid. Barium was precipitated as the carbonate by adding ammonia and sodium carbonate solution. This was repeated several times to ensure the precipitation of all barium present in the target. Caesium was precipitated as the perchlorate by adding perchloric acid, filtered and dried with alcohol.

Sources of ^{134}La were produced by an (α, 3n) reaction on caesium. Caesium chloride was irradiated with alpha particles of $\approx$ 45 MeV for $\approx$ 5 minutes in the synchrocyclotron, in order to suppress the formation of the 10 minutes ^{136}La which is produced by the accompanying (α, n) reaction. The same chemical procedure described in a previous article [5]) on ^{136}La was applied. The complete lanthanum separation took approximately 10 minutes.

3. Measurements and Results

3.1. DIRECT SPECTRUM OF ^{134}Cs

The direct spectrum was investigated with a cylindrical NaI(Tl) crystal of 2.5 cm diameter $\times$ 2.5 cm height optically coupled to a 6292 DuMont photomultiplier. The results were confirmed by using another cylindrical NaI(Tl) crystal of 6.2 cm diameter $\times$ 6.2 cm height optically coupled to a 6393 DuMont photomultiplier. These two combinations were calibrated for detecting efficiency in the energy region of interest. In both cases, sources were placed high enough to avoid summing effects. The source-crystal distance was 12 cm for the smaller crystal, and 25 cm for the larger one. The spectra were displayed on a 100 channel analyzer (RIDL). Figure 1 and 2 show the characteristic spectra of ^{134}Cs as detected by the smaller crystal in two different regions, the first from 100 to 900 keV, the second from 400 to 2000 keV. The region of overlap contained both the 605 and the 800 keV peaks, which provides a further check on the intensity values. The pulse height distribution was analyzed by successively peeling off the various peaks starting with the high energy ones [6]). The shapes of these peaks were interpolated from standard peaks of ^{88}Y, ^{42}K, ^{22}Na, ^{65}Zn, ^{54}Mn, ^{137}Cs, ^{85}Sr and ^{198}Au. The intensity values as found from the analysis of the spectra measured with the two different crystals were in excellent agreement. Table 1 gives the average values of the intensities of the various gamma rays resolved from the pulse height distributions of ^{134}Cs, together with the results reported

by various groups [2,7–12]). (Only those references are quoted which report relative intensities.) The agreement between the results obtained from the present work and those from the other investigations is very good. The two components at 800 keV could not be resolved owing to the fact that they are very close in energy (797 and 802 keV). The same applies for the couple of gamma rays at ≈ 570 keV (563 and 570 keV).

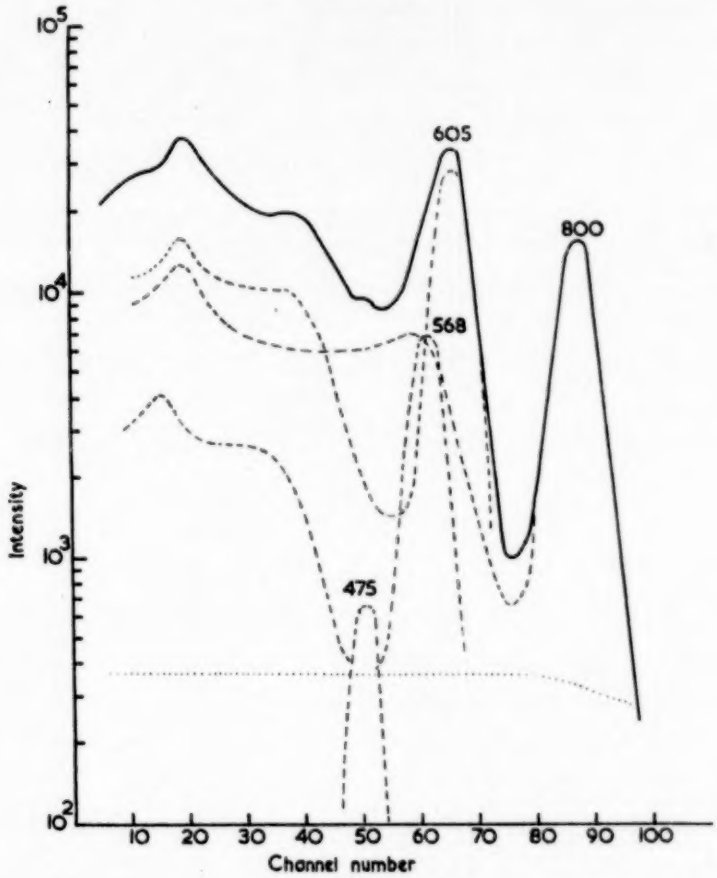

Fig. 1. The pulse height distribution from ^{134}Cs in a region of energy from ≈ 100 keV to 900 keV. The bump at ≈ 200 keV is due to back-scattering. The dashed line represents the resolved peaks, while the dotted line represents the pulse height distribution of higher energy peaks.

In addition to the gamma rays, reported so far, two new weak gamma rays were found, of 960 and 1570 keV. There is no possible combination of gamma rays in ^{134}Cs that could result in a summing peak of these energies, except the 605 keV and the new peak at 960 keV. However, the observed peak at 1570 cannot be a summing peak since the 960 keV gamma ray is too weak to cause such a large amount of summing in the geometry used in the present investigation. The two new gamma rays were resolved in both the spectra obtained with the two different crystals and with the same intensities.

The 470 keV gamma ray is certainly present, it can be seen as a small bump in the valley of the 605 keV peak. No gamma rays of energy lower than 470 keV could be found (< 2 %). The presence of weak gamma rays in this region with intensity < 2 % is not excluded since these would be difficult to resolve especially in the neighbourhood of the back-scattering bump ($\approx$ 200 keV).

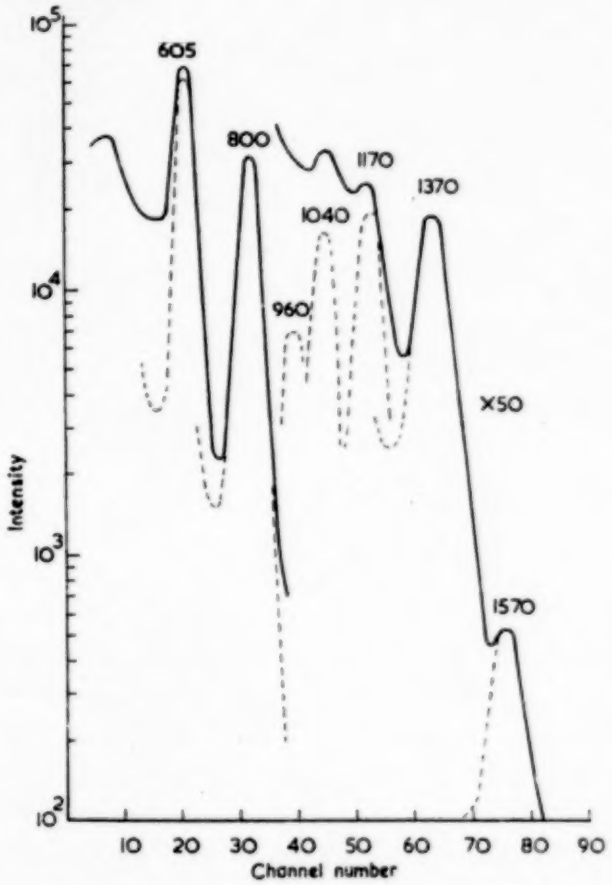

Fig. 2. The pulse height distribution from ^{134}Cs in a higher energy region. The dashed line represents the resolved peaks.

3.2. DIRECT SPECTRUM OF ^{134}La

The gamma ray spectrum of ^{134}La was examined using the 2.5 cm $\times$ 2.5 cm NaI(Tl) crystal only. The sources were followed for several hours in order to determine the contribution due to the 19 hour ^{135}La in the source; this contribution was subtracted. This long lived activity formed < 1 % of the total activity at the beginning of the experiment. No 10 minute ^{136}La component was found in the sources. This was concluded from the absence of this period in the decay of the 511 keV annihilation peak and from the absence of the characteristic 830 keV peak which is known [5]) to follow the

TABLE I

Energies and relative intensities of various gamma rays resolved in the spectrum of ^{134}Cs as found by iffer
605 keV rans

Joshi [7]) sl pe		Bashilov [8]) s		Verhaeghe [9]) sd, ce, pe		Forster [10]) scin, sle ce, pe	
Energy	Int.	Energy	Int.	Energy	Int.	Energy	Int.
				200.4±1.5	4		
						204±5	10
				208.3±1.5	4		
467±15	3.5			475 ±3	4	475±5	4
553± 7		563±2	10 ± 1	565.2±0.7	15	562±2	14
571± 7	21	569±2	18 ± 2	570.9±0.7	20	569±1	12
607± 5		604±2	100	605.8±0.7	100	604±1	100
				661.8±2.0	2	658?	weak
		796±3	103 ±10	797.0±0.6	100	796±1	72
794± 3	100						
		802±3	8 ± 1	802.2±0.6	15	802±1	11
1027±15		1038±4?	1.1± 0.6	1034.5±2.0	4	1035±3	5
1164±10	4	1166±4?	1.7± 0.6	1168 ±3	4		
1368± 5	5	1367±4	2.8± 0.6	1370 ±3	4	1369±3	5
1401±15							

[a]) sl pe only

decay of ^{136}La. The half life of the short lived component in the source, assumed to be ^{134}La was found to be 6.8±0.2 minutes in good agreement with a previous determination by Stover [13]).

Only one gamma ray of 605 keV was found to be present in addition to the 511 keV annihilation peak. The intensity of this peak was determined after subtracting the annihilation in flight continuum as interpolated from previously determined distributions using the same set up. (see ref.[14])). A value of 2.7 MeV [13]) for the end point of the positon spectrum of ^{134}La was adopted. The intensity of the 605 keV peak was found to be 5.0±0.7 % of the annihilation peak. (The complete annihilation of the positons at the source position was ensured by sandwiching the source between two aluminium discs of 5 mm thickness each; corrections for absorption in the annihilators were applied). Fig. 3 shows the gamma ray spectrum of ^{134}La in the region of interest between ≈ 100 keV and 1000 keV. The dashed line represents the continuum due to the annihilation in flight of positons. A very weak bump (< 0.3 %) at ≈ 680 keV can be seen above this continuum; this bump is most probably due to residual summing of the 511 keV gamma ray with the backscattering peak of its annihilation partner.

ifferent groups and from the present investigation. The intensity values are normalized to 100 for the ransition.

Bertolini [2]) scin, sl ce, pe		Keister [11]) sl ce, pe		Johansson [12]) scin		Present work scin	
Energy	Int.	Energy	Int.	Energy	Int.	Energy	Int.
				210?	weak		
≈250 [a]?							
		473±2	1.8±0.5	475?	<1	475±10	1.3 ±0.4
505[a]± 4							
		563±1	9 ±2				
				566±4	19	568±10	24 ±4
		569±1	13 ±2				
601± 1	100	605±1	100	603±1	100	605	100
		796±1	91 ±4				
795± 1	90			797±2	96	800± 5	92 ±7
		801±2	18 ±4				
						960±10	0.6 ±0.2
1039±12		1038±4	0.9±0.2			1040±10	1.5 ±0.3
1163±12		1168±5	3.0±0.4			1170±10	2.2 ±0.3
1350± 7	1	1367±5	4.6±0.3			1370±10	3.3 ±0.5
						1570±20	0.12±0.05

After subtraction of the pulse height distribution corresponding to a single gamma ray of 605 keV from the total spectrum, the remaining distribution above ≈ 400 keV can be fit exactly to that of the 513 keV peak of ^{85}Sr. The presence of a 560 keV gamma ray, which may correspond to the stop-over transition from the possible second 2^+ state in ^{134}Ba at 1170 keV, could not be confirmed.

4. The summing spectrum of ^{134}Cs

The summing spectrum of ^{134}Cs was examined with the cylindrical NaI(Tl) crystal of 6.2 cm × 6.2 cm dimensions. This crystal has a hole of 9 mm diameter and 31 mm depth. Sources were contained in a glas tube which fits in a copper tube with 2 mm thick walls; electrons with energy up to ≈ 4 MeV will be stopped by this absorber thickness.

Sources of ^{134}Cs were examined when placed inside the hole, when placed just outside on top of the crystal, and also when placed at different distances from the crystal. Fig. 4 shows the summing spectrum with the sources placed inside the hole, for an energy region from ≈ 400 to 2000 keV. The

dashed line represents the spectrum in this region with the source at a distance of 25 cm above the crystal. Summing peaks at 1.97, 1.40 and 1.17 MeV can be easily seen confirming the results obtained by Lu *et al.* [4]). The summing peaks which may result from expected levels at 1.64 and 1.77 MeV should lie in the valley and on the Compton distribution of the strong 1.97 MeV peak.

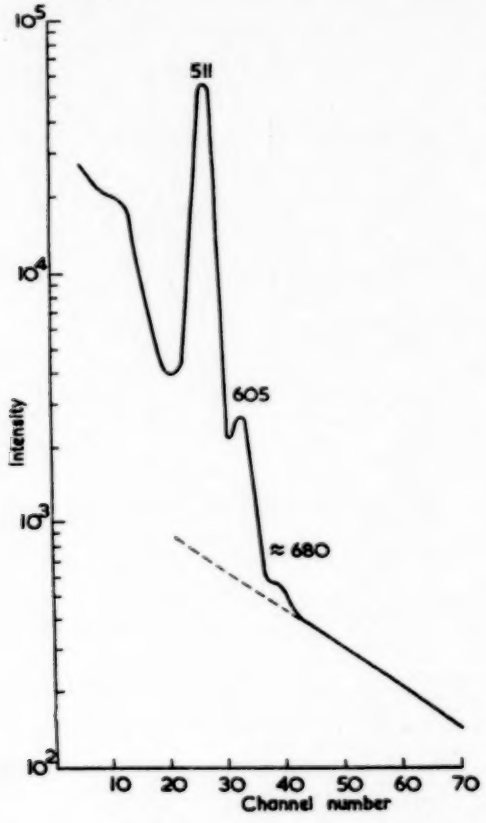

Fig. 3. The gamma ray spectrum of ^{134}La, the dashed line represents the annihilation of positons in flight.

In order to decide whether these additional summing peaks are present, it is necessary to subtract the pulse height distribution corresponding to a summing peak at 1.97 MeV. The exact shape of this distribution depends on the number and on the energy of the constituents. The 1.97 MeV peak is mainly due to triple summing (605+563+801) keV and (605+796+569 keV); the part due to double summing is weak, since it involves the 1.370 MeV gamma ray, which occurs only for 12 % in the total deexcitation of the 1.97 MeV level. (see fig. 6). Unfortunately, there do not exist too many cases with simple decay schemes from which the general structure of double and triple summing spectra can be deduced. A number of cases was studied and the results are reported in an appendix to this article; from this reason-

able semi-quantitative conclusions can be drawn about the energy dependence of summing spectra.

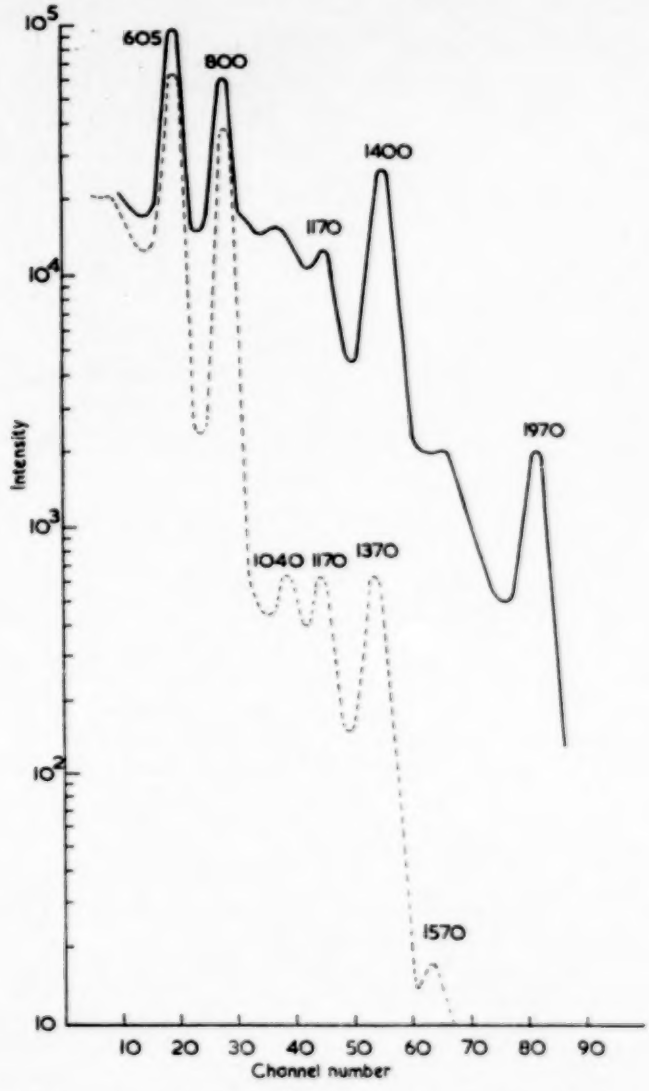

Fig. 4. The summing spectrum of ^{134}Cs when placed inside the hole, the dashed line represents the direct spectrum with the source at a distance of 25 cm from the same crystal in an energy region from $\approx$ 400 keV to 2000 keV. The actual statistics obtained for the 1.57 MeV peak in the direct spectrum was higher than that inferred from the graph.

The 2.30 MeV summing peak of ^{22}Na was assumed to give an acceptable pulse height distribution for comparison with the 1.97 MeV summing peak of ^{134}Cs, since it also arises from triple summing (511+511+1277 keV). The relative intensity of the Compton distribution of the 1.97 MeV peak should be somewhat lower than that due to the 2.30 MeV peak, firstly because of the lower energy of the summing peak and secondly because some double summing is involved in the 1.97 MeV peak (see appendix). It can be seen in

fig. 5a, however, that the reverse is the case, which proves that there are additional weak peaks present in the region of the Compton distribution due to the 1.97 MeV peak in ^{134}Cs.

For a further check the spectrum was studied with the source placed right on top of the crystal, in the aim of suppressing the triple coincidence summing (see appendix). Fig. 5b shows the spectrum in the energy region

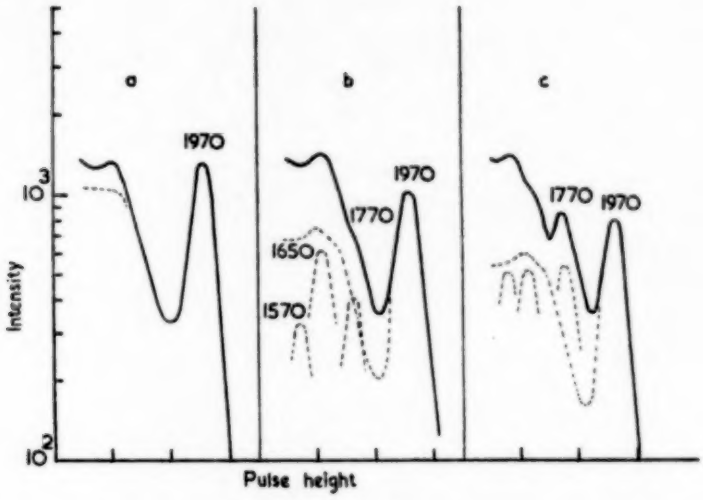

Fig. 5. The summing spectrum of ^{134}Cs in an energy region from ≈ 1500 keV to 2000 keV in different geometries: a) source inside the hole b) source placed right on top of the crystal c) source at a distance of 2 cm from the crystal. The dashed lines represent the resolved peaks.

from ≈ 1500 to 2000 keV. The dashed line represents the summing peak of 1.79 MeV (0.511+1.277 MeV) in ^{22}Na when this source is placed in the same geometry. Three peaks were found in the valley and on the Compton distribution of the 1.97 MeV summing peak. These peaks lie at 1.77, 1.65 and 1.57 MeV. The energy difference between the 1.97 MeV peak and the 1.79 MeV comparison-peak connot be responsible for this surplus, since the same picture was obtained by using the 2.34 MeV (0.57+1.77 MeV) summing peak in ^{207}Bi obtained in the same geometry. The new peaks show up even more clearly when the spectrum was displayed with the ^{134}Cs source placed 2 cm above the crystal. Fig. 5c shows the pulse height distribution obtained in this geometry for the same energy region mentioned above. The 1.79 MeV peak in ^{22}Na obtained in the same geometry was used for comparsion.

The summing peaks at 1.77 and 1.65 MeV correspond to cascades from expected levels with these energies while the 1.57 MeV peak corresponds to the peak with the same energy in the direct spectrum; it is probably due to summing of the 605 keV gamma ray with that at 960 keV. Table 2 gives the summing peaks and their interpretation.

TABLE 2

Energies of various summing peaks observed using the well-type crystal, and interpretation of their origin.

Summing peak (MeV)	Constituents	Level of origin (MeV)
1.17	0.605+0.563	1.168
1.40	0.605+0.796	1.401
1.57	0.605+0.960	1.57
1.65	0.605+0.563+0.473	1.641
	0.605+1.04	1.641
1.77	0.605+1.17	1.770
	0.605+0.563+0.605?	1.770
1.97	0.605+0.563+0.801	1.970
	0.605+0.796+0.570	1.970
	0.605+1.37	1.970
	1.17 +0.801	1.970

5. Discussion

The present work substantiates the level scheme of ^{134}Ba adopted by the Nuclear Data Group [1]). Fig. 6 gives this level scheme. A new level at 1.570 MeV is added. The energies and intensities of the various gamma rays following the decay of ^{134}Cs as found from the present investigation are given on the level scheme. For the couples of unresolved gamma ray peaks at 800 and 565 keV the intensities of the components were estimated from the average of their intensity ratios as reported by other groups. [2, 7–12]).

The position of the first 2^+ level at 605 keV is beyond doubt since the only gamma ray observed in the spectrum of ^{134}La has this energy. The existence of a level at 1.17 MeV seems to be well established from summing experiments, gamma-gamma coincidence measurements [2, 3, 4]) and angular correlation work [11, 15, 16, 17]) on ^{134}Cs. This level de-excites both to the first 2^+ level and to the ground state. The presence of this last transition is confirmed by the work of Everett *et al.* [15]). The features of this level strongly suggest [18]) a spin of 2^+. The presence of a level at 1.401 MeV is certain. The absence of a ground state transition from this level (< 0.3 %) suggests a spin $\geqq 3$ in agreement with a value 4 found from angular correlation measurements[15, 17]). The same arguments apply to the level at 1.970 MeV. Levels at 1770, 1641 and 1570 keV are suggested from the summing studies performed in this work. The total decay energy [1]) of ^{134}Cs being $\approx$ 2.07 MeV does not allow placing any one of these gamma rays higher in the level scheme. The first two levels are supported by the presence of two beta branches of 280 keV and 410 keV which may populate such levels [10]). The absence of ground state transitions from these levels (< 0.1 %) would be compatible with spins $\geqq 3$. The level at 1570 keV is suggested from the present direct gamma ray measurements

and also from the summing experiments. A spin ≤ 2 would follow for this level since a ground state transition deexciting it was observed. The presence of a weak beta ray branch populating this level is not excluded; it would probably be too weak to be easily resolvable from the complicated beta ray spectrum [1]). On the other hand it is possible that the 1.57 MeV level is populated by a weak gamma ray transition of low energy. The assignment

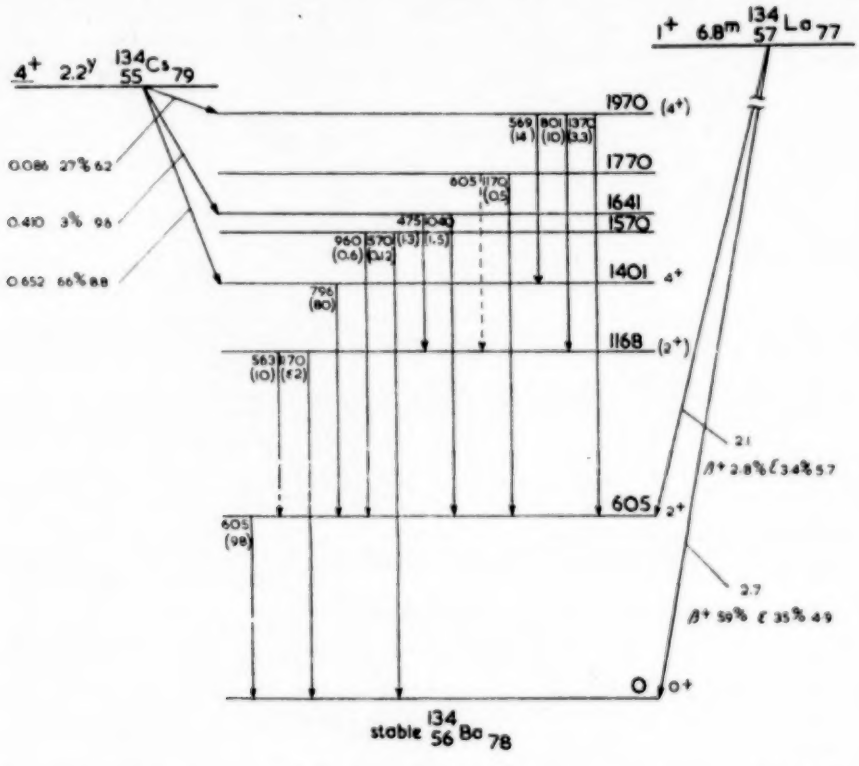

Fig. 6. Proposed level scheme of ^{134}Ba. The energy values written on the left hand side of the various transitions represent the gamma rays following the decay of ^{134}Cs. The numbers in brackets represent their relative intensities in percentage per disintegrations assuming all disintegrations to go through either the 605 or the 1170 keV transition. The uncertain 60$\dot{5}$ keV transition de-exciting the level at 1170 keV is drawn in as a dashed line. The characteristics of the beta branches following the decay of ^{134}Cs and those following the decay of ^{134}La are shown on the graph in the following order: energy of the branch, intensity in percentages per disintegration, and the log *ft* value. These values are calculated from the various gamma rays populating and de-exciting different levels.

of the weak peaks at 960 and 1570 keV to ^{134}Cs cannot be claimed to be certain since the half life of these peaks was not determined. However, the presence of these peaks in both the spectra as detected by the two different crystals, together with the presence of a summing peak at 1.57 MeV supports this assignment. If these gamma rays are due to an impurity, it should be a long-lived one ($>$ 20 day period)† with gamma rays of $\approx$ 600, 960 and 1570 keV. None of the possible impurities which may be present in the Cs-source could produce activities with these characteristics.

† See note added in proof, p. 687.

The intensity balance between the various gamma rays populating and de-exciting levels up to 1.168 MeV excitation energy is very satisfactory, even within limits much narrower than those suggested by the errors placed on the relative intensities of the various gamma rays.

The intensities and the log *ft* values for the important beta ray branches in the decay of ^{134}Cs, as calculated from the proposed decay scheme are shown in fig. 6. They are in good agreement with directly measured values for these branches as reported by various groups [1]). The log *ft* values for these branches seem to be higher than normal. For example the beta branch of 652 keV energy populating the level at 1.401 MeV has a log *ft* of 8.8. This branch should have an allowed transition character since the spin of this level at 1.401 MeV seems to be certainly 4^+ as shown by gamma-gamma angular correlation measurements [15, 17]) and polarization correlation measurements [19]).

The characteristics of the decay of ^{134}La are shown on the decay scheme (fig. 6). Two positon branches of energies 2.1 MeV and 2.7 MeV should follow the decay of ^{134}La, the first of intensity 2.8 % per disintegration and populating the first 2^+ level in ^{134}Ba, the second being a ground state transition of intensity of 59 % per disintegration. The energy values are based on the measurement of the end point of the ^{134}La positon spectrum made by Stover [13]). The log *ft* values for the two branches suggest allowed transitions, indicating spin 1^+ for the 6.8 minute ^{134}La.

Appendix

SOME FEATURES OF THE NaI SUMMING SPECTROMETER

Lu and Wiedenbeck [4]) used the NaI summing spectrometer to confirm the presence of some levels in various nuclei by comparing the spectra produced by a source placed either outside a crystal or inside a hole drilled into the NaI(Tl) crystal. Gupta and Jha [20]), Shapiro and Higgs [21]) and Schmidt-Ott [22]) discussed methods for obtaining the photopeak efficiency of such a spectrometer when the sources were placed inside the hole. It is evident from the preceding report on ^{134}Cs that interesting information can be obtained with this type of spectrometer if the spectra are compared when the sources are placed either inside or in various geometries outside the hole, in particular when complicated spectra are examined. It was thought worthwhile to show some spectra examined under different geometrical conditions using the summing crystal described in the previous article; the results give some insight into the properties of this type of spectrometers.

1) *The spectrum due to a single gamma ray*

The ^{54}Mn source was chosen to demonstrate the variation in the Compton

distribution of a single gamma ray when examined with the summing spectrometer. No important secondary effects are present in this spectrum such as an intense bremsstrahlung continuum or the presence of positons or a strong X ray. Fig. 7 shows this spectrum for three different geometries, namely inside the hole, right on top of the crystal and far from the crystal. The intensity of the Compton distribution of the 835 keV gamma ray is

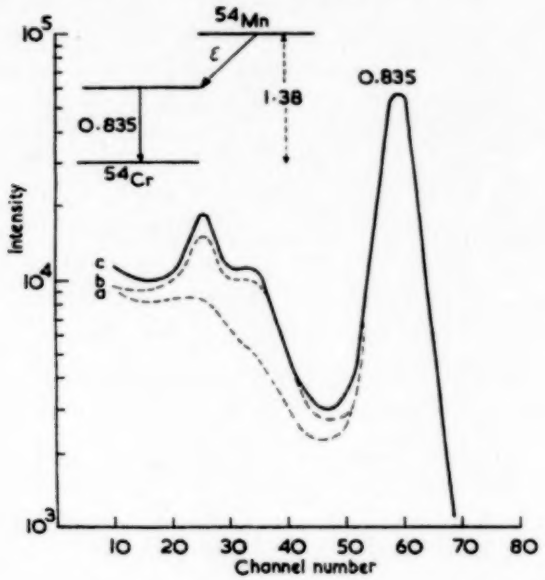

Fig. 7. The ^{54}Mn 835 keV peak examined with the summing crystal in different geometries: a) source inside the hole, b) source on top of the crystal, c) source high above the crystal. Some features of the decay scheme of ^{54}Mn are shown in the insert.

reduced when the source is placed in the hole, in other words there is a gain in the photopeak detecting efficiency in this geometry. This is obviously due to the smaller escape probability of the degraded Compton scattered gamma rays for this geometry. Especially the Compton shoulder is suppressed since in this case there is only a small amount of energy left for the scattered gamma ray after the first collision.

2) *Source having cascades of two gamma rays only*

When cascades of two gamma rays are involved, the intensity of the summing peak is $N\,\varepsilon_1\varepsilon_2\omega^2$ where N is the intensity of the cascade, ε_1 and ε_2 are the photopeak efficiencies for the two gamma rays, members of the cascade, and ω is the solid angle subtended by the crystal as seen from the source position.

In those cases where two or more independent cascades †) of the type

† Cascades are called independent when there is only one gamma transition entering or leaving the various levels involved.

mentioned above are present, the relative intensities of the various summing peaks are practically independent of the geometry. The difference in the relative detecting efficiencies of the constituent gamma rays for different geometries causes only a negligible correction. This was shown explicitly in a study with the 2.5 cm crystal when the source distance was increased from 2 cm to 8 cm.

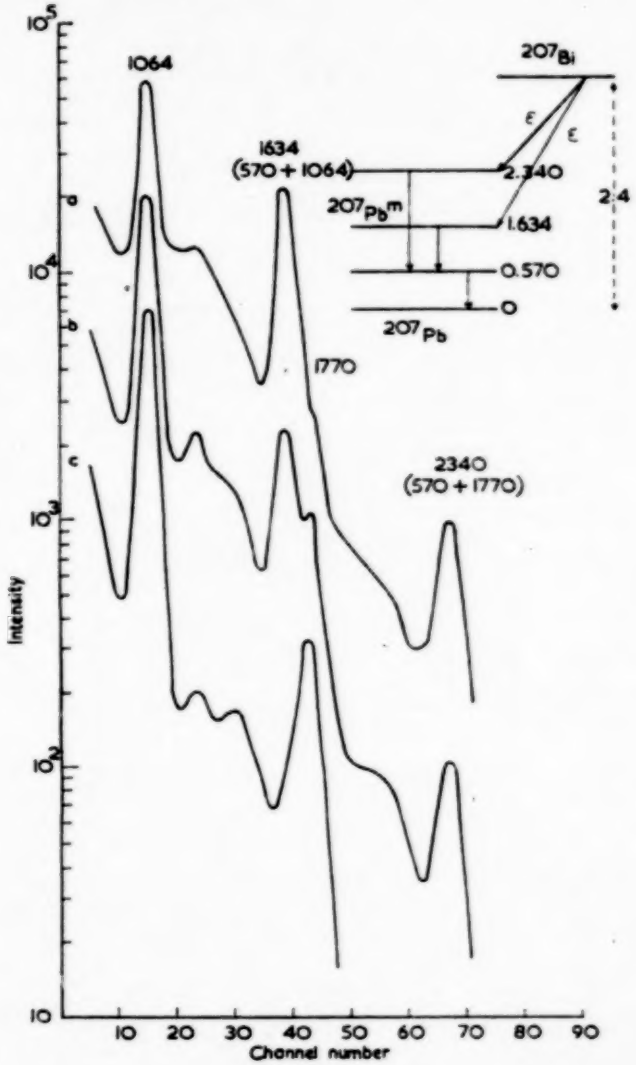

Fig. 8. The ^{207}Bi spectrum examined with the summing crystal in different geometries: a) source inside the hole, b) source on top of the crystal, c) source high above the crystal. Some features of the decay scheme of ^{207}Bi are shown in the insert.

A typical example of such sources is ^{207}Bi, its decay scheme is shown in the insert of fig. 8, This figure also gives the spectra of ^{207}Bi in an energy region between $\approx$ 1 and 2.5 MeV in three different geometries. One of these is the

direct spectrum of this source, i.e. the spectrum free from summing effects. It can be seen from the other two spectra, with the source inside and on top of the crystal, that the ratio between the summing peaks at 2.34 and 1.64 MeV stays practically the same, thus confirming the conclusion mentioned above.

The reduction in intensity of the Compton distributions for peaks when sources are placed in the well can also be seen in these spectra.

3) *Sources having cascades of more than two gamma rays*

Consider a simple case of three excited levels of energies E_3, E_2 and E_1

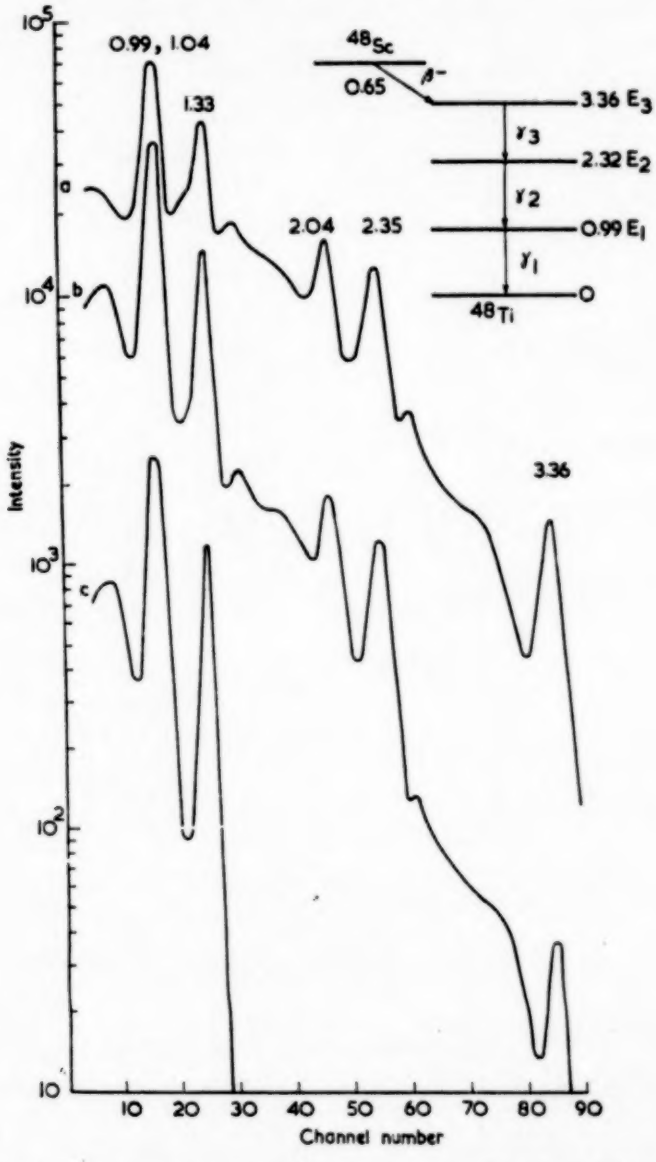

Fig. 9. The ^{48}Sc spectrum examined with the summing crystal in different geometries: a) source inside the hole, b) source on top of the crystal, c) source high above the crystal. Some features of the decay scheme of ^{48}Sc are shown in the insert.

de-excited by three cascading gamma rays γ_3, γ_2 and γ_1 respectively (see insert of fig. 9), of intensity N. The summing spectrum will consist of the gamma rays γ_1, γ_2, γ_3, the double summing peaks γ_{12}, γ_{13}, γ_{23} and the triple summing peak γ_{123} in a self explanatory notation. The intensities of these peaks are

$$N_{ij} = N\,\varepsilon_i\varepsilon_j\omega^2 \quad \text{and} \quad N_{123} = N\varepsilon_1\varepsilon_2\varepsilon_3\omega^3.$$

This means that the triple coincidence summing peak decreases faster in intensity than a double coincidence summing peak with decreasing solid angle.

The nucleide ^{48}Sc is a simple case to check the above argument. The decay of this isotope consists of one negaton group with an endpoint of 0.65 MeV followed by three gamma rays [23]) of 1.04, 1.33 and 0.99 MeV in cascade. The decay scheme is shown in the insert of fig. 9. The negatons present in the decay of ^{48}Sc, being of low energy do not disturb the spectrum in the region of interest. The spectra are displayed for various geometries. It is clear that the triple coincidence summing peak at 3.36 MeV gains considerably in intensity when the source is placed inside the hole which confirms the conclusion mentioned above. This behaviour therefore provides a means of distinguishing between double and triple summing when studying complicated decay schemes.

The authors wish to thank Prof. Dr. P. C. Gugelot, Prof. Dr. A. H. W. Aten Jr. and Prof. Dr. A. H. Wapstra for their interest in this work, Mrs. A. Funke-Klopper and Miss J. C. Kapteijn for performing the chemical separations and the personnel of the cyclotron for the irradiations.

One of the authors (R. K. G.) is indebted to the Egyptian Atomic Energy Commission for a grant.

This work was performed as part of the research program of the „Stichting voor Fundamenteel Onderzoek der Materie (F.O.M.)", which is financially supported by the „Nederlandse Organisatie voor Zuiver-Wetenschappelijk Onderzoek (Z.W.O.)"

Note added in proof. A new measurement of the gamma ray spectrum from the same source was undertaken 150 days after the first series. The two new gamma rays are still present with the same relative abundance. Their half life therefore lies between 0.8 and 4 years; the assignment to ^{134}Cs can be regarded as reasonably certain.

References

1) Nuclear Data Sheets, National Research Council, Washington, D. C. U.S.A.
2) G. Bertolini, M. Bettoni and E. Lazzarini, Nuovo Cimento **2** (1955) 273; **1** (1955) 746
3) A. Chandra, Proc. Indian Acad. Sci. A **44** (1956) 194
4) D. C. Lu and M. L. Wiedenbeck, Phys. Rev. **94** (1954) 501

5) R. K. Girgis and R. van Lieshout, Nuclear Physics **12** (1959) 204
6) R. K. Girgis, R. A. Ricci and R. van Lieshout, to be published
7) M. C. Joshi and B. V. Thosar, Phys. Rev. **96** (1954) 1022
8) A. A. Bashilov, N. M. Anton'eva, M. V. Blinov and B. Džhelepov, Izvest. Akad. Nauk., S.S.S.R. Ser. Fiz. **18** (1954) 43
9) J. Verhaeghe and J. Demuynck, Compt. rend. **239** (1954) 1374
10) H. H. Forster and J. S. Wiggins, Nuovo Cimento **2** (1955) 854; Phys. Rev. **99** (1955) 660 A
11) G. L. Keister, E. B. Lee and F. H. Schmidt, Phys. Rev. **97** (1955) 451
12) K. E. Johansson, Arkiv Fysik **10** (1956) 247
13) B. J. Stover, Phys. Rev. **81** (1951) 8
14) R. A. Ricci, R. K. Girgis and R. van Lieshout, Nuovo Cimento **11** (1959) 156
15) A. E. Everett and M. J. Glaubman, Phys. Rev. **100** (1955) 955 A
16) E. D. Klema, Phys. Rev. **100** (1955) 66
17) M. G. Stewart, R. P. Scharenberg and M. L. Wiedenbeck, Phys. Rev. **99** (1955) 691
18) G. Scharff-Goldhaber and J. Weneser, Phys. Rev. **98** (1955) 212;
K. Way, D. M. Kundu, C. L. McGinnis and R. van Lieshout, Annual Review of Nuclear Science **6** (1956) 129
19) R. M. Kloepper, E. S. Lennox and M. L. Wiedenbeck, Phys. Rev. **88** (1952) 695;
B. L. Robinson and L. Madansky, Phys. Rev. **88** (1952) 1065
20) R. K. Gupta and S. Jha, Nuclear Physics **1** (1956) 2
21) P. Shapiro and R. W. Higgs, Rev. Sci. Instrum. **28** (1957) 939
22) W. D. Schmidt-Ott, Zeits. Phys. **154** (1959) 294
23) K. Way, R. W. King, C. L. McGinnis and R. van Lieshout, Nuclear level Schemes, TID—5300, N.R.C. (Washington, 1955)

AUTHOR INDEX

ARIMA, A. and S. YOSHIDA, Analysis of a rotational state in terms of the shell model states 139
ARMBRUSTER, R., *see* GORODETZKY
BABA, C. V. K., *see* BHATTACHERJEE
BATTAT, M. E., *see* LOS ALAMOS PHYSICS AND CRYOGENICS GROUPS
BELL, J. S., Particle-hole conjugation in the shell model 117
BELL, R. E. and M. H. JØRGENSEN, Half-lives of two excited states of Gd^{156} 413
BHATTACHERJEE, S. K., BALDEV SAHAI and C. V. K. BABA, Decay of Pm^{148} 356
BIAŁYNICKI-BIRULA, I., Lee model and the local field theory 309
BISWAS, S. N., *see* PANDIT
BLANKENBECLER, RICHARD, MARVIN L. GOLDBERGER and FRANCIS R. HALPERN, Elastic neutron-deuteron scattering 629
BOLLINGER, L. M., *see* KENNETT
BONDELID, R. O., *see* LOS ALAMOS PHYSICS AND CRYOGENICS GROUPS
BOSKMA, P. and H. DE WAARD, Excited states of ^{166}Er 533
BOWCOCK, J. and D. WALECKA, Analytic properties of the Schrödinger amplitude at a fixed angle 371
BRINK, D. M. and A. K. KERMAN, Two body forces in light deformed nuclei 314
BROWNE, CORNELIUS P., Energy levels of Na^{22} from the $Mg^{24}(d, \alpha)Na^{22}$ and $Mg^{25}(p, \alpha)Na^{22}$ reactions 662
CHEVALLIER, P. *see* GORODETZKY
COHEN, L., *see* OLKOWSKY
COON, J. H., *see* LOS ALAMOS PHYSICS AND CRYOGENICS GROUPS
CRANBERG, L., *see* LOS ALAMOS PHYSICS AND CRYOGENICS GROUPS
DAHL, P., *see* MAACK BISGÅRD
DAVYDOV, A. S. and V. S. ROSTOVSKY, Relative transition probabilities between rotational levels of non-axial nuclei 58
DAY, R. B., *see* LOS ALAMOS PHYSICS AND CRYOGENICS GROUPS
DE WAARD, H., *see* BOSKMA
EDESKUTY, F., *see* LOS ALAMOS PHYSICS AND CRYOGENICS GROUPS
EDGE, R. D., The altitude dependence of atmospheric cosmic-ray neutrons and the slow neutron density below a water surface . . 182
EGARDT, L., A note on the inelastic scattering of high energy protons by light nuclei 84

EISBERG, R. M., *see* GRIFFITHS
EMERY, V. J., On the existence of solutions of the Brueckner equations for a many-fermion system 69
EVANS, J. E., *see* WATERS
FARWELL, G. W., *see* YAVIN
FERGUSON, A. T. G. and E. B. PAUL, A study of the energy levels of A^{37}, Sc^{48} and Cr^{51}. 426
FERGUSON, J. M., Fe^{59} decay scheme. 579
FIRK, F. W. K. and M. C. MOXON, The determination of neutron resonance parameters of tungsten by the transmission method . . 552
FRADKIN, E. S., The Green's function method in quantum statistics . 465
FRENTROP, A. H., *see* LOS ALAMOS PHYSICS AND CRYOGENICS GROUPS
GILL, P. S., *see* SEHGAL
GIRGIS, R. K. and R. VAN LIESHOUT, The level scheme of ^{136}Ba . . . 204
GIRGIS, R. K. and R. VAN LIESHOUT, The level scheme of ^{134}Ba. Some features of the NaI summing spectrometer 672
GOLDANSKY, V. I., B. B. GOVORKOV and R. G. VASSILKOV, Photoproduction of neutral prions on hydrogen near the threshold . . . 327
GOLDBERGER, MARVIN L., *see* BLANKENBECLER
GOLDFARB, L. J. B. and J. R. ROOK, The polarization of deuterons and particle of arbitrary spin II 494
GOLDFARB, L. J. B., On the detection of deuteron polarization. . . . 657
GOODING, T. J., Proton total reaction cross sections at 34 MeV . . . 241
GORODETZKY, S., P. CHEVALLIER, R. ARMBRUSTER et G. SUTTER, Corrélation angulaire de paires de conversion interne détectées dans un fond de neutrons et de rayonnement γ. Application à ^{14}N, ^{10}Be, ^{10}B. 349
GOVORKOV, B. B., *see* GOLDANSKY
GRATOT, I., *see* OLKOWSKY
GREGERS HANSEN, P., O. B. NIELSEN and R. K. SHELINE, Levels in Gd^{156} excited in the decay of 5.6 d Tb^{156} 389
GRIFFITHS, R. J. and R. M. EISBERG, The mechanism of the direct interaction process at intermediate energies 225
HANS, H. S., *see* SEHGAL
HALPERN, FRANCIS R., *see* BLANKENBECLER
HELMERS, K., On symplectic invariance of the energy matrix in a nuclear j^N configuration. 647
HENKEL, R. L., *see* LOS ALAMOS PHYSICS AND CRYOGENICS GROUPS
HILLMAN, PETER, ARNE JOHANSSON, GUNNAR TIBELL and HELGE TYRÉN, Inelastic scattering of high energy protons by helium: an excited level? 596
IZBICKI, HERBERT, Note on "double binomial coefficients" 532

JEZAK, E. V., *see* MCCARTHY
JOHANSSON, ARNE, *see* HILLMAN
JOHANSSON, SVEN A. E., On spontaneous fission rates 449
JOHANSSON, SVEN A. E., *see* PERSSON
JONES, G. A., Energy dependence of the (p, n) reaction near $A = 70$. 167
JØRGENSEN, M. H., *see* BELL
KENNETT, T. J. and L. M. BOLLINGER, The multiple scattering of neutrons at resonances 249
KERMAN, A. K., *see* BRINK
KIKUCHI, KEN, Distribution of the imaginary part of the optical potential. 305
KINSEY, B. B., *see* WATERS
KOMAR, A. A. and M. A. MARKOV, An example of a field theory with indefinite metric in Hilbert space II 190
KROMMINGA, A. J., *see* MCCARTHY
LAURIKAINEN, K. V. and O. VARHO, Phenomenological two-nucleon potentials and the deuteron, II 606
LEMMER, R. H., TH. A. J. MARIS and Y. C. TANG, On the imaginary optical potential 619
LE PAPE, M., *see* OLKOWSKY
LOS ALAMOS PHYSICS AND CRYOGENICS GROUPS, Total neutron cross sections of the hydrogen and helium isotopes 291
MAACK BISGÅRD, K., P. DAHL and K. OLESEN, Multipolarities of U^{233} transitions 612
MCCARTHY, I. E., E. V. JEZAK and A. J. KROMMINGA, Momentum distribution of nucleons in the nuclear surface 274
MARCH, N. H. and W. H. YOUNG, Approximate solutions of the density matrix equation for a local average field 237
MARIS, TH. A. J., *see* LEMMER
MARKOV, M. A., *see* KOMAR
MARX, G. and K. L. NAGY, A proposed strong interaction of muons . 125
MEHTA, M. L., On the singularities of a generalized Brueckner t-matrix 333
MILLS, R. L., *see* LOS ALAMOS PHYSICS AND CRYOGENICS GROUPS
MINARDI, ETTORE, Connection between masses and isobaric spin . . 35
MITRA, A. N., Pion-baryon interactions and "closed loop" phenomena 133
MOXON, M. C., *see* FIRK
NAGY, K. L., *see* MARX
NIELSEN, O. B., *see* GREGERS HANSEN
NING HU, The proper field of a physical nucleon 87
NOBLES, R. A., *see* LOS ALAMOS PHYSICS AND CRYOGENICS GROUPS
OLESEN, K., *see* MAACK BISGÅRD
OLKOWSKY, J., I. GRATOT, M. LE PAPE et L. COHEN, Un nouvel

isotope du terbium de masse 152, émetteur alpha 159
OLKOWSKY, J., M. LE PAPE, I. GRATOT et L. COHEN, Un nouvel isotope du gadolinium très déficient en neutrons 527
PANDIT, L. K. and S. N. BISWAS, K^+-meson—nucleon scattering and K^+—Y relative parity 521
PAUL, E. B., *see* FERGUSON
PERRY, J. E., *see* LOS ALAMOS PHYSICS AND CRYOGENICS GROUPS
PERSSON, BÖRJE and SVEN A. E. JOHANSSON, Internal bremsstrahlung from P^{32}. 432
PHILLIPS, D. D., *see* LOS ALAMOS PHYSICS AND CRYOGENICS GROUPS
PILKUHN, HARTMUT, Quadrupole interaction in SU_2-coupling and cranking model. 269
REDMOND, PETER, J., *see* URETSKY
ROBERTS, T. R., *see* LOS ALAMOS PHYSICS AND CRYOGENICS GROUPS
ROOK, J. R., *see* GOLDFARB
ROSE, H. J., W. TROST and F. RIESS, The spin assignments of the 9.16-MeV and 6.44-MeV states in N^{14} 510
ROSTOVSKY, V. S., *see* DAVYDOV
RIAZUDDIN, K^0—K^+ mass excess. 342
RIESS, F., *see* ROSE
SAHAI, BALDEV, *see* BHATTACHERJEE
SEHGAL, M. L., H. S. HANS and P. S. GILL, Thermal neutron cross-sections for producing some isomers 261
SHELINE, R. K., *see* GREGERS HANSEN
SOOD, P. C., *see* TRAINOR
SRINIVASAN, S. K. and K. VENKATESAN, Photoproduction of pion pairs by a nucleon 418
SUTTER, G., *see* GORODETZKY
SYDORIAK, S. G., *see* LOS ALAMOS PHYSICS AND CRYOGENICS GROUPS
TANG, Y. C., *see* LEMMER
TIBELL, GUNNAR, *see* HILLMAN
TRAINOR, L. E. H. and P. C. SOOD, Nature of nuclear matter in the free-meson lattice model. 625
TROST, W., *see* ROSE
TYRÉN, HELGE, *see* HILLMAN
UHLMANN, A., Untersuchungen über Quantentheorien mit indefiniter Metrik. 103
URETSKY, JACK L. and PETER J. REDMOND, Calculation of the magnetic moments of nucleons by use of a modified propagator . . 485
VAN LIESHOUT, R., *see* GIRGIS
VARHO, O., *see* LAURIKAINEN
VASSILKOV, R. G., *see* GOLDANSKY

VENKATESAN, K., *see* SRINIVASAN
WALECKA, D., *see* BOWCOCK
WATERS, J. R., J. E. EVANS, B. B. KINSEY and G. H. WILLIAMS, Spins and radiation widths of the low energy neutron resonances in tungsten 563
WILLIAMS, G. H., *see* WATERS
YAVIN, A. I. and G. W. FARWELL, Angular distributions for elastic and inelastic scattering of 40-MeV alpha particles by carbon, nitrogen, oxygen, and argon 1
YNTEMA, J. L., *see* ZEIDMAN
YONEZAWA, MINORU, Remarks on the decay interactions in the K_{e3} process 589
YOSHIDA, S., *see* ARIMA
YOUNG, W. H., *see* MARCH
ZEIDMAN, B. and J. L. YNTEMA, (α, d) reactions on N^{14} and Li^{6} . . . 298

SUBJECT INDEX

1. Nuclear Structure

1.B *Two- and three-body problems*

Phenomenological two-nucleon potentials and the deuteron, II, K. V. Laurikainen and O. Varho 606
Elastic neutron-deuteron scattering, Richard Blankenbecler, Marvin L. Goldberger and Francis R. Halpern 629

1.C *Many-particle systems*

On the existence of solutions of the Brueckner equations for a many-fermion system, V. J. Emery 69
Approximate solutions of the density matrix equation for a local average field, N. H. March and W. H. Young 237
On the singularities of a generalized Brueckner t-matrix, M. L. Mehta . . 333
The Green's function method in quantum statistics, E. S. Fradkin 465

1.D *Nuclear models*

1.D.1 *Shell model*

Particle-hole conjugation in the shell model, J. S. Bell 117
Note on "double binomial coefficients", Herbert Izbicki 532
On symplectic invariance of the energy matrix in a nuclear j_N configuration, K. Helmers 647

1.D.2 *Collective model*

Relative transition probabilities between rotational levels of non-axial nuclei, A. S. Davydov and V. S. Rostovsky. 58
Two body forces in light deformed nuclei, D. M. Brink and A. K. Kerman 314
Levels in Gd^{156} excited in the decay of 5.6 d Tb^{156}, P. Gregers Hansen, O. B. Nielsen and R. K. Sheline 389
Half-lives of two excited states of Gd^{156}, R. E. Bell and M. H. Jørgensen. 413

1.D.3 *Other models*

Nature of nuclear matter in the free-meson lattice model, L. E. H. Trainor and P. C. Sood 625

1.D.4 *Relationship between different models*

Analysis of a rotational state in terms of the shell model states, A. Arima and S. Yoshida 139
Quadrupole interaction in SU_3-coupling and cranking model, Hartmut Pilkuhn. 269

1.E *Properties of nuclei*

1.E.1 *Energy levels*

The level scheme of ^{136}Ba, R. K. Girgis and R. van Lieshout 204
Decay of Pm^{148}, S. K. Bhattacherjee, Baldev Sahai and C. V. K. Baba 356
Levels in Gd^{156} excited in the decay of 5.6. d Tb^{156}, P. Gregers Hansen, O. B. Nielsen and R. K. Sheline 389
A study of the energy levels of A^{37}, Sc^{48} and Cr^{51}, A. T. G. Ferguson and E. B. Paul 426
The spin assignments of the 9.16-MeV and 6.44-MeV states in N^{14}, H. J. Rose, W. Trost and F. Riess 510
Excited states of ^{166}Er, P. Boskma and H. de Waard 533
Fe^{59} decay scheme, J. M. Ferguson 579
Multipolarities of U^{233} transitions, K. Maack Bisgård, P. Dahl and K. Olesen 612
The level scheme of ^{134}Ba. Some features of the NaI summing spectrometer, R. K. Girgis and R. van Lieshout 672

1.E.4 *Transition probabilities; Cross sections*

Half-lives of two excited states of Gd^{156}, R. E. Bell and M. H. Jørgensen 413

1.E.7 *Isobaric spin effects*

Energy levels of Na^{22} from the Mg^{24}(d, α)Na^{22} and Mg^{25}(p, α)Na^{22} reactions, Cornelius P. Browne 662

2. Nuclear Reactions

2.A *General properties*

2.A.1 *Cross sections, energy relations*

The multiple scattering of neutrons at resonances, T. J. Kennett and L. M. Bollinger 249
Total neutron cross sections of the hydrogen and helium isotopes, Los Alamos Physics and Cryogenics Groups 291
A study of the energy levels of A^{37}, Sc^{48} and Cr^{51}, A. T. G. Ferguson and E. B. Paul 426

2.B *Angular distributions, Correlations; Polarization*

(α, d) reactions on N^{14} and Li^{6}, B. Zeidman and J. L. Yntema 298
The polarization of deuterons and particles of arbitrary spin II, L. J. B. Goldfarb and J. R. Rook 494
On the detection of deuteron polarization, L. J. B. Goldfarb 656

2.C *Resonance reactions; R-matrix theory*

The determination of neutron resonance parameters of tungsten by the transmission method, F. W. K. Firk and M. C. Moxon 552
Spins and radiation widths of the low energy neutron resonances in tungsten, J. R. Waters, J. E. Evans, B. B. Kinsey and G. H. Williams 563
Energy levels of Na^{22} from the Mg^{24}(d, α)Na^{22} and Mg^{25}(p, α)Na^{22} reactions, Cornelius P. Browne. 662

2.E *Optical model*

Energy dependence of the (p, n) reaction near $A = 70$, G. A. Jones . . . 167
Proton total reaction cross sections at 34 MeV, T. J. Gooding 241
Distribution of the imaginary part of the optical potential, Ken Kikuchi . 305
On the imaginary optical potential, R. H. Lemmer, Th. A. J. Maris and Y. C. Tang 619

2.F *Direct interaction (other than stripping)*

The mechanism of the direct interaction process at intermediate energies, R. J. Griffiths and R. M. Eisberg 225
Momentum distribution of nucleons in the nuclear surface, I. E. McCarthy, E. V. Jezak and A. J. Kromminga. 274

2.J *Fission and spallation*

On spontaneous fission rates, Sven A. E. Johansson 449
Un nouvel isotope du gadolinium très déficient en neutrons, J. Olkowsky, M. le Pape, I. Gratot et L. Cohen 527

2.L *Scattering processes (except two-nucleon system and meson scattering)*

Angular distributions for elastic and inelastic scattering of 40-MeV alpha particles by carbon, nitrogen, oxygen, and argon, A. I. Yavin and G. W. Farwell 1
A note on the inelastic scattering of high energy protons by light nuclei, L. Egardt 84
Inelastic scattering of high energy protons by helium: an excited level?, Peter Hillman, Arne Johansson, Gunnar Tibell and Helge Tyrén 596

3. Electromagnetic Radiation

3.A *Gamma radiation*

The level scheme of ^{136}Ba, R. K. Girgis and R. van Lieshout 204
Thermal neutron cross-sections for producing some isomers, M. L. Sehgal, H. S. Hans and P. S. Gill. 261
Levels in Gd^{156} excited in the decay of 5.6 d Tb^{156}, P. Gregers Hansen, O. B. Nielsen and R. K. Sheline 389
Half-lives of two excited states of Gd^{156}, R. E. Bell and M. H. Jørgensen . 413
The spin assignments of the 9.16-MeV and 6.44-MeV states in N^{14}, H. J. Rose, W. Trost and F. Riess 510
Fe^{59} decay scheme, J. M. Ferguson. 579
The level scheme of ^{134}Ba. Some features of the NaI summing spectrometer, R. K. Girgis and R. van Lieshout. 672

3.B *Internal conversion*

Corrélation angulaire de paires de conversion interne détectées dans un fond de neutrons et de rayonnement γ. Application à ^{14}N, ^{10}Be, ^{10}B, S. Gorodetzky, P. Chevallier, R. Armbruster et G. Sutter 349
Multipolarities of U^{233} transitions, K. Maack Bisgård, P. Dahl and K. Olesen 612

4. Beta decay; Parity

4.E *Analysis of data*

Un nouvel isotope du terbium de masse 152, émetteur alpha, J. Olkowsky, I. Gratot, M. le Pape et L. Cohen 159

Decay of Pm^{148}, S. K. Bhattacherjee, Baldev Sahai and C. V. K. Baba . . 356
Internal bremsstrahlung from P^{32}, Börje Persson and Sven A. E. Johansson 432
Un nouvel isotope du gadolinium très déficient en neutrons, J. Olkowsky, M. le Pape, I. Gratot et L. Cohen 527
Excited states of ^{166}Er, P. Boskma and H. de Waard 533
Fe^{59} decay scheme, J. M. Ferguson 579

5. Alpha Decay

Un nouvel isotope du terbium de masse 152, émetteur alpha, J. Olkowsky, I. Gratot, M. le Pape et L. Cohen 159

6. Methods and Instruments

6.A *Experimental*

The multiple scattering of neutrons at resonances, T. J. Kennett and L. M. Bollinger 249

6.D *Tables and computational aids*

Phenomenological two-nucleon potentials and the deuteron, II, K. V. Laurikainen and O. Varho 606

7. Quantum Field Theory

7.A *General*

The proper field of a physical nucleon, Ning Hu 87
Analytic properties of the Schrödinger amplitude at a fixed angle, J. Bowcock and D. Walecka 371
Calculation of the magnetic moments of nucleons by use of a modified propagator, Jack L. Uretsky and Peter J. Redmond 485
Elastic neutron-deuteron scattering, Richard Blankenbecler, Marvin L. Goldberger and Francis R. Halpern 629

7.C *π-meson field (scattering and nuclear forces)*

Photoproduction of neutral pions on hydrogen near the threshold, V. I. Goldansky, B. B. Govorkov and R. G. Vassilkov 327
Photo-production of pion pairs by a nucleon, S. K. Srinivasan and K. Venkatesan 418
Nature of nuclear matter in the free-meson lattice model, L. E. H. Trainor and P. C. Sood 625

8. Elementary Particles

8.B *Theory: interactions, transformation properties*

A proposed strong interaction of muons, G. Marx and K. L. Nagy 125
Pion-baryon interactions and "closed loop" phenomena, A. N. Mitra . . . 133
K^0—K^+ mass excess, Riazuddin 342
K^+-meson—nucleon scattering and K^+—Y relative parity, L. K. Pandit and S. N. Biswas 521
Remarks on the decay interaction in the K_{e3} process, Minoru Yonezawa . 589

8.C *Fundamental theory of matter*

Connection between masses and isobaric spin, Ettore Minardi 35
Untersuchungen über Quantentheorien mit indefiniter Metrik, A. Uhlmann 103
An example of a field theory with indefinite metric in Hilbert space II, A. A. Komar and M. A. Markov 190
Lee model and the local field theory, I. Białynicki-Birula 309

9. Cosmic Radiation

9.A *General*

The altitude dependence of atmospheric cosmic-ray neutrons and the slow neutron density below a water surface, R. D. Edge 182

10. News Items

10.A *News items*

CERN Council Meeting in Geneva (26 May 1959) 218
Institute of Physics "Notes for Authors" 218

10.D *Book reviews*

Bowen, J. H. and E. F. O. Masters, Nuclear reactor control and instrumentation (P. L. Ølgaard) 219
Galbraith, William, Extensive air showers (J. G. Wilson) 447
Goldstein, Herbert, Fundamental aspects of reactor shielding (P. L. Ølgaard) 224
Haïssinsky, M., editor, Les peroxydes organiques en radiobiologie, fourth series of actions chimiques et biologiques des radiations (Derek B. Hoge) 448
Harrison, J. R., Nuclear reactor shielding (B. Micheelsen) 219
Hocker, K. H. and K. Weimer, editors, Lexikon der Kern- und Reaktortechnik (O. Kofoed-Hansen) 446
International atomic energy agency bulletin (L. R.) 219
Koppeman, Bernard, editor, Materials for nuclear reactors (Niels Hansen) 222
Kunz, W. und J. Schintlmeister, Tabellen der Atomkerne, Teil I: Eigenschaften der Atomkerne, Bd. 1: Die Elemente Neutron bis Zinn (L. R.) . 222
Neary, G. J., R. J. Munson and R. H. Mole, Chronic radiation hazards - An experimental study with fast neutrons (W. Yourgrau) 223
Riezler, Wolfgang and Wilhelm Walcher, editors, with particular co-operation of Wolfgang Finkelnburg and Heinz Maier-Leibnitz, Kerntechnik: Physik-Technologie-Reaktoren (Sven Holm) 221
Šimáně, Č., Accelerators of ions and electrons (J. H. Bjerregaard) 220
Slack, L. and K. Way, Radiations from radioactive atoms in frequent use (L. R.) 220
Way, K., editor, 1959 nuclear data tables (L. R.) 220
Wootton, W. R., Steam cycles for nuclear power plant (H. Abel-Larsen) 447

NUCLEAR PHYSICS

ASSISTANT EDITOR

The Editor of NUCLEAR PHYSICS requires the assistance of a theoretical physicist for the reading and preparation of manuscripts for the press. The main requirements are:

(1) interest in and acquaintance with the methods of field theory and nuclear physics,

(2) interest in obtaining experience in the techniques of typography and editing,

(3) good knowledge of English.

The candidate is expected to reside in Copenhagen and may

(a) either be engaged on a full-time basis

(b) or be given the opportunity of pursuing research on a part-time basis.

The conditions of employment (salary, pension scheme, etc.) will be on the academic level, depending on the status and experience of the candidate.

Applications with details of scientific education and references should be sent to:
Professor L. Rosenfeld, NORDITA, Blegdamsvej 17,
COPENHAGEN, Denmark

ENERGY LEVELS OF LIGHT NUCLEI. VI

by

E. AJZENBERG-SELOVE
Department of Physics, Haverford College, Haverford, Pennsylvania

and

T. LAURITSEN
Kellog Radiation Laboratory, California
Institute of Technology, Pasadena, California

volume 11 (1959) no. 1
320 pages, 40s., $ 5.30

NORTH-HOLLAND PUBLISHING COMPANY
NIEUWE ZIJDS VOORBURGWAL 68-70 AMSTERDAM-C HOLLAND

NORTH-HOLLAND BOOKS

ANALYTICAL and CANONICAL FORMALISM in PHYSICS

by ANDRÉ MERCIER

Head of the Department of Theoretical Physics University of Berne

6×9″ VIII + 222 pp. Guilders 20.00 (40s.)

CONTENTS

i. Lagrangian Formalism
ii. Lagrangian Density
iii. Canonical Formalism
iv. Canonical Form of Electrodynamics
v. Hamiltonian Densities
vi. Transformations
vii. Canonical Formalism with Vanishing Jacobian Determinant

Those who are not highly specialized in these matters but do want to get a fairly broad knowledge of the subject are not aware of the fact that the greater parts of this formalism, including many specific conclusions of physical concern, do not involve in the least quantum theory, i.e. "quantization" of the fields. To show this and to provide the reader with a fairly complete presentation of the *classical* (i.e. not yet quantized) theory of fields is one of the main aims of the book.

This formalism is presented with great generality. Some special topics have also been included when they are found to be of importance in connection with the problems raised; however, they are not elaborated with the same generality, but just formulated as far as is found necessary for the understanding of these connections; for instance we can name: tensorial formalism and spinorial formalism.

A special chapter has been devoted to transformations of several kinds including canonical transformations, reversibility and the like as well as their interrelations, so that the ground is prepared for an understanding of the CPT-Theorems.

A short chapter on Dirac's dynamics with vanishing Jacobian closes the book.

The work builds upon the well-known *Principles of Analytical Dynamics* by the same author (in French), where particular weight is laid upon the homogeneous formalism, but it can easily be read with profit without knowledge of the latter by any advanced students in physics, astronomy or mathematics as well as by research workers who want to get a thorough practice in the use of these methods.

Many examples and as many as 124 problems illustrate the formalism exposed.

Sole Agency for U.S.A.: Interscience Publishers Inc. - New York

NORTH-HOLLAND PUBLISHING COMPANY - AMSTERDAM